Oxidative Medicine and Cellular Longevity

Oxidative Stress and Antioxidant Strategies in Cardiovascular Disease

Guest Editors: Adriane Belló-Klein, Neelam Khaper, Susana Llesuy, Dalton Valentim Vassallo, and Constantinos Pantos

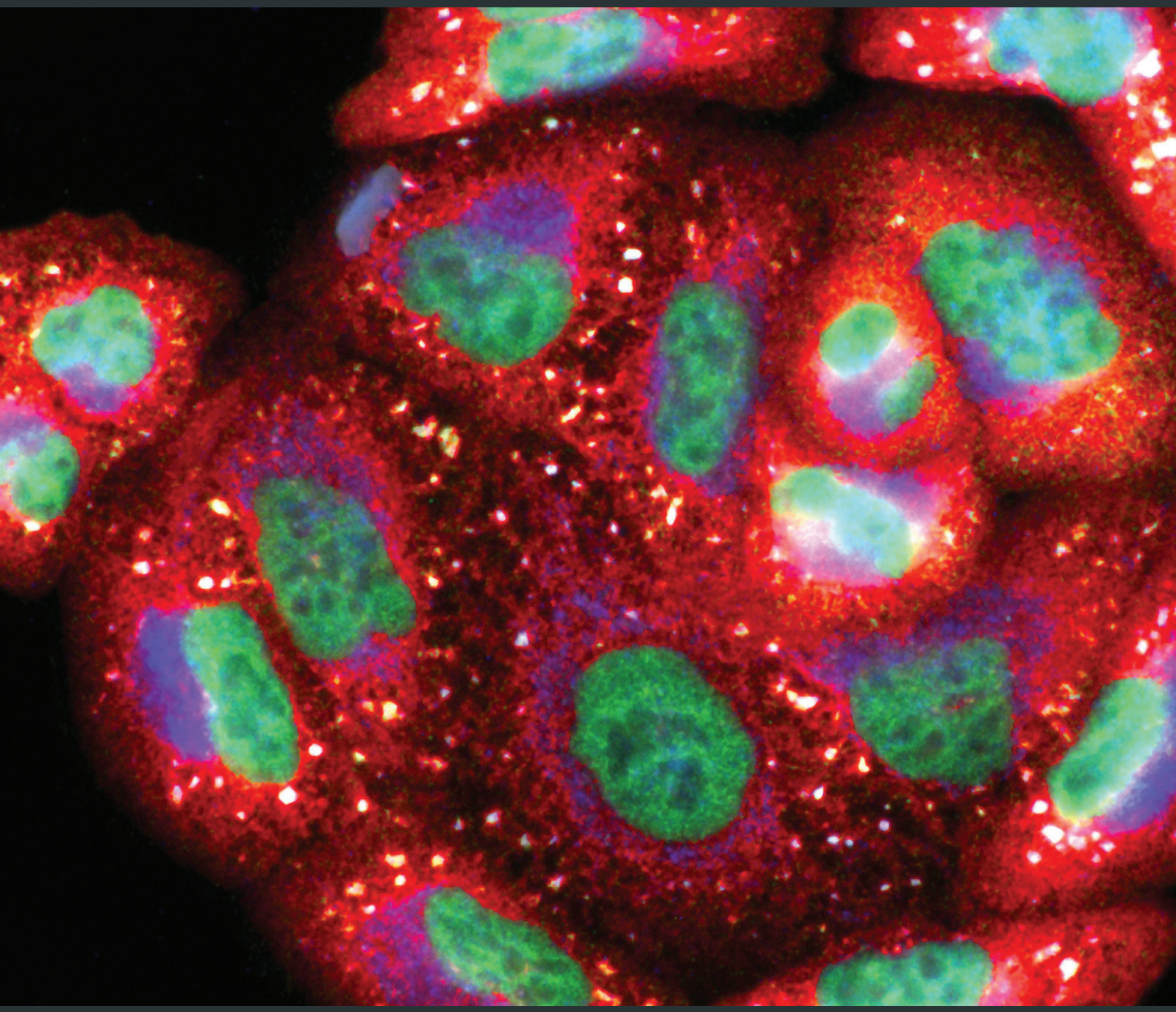

Oxidative Stress and Antioxidant Strategies in Cardiovascular Disease

Oxidative Medicine and Cellular Longevity

Oxidative Stress and Antioxidant Strategies in Cardiovascular Disease

Guest Editors: Adriane Belló-Klein, Neelam Khaper, Susana Llesuy, Dalton Valentim Vassallo, and Constantinos Pantos

Editorial Board

Contents

Hindawi Publishing Corporation
Oxidative Medicine and Cellular Longevity
Volume 2014, Article ID 678741, 2 pages
http://dx.doi.org/10.1155/2014/678741

Editorial

Oxidative Stress and Antioxidant Strategies in Cardiovascular Disease

Adriane Belló-Klein,[1] Neelam Khaper,[2] Susana Llesuy,[3] Dalton Valentim Vassallo,[4] and Constantinos Pantos[5]

[1] *Physiology Department, Federal University of Rio Grande do Sul, 90050-170 Porto Alegre, RS, Brazil*
[2] *Northern Ontario School of Medicine, Lakehead University, Thunder Bay, Canada P7B 5E1*
[3] *Faculty of Pharmacy, University of Buenos Aires, Buenos Aires 1121, Argentina*
[4] *Santa Casa de Misericórdia School of Medicine (EMESCAM), 29027-502 Vitória, ES, Brazil*
[5] *Pharmacology Department, University of Athens, 11527 Athens, Greece*

Correspondence should be addressed to Adriane Belló-Klein; belklein@ufrgs.br

Received 25 May 2014; Accepted 25 May 2014; Published 17 June 2014

The notion of oxidative stress has changed over the past decades from the idea of being a phenomenon involved exclusively with oxidative damage to a more contemporary concept that includes its role in intracellular signaling pathways. Reactive oxygen species (ROS) such as superoxide anion ($O_2{\cdot}^-$), hydroxyl radical ($OH^\bullet$), and hydrogen peroxide (H_2O_2) can be generated by different intracellular sources such as NAD(P)H oxidase, xanthine oxidase, myeloperoxidase, and uncoupled nitric oxide synthase [1]. ROS are capable of reacting with several cellular components, resulting in lipid peroxidation, and damage to proteins and DNA. In order to counterregulate these oxidative processes, cells have developed enzymatic and nonenzymatic antioxidant systems that can offer protection by regulating antioxidant response element signaling pathways [2]. In this regard, some phytochemicals, such as sulforaphane, brazilin, chalcone, resveratrol, and curcumin, are reported to modulate translocation and activation of the nuclear factor-erythroid-2-related factor (Nrf2) and regulate antioxidant response [3]. The primary aim of this special issue is to highlight the central role of antioxidants in various experimental models of heart failure and endothelial dysfunction as well as in human studies.

This special issue contains a review article and primary research articles covering a broad range of topics related to the therapeutic potential of antioxidants in heart failure. In a study by Y. Wang et al., *sulforaphane* attenuation of type-2 diabetes induced aortic fibrosis was associated with the upregulation of Nrf2 expression and function in mice. In another interesting study by M. H. Lee et al., *resveratrol* inhibited rat aortic vascular smooth muscle cell proliferation, dedifferentiation, and phenotype modulation. This finding was attributed to a differential regulation of prosurvival pathways by resveratrol, reinforcing the protective role of flavonoids by altering the phosphorylation state of some targeted molecules. Another polyphenol covered in this special issue is *methyl gallate* and its ability to afford cardioprotection against cobalt or H_2O_2-induced oxidative stress. This polyphenol was able to scavenge ROS, safeguarding mitochondria and cellular DNA and inhibiting the intrinsic apoptotic pathway.

Apoptosis is an important element of the cardiac remodeling process [4]. Suppression of apoptosis is a key target in attenuating adverse remodeling process [5]. In a related article featured in this special issue, a *microRNA* (miRNA) that targets glutathione peroxidase was utilized to explore its potential cardioprotective role against oxidative stress-induced apoptosis. This miRNA was markedly upregulated in apoptotic cells and its downregulation reduced the mitochondrial apoptotic pathway in cardiomyocytes exposed to oxidative stress. These novel findings may have some therapeutic

implications for a variety of cardiovascular diseases related to ROS, including atherosclerosis.

The role of antioxidants in *atherosclerosis* was another key topic explored in this special issue. An elegant paper by A. J. Lepedda et al. demonstrated that the prooxidant environment present in atherosclerotic plaque may oxidatively modify filtered albumin and the contribution of glutathione in maintaining the *intraplaque thiols equilibrium*. Another interesting study by M. Macharia et al. featured in this issue evaluated the association of indices of *paraoxonase*, an enzyme that prevents the oxidation of LDL cholesterol, as well as the oxidative status with subclinical cardiovascular disease in mixed-ancestry South Africans. Diabetic subjects of this population displayed a significant decrease in paraoxonase and antioxidants as well as an increase in oxidized LDL and lipid peroxidation. Carotid intima-media thickness of these patients was negatively correlated with indices of antioxidant activity and positively correlated with measures of lipid oxidation. E. Tuncay et al. also explored the role of antioxidants in diabetes. The authors elegantly demonstrated that an enhancement of antioxidant defense in diabetics prevented diastolic dysfunction due to modulation of the ryanodine receptor, leading to normalized intracellular concentrations of calcium and zinc in cardiomyocytes.

Estrogen therapy as another antioxidant strategy is explored by two articles featured in this issue. The influence of estrogen on *coronary resistance* was studied by P. C. Schenkel et al. where they investigated the modulatory role of nitric oxide and H_2O_2 levels in female rats. The data suggest that, in the absence of estrogen, coronary resistance regulation seems to be more dependent on H_2O_2 which is maintained at low levels by increased catalase activity. The data provides a new insight regarding the role of oxidative stress balance in the regulation of coronary tone. One compelling question that is always raised regarding estrogen therapy is the optimal dose that should be used. An interesting paper by C. Campos et al. indicates that a *low dose of estrogen* (40% less than the pharmacological dose) was just as effective as a high dose for promoting improvement in cardiovascular function and reducing oxidative stress, thereby supporting the approach of using low dose of estrogen in clinical settings to minimize the risks associated with estrogen therapy.

The cardioprotective role of *thyroid hormones* has also been featured in this special issue. Administration of this hormone has been associated with increased ROS, Nrf2, thioredoxin, and heme-oxygenase levels in cardiac tissue [6]. It seems that a thyroid hormone-dependent counterregulatory response could represent a hormetic effect, in order to stabilize redox environment and provide cell survival [7]. An elegant review by C. Pantos and I. Mourouzis highlights the role of thyroid hormones in ischemia/reperfusion injury and the conversion from pathologic to physiologic growth after myocardial infarction via TRα1 receptor.

In summary, this special issue covers a wide range of topics addressing the role of oxidative stress and antioxidants in the pathophysiology of heart failure. These articles not only enrich our understanding of how oxidative stress plays an important role in heart failure but also provide evidence on antioxidant therapies in this condition.

Acknowledgment

We would like to acknowledge the reviewers for their expert assistance and all authors for their contribution to the issue.

Adriane Belló-Klein
Neelam Khaper
Susana Llesuy
Dalton Valentim Vassallo
Constantinos Pantos

References

[1] H. Tsutsui, S. Kinugawa, and S. Matsushima, "Oxidative stress and heart failure," *American Journal of Physiology: Heart and Circulatory Physiology*, vol. 301, no. 6, pp. 2181–2190, 2011.

[2] B. Halliwell, "Oxidative stress and neurodegeneration: where are we now?" *Journal of Neurochemistry*, vol. 97, no. 6, pp. 1634–1658, 2006.

[3] Y.-J. Surh, J. K. Kundu, and H.-K. Na, "Nrf2 as a master redox switch in turning on the cellular signaling involved in the induction of cytoprotective genes by some chemopreventive phytochemicals," *Planta Medica*, vol. 74, no. 13, pp. 1526–1539, 2008.

[4] A. Abbate and J. Narula, "Role of apoptosis in adverse ventricular remodeling," *Heart Failure Clinics*, vol. 8, no. 1, pp. 79–86, 2012.

[5] D. Wencker, M. Chandra, K. Nguyen et al., "A mechanistic role for cardiac myocyte apoptosis in heart failure," *The Journal of Clinical Investigation*, vol. 111, no. 10, pp. 1497–1504, 2003.

[6] D. Baraldi, K. Casali, R. O. Fernandes et al., "The role of AT1-receptor blockade on reactive oxygen species and cardiac autonomic drive in experimental hyperthyroidism," *Autonomic Neuroscience: Basic and Clinical*, vol. 177, no. 2, pp. 163–169, 2013.

[7] L. A. Videla, "Cytoprotective and suicidal signaling in oxidative stress," *Biological Research*, vol. 43, no. 3, pp. 363–369, 2010.

Hindawi Publishing Corporation
Oxidative Medicine and Cellular Longevity
Volume 2014, Article ID 587083, 8 pages
http://dx.doi.org/10.1155/2014/587083

Clinical Study

Xanthine Oxidase Activity Is Associated with Risk Factors for Cardiovascular Disease and Inflammatory and Oxidative Status Markers in Metabolic Syndrome: Effects of a Single Exercise Session

Ana Maria Pandolfo Feoli,[1] Fabrício Edler Macagnan,[2] Carla Haas Piovesan,[1,2] Luiz Carlos Bodanese,[2] and Ionara Rodrigues Siqueira[3]

[1] *Faculdade de Enfermagem, Nutrição e Fisioterapia, Pontifícia Universidade Católica do Rio Grande do Sul, Avenida Ipiranga 6681, Prédio 12, 8° andar, 90619-900 Porto Alegre, RS, Brazil*
[2] *Programa de Pós-Graduação em Medicina e Ciências da Saúde, Pontifícia Universidade Católica do Rio Grande do Sul, Avenida Ipiranga 6690, 90610-000 Porto Alegre, RS, Brazil*
[3] *Departamento de Farmacologia, Instituto de Ciências Básicas da Saúde, Universidade Federal do Rio Grande do Sul, Rua Sarmento Leite 500, 90050-170 Porto Alegre, RS, Brazil*

Correspondence should be addressed to Ana Maria Pandolfo Feoli; anamariafeoli@hotmail.com

Received 22 November 2013; Revised 5 April 2014; Accepted 19 April 2014; Published 21 May 2014

Academic Editor: Neelam Khaper

Objective. The main goal of the present study was to investigate the xanthine oxidase (XO) activity in metabolic syndrome in subjects submitted to a single exercise session. We also investigated parameters of oxidative and inflammatory status. *Materials/Methods*. A case-control study (9 healthy and 8 MS volunteers) was performed to measure XO, superoxide dismutase (SOD), glutathione peroxidase activities, lipid peroxidation, high-sensitivity C-reactive protein (hsCRP) content, glucose levels, and lipid profile. Body mass indices, abdominal circumference, systolic and diastolic blood pressure, and TG levels were also determined. The exercise session consisted of 3 minutes of stretching, 3 minutes of warm-up, 30 minutes at a constant dynamic workload at a moderate intensity, and 3 minutes at a low speed. The blood samples were collected before and 15 minutes after the exercise session. *Results*. Serum XO activity was higher in MS group compared to control group. SOD activity was lower in MS subjects. XO activity was correlated with SOD, abdominal circumference, body mass indices, and hsCRP. The single exercise session reduced the SOD activity in the control group. *Conclusions*. Our data support the association between oxidative stress and risk factors for cardiovascular diseases and suggest XO is present in the pathogenesis of metabolic syndrome.

1. Introduction

The metabolic syndrome (MS) is mainly characterized by obesity, blood hypertension, hyperglycemia, or serum dyslipidemia as defined by the third report of the National Cholesterol Education Program Adult Treatment Panel III [1] and the International Diabetes Federation [2]. It has been demonstrated that the metabolic syndrome is associated with double risk of cardiovascular disease and mortality as well as stroke, even without type 2 diabetes mellitus [3]. However, the pathophysiological mechanisms by which the metabolic syndrome increases cardiovascular risk have not been fully clarified yet [4].

Epidemiological studies have also demonstrated the relationship between the uric acid and MS [5] and individual components of metabolic syndrome such as obesity,

hypertension, dyslipidemia, [6], insulin resistance, higher C-reactive protein (CRP) concentration [7], and endothelial dysfunction [8].

According to Mankovsky et al. [9], cardiovascular events have also been related to uric acid levels. In addition, epidemiological studies demonstrated that uric acid is an independent risk factor for cardiovascular diseases [4, 10], particularly in hypertensive and diabetic individuals [11]. Although uric acid is considered an important water soluble antioxidant, several authors have discussed the dual role of uric acid as a detrimental or protective factor [12, 13]. Uric acid is generated by xanthine oxidase (XO); this enzyme catalyses the conversion of hypoxanthine to uric acid and superoxide anion radical [14]. Although hyperuricemia has been linked to metabolic syndrome, the role of xanthine oxidase remains poorly understood.

As described above, XO is a source of reactive oxygen species, generating superoxide anion radical. Several studies have reported that oxidative stress, the imbalance between free radical levels and antioxidant capacity, plays a significant role in the pathogenesis of cardiovascular disease [15] and diabetes [16]. However, few data are available concerning the associations between circulating concentrations of oxidative biomarkers and MS. Specifically, metabolic syndrome-related oxidative changes in macromolecules and antioxidant enzymatic system have been described, although these results are contradictory, pointing to a rather complex relationship to link oxidative status with the metabolic syndrome [4]. Besides, despite the oxidative status heterogeneity in different ethnic groups [17], the oxidative stress markers in metabolic syndrome in Brazilian patients have received little attention.

Furthermore, the inflammation process has been widely connected to metabolic syndrome. Adipose tissue produces proinflammatory cytokines, called adipocytokines, which could increase C-reactive protein (CRP) synthesis [16]. The ultrasensitive C-reactive protein (hsCRP) has been widely used to evaluate vascular inflammation and cardiovascular risk [18]. Interestingly, cytokines can irreversibly convert endothelial xanthine dehydrogenase to its active form, XO [19].

Epidemiological and experimental studies have demonstrated that exercise may be able to prevent and treat metabolic syndrome and its components, such as type 2 diabetes and cardiovascular disease [20]. The beneficial effect has been related to training-induced adaptations in oxidative status; this hypothesis is based on the fact that acute exercise session would induce an increase in reactive species levels, although to our knowledge there are no studies reporting the impact of acute exercise on oxidative status in metabolic syndrome.

Our working hypothesis was that xanthine oxidase activity is increased in metabolic syndrome and this parameter is correlated to clinical criteria, oxidative stress, and inflammatory markers and the acute exercise would be able to alter these parameters.

The main goal of the present study was to investigate the plasma XO activity in metabolic syndrome patients. We also investigated lipid peroxidation and antioxidant enzyme activities, namely, superoxide dismutase and glutathione peroxidase. Besides, CRP levels were detected as a low-grade inflammatory marker. The acute effects of single exercise session on these parameters were also investigated.

2. Methods

2.1. Subjects. Subjects were examined by the same physician at the Rehabilitation Center, Pontifical Catholic University of Rio Grande do Sul state (PUCRS). The characteristics of the subjects are shown in Table 1. The study included 17 subjects (09 men and 08 women; mean age: 50.28 ± 6.5 years). The control group consisted of 9 healthy subjects, and 8 patients were diagnosed with MS. All subjects were sedentary with no regular physical activity. Based on previous report comparing plasma XO activity between control subjects and patients with hyperlipidemia [21], a sample size of 7 subjects in each group was needed to detect the effect for a 90% power at a 0.05 significance level.

The diagnostic criteria for MS were made using the NCEP ATP III [1], following three or more criteria [11]: abdominal obesity based on abdominal circumference (men, >102 cm; women, >88 cm); triglycerides (≥150 mg/dL); high-density lipoprotein- (HDL-) cholesterol (men, <40 mg/dL; women, <50 mg/dL); blood pressure (≥130/85 mm Hg); and fasting glucose (≥110 mg/dL). Exclusion criteria were clinical manifestations of cardiovascular disease, diabetes, hypertension, other chronic diseases, renal or hepatic insufficiency and hypothyroidism, use of drugs capable of modifying the lipid profile, inflammation that could not be withdrawn 6 weeks before initiating the study, and any infection or inflammatory disease within the 6 weeks prior to the study. The study protocol and the procedures were approved by Ethics Committee of PUCRS (0603024) and the subjects gave informed consent.

2.2. Chemicals. All chemicals used in this study were purchased from Sigma Chemical Co. (St. Louis, MO, USA) and were of analytical grade or the highest grade available.

2.3. Clinical and Anthropometric Parameters. Blood pressure was measured with subjects in the sitting position using a mercury sphygmomanometer after a 10-min period of rest, two separated measurements being performed. Anthropometrical measurements included weight, height, and abdominal circumference. Weight was obtained using calibrated scales (Filizola, Brazil) while subjects wore light clothing and no shoes and height was measured by a fixed stadiometer. BMI was calculated as weight divided by height square. Abdominal circumference was measured in orthostatic position at the midpoint between the low costal rim and the iliac crest.

2.4. Physical Activity Session. The physical activity session was supervised at all times and took about 40 minutes divided as follows: 3 minutes spent in stretching, 3 minutes in warming up (walking on the treadmill at 3.2 km/h without grate), 30 minutes in a constant dynamic workload on moderate intensity (speed and grate were sufficiently increased to reach

Table 1: Clinical characteristics of the study populations.

Parameters	Controls ($n = 9$)	MS ($n = 8$)	P
Sex (F/M)	(5/4)	(4/4)	
Age (years)	50.56 ± 5.36	50.00 ± 7.69	0.863
BMI (kg/m^2)	24.47 ± 1.10	37.14 ± 5.19	<0.001
AC (cm)			
Female	74.60 ± 9.69	114.63 ± 10.96	0.001
Male	94.00 ± 4.69	120.88 ± 10.38	0.003
Total-C (mg/dL)	198.44 ± 31.16	218.88 ± 39.77	0.253
LDL-C (mg/dL)	167.60 ± 29.28	167.30 ± 28.82	0.983
HDL-C (mg/dL)			
Female	63.80 ± 10.13	48.50 ± 7.59	0.041
Male	63.50 ± 4.95	43.67 ± 8.02	0.048
TG (mg/dL)	90.67 ± 30.81	211.25 ± 76.30	<0.001
AIP	0.13 ± 0.18	0.63 ± 0.21	<0.001
Glucose (mmol/L)	86.00 ± 5.32	104.38 ± 13.50	0.001
Insulin	4.23 ± 1.52	19.84 ± 5.80	0.003
HOMA	0.90 ± 0.34	5.22 ± 2.12	0.000
hsCRP (mg/dL)	0.12 ± 0.09	0.79 ± 0.29	<0.001
SBP (mmHg)	115.56 ± 13.79	145.13 ± 10.97	0.002
DBP (mmHg)	77.11 ± 13.38	93.75 ± 8.76	0.009

Data are expressed as mean ± SD. BMI: body mass indices, AC: abdominal circumference, Total-C: total cholesterol, LDL-C: low density lipoprotein cholesterol, HDL-C: high density lipoprotein cholesterol, TG: triglycerides, AIP: log.(TG/HDL-c); atherogenic index of plasma, HOMA: ((Glucose/18) ∗ insulin)/22,5; homeostatic model assessment for insulin resistance, hsCPR: high sensitive C protein reactivity, SBP: systolic blood pressure, DBP: diastolic blood pressure. Student' t-test.

the set point of the heart rate (HR), and 3 minutes at a low velocity (3.2 km/h) to cool down. A HR monitor (POLAR) was used to control and keep the HR on target as suggested by the Brazilian Guideline for MS diagnosis and treatment [11]. The range of the heart rate (HR) between 65 and 75% of the age predicted maximum HR is a common method. This method was used to set individual workload on treadmill (Inbrasport, Export model). The velocity and grate of the treadmill were progressively increased until HR reached the set point.

2.5. Biochemical Parameters. All blood samples were collected in the morning after overnight fast (before exercise) and 15 minutes after the acute exercise session. Blood samples were collected in heparinized tubes and immediately centrifuged at room temperature for 10 min at 3000 rpm. The supernatant was transferred to cryotubes and aliquots were stored at −70°C until assay for xanthine oxidase (XO), superoxide dismutase (SOD), glutathione peroxidase (GSHPx), lipid peroxidation (TBARS), high-sensitivity CRP, glucose, and lipid parameters were determined. Plasma glucose, total serum cholesterol, serum triglyceride, and serum HDL-cholesterol levels were measured by standard enzymatic methods using reagents in a fully automated analyzer (Vitros 950 dry chemistry system; Johnson & Johnson, Rochester, NY). LDL-cholesterol was estimated using the Friedewald equation [22]. High-sensitivity CRP (hsCRP) was measured using the ADVIA Centaur immunoassay on the ADVIA Centaur analyzer (Siemens Medical Solutions Diagnostics, Frimley, Surrey, UK).

2.6. Atherogenic Index of Plasma (AIP). The new atherogenic plasma index (AIP) is a logarithmic transformation of the ratio of the molar triglyceride (TG) concentration and high density lipoprotein cholesterol (HDL-C). AIP correlates closely with the particle size of LDL ($r = 0.8$) and the esterification rate of plasma cholesterol devoid of apo B lipoproteins (FERHDL), $r = 0.9$, which are considered at present the most sensitive indicators of the atherogenic plasma profile. The mean AIP values of nonrisk groups equaled zero or were lower, while atherogenic risk AIP reached positive values [7].

2.7. Determination of XO Activity. Serum XO activity (cytoplasmic xanthine oxidase (EC1.17.3.2)) was measured according to the method of Prajda and Weber, where activity is measured by determination of uric acid from xanthine [23]. Serum was incubated for 30 min at 37°C in phosphate buffer (pH 7.5, 50 mM) containing xanthine (4 mM). The reaction was stopped adding 20 μL 100% TCA. The mixture was then centrifuged at 4000 ×g for 20 min. Uric acid was determined in the supernatant by absorbance at 292 nm against a blank. The results are expressed as units per milliliter (U/mL).

2.8. Determination of SOD Activity. Superoxide dismutase activity was determined with a RANSOD kit (Randox Laboratories, San Diego, CA, USA). This method employs xanthine and xanthine oxidase to generate superoxide radical, which reacts with 2-(4-iodophenyl)-3-(4-nitrophenol)-5-phenyltetrazolium chloride to form a red formazan dye that is assayed spectrophotometrically at 505 nm and 37°C.

Inhibition of production of the chromogen is proportional to SOD activity in the sample. SOD activity was expressed as units per μg protein.

2.9. Determination of GPx Activity. GPx activity was determined according to Wendel [24]. The reaction was carried out at 25°C in 600 μL of solution containing 100 mM pH 7.7 potassium phosphate buffer, 1 mM EDTA, 0.4 mM sodium azide, 2 mM GSH, 0.1 mM NADPH, and 0.62 U of GSH reductase. The activity of selenium-dependent GPx was measured taking *tert*-butyl hydroperoxide as substrate at 340 nm. The contribution of spontaneous NADPH oxidation was always subtracted from the overall reaction rate. GPx activity was expressed as nmol NADPH oxidized per minute per mg protein.

2.10. Lipid Peroxidation (TBARS). The formation of thiobarbituric acid reactive substances (TBARS) was based on the methods described by Buege [25]. Aliquots of samples were incubated with 10% trichloroacetic acid (TCA) and 0.67% thiobarbituric acid (TBA). The mixture was heated in a boiling water bath. Afterwards, *n*-butanol was added and the mixture was centrifuged. The organic phase was collected to measure fluorescence at excitation and emission wavelengths of 515 and 553 nm [26], respectively; 1,1,3,3-tetramethoxypropane, which is converted to malondialdehyde (MDA), was used as standard. The results were expressed as nmol MDA formed/mg protein.

2.11. Statistical Analysis. Statistical evaluation was carried out with the SPSS 11.0 (Statistical Packages for Social Sciences; SPSS Inc, Chicago, Illinois, USA). Results were expressed as mean (±SD). Baseline results were compared by the Student's *t*-test (see Table 1). Pearson correlation and linear regression analysis were used to study the relationships between all evaluated parameters. To test the effect of single session treadmill on oxidative status markers in patients with metabolic syndrome, we used two-way ANOVA for repeated measurements. The post hoc test was performed by Tukey test. A value of $P \leq 0.05$ was considered significant.

3. Results

Baseline clinical and biochemical characteristics of control and MS groups are shown in Table 1. MS subjects showed higher levels of BMI, abdominal circumference, systolic and diastolic blood pressure, and TG levels, while HDL-C was decreased in this group.

MS was able to alter some oxidative stress parameters, especially XO activity which increased in MS group ($P = 0.002$, Figure 1). The impact of MS and acute exercise on the antioxidant enzymes studied is presented in Figure 2. SOD activity was reduced in MS group (Figure 2(a); $P = 0.019$). On the other hand, no differences on the GSHPx activity were found in MS subjects (Figure 2(b)). Figure 3 illustrates the effect of MS and acute exercise on lipid peroxidation evaluated by TBARS levels. MS did not alter significantly TBARS levels.

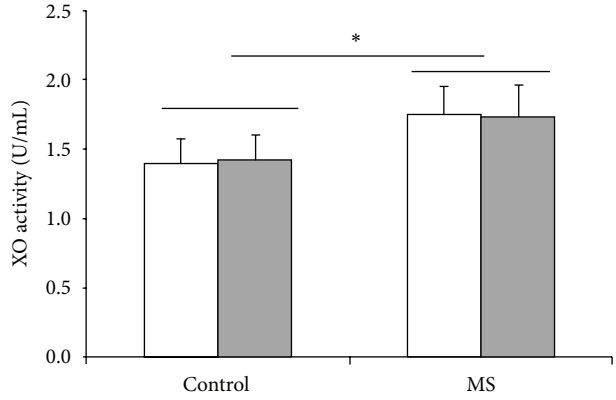

Figure 1: Effects of metabolic syndrome (MS) and single treadmill session on XO activity. White bar = before exercise; shadowed bar = after exercise; two-way ANOVA followed by Tukey test. * Significant difference between control and SM groups; $P < 0.05$.

Table 2: Pearson correlation with XO and clinical parameters ($n = 17$).

XO activity versus	r	P
SOD activity	−0.71	0.005
Abdominal circumference	0.61	0.010
BMI	0.66	0.007
hsCRP	0.70	0.005

BMI: body mass indices; hsCRP: high sensitive reactive C protein. Pearson correlation and linear regression analysis were used to study the relationships between parameters.

There was a significant correlation between XO activity and metabolic syndrome markers. Pearson correlation coefficients between XO activity and anthropometric and biochemical and oxidative stress parameters are shown in Table 2. XO activity was correlated positively with BMI, abdominal waist, and hsCRP and negatively with SOD activity. Besides, there was a significant correlation between SOD activity and metabolic syndrome markers (data not shown).

The single exercise session induced a reduction in SOD activity (Figure 2(a)) in the control group, without any effect in MS group. This exercise protocol did not alter XO activity, TBARS levels, and GSHPx activity.

4. Discussion

This study adds evidence to the pathophysiological mechanisms in the metabolic syndrome, principally to role of oxidative stress in MS and its components.

Our results provide the first evidence that higher XO activity may have a central role in MS. MS subjects showed increased XO activity; besides XO activity was correlated to metabolic syndrome markers. Accordingly, uric acid levels have been related to cardiovascular events [9], which is relevant since XO is a metabolic pathway for uric acid generation. It has been suggested that higher uric acid levels are associated with their lower renal excretion [27], although the results presented here could suggest an increase in uric acid

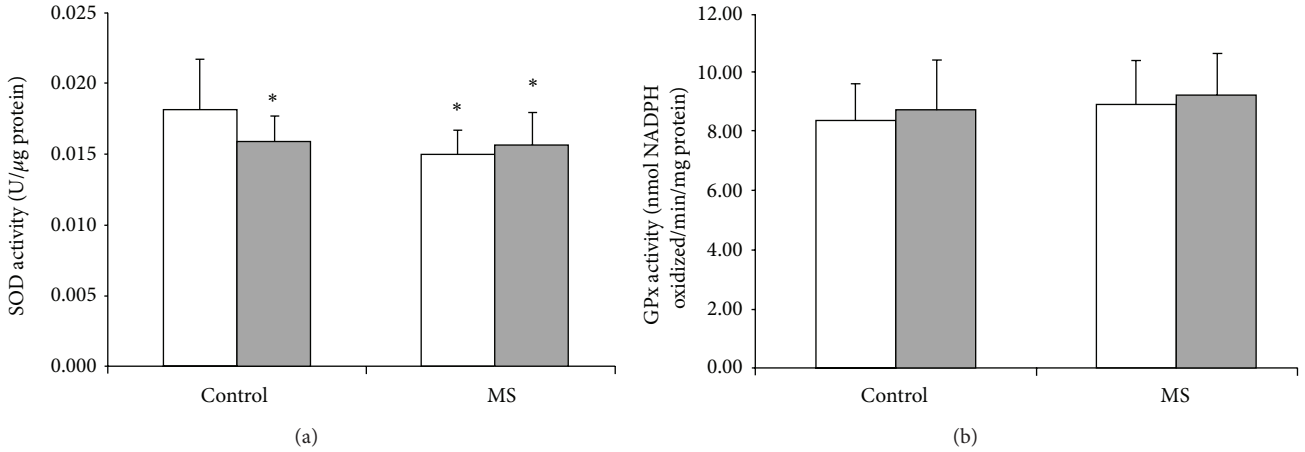

Figure 2: Effects of metabolic syndrome (MS) and single treadmill session on antioxidant enzymes activities, SOD (a) and GPx (b). White bar = before exercise; shadowed bar = after exercise; two-way ANOVA followed by Tukey test. *Significantly different as compared to control group before acute exercise; $P < 0.05$.

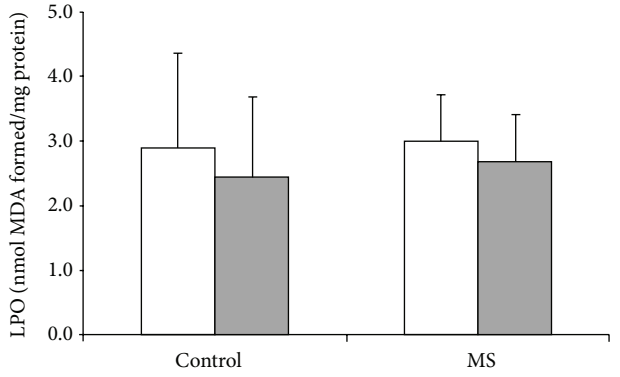

Figure 3: Effects of metabolic syndrome (MS) and single treadmill session on lipid peroxidation through TBARS. White bar = before exercise; shadowed bar = after exercise; two-way ANOVA followed by Tukey test.

production induced by augmented XO activity. Nevertheless, our results do not exclude the participation of lower renal excretion.

Also, it is important to note that uric acid nephrolithiasis is significantly more frequent among patients with the metabolic syndrome and obesity [28], which can be related to enhanced xanthine oxidase activity. Moreover, it has been demonstrated that there is an association between kidney stones and atherosclerosis [29].

It is important to note that excessive dietary sucrose or high-fructose corn syrup has been related to risk factors for cardiovascular disease and metabolic syndrome. It has been suggested that this effect is linked to increased uric acid levels produced by fructokinase pathway [30]. Then a causal role of uric acid in fructose-induced MS has been hypothesized; however it can be supposed that altered XO activity and fructose-induced higher levels of uric acid can produce synergistic deleterious effect.

In addition, our results could provide a new perspective for pharmacological prevention and/or MS treatment, at least as adjuvant strategies. In this sense, XO inhibitors, such as allopurinol and oxypurinol, have been suggested for the prevention of cardiovascular diseases [14].

Considering that an increase in XO activity was observed, whose reactions have superoxide anion radical as a byproduct [31], the role of this enzyme in MS might be suggested in producing an imbalance between free radical levels and antioxidant capacity. Our results corroborate the hypothesis that oxidative stress is involved in MS pathogenesis.

Additionally, in an effort to compare our findings with results reported in the literature, we also investigated some parameters of oxidative status, lipid peroxidation, and antioxidant enzyme activities, namely, superoxide dismutase and glutathione peroxidase.

SOD activity, a major intracellular and extracellular enzymatic defense system against superoxide, was significantly lower in MS subjects, and there was a negative correlation between SOD and XO activities. An increased XO activity generating superoxide anion radical and a concomitantly decreased SOD activity were found in MS patients of this study, indicating an increase in production and a decrease in removal of superoxide radicals. This disturbed superoxide content may be important in the pathogenesis of MS, since excessive content of reactive species may induce endothelial dysfunction [16, 32], which is associated with different stages of atherosclerosis [33–35]. Moreover, in agreement with Isogawa et al. [21], SOD activity was negatively correlated with some metabolic syndrome markers, namely, abdominal waist, BMI, and hsCRP.

It is important to note that SOD activity results are contradictory in different ethnicities, since Japanese and Taiwanese MS patients have significantly lower SOD activity [36, 37], while Caucasians recruited in Prague demonstrated higher SOD activity [6]. These findings support the idea that oxidative parameters must be tested in specific populations [17].

The evaluated metabolic syndrome parameters can be related to endothelial cell dysfunction. In this context, our

findings can corroborate the hypothesis that endothelial dysfunction is related to decreased nitric oxide (NO) content through inactivation of NO by superoxide, considering that NO modulates vascular tone through its vasodilator action [38]. The interaction of NO with superoxide may yield peroxynitrite, which breaks down to form a hydroxyl radical, thereby resulting in increased oxidative stress [39].

In contrast to previous data, MS did not modify TBARS levels. It is possible to infer that TBARS levels were unchanged because glutathione peroxidase activity, which breaks down peroxides (notably those derived from the oxidation of membrane phospholipids), remained unaltered [37]. This finding may suggest that increases in lipoperoxidation levels may not be crucial in MS; therefore, other molecular mechanisms cannot be ruled out.

This work demonstrated that XO activity correlated positively with hsCRP, a marker of low-grade inflammation. Also, Martinez-Hervas et al. [40] found a positive association between XO activity and hsCRP in a study with familial combined hyperlipidemia. It is possible to infer that inflammatory mediators, such as cytokines, are involved in the activation of XO [19]. It is interesting to comment that a growing body of evidence suggests that inflammation markers are closely related to MS and its consequences [33].

Our data indicate an association between increased abdominal circumference and XO activity. It is possible to hypothesize that XO-generated superoxide can be, at least in part, related to visceral adiposity. Obesity, characterized by enlarged adipocytes, and insulin resistance are associated with impaired adipogenesis and a low-grade chronic inflammation. Visceral adiposity plays an important role in the progression of cardiovascular diseases, insulin resistance, and type 2 diabetes [32, 34].

Although regular exercise has been suggested for the management of MS and its components, changes in human performance and physiological conditions after acute exercise session have only recently attracted attention. It is important to describe that the beneficial effect of exercise has been linked to free radicals production achieving adaptations in antioxidant system. Considering this hypothesis, we could expect that a single session of exercise would be able to induce an oxidative stress status; however, our acute session exercise protocol reduced SOD activity in healthy control subjects, without any effect in MS group, showing different profiles between these groups. It is impossible to establish, at this moment, a mechanism by which the exercise alters this parameter only in healthy subjects, although it is possible to postulate that MS condition may induce sustained adaptations which a single exercise session was unable to impact. Besides, the physiological impact of this effect in healthy subjects remains unsolved, since reduced SOD activity could increase the superoxide radical content, although it might reduce the hydrogen peroxide generation, as reactive oxygen species that combined to metal iron would originate hydroxyl radicals, inducing a hazardous state.

It is possible to suggest that types, regimen, and intensities of physical activity protocols can be determinant to impact oxidative status parameters. In this context, it is interesting to note that walking and stretching or resistance exercise training during 12 weeks without diet-induced weight loss did not alter oxidative stress in middle-aged men with MS [41]. Besides, aerobic exercise or Hatha yoga for 12 weeks did not alter lipid or protein oxidative damage [42], while longer exercise protocols have attenuated oxidative stress parameters in patients with type 2 diabetes [42, 43].

In accordance with the results presented here, the acute session exercise did not alter the plasma levels of pro- or anti-inflammatory cytokines in women with MS [44]; however, Greene et al. demonstrated that acute exercise increased hsCRP in subjects [45].

Our results support the hypothesis that increased XO activity has a central role in metabolic syndrome. The single exercise session protocol was able to alter SOD activity in healthy control group, without any impact on the MS subjects. Additional work will be required to investigate the molecular mechanisms behind these findings.

Abbreviations

MS:	Metabolic syndrome
NCEP ATP III:	Third Report of the National Cholesterol Education Program Adult Treatment Panel III
XO:	Xanthine oxidase
SOD:	Superoxide dismutase
GSHPx:	Glutathione peroxidase
hsCRP:	High-sensitivity CRP
TBARS:	Thiobarbituric acid reactive substances
NO:	Nitric oxide.

Conflict of Interests

The present study does not have real or apparent conflict of interests.

Authors' Contribution

Ana Maria Pandolfo Feoli, Fabrício Edler Macagnan, Carla Haas Piovesan, and Ionara Rodrigues Siqueira worked on data collection and analysis, data interpretation, and paper writing. Luiz Carlos Bodanese contributed to paper writing.

References

[1] National Institutes of Health et al., *ATP III Guidelines At-A-Glance Quick Desk Reference*, NIH Publication, 2001.

[2] Atlas Diabetes, "International Diabetes Federation," 2000, http://www.idf.org/diabetesatlas.

[3] S. Mottillo, K. B. Filion, J. Genest et al., "The metabolic syndrome and cardiovascular risk: a systematic review and meta-analysis," *Journal of the American College of Cardiology*, vol. 56, no. 14, pp. 1113–1132, 2010.

[4] K. G. M. M. Alberti, R. H. Eckel, S. M. Grundy et al., "Harmonizing the metabolic syndrome: a joint interim statement of the international diabetes federation task force on epidemiology and prevention; National heart, lung, and blood institute; American heart association; World heart federation; International atherosclerosis society; And international association for

the study of obesity," *Circulation*, vol. 120, no. 16, pp. 1640–1645, 2009.

[5] X. Sui, T. S. Church, R. A. Meriwether, F. Lobelo, and S. N. Blair, "Uric acid and the development of metabolic syndrome in women and men," *Metabolism: Clinical and Experimental*, vol. 57, no. 6, pp. 845–852, 2008.

[6] L. Vávrová, J. Kodydková, M. Zeman et al., "Altered activities of antioxidant enzymes in patients with metabolic syndrome," *Obesity Facts*, vol. 6, no. 1, pp. 39–47, 2013.

[7] M. Dobiasova, "AIP-atherogenic index of plasma as a significant predictor of cardiovascular risk: from research to practice," *Vnitřní lékařnství*, vol. 52, no. 1, pp. 64–71, 2006.

[8] C. A. J. Farquharson, R. Butler, A. Hill, J. J. F. Belch, and A. D. Struthers, "Allopurinol improves endothelial dysfunction in chronic heart failure," *Circulation*, vol. 106, no. 2, pp. 221–226, 2002.

[9] B. Mankovsky, R. Kurashvili, and S. Sadikot, "Is serum uric acid a risk factor for atherosclerotic cardiovascular disease?: a review of the clinical evidence. Part 1," *Diabetes and Metabolic Syndrome: Clinical Research and Reviews*, vol. 4, no. 3, pp. 176–184, 2010.

[10] M. Kanbay, M. Segal, B. Afsar, D. H. Kang, B. Rodriguez-Iturbe, and R. J. Johnson, "The role of uric acid in the pathogenesis of human cardiovascular disease," *Heart*, vol. 99, no. 11, pp. 759–766, 2013.

[11] A. Brandão, A. A. Brandão, A. da Rocha Nogueira et al., "I Diretriz brasileira de diagnóstico e tratamento da síndrome metabólica," *Brasileiros de Cardiologia*, vol. 84, supplement I, pp. 1–28, 2005.

[12] A. G. Ioachimescu, D. M. Brennan, B. M. Hoar, S. L. Hazen, and B. J. Hoogwerf, "Serum uric acid is an independent predictor of all-cause mortality in patients at high risk of cardiovascular disease: a Preventive Cardiology Information System (PreCIS) database cohort study," *Arthritis and Rheumatism*, vol. 58, no. 2, pp. 623–630, 2008.

[13] K. Okamoto, B. T. Eger, T. Nishino, S. Kondo, E. F. Pai, and T. Nishino, "An extremely potent inhibitor of xanthine oxidoreductase: crystal structure of the enzyme-inhibitor complex and mechanism of inhibition," *The Journal of Biological Chemistry*, vol. 278, no. 3, pp. 1848–1855, 2003.

[14] P. Puddu, G. M. Puddu, E. Cravero, L. Vizioli, and A. Muscari, "The relationships among hyperuricemia, endothelial dysfunction, and cardiovascular diseases: molecular mechanisms and clinical implications," *Journal of Cardiology*, vol. 59, no. 3, pp. 235–242, 2012.

[15] S. Furukawa, T. Fujita, M. Shimabukuro et al., "Increased oxidative stress in obesity and its impact on metabolic syndrome," *Journal of Clinical Investigation*, vol. 114, no. 12, pp. 1752–1761, 2004.

[16] V. O. Palmieri, I. Grattagliano, P. Portincasa, and G. Palasciano, "Systemic oxidative alterations are associated with visceral adiposity and liver steatosis in patients with metabolic syndrome," *The Journal of Nutrition*, vol. 136, no. 12, pp. 3022–3026, 2006.

[17] P. Galassetti, "Inflammation and oxidative stress in obesity, metabolic syndrome, and diabetes," *Experimental Diabetes Research*, vol. 2012, Article ID 943706, 2012.

[18] S. Devaraj, U. Singh, and I. Jialal, "Human C-reactive protein and the metabolic syndrome," *Current Opinion in Lipidology*, vol. 20, no. 3, pp. 182–189, 2009.

[19] C. Vorbach, R. Harrison, and M. R. Capecchi, "Xanthine oxidoreductase is central to the evolution and function of the innate immune system," *Trends in Immunology*, vol. 24, no. 9, pp. 512–517, 2003.

[20] M. Valko, D. Leibfritz, J. Moncol, M. T. D. Cronin, M. Mazur, and J. Telser, "Free radicals and antioxidants in normal physiological functions and human disease," *International Journal of Biochemistry and Cell Biology*, vol. 39, no. 1, pp. 44–84, 2007.

[21] A. Isogawa, M. Yamakado, M. Yano, and T. Shiba, "Serum superoxide dismutase activity correlates with the components of metabolic syndrome or carotid artery intima-media thickness," *Diabetes Research and Clinical Practice*, vol. 86, no. 3, pp. 213–218, 2009.

[22] W. T. Friedewald, R. I. Levy, and D. S. Fredrickson, "Estimation of the concentration of low-density lipoprotein cholesterol in plasma, without use of the preparative ultracentrifuge," *Clinical Chemistry*, vol. 18, no. 6, pp. 499–502, 1972.

[23] N. Prajda and G. Weber, "Malignant transformation linked imbalance: decreased xanthine oxidase activity in hepatomas," *FEBS Letters*, vol. 59, no. 2, pp. 245–249, 1975.

[24] A. Wendel, "Glutathione peroxidase," in *Enzymatic Basis of Detoxification*, W. B. Jakoby, Ed., vol. 1, pp. 333–353, Academic Press, New York, NY, USA, 1980.

[25] J. Buege, "Microsomal lipid peroxidation," in *Methods in Enzymology*, S. Fleischer and L. Packer, Eds., pp. 302–310, Academic Press, New York, NY, USA, 52 edition, 1978.

[26] K. Yagi, "Simple assay for the level of total lipid peroxides in serum or plasma," *Methods in Molecular Biology*, vol. 108, pp. 101–106, 1998.

[27] F. Facchini, Y.-D. I. Chen, C. B. Hollenbeck, and G. M. Reaven, "Relationship between resistance to insulin-mediated glucose uptake, urinary uric acid clearance, and plasma uric acid concentration," *Journal of the American Medical Association*, vol. 266, no. 21, pp. 3008–3011, 1991.

[28] D. Pasalic, N. Marinkovic, and L. Feher-Turkovic, "Uric acid as one of the important factors in multifactorial disorders—facts and controversies," *Biochemia Medica*, vol. 22, no. 1, pp. 63–75, 2012.

[29] Y. Fujii, A. Okada, T. Yasui et al., "Effect of adiponectin on kidney crystal formation in metabolic syndrome model mice via inhibition of inflammation and apoptosis," *PloS ONE*, vol. 8, no. 4, Article ID e61343, 2013.

[30] K. Stanhope, J. Schwarz, and P. Havel, "Adverse metabolic effects of dietary fructose: results from the recent epidemiological, clinical, and mechanistic studies," *Current Opinion in Lipidology*, vol. 24, no. 3, pp. 198–206, 2013.

[31] G. Baskol, M. Baskol, and D. Kocer, "Oxidative stress and antioxidant defenses in serum of patients with non-alcoholic steatohepatitis," *Clinical Biochemistry*, vol. 40, no. 11, pp. 776–780, 2007.

[32] H. L. Kin, L. C. Yu, B. C. Wing, J. C. N. Chan, and C. W. W. Chu, "Mesenteric fat thickness is an independent determinant of metabolic syndrome and identifies subjects with increased carotid intima-media thickness," *Diabetes Care*, vol. 29, no. 2, pp. 379–384, 2006.

[33] B. Gustafson, A. Hammarstedt, C. X. Andersson, and U. Smith, "Inflamed adipose tissue: a culprit underlying the metabolic syndrome and atherosclerosis," *Arteriosclerosis, Thrombosis, and Vascular Biology*, vol. 27, no. 11, pp. 2276–2283, 2007.

[34] B. Gustafson, "Adipose tissue, inflammation and atherosclerosis," *Journal of Atherosclerosis and Thrombosis*, vol. 17, no. 4, pp. 332–341, 2010.

[35] N. Villanova, S. Moscatiello, S. Ramilli et al., "Endothelial dysfunction and cardiovascular risk profile in nonalcoholic fatty liver disease," *Hepatology*, vol. 42, no. 2, pp. 473–480, 2005.

[36] T. Yokota, S. Kinugawa, M. Yamato et al., "Systemic oxidative stress is associated with lower aerobic capacity and impaired skeletal muscle energy metabolism in patients with metabolic syndrome," *Diabetes Care*, vol. 36, no. 5, pp. 1341–1346, 2013.

[37] S. Chen, C. H. Yen, Y. C. Huang, B. J. Lee, S. Hsia, and P. T. Lin, "Relationships between inflammation, adiponectin, and oxidative stress in metabolic syndrome," *PLoS ONE*, vol. 7, no. 9, Article ID e45693, 2012.

[38] P. L. Huang, "eNOS, metabolic syndrome and cardiovascular disease," *Trends in Endocrinology and Metabolism*, vol. 20, no. 6, pp. 295–302, 2009.

[39] D. Jourd'heuil, F. L. Jourd'heuil, P. S. Kutchukian, R. A. Musah, D. A. Wink, and M. B. Grisham, "Reaction of superoxide and nitric oxide with peroxynitrite. Implications for peroxynitrite-mediated oxidation reactions in vivo," *The Journal of Biological Chemistry*, vol. 276, no. 31, pp. 28799–28805, 2001.

[40] S. Martinez-Hervas, J. T. Real, C. Ivorra et al., "Increased plasma xanthine oxidase activity is related to nuclear factor kappa beta activation and inflammatory markers in familial combined hyperlipidemia," *Nutrition, Metabolism and Cardiovascular Diseases*, vol. 20, no. 10, pp. 734–739, 2010.

[41] M. Venojärvi, A. Korkmaz, N. Wasenius et al., "12 Weeks' aerobic and resistance training without dietary intervention did not influence oxidative stress but aerobic training decreased atherogenic index in middle-aged men with impaired glucose regulation," *Food and Chemical Toxicology*, vol. 61, pp. 127–135, 2013.

[42] L. A. Gordon, E. Y. Morrison, D. A. McGrowder et al., "Effect of exercise therapy on lipid profile and oxidative stress indicators in patients with type 2 diabetes," *BMC Complementary and Alternative Medicine*, vol. 8, article 21, pp. 1–10, 2008.

[43] G. Lazarevic, S. Antic, T. Cvetkovic, V. Djordjevic, P. Vlahovic, and V. Stefanovic, "Effects of regular exercise on cardiovascular risk factors profile and oxidative stress in obese type 2 diabetic patients in regard to SCORE risk," *Acta Cardiologica*, vol. 63, no. 4, pp. 485–491, 2008.

[44] G. Pereira, R. A. Tibana, J. Navalta et al., "Acute effects of resistance training on cytokines and osteoprotegerin in women with metabolic syndrome," *Clinical Physiology and Functional Imaging*, vol. 33, no. 2, pp. 122–130, 2012.

[45] N. Greene, S. Martin, and S. Crouse, "Acute exercise and training alter blood lipid and lipoprotein profiles differently in overweight and obese men and women," *Obesity*, vol. 20, no. 8, pp. 1618–1627, 2012.

Hindawi Publishing Corporation
Oxidative Medicine and Cellular Longevity
Volume 2014, Article ID 135650, 10 pages
http://dx.doi.org/10.1155/2014/135650

Research Article

Indices of Paraoxonase and Oxidative Status Do Not Enhance the Prediction of Subclinical Cardiovascular Disease in Mixed-Ancestry South Africans

M. Macharia,[1] A. P. Kengne,[2] D. M. Blackhurst,[3] R. T. Erasmus,[1] M. Hoffmann,[1] and T. E. Matsha[4]

[1] *Division of Chemical Pathology, Faculty of Health Sciences, National Health Laboratory Service (NHLS) and University of Stellenbosch, Cape Town, South Africa*
[2] *NCRP for Cardiovascular and Metabolic Diseases, South African Medical Research Council & and University of Cape Town, Cape Town, South Africa*
[3] *Division of Chemical Pathology, University of Cape Town, Cape Town, South Africa*
[4] *Department of Biomedical Sciences, Faculty of Health and Wellness Science, Cape Peninsula University of Technology, P.O. Box 1906, Bellville, Cape Town 7530, South Africa*

Correspondence should be addressed to T. E. Matsha; matshat@cput.ac.za

Received 30 September 2013; Accepted 2 March 2014; Published 27 March 2014

Academic Editor: Dalton Valentim Vassallo

We evaluated the association of indices of paraoxonase (PON1) and oxidative status with subclinical cardiovascular disease (CVD) in mixed-ancestry South Africans. Participants were 491 adults (126 men) who were stratified by diabetes status and body mass index (BMI). Carotid intima-media thickness (CIMT) was used as a measure of subclinical CVD. Indices of PON1 and oxidative status were determined by measuring levels and activities (paraoxonase and arylesterase) of PON1, antioxidant activity (ferric reducing antioxidant power and trolox equivalent antioxidant capacity), and lipid peroxidation markers (malondialdehyde and oxidized LDL). Diabetic subjects (28.9%) displayed a significant decrease in PON1 status and antioxidant activity as well as increase in oxidized LDL and malondialdehyde. A similar profile was apparent across increasing BMI categories. CIMT was higher in diabetic than nondiabetic subjects ($P < 0.0001$) but showed no variation across BMI categories. Overall, CIMT correlated negatively with indices of antioxidant activity and positively with measures of lipid oxidation. Sex, age, BMI, and diabetes altogether explained 29.2% of CIMT, with no further improvement from adding PON1 and/or antioxidant status indices. Though indices of PON1 and oxidative status correlate with CIMT, their measurements may not be useful for identifying subjects at high CVD risk in this population.

1. Introduction

Early identification of people at high risk of atherosclerotic cardiovascular diseases (CVDs), followed by the implementation of lifestyle and drug interventions with proven beneficial effects, has been largely emphasized in strategies to reduce the mortality and morbidity from cardiovascular disease [1]. This is particularly relevant in some individuals including diabetic or obese people in whom risk factors for CVD tend to cluster and confer a very high risk of CVD [2]. Indeed, compared with their nondiabetic counterparts, people with type 2 diabetes have 2–6-fold higher risk for future CVD which accounts for up to 75% of mortality in this population [3]. The relation between adiposity and cardiovascular health was for a long time thought to be mediated solely by coincident CVD risk factors [4]. Several studies have however shown that obesity not only relates to but also independently predicts CVD [5, 6]. Nonetheless, there is no denying of the correlation between diabetes and obesity. Both conditions are increasingly viewed as proinflammatory states associated with an altered metabolic profile, endothelial dysfunction, and oxidative stress [5, 6]. Oxidative stress has been hypothesized as a mechanism linking the two conditions as well as accounting for their initiation, progression, and possible link with early atherosclerosis [5, 6]. It is plausible therefore that the association between increased

body mass index (BMI) and diabetes and early atherosclerosis is largely due to underlying oxidative stress. The present study was undertaken to evaluate our hypothesis that specific indices of oxidative stress are associated with markers of subclinical CVD and may aid early CVD risk stratification in a population with a high prevalence of diabetes and obesity. For this purpose, indices of PON1 and oxidative status were determined by measuring levels and activities (paraoxonase and arylesterase) of paraoxonase (PON) 1, antioxidant activity (ferric reducing antioxidant power and trolox equivalent antioxidant capacity), and lipid peroxidation markers (malondialdehyde and oxidized LDL). The association of subclinical atherosclerosis with PON1 activity and oxidative stress has been reported in previous studies [7, 8]. Similar to the increasing rates of CVD worldwide, CVD contributes significantly to the public health burden in South Africa where interethnic differences in CHD prevalence and mortality are apparent [9]. The mixed ancestry is a heterogeneous South African ethnic group with a high risk for CVD demonstrated by very high prevalence of obesity, diabetes, and metabolic syndrome [10, 11]. Furthermore, we had also demonstrated high lifetime CVD risk in mixed-ancestry subjects with normoglycemia and those younger than 35 years [11].

2. Materials and Methods

2.1. Study Setting and Population. The study setting has been described in detail elsewhere [10, 11] and is located in a mixed-ancestry township (Bellville South) located within the Northern suburbs of Cape Town, Western Cape, South Africa. The mixed ancestry is a heterogeneous South African population comprising 32–43% Khoisan, 20–36% Bantu-speaking African, 21–28% European, and 9–11% Asian ancestry [12]. This specific study involved participants that took part in the survey during January 2011–November 2011. The study was approved by the research ethics committees of Stellenbosch University (Reference Number: N10/04/118) and the Cape Peninsula University of Technology (CPUT/HW-REC 2010/H017). The study was conducted according to the Code of Ethics of the World Medical Association (Declaration of Helsinki). All participants signed written informed consent after all the procedures were fully explained in the language of their choice.

2.2. Clinical Data. All consenting participants completed a questionnaire designed to obtain information on lifestyle factors such as smoking and alcohol consumption, physical activity, diet, family history of CVD, diabetes mellitus, and demographics. Blood pressure measurements were performed according to the World Health Organization (WHO) guidelines [13] using a semiautomatic digital blood pressure monitor (Rossmax, PA, USA) on the right arm in a sitting position. Other clinical measurements included the body weight, height, waist, and hip circumferences. Weight (to the nearest 0.1 kg) was determined in a subject wearing light clothing and without shoes and socks, using a Sunbeam EB710 digital bathroom scale, which was calibrated using a standard object of known mass. Waist circumference was measured using a nonelastic tape at the level of the narrowest part of the torso, as seen from the anterior view. The hip circumference was also measured using a nonelastic tape around the widest portion of the buttocks. All anthropometric measurements were performed three times and their average was used for analysis. Diabetes status was based on a history of doctor diagnosis, a fasting plasma glucose ≥7.0 mmol/L, and/or a 2-hour postoral glucose tolerance test (OGTT) plasma glucose >11.1 mmol/L as recommended by the WHO [14]. Adiposity was described according to body mass index (BMI in kg/m^2) as normal weight (<25), overweight (25–30), and obese (>30).

2.3. Measurement of Carotid Intima-Media Thickness (CIMT). Two qualified sonographers measured CIMT in longitudinal section at the far wall of the distal common carotid arteries, 2 cm from the bifurcation, at 3 consecutive end-points, 5–10 mm apart. The mean of six readings (3 from each side) was calculated for each participant using a portable B-mode and spectral Doppler ultrasound scanner equipped with cardiovascular imaging software. The GE LOGIQ e (General Electric Healthcare, Germany) high performance multipurpose colour compact ultrasound system included new imaging CrossXBeam technologies with multifrequency virtual apex on phased array cardiac transducer (3S-RS wide band phased probe 1.7–4.0 MHz) for echocardiography and a linear wideband vascular transducer (8L-RS 4.0–12 MHz linear probe) used for improved diagnostic confidence and imaging clarity for the carotids.

2.4. Laboratory Measurements. Blood samples were collected after an overnight fast and processed for further biochemical analyses. The Cobas 6000 immunometric analyzer (Roche Diagnostics) was used to measure levels of fasting plasma glucose (FBG), glycated haemoglobin (HbA1c), total cholesterol, high density lipoprotein cholesterol (HDL-c), triglycerides (TG) and γ-glutamyltransferase (GGT), and high sensitive C-reactive protein (hsCRP). Low density lipoprotein cholesterol (LDL-c) was calculated using Friedewald's formula [15]. An enzyme linked immunosorbent assay (ELISA) kit was used to measure plasma levels of paraoxonase 1 (PON1) following the manufacturer's instructions (Aviscera biosciences, Santa Clara, California). This assay employs a quantitative sandwich enzyme immunoassay technique.

2.5. Total Antioxidant Capacity. The total antioxidant capacity in plasma samples was assessed using the ferric reducing antioxidant power (FRAP) and trolox equivalent antioxidant capacity (TEAC) assays. FRAP was done according to the method of Benzie and Strain [16]. Briefly, plasma samples were mixed with FRAP reagent, incubated for 30 min at 37°C, and the absorbance at 593 nm was recorded using a spectrophotometer (Spectramax plus384 Molecular devices, USA). The TEAC assay was according to Re et al. [17] and is based on monitoring (at 734 nm) the oxidation of 2, 2′-azinobis-(3-ethylbenzothiazoline-6-sulfonic acid) radical (ABTS) cation formed by reacting ABTS, and potassium persulfate. Distilled water was used instead of PBS to dilute the ABTS$^+$ radical solution.

2.6. Paraoxonase Activity. Paraoxonase (PONase) and arylesterase (AREase) activities were measured using paraoxon and phenylacetate (Sigma Aldrich, SA) as substrates, respectively. PONase activity was measured using Richter and Furlong's method [18] from the initial velocity of p-nitrophenol production at 37°C and the increased absorbance at 405 nm was monitored on a spectrophotometer (Spectramax plus384, Molecular devices, USA). Each serum sample was incubated with 5-mmol/L eserine (Sigma Aldrich, SA) for 15 minutes at room temperature to inhibit serum cholinesterase activity which is usually elevated in diabetes and would otherwise interfere with the determination of paraoxonase activity in serum from diabetic individuals. PON-1 activity of 1 U/L was defined as 1 μmol of p-nitrophenol hydrolyzed per minute. A slightly modified method of Browne et al. [19] was used to measure AREase activity. The working reagent consisted of 20 mmol/L Tris-HCl, 4 mmol/L phenyl acetate, pH 8.0, with 1.0 mmol/L $CaCl_2$ (Sigma Aldrich, SA). The reaction was initiated by adding 5 μL of 40-fold tris-diluted samples to 345 μL of the working reagent at 25°C. The change in absorbance at 270 nm was recorded for 60 minutes after a 20-second lag time on a Spectramax plus384 spectrophotometer. The activity, expressed as kU/L, was based on the molar absorptivity (1310) of phenol at 270 nm. In both assays, the rates used to generate the data points were derived from the linear portions of the rate versus time plots.

2.7. Lipid Peroxidation. Plasma MDA and ox-LDL were used as markers of lipid peroxidation (LPO). The method of Jentzsch et al. [20] was used to estimate the thiobarbituric acid reactive substances (TBARS) which reflect the production of MDA. Plasma ox-LDLs were measured using a quantitative sandwich ELISA kit (Cellbiolabs, San Diego, California).

2.8. Statistical Analyses. Data are presented as mean standard deviation, SD, or median of 25th–75th percentiles for continuous variables and as count and percentage for categorical variables. For group (sex, diabetes status, and BMI, quarters of CIMT) comparisons, chi square test, student's t-test, and analysis of the variance (ANOVA) and nonparametric equivalents were used. Continuous associations between CIMT and the indices were assessed graphically with the use of correlation matrix, before and after applying the Box-Cox [21] power transformations to improve the shape of the associations; then the "Covariance Estimation for Multivariate t Distribution" [22] method was used to derive the correlation coefficients, while minimizing the potential effects of outliers. The Steiger t-test was used to compare correlation coefficients among indices. Regression coefficients to indicate the size of the association of each of the indices with CIMT were derived from robust multiple linear regression models that included each of the 4 variables of interest, age, sex, body mass index, and diabetes status. Analyses were carried out using R statistical software version 3.0.0 [03-04-2013], (The R Foundation for Statistical Computing, Vienna, Austria). The significance level was set at 0.05.

3. Results

3.1. Participants' Basic Profile. Of the 651 participants (men 170, 26%) who took part in the study, 160 (25%) were excluded from this analysis as they had missing values for CIMT and/or other relevant variables. Baseline characteristics of participants included and excluded from analyses were very similar. The final analytic sample comprised 491 participants (men 126, 25.7%) with a mean age of 54.6 (13.2) years. Among them, 142 (29%) had diabetes, 137 (28%) were overweight, and 261 (53%) were obese. The average BMI was 31.4 (8.1) kg/m^2 (Table 1). There were no age differences between men and women and across the BMI profiles but diabetic subjects were significantly older than nondiabetic ones (59.6 versus 52.5 years, $P < 0.0001$) and had higher BMI (33.4 versus 30.6 kg/m^2, $P = 0.002$). Women had significantly higher levels of HbA1c, BMI, and waist circumference. In general, there were no differences between the genders with regard to the lipid profile. Triglyceride levels increased while HDL-cholesterol decreased across BMI categories (both $P < 0.0001$, ANOVA).

3.2. Paraoxonase and Oxidative Status Profile. Men had significantly higher FRAP (732 versus 655 μM, $P = 0.006$) and ox-LDL (5141 versus 4110 ng/mL, $P < 0.0001$) and lower AREase activity and PON 1 levels (91 versus 117 kU/L; 88 versus 98 μg/mL, $P < 0.0001$) respectively, compared to women. In diabetic subjects, a less favorable profile was observed for PON1 (mass and activity) and oxidative status (decreased FRAP and TEAC; elevated Ox-LDL and TBARS). A similar less favorable profile was also apparent across increasing BMI categories (Table 1).

3.3. CIMT Profile and Associations with PON1 and Oxidative Profiles. The median CIMT was 0.82 mm. It was higher in men than in women (0.95 versus 0.80 mm, $P < 0.0001$) and in diabetic than in nondiabetic subjects (0.98 versus 0.77 mm, $P < 0.0001$). However, there was neither a significant difference ($P > 0.227$) nor a linear trend in the distribution of CIMT levels across BMI categories (Table 1). Overall, CIMT correlated negatively with all indices of antioxidant activity and positively with the measures of lipid oxidation (Table 2, Figure 1). Correlation coefficients however were very weak, with borderline significant differences by diabetes status for the correlations of CIMT with TEAC ($P = 0.04$), Ox-LDL ($P = 0.02$), and TBARS ($P = 0.04$). In stratified analyses, the correlation coefficients for each of these three indices always appeared to be significant and stronger in nondiabetics and weak and nonsignificant in diabetics (Table 2, Figure 1). The distribution of participants' characteristics across quarters of CIMT is shown in Table 3 showing increasing age, systolic blood pressure, waist/hip ratio, fasting glucose, total cholesterol, and decreasing proportion of women across increasing quarters of CIMT.

3.4. Multivariable Analysis. In a model comprising sex, age, and BMI, each of the three variables was significantly associated with CIMT. This basic model explained 26.4% of the variation in CIMT levels. When this model was expanded

Table 1: General characteristics of the participants.

Variables	Overall	Sex			Diabetes			BMI			
		Men	Women	*P*	No	Yes	*P*	Normal	Overweight	Obese	*P*
N	491	126	365		349	142		93	137	261	
Female, *n* (%)	365 (74.3)	0	365 (100)		257 (73.6)	108 (76.1)	0.578	47 (50.5)	93 (67.9)	235 (90.0)	<0.0001
Age (years)	54.6 (13.2)	55.4 (13.3)	54.3 (13.2)	0.401	52.5 (13.4)	59.6 (11.5)	<0.0001	55.3 (15.2)	53.6 (13.3)	54.8 (12.6)	0.568
BMI (kg/m^2)	31.4 (8.1)	27.5 (7.0)	32.8 (8.0)	<0.0001	30.6 (7.3)	33.4 (9.5)	0.002	21.5 (3.1)	27.6 (1.4)	37.0 (6.7)	<0.0001
Waist circumference (cm)	96.4 (15.4)	94.9 (14.5)	96.9 (15.7)	0.208	94.6 (16.1)	100.8 (12.9)	<0.0001	80.5 (17.1)	90.7 (8.4)	105.1 (11.2)	<0.0001
Waist/hip ratio	0.89 (0.12)	0.93 (0.12)	0.87 (0.12)	<0.0001	0.88 (0.12)	0.92 (0.12)	0.001	0.85 (0.19)	0.89 (0.09)	0.90 (0.10)	0.010
Systolic BP (mmHg)	136 (26)	138 (24)	136 (27)	0.309	133 (23)	144 (31)	0.0001	133 (31)	135 (25)	136 (25)	0.138
Diastolic BP (mmHg)	82 (14)	84 (15)	81 (13)	0.030	81 (14)	84 (14)	0.055	78 (12)	81 (12)	83 (15)	0.002
FPG (mmol/L)	6.4 (2.9)	6.2 (2.5)	6.5 (3.1)	0.292	5.1 (0.7)	9.5 (3.9)	<0.0001	5.3 (1.5)	6.6 (3.4)	6.7 (3.0)	0.0003
HbA1c (%)	6.6 (1.6)	6.3 (1.4)	6.7 (1.7)	0.025	5.9 (0.4)	8.3 (2.2)	<0.0001	5.9 (1.0)	6.8 (2.0)	6.7 (1.6)	<0.0001
Creatinine (μM)	74.8 (25.5)	89.5 (35.5)	69.6 (18.5)	<0.0001	75.3 (20.0)	81.1 (42.8)	0.21	79.4 (19.1)	75.0 (19.3)	73.7 (30.0)	0.480
C-reactive protein (mg/L)	5.1 [2.0–8.9]	3.7 [1.5–7.6]	5.6 [2.2–9.2]	0.025	5.0 [1.9–8.4]	5.5 [2.5–10.2]	0.126	3.0 [1.0–5.6]	2.9 [1.4–6.6]	6.8 [3.5–11.1]	0.375
GGT (IU/L)	27 [19–43]	31 [24–46]	25 [17–41]	<0.0001	25 [18–41]	29 [23–50]	0.003	26 [18–42]	25 [18–43]	28 [20–43]	0.451
Total cholesterol (mmol/L)	5.5 (1.1)	5.4 (1.0)	5.5 (1.1)	0.494	5.5 (1.1)	5.5 (1.2)	0.360	5.4 (1.1)	5.7 (1.1)	5.4 (1.0)	0.072
HDL cholesterol (mmol/L)	1.4 (0.4)	1.3 (0.5)	1.4 (0.4)	0.058	1.4 (0.4)	1.3 (0.4)	0.009	1.6 (0.5)	1.3 (0.4)	1.3 (0.3)	<0.0001
LDL cholesterol (mmol/L)	3.4 (1.0)	3.4 (0.9)	3.4 (1.0)	0.525	3.4 (0.9)	3.4 (1.0)	0.990	3.3 (1.1)	3.6 (1.0)	3.4 0.9)	0.026
Triglycerides (mmol/L)	1.5 (0.9)	1.7 (1.1)	1.5 (0.8)	0.047	1.4 (0.8)	1.8 (1.0)	<0.0001	1.2 (0.8)	1.6 (0.9)	1.6 (0.9)	0.0001
CIMT (mm)	0.82 [0.67–1.02]	0.95 [0.72–1.22]	0.80 [0.65–0.95]	<0.0001	0.77 [0.65–0.93]	0.98 [0.77–1.15]	<0.0001	0.85 [0.65–1.08]	0.80 [0.70–0.92]	0.82 [0.68–1.00]	0.227
PON1 (μg/mL)	96 [74–111]	88 [69–105]	98 [78–112]	0.002	99 [77–112]	91 [66–107]	0.0005	107 [92–115]	99 [77–111]	91 [71–108]	0.0006
PONase (U/L)	184 [131–220]	194 [158–218]	183 [124–221]	0.091	204 [167–225]	156 [96–182]	<0.0001	221 [186–244]	198 [156–226]	172 [102–206]	<0.0001
AREase (kU/L)	107 [82–132]	91 [65–104]	117 [90–137]	<0.0001	113 [91–137]	90 [63–115]	<0.0001	118 [96–147]	107 [80–132]	98 [77–123]	<0.0001
FRAP (μM)	677 [545–827]	732 [592–861]	655 [537–811]	0.006	722 [588–852]	614 [471–732]	<0.0001	754 [642–911]	725 [583–852]	638 [523–749]	<0.0001
TEAC (nM)	1279 [944–1654]	1366 [1018–1742]	1271 [936–1631]	0.086	1423 [1077–1746]	1051 [681–1320]	<0.0001	1570 [1238–1882]	1366 [1153–1846]	1206 [879–1505]	<0.0001
Ox-LDL (ng/mL)	4408 [3143–5911]	5141 [3979–6333]	4110 [2834–5484]	<0.0001	3916 [2755–5138]	5885 [4602–6944]	<0.0001	3535 [2511–4747]	4337 [2859–5736]	4780 [3683–6216]	<0.0001
TBARS (nM)	2277 [1559–3132]	2042 [1527–2772]	2304 [1625–3214]	0.203	1982 [1406–2672]	3152 [2380–3655]	<0.0001	1546 [1046–2369]	2238 [1546–3115]	2533 [1924–3281]	<0.0001

FPG: fasting plasma glucose; BMI: body mass index; BP blood pressure; GGT: gamma glutamyl transferase; HDL: high density lipoprotein; LDL: low density lipoprotein; CIMT: carotid intima-media thickness; PON1: paraoxonase 1; PONase: paraoxonase; AREase: arylesterase; FRAP: ferric reducing ability of plasma; TEAC: trolox equivalent antioxidant capacity; Ox-LDL: oxidized LDL; TBARS: thiobarbituric acid reactive substances.

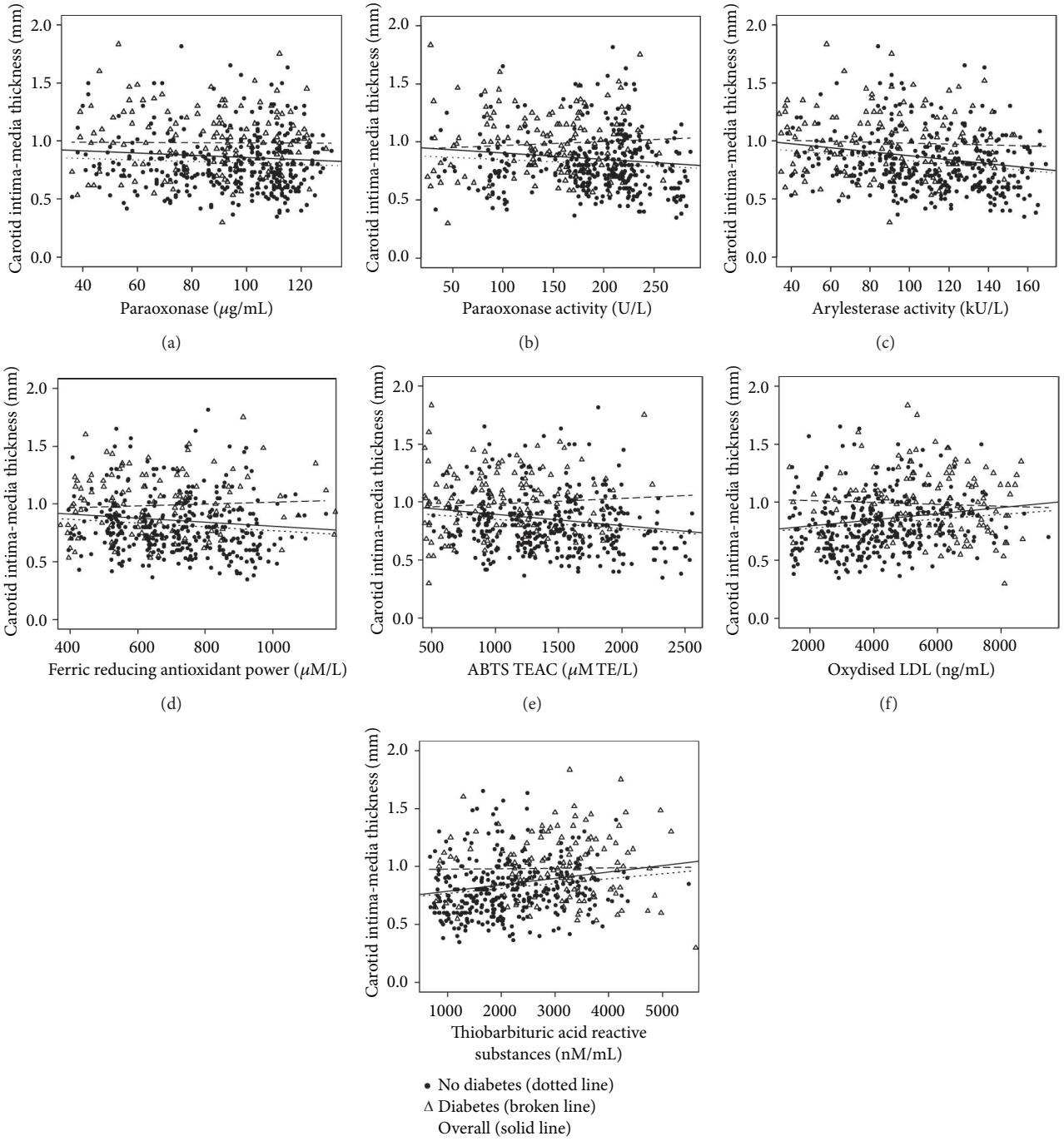

Figure 1: Correlations of paraoxonase, paraoxonase activity, arylesterase ferric reducing antioxidant power, TEAC, oxidized LDL, and thiobarbituric acid reactive substances activity with carotid intima-media thickness. Participants are grouped by diabetes status with the triangles representing those with diabetes and the solid circles representing those without diabetes. The superimposed regression lines are for the overall sample (solid line), and participants with (broken line) and without diabetes (dotted lines). Accompanying correlations coefficients are shown in Table 2.

with the inclusion of diabetes status, all variables in the model remained significantly associated with CIMT and further explained 29.2% of the variation. However, as shown in Table 4, none of the indices of PON1 and antioxidant status significantly associated with CIMT in the presence of the four basic variables and furthermore did not improve the fit of models in predicting the variability of CIMT. In the presence of variables in the basic model, SBP ($\beta = 0.002$, $P < 0.0001$), but not DBP ($\beta = 0.001$, $P = 0.066$), was significantly associated with CIMT. In the same basic model, neither waist

Table 2: Robust correlation of CIMT with PON and antioxidant status.

Correlates	Overall	No diabetes	Diabetes	*P* value
PON1	−0.09 (−0.17 to 0.00)	−0.04 (−0.14 to 0.07)	−0.01 (−0.17 to 0.16)	0.74
PONase	−0.17 (−0.25 to −0.08)	−0.11 (−0.21 to 0)	0.04 (−0.13 to 0.20)	0.15
AREase	−0.24 (−0.32 to −0.15)	−0.20 (−0.30 to −0.09)	−0.05 (−0.21 to 0.12)	0.13
FRAP	−0.17 (−0.26 to −0.09)	−0.12 (−0.22 to −0.02)	0.03 (−0.13 to 0.20)	0.12
TEAC	−0.22 (−0.30 to −0.13)	−0.16 (−0.26 to −0.06)	0.04 (−0.12 to 0.21)	0.04
Ox-LDL	0.25 (0.17 to 0.34)	0.21 (0.10 to 0.30)	−0.03 (−0.20 to 0.13)	0.02
TBARS	0.26 (0.17 to 0.34)	0.19 (0.09 to 0.29)	−0.01 (−0.17 to 0.16)	0.04

Paraoxonase 1; PONase: paraoxonase; AREase: arylesterase; FRAP: ferric reducing ability of plasma; TEAC: trolox equivalent antioxidant capacity; Ox-LDL: oxidized LDL; TBARS: thiobarbituric acid reactive substances.

Table 3: Characteristics of the participants by quarters of CIMT.

Variables	Quartiles of CIMT				*P* value
	Q1	Q2	Q3	Q4	
N	123	131	118	119	NA
CIMT [min–max]	0.30–0.67	0.68–0.82	0.83–1.02	1.03–2.18	NA
Female, *n* (%)	101 (82.1)	104 (79.4)	97 (82.2)	63 (52.9)	<0.0001
Age (years)	44.9 (12.9)	53.3 (11.8)	57.6 (11.3)	63.0 (9.8)	<0.0001
BMI (kg/m^2)	30.5 (6.7)	31.5 (8.0)	32.3 (8.0)	31.5 (9.5)	0.234
Waist circumference (cm)	94.0 (18.7)	97.1 (13.5)	96.3 (14.0)	98.2 (14.9)	0.060
Waist/hip ratio	0.86 (0.15)	0.87 (0.12)	0.89 (0.10)	0.93 (0.10)	<0.0001
Systolic BP (mmHg)	125 (19)	135 (26)	138 (21)	149 (31)	<0.0001
Diastolic BP (mmHg)	78 (12)	83 (16)	82 (11)	84 (15)	0.007
FPG (mmol/L)	5.7 (2.2)	6.0 (2.3)	6.4 (2.8)	7.6 (3.9)	<0.0001
HbA1c (%)	6.2 (1.1)	6.2 (1.0)	6.7 (1.6)	7.4 (2.3)	<0.0001
Creatinine (μM)	68.8 (14.3)	72.8 (19.0)	72.2 (18.6)	85.8 (39.8)	<0.0001
C-reactive protein (mg/L)	4.4 [1.4–7.6]	5.1 [2.2–8.7]	5.4 [2.5–9.2]	5.3 [2.0–9.2]	0.222
GGT (IU/L)	24 [17–38]	29 [19–49]	28 [19–41]	29 [21–43]	0.145
Total cholesterol (mmol/L)	5.2 (0.9)	5.4 (1.1)	5.7 (1.2)	5.7 (1.1)	<0.0001
HDL cholesterol (mmol/L)	1.4 (0.4)	1.3 (0.4)	1.4 (0.4)	1.4 (0.4)	0.708
LDL cholesterol (mmol/L)	3.2 (0.8)	3.4 (1.0)	3.6 (1.0)	3.6 (1.0)	0.003
Triglycerides (mmol/L)	1.3 (0.7)	1.5 (0.9)	1.7 (1.0)	1.6 (0.9)	0.0008
PON1 (μg/mL)	102 [78–112]	94 [77–110]	98 [77–112]	94 [70–110]	0.290
PONase (U/L)	204 [170–233]	184 [130–215]	182 [136–218]	177 [119–217]	0.005
AREase (kU/L)	118 [97–141]	103 [84–126]	94 [75–132]	95 [76–120]	<0.0001
FRAP (μM)	734 [602–887]	672 [573–809]	636 [533–795]	667 [534–785]	0.014
TEAC (nM)	1484 [1068–1858]	1316 [947–1628]	1206 [929–1595]	1235 [904–1568]	0.001
Ox-LDL (ng/mL)	3618 [2641–5102]	4576 [3230–5844]	4747 [3638–6176]	4975 [3545–6333]	<0.0001
TBARS (nM)	1857 [1251–2504]	2280 [1544–3042]	2447 [1919–3256]	2571 [1905–3666]	<0.0001

FPG: fasting plasma glucose; BMI: body mass index; BP blood pressure; GGT: gamma glutamyl transferase; HDL: high density lipoprotein; LDL: low density lipoprotein; CIMT: carotid intima-media thickness; PON1: paraoxonase 1; PONase: paraoxonase; AREase: arylesterase; FRAP: ferric reducing ability of plasma; TEAC: trolox equivalent antioxidant capacity; Ox-LDL: oxidized LDL; TBARS: thiobarbituric acid reactive substances.

circumference ($\beta = -0.0007$, $P = 0.434$) nor waist/hip ratio ($\beta = 0.031$, $P = 0.724$) was associated with CIMT, even when they were allowed to replace BMI in the model (both $P >= 0.364$).

4. Discussion

The prominent role of oxidative stress in the occurrence of atherosclerosis and related complications is well recognized, with suggestions that measurement of oxidative stress may aid risk stratification and effective prevention of atherothrombotic diseases. In this study, we evaluated the profile of several indices of PON1 and oxidative status and their relationship with CIMT, which is a marker of subclinical cardiovascular disease. Our findings demonstrate that measures of oxidative stress together with PON1 are only superficially associated with CIMT. Instead, conventional risk factors such as age, gender, adiposity, and chronic hyperglycemia and not measures of oxidative stress may be more important in estimating CVD risk in our population.

Table 4: Regression coefficients from multiple robust linear models for the prediction of CIMT by indices of PON1 and antioxidant status accounting for the potential effect of sex, age, diabetes, and adiposity.

	Age—sex—BMI		Diabetes		PON1		PONase		AREase		FRAP		TEAC		Ox-LDL		TBARS	
	β	P	β	P	β	P	β	P	β	P	β	P	β	P	β	P	β	P
Index	—	—	—	—	−0.0002	0.723	−0.00006	0.730	−0.0003	0.390	−0.00002	0.743	−0.00002	0.571	0.000004	0.539	0.00001	0.255
Age	0.009	<0.0001	0.008	<0.0001	0.008	<0.0001	0.008	<0.0001	0.008	<0. 0001	0.008	<0.0001	0.008	<0.0001	0.008	<0.0001	0.008	<0.0001
Sex (men)	0.151	<0.0001	0.150	<0.0001	0.149	<0.0001	0.150	<0.0001	0.141	<0.0001	0.151	<0.0001	0.150	<0.0001	0.145	<0.0001	0.145	<0.0001
BMI	0.004	0.002	0.003	0.017	0.003	0.029	0.003	0.030	0.003	0.041	0.003	0.030	0.003	0.035	0.003	0.027	0.003	0.043
Diabetes	—	—	0.124	<0.0001	0.122	<0.0001	0.121	<0.001	0.118	<0.0001	0.121	<0.0001	0.120	<0.0001	0.119	<0.0001	0.114	<0.0001
R^2	0.264		0.292		0.292		0.293		0.291		0.295		0.293		0.292		0.294	

BMI: body mass index; paraoxonase 1; PONase: paraoxonase; AREase: arylesterase; FRAP: ferric reducing ability of plasma; TEAC: trolox equivalent antioxidant capacity; Ox-LDL: oxidized LDL; TBARS: thiobarbituric acid reactive substances.

The physiological role of PON1 in reducing atherosclerosis stems from its ability to inhibit the oxidation of low density lipoprotein (LDL) [23] and its ability to stimulate cholesterol efflux from macrophages [24]. In this regard, decreased activities of PON1 and/or other antioxidant species have been demonstrated in obesity, diabetes, and other oxidative stress-related conditions [25–27]. In our study, we found PON1 activities to be significantly reduced in obese and diabetic subjects. It has previously been suggested that decreased PON1 activity in diabetes may be due to glycation-induced changes to HDL and/or PON1, thereby affecting its association with HDL that has been related to its antiatherogenic properties [28]. Similar to diabetes, obesity is strongly associated with oxidative stress and proinflammatory state which in this study is corroborated by significantly raised oxidative stress markers (ox-LDL and TBARS) in obese subjects.

Proinflammatory markers and oxidative stress have been shown to modulate and inactivate PON1 activity [29–32]. Adipose tissue expresses inflammatory cytokines, interleukin-6 (IL-6), and tumor necrosis factor-α (TNF-α) which are associated with oxidative stress [33]. In a study which introduced a mixture of IL-6, IL-1, and TNF-α in murine hepatoma cell line Hepa 1–6, a reduction in PON1 mRNA was observed [29]. In addition, obesity alters the composition of HDL in a manner that may impair binding of PON1 to HDL surface such as lowering both HDL's largest subfraction (HDL2) and its major binding protein (apo A1) [34]. Since PON1 is a lipid-dependent enzyme whose activity hinges on its conformation within HDL, the impaired binding in results decreased enzyme activity.

Measurements of oxidative stress have previously been proposed as a predictor of atherosclerosis in end stage renal disease patients [7]. In their study, Dursan et al. [7] demonstrated significant positive correlation between CIMT and serum TBARS and nitrite/nitrate levels and a significant negative correlation between CIMT and antioxidant markers superoxide dismutase (SOD), catalase (CAT), and plasma sulfhydryl (P-SH) levels in patients on chronic haemodialysis. We found total antioxidants (FRAP, AREase) to be negatively correlated with CIMT, whilst markers of oxidative stress (ox-LDL and TBARS) showed a positive correlation, but the association was not retained in further adjusted regression analyses and there were suggestions that diabetes affects these associations since they were generally stronger and significant in nondiabetics compared to diabetics. Instead, traditional CVD risk factors, age, gender, obesity, and diabetes, were significant determinants of subclinical atherosclerosis, accounting for 29.2% of CIMT variability. Previous studies have demonstrated that only a fraction of CVD risk is explained by traditional risk factors [35, 36] prompting a search for alternate and additional predictors. Emerging data from around the world support the pivotal role of chronic inflammation in the occurrence of CVD complications. Although influences of PON1 and oxidative stress have been demonstrated to be on the early steps of atherosclerosis [37], our results exclude measurements of PON1 activity and indices of antioxidant status in prediction of atherosclerotic risk.

Some limitations should be accounted for when interpreting our findings. First, the cross-sectional design of our study precludes drawing inferences on the direction of the associations. Second, we did not establish the intraobserver variability between the sonographers who performed CIMT measurements; however we used multiple measurements at different points. Third, because our study population was ethnically exclusive, our results can only be generalized to mixed-ancestry South African subjects. Fourth, we used BMI as the marker of obesity although it cannot distinguish between visceral and subcutaneous fat. Visceral fat is particularly strongly associated with atherosclerotic CVD risk [38]. Fifth, we did not evaluate other residual confounders that may affect oxidative stress markers such as dietary factors. Lastly, the number of males versus that of females is skewed, with this being a common trend in South African population studies. Nonetheless, we used two methods for each of the three measures of oxidative status. Besides allowing us to demonstrate the consistency of our findings, this approach reinforces the accuracy of antioxidant status results since the measured total antioxidant status of biological samples is known to be method specific [39]. Furthermore, the nonspecific nature of the MDA-TBARS method requires corroboration. Since PON1 is purported to function as an antioxidant, another key strength distinguishing this study from several others is the evaluation of its activity in the context of antioxidant status.

In conclusion, although atherosclerosis is considered an inflammatory/oxidative condition, our results argue against a major role of PON1 and oxidative status in prediction of atherosclerotic risk as none of these indices impacted on the model's value in explaining the variability of CIMT. Rather, the findings reaffirm the importance of conventional risk factors such as age, gender, adiposity, and chronic hyperglycemia in estimating CVD risk in this mixed-ancestry population.

Conflict of Interests

The authors declare that there is no conflict of interests regarding the publication of this paper.

Acknowledgments

The authors would like to thank the Bellville South Community of Cape Town, South Africa. This study was funded by the University Research Fund of the Cape Peninsula University of Technology, South Africa, South African Medical Research Council, Harry Crossley Foundation, and University of Stellenbosch.

References

[1] World Health Organization, *Prevention of Cardiovascular Disease: Guidelines for Assessment and Management of Total Cardiovascular Risk*, World Health Organization, Geneva, Switzerland, 2007.

[2] S. A. Matheus, L. R. M. Tannus, R. A. Cobas, C. C. S. Palma, C. A. Negrato, and M. B. Gomes, "Impact of diabetes on cardiovas-

cular disease: an update," *International Journal of Hypertension*, vol. 2013, Article ID 653789, 15 pages, 2013.

[3] M. K. Ali, K. M. V. Narayan, and N. Tandon, "Diabetes & coronary heart disease: current perspectives," *Indian Journal of Medical Research*, vol. 132, no. 11, pp. 584–597, 2010.

[4] P. Poirier, T. D. Giles, G. A. Bray et al., "Obesity and cardiovascular disease: pathophysiology, evaluation, and effect of weight loss: an update of the 1997 American Heart Association Scientific Statement on obesity and heart disease from the Obesity Committee of the Council on Nutrition, Physical Activity, and Metabolism," *Circulation*, vol. 113, no. 6, pp. 898–918, 2006.

[5] I. Bondia-Pons, L. Ryan, and J. A. Martinez, "Oxidative stress and inflammation interactions in human obesity," *Journal of Physiology and Biochemistry*, vol. 68, pp. 701–711, 2012.

[6] J. Logue, H. M. Murray, P. Welsh et al., "Obesity is associated with fatal coronary heart disease independently of traditional risk factors and deprivation," *Heart*, vol. 97, no. 7, pp. 564–568, 2011.

[7] B. Dursun, E. Dursun, G. Suleymanlar et al., "Carotid artery intima-media thickness correlates with oxidative stress in chronic haemodialysis patients with accelerated atherosclerosis," *Nephrology Dialysis Transplantation*, vol. 23, no. 5, pp. 1697–1703, 2008.

[8] H. A. Labib, R. L. Etewa, O. A. Gaber, M. Atfy, T. M. Mostafa, and I. Barsoum, "Paraoxonase-1 and oxidative status in common Mediterranean β-thalassaemia mutations trait, and their relations to atherosclerosis," *Journal of Clinical Pathology*, vol. 64, no. 5, pp. 437–442, 2011.

[9] R. Norman, D. Bradshaw, M. Schneider, D. Pieterse, and P. Groenwald, *Revised Burden of Disease Estimates for fhe Comparative Risk Factor Assessment, South Africa 2000*, Medical Research Council, Cape Town, South Africa, 2006.

[10] R. T. Erasmus, D. J. Soita, M. S. Hassan et al., "High prevalence of diabetes mellitus and metabolic syndrome in a South African coloured population: baseline data of a study in Bellville, Cape Town," *South African Medical Journal*, vol. 102, no. 11, part 1, pp. 841–844, 2012.

[11] T. E. Matsha, M. S. Hassan, M. Kidd, and R. T. Erasmus, "The 30-year cardiovascular risk profile of South Africans with diagnosed diabetes, undiagnosed diabetes, pre-diabetes or normoglycaemia: the Bellville, South Africa pilot study," *Cardiovascular Journal of Africa*, vol. 23, no. 1, pp. 5–11, 2012.

[12] E. de Wit, W. Delport, C. E. Rugamika et al., "Genome-wide analysis of the structure of the South African Coloured Population in the Western Cape," *Human Genetics*, vol. 128, no. 2, pp. 145–153, 2010.

[13] J. Chalmers, S. MacMahon, G. Mancia et al., "1999 World Health Organization-International Society of Hypertension Guidelines for the management of hypertension. Guidelines subcommittee of the World Health Organization," vol. 21, no. 5-6, pp. 1009–1060, 1999.

[14] K. G. Alberti and P. Z. Zimmet, "Definition, diagnosis and classification of diabetes mellitus and its complications. Part 1: diagnosis and classification of diabetes mellitus provisional report of a WHO consultation," *Diabetic Medicine*, vol. 15, no. 7, pp. 539–553, 1998.

[15] W. T. Friedewald, R. I. Levy, and D. S. Fredrickson, "Estimation of the concentration of low-density lipoprotein cholesterol in plasma, without use of the preparative ultracentrifuge," *Clinical Chemistry*, vol. 18, no. 6, pp. 499–502, 1972.

[16] I. F. F. Benzie and J. J. Strain, "The ferric reducing ability of plasma (FRAP) as a measure of 'antioxidant power': the FRAP assay," *Analytical Biochemistry*, vol. 239, no. 1, pp. 70–76, 1996.

[17] R. Re, N. Pellegrini, A. Proteggente, A. Pannala, M. Yang, and C. Rice-Evans, "Antioxidant activity applying an improved ABTS radical cation decolorization assay," *Free Radical Biology and Medicine*, vol. 26, no. 9-10, pp. 1231–1237, 1999.

[18] R. J. Richter and C. E. Furlong, "Determination of paraoxonase (PON1) status requires more than genotyping," *Pharmacogenetics*, vol. 9, no. 6, pp. 745–753, 1999.

[19] R. W. Browne, S. T. Koury, S. Marion, G. Wilding, P. Muti, and M. Trevisan, "Accuracy and biological variation of human serum paraoxonase 1 activity and polymorphism (Q192R) by kinetic enzyme assay," *Clinical Chemistry*, vol. 53, no. 2, pp. 310–317, 2007.

[20] A. M. Jentzsch, H. Bachmann, P. Fürst, and H. K. Biesalski, "Improved analysis of malondialdehyde in human body fluids," *Free Radical Biology and Medicine*, vol. 20, no. 2, pp. 251–256, 1996.

[21] G. E. P. Box and D. R. Cox, "An analysis of transformations," *Jou rnal of the Royal Statistical Society B: Statistical Methodology*, vol. 26, no. 2, pp. 211–252, 1964.

[22] J. T. Kent, D. E. Tyler, and Y. A. Vardi, "Curious likelihood identity for the multivariate t-distribution," *Communications in Statistics-Simulation and Computation*, vol. 23, no. 2, pp. 441–453, 1994.

[23] M. I. Mackness, S. Arrol, and P. N. Durrington, "Paraoxonase prevents accumulation of lipoperoxides in low-density lipoprotein," *FEBS Letters*, vol. 286, no. 1-2, pp. 152–154, 1991.

[24] M. Rosenblat, L. Gaidukov, O. Khersonsky et al., "The catalytic histidine dyad of high density lipoprotein-associated serum paraoxonase-1 (PON1) is essential for PON1-mediated inhibition of low density lipoprotein oxidation and stimulation of macrophage cholesterol efflux," *Journal of Biological Chemistry*, vol. 281, no. 11, pp. 7657–7665, 2006.

[25] B. Mackness, P. Durrington, P. McElduff et al., "Low paraoxonase activity predicts coronary events in the Caerphilly Prospective Study," *Circulation*, vol. 107, no. 22, pp. 2775–2779, 2003.

[26] C. A. Abbott, M. I. Mackness, S. Kumar, A. J. Boulton, and P. N. Durrington, "Serum paraoxonase activity, concentration, and phenotype distribution in diabetes mellitus and its relationship to serum lipids and lipoproteins," *Arteriosclerosis, Thrombosis, and Vascular Biology*, vol. 15, no. 11, pp. 1812–1818, 1995.

[27] L. Bajnok, I. Seres, Z. Varga et al., "Relationship of serum resistin level to traits of metabolic syndrome and serum paraoxonase 1 activity in a population with a broad range of body mass index," *Experimental and Clinical Endocrinology and Diabetes*, vol. 116, no. 10, pp. 592–599, 2008.

[28] M. Inoue, T. Suehiro, T. Nakamura, Y. Ikeda, Y. Kumon, and K. Hashimoto, "Serum arylesterase/diazoxonase activity and genetic polymorphisms in patients with type 2 diabetes," *Metabolism: Clinical and Experimental*, vol. 49, no. 11, pp. 1400–1405, 2000.

[29] C. Y. Han, T. Chiba, J. S. Campbell et al., "Reciprocal and coordinate regulation of serum amyloid A versus apolipoprotein A-I and paraoxonase-1 by inflammation in murine hepatocytes," *Arteriosclerosis, Thrombosis, and Vascular Biology*, vol. 26, no. 8, pp. 1806–1813, 2006.

[30] Y. Kumon, Y. Nakauchi, T. Suehiro et al., "Proinflammatory cytokines but not acute phase serum amyloid A or C-reactive protein, downregulate paraoxonase 1 (PON1) expression by HepG2 cells," *Amyloid*, vol. 9, no. 3, pp. 160–164, 2002.

[31] K. R. Feingold, R. A. Memon, A. H. Moser, and C. Grunfeld, "Paraoxonase activity in the serum and hepatic mRNA levels decrease during the acute phase response," *Atherosclerosis*, vol. 139, no. 2, pp. 307–315, 1998.

[32] M. Aviram, M. Rosenblat, S. Billecke et al., "Human serum paraoxonase (PON 1) is inactivated by oxidized low density lipoprotein and preserved by antioxidants," *Free Radical Biology and Medicine*, vol. 26, no. 7-8, pp. 892–904, 1999.

[33] V. Mohamed-Ali, L. Flower, J. Sethi et al., "β-adrenergic regulation of IL-6 release from adipose tissue: in vivo and in vitro studies," *Journal of Clinical Endocrinology and Metabolism*, vol. 86, no. 12, pp. 5864–5869, 2001.

[34] G. Ferretti, T. Bacchetti, C. Moroni et al., "Paraoxonase activity in high-density lipoproteins: a comparison between healthy and obese females," *Journal of Clinical Endocrinology and Metabolism*, vol. 90, no. 3, pp. 1728–1733, 2005.

[35] U. N. Khot, M. B. Khot, C. T. Bajzer et al., "Prevalence of conventional risk factors in patients with coronary heart disease," *Journal of the American Medical Association*, vol. 290, no. 7, pp. 898–904, 2003.

[36] P. Greenland, M. D. Knoll, J. Stamler et al., "Major risk factors as antecedents of fatal and nonfatal coronary heart disease events," *Journal of the American Medical Association*, vol. 290, no. 7, pp. 891–897, 2003.

[37] D. S. Ng, T. Chu, B. Esposito, P. Hui, P. W. Connelly, and P. L. Gross, "Paraoxonase-1 deficiency in mice predisposes to vascular inflammation, oxidative stress, and thrombogenicity in the absence of hyperlipidemia," *Cardiovascular Pathology*, vol. 17, no. 4, pp. 226–232, 2008.

[38] L. M. Browning, S. D. Hsieh, and M. Ashwell, "A systematic review of waist-to-height ratio as a screening tool for the prediction of cardiovascular disease and diabetes: 0.5 could be a suitable global boundary value," *Nutrition Research Reviews*, vol. 23, no. 2, pp. 247–269, 2010.

[39] B. Palmieri and V. Sblendorio, "Oxidative stress tests: overview on reliability and use—part I," *European Review for Medical and Pharmacological Sciences*, vol. 11, no. 5, pp. 309–342, 2007.

Hindawi Publishing Corporation
Oxidative Medicine and Cellular Longevity
Volume 2014, Article ID 572430, 9 pages
http://dx.doi.org/10.1155/2014/572430

Research Article

Resveratrol Inhibits Phenotype Modulation by Platelet Derived Growth Factor-bb in Rat Aortic Smooth Muscle Cells

Mi Hee Lee,[1] Byeong-Ju Kwon,[1,2] Hyok Jin Seo,[1,2] Kyeong Eun Yoo,[1,2] Min Sung Kim,[1,2] Min-Ah Koo,[1,2] and Jong-Chul Park[1,2]

[1] *Cellbiocontrol Laboratory, Department of Medical Engineering, Yonsei University College of Medicine, 134 Shinchon-Dong, Seodaemun-Gu, Seoul 120-752, Republic of Korea*
[2] *Brain Korea 21 PLUS Project for Medical Science, Yonsei University, 134 Shinchon-Dong, Seodaemun-Gu, Seoul 120-752, Republic of Korea*

Correspondence should be addressed to Jong-Chul Park; parkjc@yuhs.ac

Received 8 November 2013; Revised 8 January 2014; Accepted 27 January 2014; Published 10 March 2014

Academic Editor: Constantinos Pantos

Dedifferentiated vascular smooth muscle cells (VSMCs) are phenotypically modulated from the contractile state to the active synthetic state in the vessel wall. In this study, we investigated the effects of resveratrol on phenotype modulation by dedifferentiation and the intracellular signal transduction pathways of platelet derived growth factor-bb (PDGF-bb) in rat aortic vascular smooth muscle cells (RAOSMCs). Treatment of RAOSMCs with resveratrol showed dose-dependent inhibition of PDGF-bb-stimulated proliferation. Resveratrol treatment inhibited this phenotype change and disassembly of actin filaments and maintained the expression of contractile phenotype-related proteins such as calponin and smooth muscle actin-alpha in comparison with only PDGF-bb stimulated RAOSMC. Although PDGF stimulation elicited strong and detectable Akt and mTOR phosphorylations lasting for several hours, Akt activation was much weaker when PDGF was used with resveratrol. In contrast, resveratrol only slightly inhibited phosphorylations of 42/44 MAPK and p38 MAPK. In conclusion, RAOSMC dedifferentiation, phenotype, and proliferation rate were inhibited by resveratrol via interruption of the balance of Akt, 42/44MAPK, and p38MAPK pathway activation stimulated by PDGF-bb.

1. Introduction

Vascular smooth muscle cells (VSMC) exhibit differentiated, biosynthetic, contractile roles in the media layer of mature blood vessels. However, VSMC dedifferentiation is induced in response to injury in a vessel, followed by phenotypic modulation toward a proliferative, migratory, and synthetic phenotype with extracellular matrix protein deposition, which contributes to intimal hyperplasia [1–3]. Differentiated VSMCs in normal vessels have a contractile phenotype, a spindle-like elongated morphology, and a smaller cell size. In contrast, dedifferentiated VSMCs in injured vessels have a synthetic phenotype, a hypertrophic appearance, hill and valley growth, and a relatively larger size. In addition to these morphological and functional alterations, the change in VSMCs from contractile to synthetic phenotype is controlled by SMC-specific molecular markers such as caldesmon, calponin, alpha-tropomysin, smooth muscle myosin heavy chain, SM22α, and smooth muscle alpha actin (αSMA) [4–6].

Platelet derived growth factor-bb (PDGF-bb) is one of the most potent mitogens and chemoattractants for VSMCs. PDGF-bb binds to the PDGF receptor (PDGFR)-β and utilizes the tyrosine kinase receptor signaling leading to generation of reactive oxygen species (ROS) and subsequently activates several intracellular signaling cascades, including the extracellular signal-regulated kinase (ERK) and p38 mitogen-activated protein kinase (MAPK) pathways and the phosphatidylinositol 3-kinase-Akt (PI3K-Akt) pathway. It has also been shown to stimulate VSMC dedifferentiation [7–9]. Akt is the major signal transducer in growth factor-mediated transcription and promotes cell survival by inhibiting apoptosis. Furthermore, the Akt pathway is the key trigger of mTOR signaling, and Akt-mediated phosphorylation is directly related to mTOR activation. The mTOR protein has

been implicated in cardiovascular diseases and specifically in cardiac hypertrophy [10, 11].

Resveratrol (3,4′,5-trihydroxystilbene), a naturally occurring molecule known as a phytoalexin, is a polyphonic compound found in grapes and red wine. Resveratrol is also known to possess antioxidant, anti-inflammatory, antithrombotic, and antiproliferative effects. Additionally, various studies have shown that resveratrol inhibits the oxidation of low-density lipoprotein (oxLDL) and the early progression of atherosclerotic lesions and also protects cardiomyocytes against ischemia-reperfusion injury [12–14]. Although numerous studies have addressed the effects of red wine consumption on cardioprotection, alcohol contained in red wine interacts with resveratrol to elicit the desired effects. For that reason, several studies have demonstrated that both resveratrol supplement and dealcoholized red wine have physiological activity for cardiovascular protection [15, 16].

In this study, we investigated the effects of resveratrol on proliferation, phenotype modulation, and intracellular signal transduction pathways in PDGF-bb-induced rat aortic vascular smooth muscle cells (RAOSMCs). Our results demonstrate the inhibitory mechanism of resveratrol on phenotype modulation of PDGF-bb-stimulated RAOSMCs.

2. Materials and Methods

2.1. Cell Culture. Primary cultured rat aortic smooth muscle cells (RAOSMCs, Biobud, Seoul, Korea) were routinely maintained in Dulbecco's modified Eagle's medium (DMEM) (Gibco, Carlsbad, CA, USA) supplemented with 10% fetal bovine serum (Sigma, St. Louis, MO, USA) and a 1% antibiotic-antimycotic solution containing 10,000 units penicillin, 10 mg streptomycin, and 25 μg/mL amphotericin B (Sigma) at 37°C in a humidified atmosphere of 5% CO_2. For experiments, cells were used between passages 5 and 10.

2.2. Cell Stimulation by PDGF-bb and Treatment of Resveratrol. RAOSMCs were grown to 80–90% confluence and synchronized in serum-free DMEM medium for 48 h before experiments. Trans-resveratrol (Sigma) was dissolved in 50% dimethylsulphoxide (DMSO) (Sigma) for a stock solution of 100 mM and then diluted to desired concentrations with media prior to cell treatment. Cells were treated with various concentrations of resveratrol: 10~200 μM in cell proliferation assay, 20 μM in cell morphology analysis, and 100 μM in western blotting on quiescent cells with or without 10 ng/mL PDGF-bb for designated times.

2.3. Cell Proliferation and DNA Synthesis. Cell viability was determined by MTT assay [reduction of 3-(4,5-dimethylthiazol-2-yl)-2,5-diphenyltetrazolium bromide to a purple formazan product, Sigma]. For the MTT assay, cells were incubated with 0.5 mg/mL MTT in the last 4 h of the culture period and tested at 37°C in the dark. The media were decanted, the produced formazan salts were dissolved in DMSO, and the absorbance was determined at 570 nm by an automatic microplate reader (Spectra Max 340, Molecular Devices Co., Sunnyvale, CA, USA). DNA synthesis was performed by a 5-bromo-2′-deoxyuridine (BrdU) incorporation assay (Roche Applied Science, Seoul, Korea). Briefly, BrdU-labeling solution was added to the cells, and cells were incubated for 2 h at 37°C. The labeling medium was then removed, and cells were incubated with fixation solution for 30 min at room temperature. After fixation of the cells, anti-BrdU-POD working solution was added, and cells were incubated for 90 min at room temperature. Then, the substrate solution was added, and the absorbance was measured at 370 nm with a 492 nm reference wavelength by an automatic microplate reader (Spectra Max 340, Molecular Devices Co.).

2.4. Immunofluorescence Assay. Cells were grown on coverslips to 50% confluence, serum-starved for 48 h, and then stimulated with or without 10 ng/mL PDGF-bb and 10 or 20 μM resveratrol. Stimulated cells were fixed in 10% formalin solution and permeabilized with 0.5% Triton X-100 in phosphate buffer saline (PBS, pH 7.6). Then, cells were blocked with 5% bovine serum albumin (BSA, Sigma) and incubated with anti-smooth muscle actin-α (αSMA, Dako North America Inc., CA, USA) and anti-calponin (Santa Cruz Biotechnology Inc., Sana Cruz, CA, USA). Cells were then incubated with the secondary antibody, goat-anti-mouse IgG-conjugated Texas Red (Santa Cruz). Alexa 488-conjugated rhodamine phalloidin (5 U/mL, Invitrogen, Carlsbad, CA, USA) was used to visualize F-actin stress fibers, and nuclei were stained with Hoechst 33528. Coverslips were mounted with aqueous mounting medium (Dako Faramount, Dako North America Inc.), and images were evaluated using fluorescence microscope (Olympus, Tokyo, Japan) equipped with a DP-71 digital camera (Olympus).

2.5. Morphology Analysis. For morphology analysis, a cell plasma membrane was visualized by staining it with Texas Red C2-maleimide (5 U/mL, Invitrogen) and Hoechst 33258 (1 μg/mL in PBS, Sigma). Images were captured on a fluorescence microscope (Olympus) equipped with a DP-71 digital camera (Olympus). Cell circularity and an area of 100 cells for each group were analyzed using ImageJ software (NIH, Bethesda, MD, USA). The circularity was measured to determine the morphological distribution between the contractile phenotype and the synthetic phenotype of RAOSMCs. Circularity was presented from 0 to 1, with values closer to 0 indicating spindle morphology and those closer to 1 indicating a circular phenotype [17, 18].

2.6. Western Blotting. After time-course stimulation with PDGF-bb, the cells were washed twice with cold PBS (10 mM, pH 7.4). Ice-cold RIPA lysis buffer (Santa Cruz Biotechnology) was added to the cells for 5 min. The cells were scraped, and the lysate was cleared by centrifugation at 14,000 ×g for 20 min at 4°C. The resultant supernatant (total cell lysate) was collected. The protein concentration was determined using a DC Bio-Rad assay kit (Bio-Rad Laboratories, Hercules, California, USA). For immunoblot analysis, proteins were separated by 10–15% SDS-PAGE and then electrotransferred onto a PVDF membrane. The membrane was blocked with

blocking buffer (5% bovine serum albumin and 1% Tween-20 in 20 mM TBS, pH 7.6) for 1 h at room temperature and then probed overnight with antibodies to phospho-PDGFR-β (p-PDGFR-β, Tyr751), total PDGFR-β, phospho-MEK1/2 (p-MEK1/2, Ser217/221), total MEK1/2, phospho-p42/44MAPK (p-p42/44MAPK, Thr202/Tyr204), total p42/44MAPK, phospho-Akt (p-Akt, Ser473), total Akt, phospho-mTOR (p-mTOR, Ser2448), total mTOR, phospho-p38 MAPK (p-p38MAPK, Thr180/Tyr182), and total p38MAPK. Antibodies were purchased from Cell Signaling Technology (Danvers, MA, USA) and used at 1 : 1,000 dilutions. Detection of horseradish peroxidase-conjugated secondary antibody (i.e., anti-rabbit IgG (1 : 2,000) and antimouse IgG (1 : 2,000) from Santa Cruz Biotechnology Inc.) was accomplished using enhanced chemiluminescence of the ECL Plus detection kit (Amersham Biosciences, Buckinghamshire, England). The band intensity was quantified using ImageJ software (NIH) and relative fold exchanges averaged across the three experiments (normalized to phosphorylated forms and total forms) are shown below each band.

2.7. Statistical Analysis. All variables were tested in three independent cultures for each experiment. The results are reported as mean ± SD compared to nontreated controls. Statistical analysis was performed using a one-way ANOVA, followed by a Tukey's HSD test for multiple comparisons using SPSS software. A P value < 0.05 was considered statistically significant.

3. Results

3.1. Inhibitory Effect of Resveratrol on PDGF-bb-Induced Proliferation in RAOSMCs. To assess whether resveratrol inhibited PDGF-bb-stimulated RAOSMC proliferation, serum-starved RAOSMCs were incubated with 10 ng/mL PDGF-bb and increasing concentrations of resveratrol for 48 h. Treatment with 10 ng/mL PDGF-bb induced proliferation of RAOSMCs in comparison with nonstimulated cells. However, the presence of resveratrol resulted in significant ($P < 0.05$) dose-dependent decreases in cell growth (Figure 1(a)). When cells were treated with increasing concentrations of resveratrol, a significant ($P < 0.05$) dose-dependent reduction in cell growth was observed starting at 50 μM. The level of DNA synthesis was also measured by cell proliferation assay. Stimulation of RAOSMCs with 10 ng/mL PDGF-bb caused a significant increase in the DNA amount, and resveratrol significantly inhibited this increase in a concentration-dependent manner (Figure 1(b)). Furthermore, increases in cell viability and DNA synthesis induced by PDGF-bb stimulation were completely suppressed in cells treated with concentrations of resveratrol greater than 100 μM. These results suggest that resveratrol exerts a potent antiproliferative effect on PDGF-bb-stimulated RAOSMC proliferation.

3.2. Inhibitory Effect of Resveratrol on PDGF-bb-Stimulated RAOSMC Morphology and Phenotype. To define phenotype exchange in PDGF stimulation, we assessed RAOSMC phenotype and morphology using immunofluorescence and

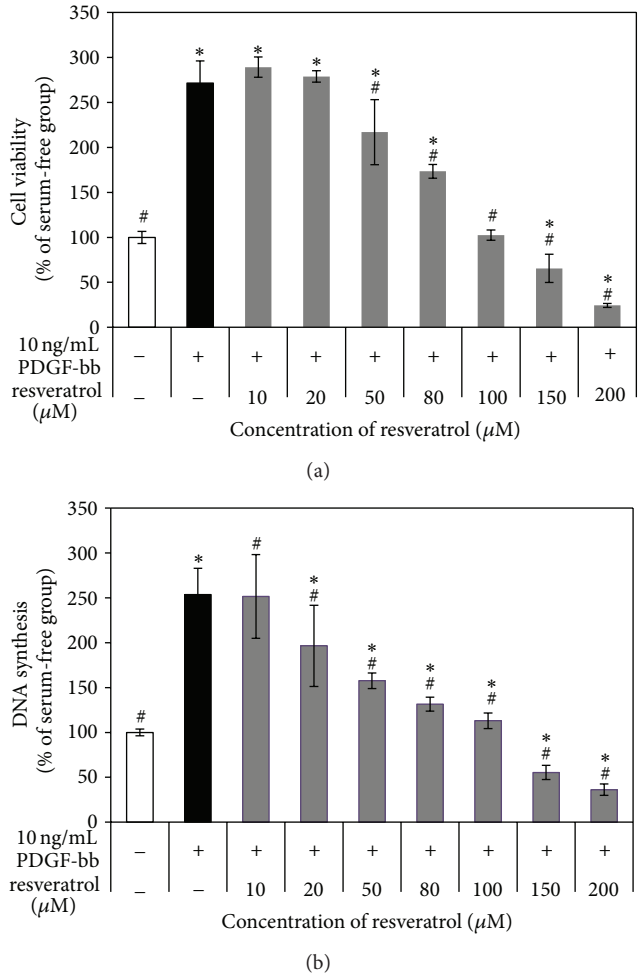

Figure 1: Antiproliferative activity of resveratrol in PDGF-bb-stimulated RAOSMCs. After 24 h of starvation with serum-free DMEM, cells were treated with 10 ng/mL PDGF-bb and increasing concentrations (10–200 μM) of resveratrol for 48 h. (a) The effect of resveratrol growth inhibition on PDGF-bb-stimulated RAOSMCs. Cell viability was detected using the MTT assay. (b) The effect of resveratrol on PDGF-bb-induced DNA synthesis in RAOSMCs. DNA synthesis was detected using the BrdU incorporation assay. $^{*}P < 0.05$ compared with nonstimulated controls; $^{\#}P < 0.05$ compared with 10 ng/mL PDGF-bb-stimulated controls.

immunocytochemical staining with antibodies against αSMA and calponin. RAOSMCs were grown on glass cover slips, starved of serum for 48 h, and stimulated in the presence and absence of PDGF-bb and resveratrol for 24 h.

RAOSMCs exhibited elongation and spindle morphology during prolonged serum deprivation. As shown in Figure 2, RAOSMCs serum-starved for 48 hr revealed an aligned arrangement of actin filaments with an organized cytoskeleton network. In contrast, PDGF-bb-stimulated RAOSMCs showed disassembled distribution and aggregation around the perinuclear region of actin filaments without clear filamentous organization. However, RAOSMCs treated with resveratrol maintained spindle-like shapes and organization of the actin filaments by inhibiting the effects of PDGF-bb-stimulation.

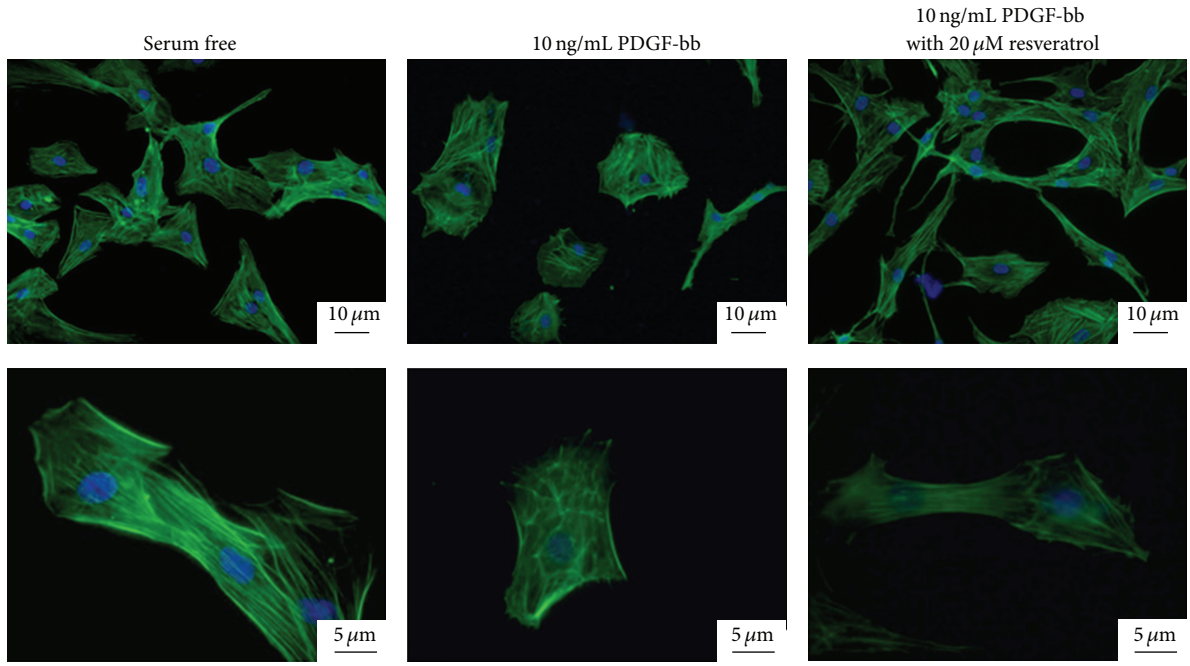

Figure 2: Arrangement of F-actin filaments of RAOSMCs with or without 10 ng/mL PDGF-bb stimulation and 20 μM resveratrol. Nuclei were stained blue with Hoechst 33528, and F-actin was green due to alexa (388)-rhodamine phalloidin. Images in the upper and low panels were obtained at ×400 and ×1000 original magnifications, respectively. The micrographs shown in this figure are representative of three independent experiments with similar results.

Therefore, cells were examined for accumulation of the contractile-related proteins, αSMA (Figure 3(a)) and calponin (Figure 3(d)), in clear actin filament organization. When RAOSMCs were stimulated with PDGF-bb, cells were observed to undergo morphological changes from spindle-shaped to polygonal, and relatively low levels of αSMA (Figure 3(b)) and calponin were noted (Figure 3(e)) with disassembled distribution of actin filaments in the cytosol. However, treatment with 20 μM resveratrol inhibited the morphological changes. Furthermore, when cells were treated with resveratrol, the actin cytoskeleton maintained parallel actin filaments by forming a complex with contractile phenotype-related proteins, including αSMA (Figure 3(c)) and calponin (Figure 3(f)). To determine the morphological distribution of the cells, circularity was measured by ImageJ analysis. Compared to serum-starved cells, PDGF-bb-stimulated cells showed a greater distribution in circularity, whereas cells treated with resveratrol exhibited lower circularity (Figure 4(a)). The average circularity of PDGF-bb-stimulated cells was significantly higher than that of nontreated cells. However, resveratrol-treated cells stimulated with PDGF-bb were not significantly different from the nontreated cells (Figure 4(b)). Therefore, PDGF-bb-stimulated RAOSMCs had a greater area compared with serum-starved RAOSMCs. Resveratrol inhibited the change in area stimulated by PDGF-bb (Figure 4(c)).

3.3. Inhibitory Mechanism of Dedifferentiation on PDGF-bb-Stimulated RAOSMCs by Resveratrol. Treatment of RAOSMCs with resveratrol significantly inhibited PDGF-bb-stimulated proliferation in a dose-dependent manner. Furthermore, treatment of cells with 100 μM resveratrol almost completely inhibited the growth of ROASMCs, as shown by DNA synthesis assay and MTT assay.

To define the effects of resveratrol on signaling pathways involved in PDGF-bb-stimulated dedifferentiation, serum-starved cells were stimulated with 10 ng/mL PDGF-bb in the absence or presence of resveratrol for specified times. Then, we analyzed the activation of p42/44MAPK, p38MAPK, and Akt, downstream effectors of PDGF-bb-induced signaling, by Western blotting.

Addition of 10 ng/mL PDGF-bb to serum-starved cells led to PDGFR-β phosphorylation that peaked within 10 min of stimulation and returnedto baseline level after 2~4 h, with similar results achieved in atleast three independent experiments (Figure 5(a)). However, resveratrol treatment inhibited PDGFR-β phosphorylation induced byPDGF-bb at only 10 min, while no inhibition of PDGFR-β phosphorylation was observed during incubations longer than 30 min.

In a similar manner, PDGF-bb stimulated the phosphorylations of downstream effectors such as MEK1/2, p42/44MAPK (Figure 5(b)), and p38 (Figure 5(c)), and resveratrol only slightly inhibited the PDGF-bb-induced phosphorylations of MEK1/2, p42/44MAPK, and p38MAPK in a time-dependent manner. However, as shown in Figure 5(d), while PDGF stimulation elicited strong and detectable signals for Akt and mTOR phosphorylations for several hours, resveratrol treatment clearly inhibited the

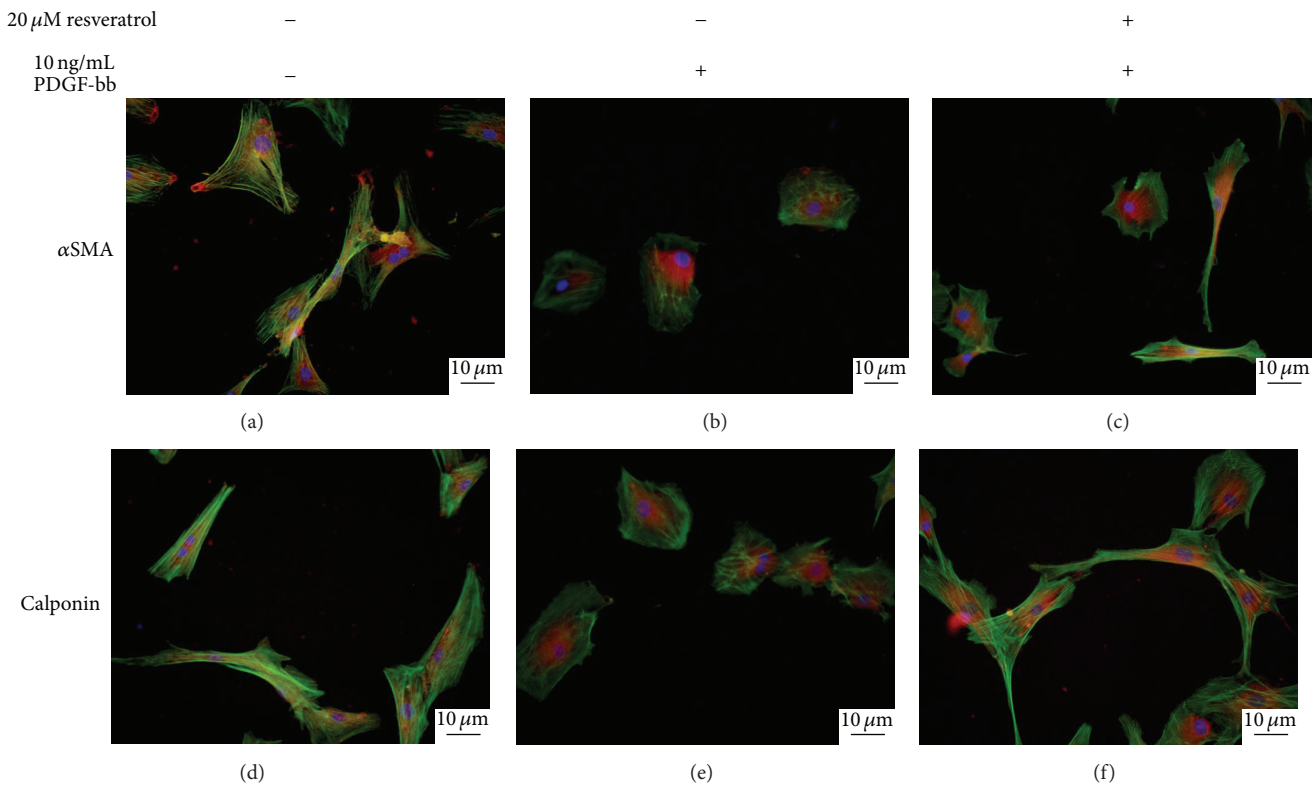

FIGURE 3: Characterization of morphology modulation by resveratrol on PDGF-bb-stimulated RAOSMCs. Cells were incubated in serum-free media (a, d), 10 ng/mL PDGF-bb (b, e), or 20 μM resveratrol with 10 ng/mL PDGF-bb (c, f). Nuclei were stained blue with Hoechst 33528, αSMA (a~c) and calponin (d~f) are red, and F-actin is green due to alexa (388)-rhodamine phalloidin. The micrographs (magnification, ×100) shown in this figure are representative of three independent experiments with similar results.

PDGF-mediated phosphorylations of Akt and mTOR, a downstream effector dependent on Akt.

4. Discussion

Changes of the differentiated VSMC play a critical role in cardiovascular diseases, such as atherosclerosis, hypertension, asthma, and vascular aneurisms. Identification of dedifferentiated VSMCs was based on morphological criteria that met the terms for "phenotypic modulation" or "phenotypic switching" in functional and structural properties. A phenotypic switch from a contractile to synthetic phenotype accompanies the proliferation and migration of cells [19, 20].

PDGF, a key mediator in the proliferation of VSMCs, plays an important role in the pathogenesis of various vascular disorders. It has already been reported that PDGF-bb is implicated in intracellular ROS generation and VSMC growth [7, 21]. Furthermore, the signaling pathways affected by PDGF are so similar to that activated by oxidative stress [22, 23]. PDGF-bb represses the characteristic VSMC gene expression by activating extracellular signal-regulated kinase 1/2-mitogen activated protein kinase (ERK1/2-MAPK), p38 MAPK, and Akt pathways in cultured VSMCs [24, 25].

This study reports that PDGF-bb treatment causes phenotypic changes typical of dedifferentiation in RAOSMCs by activating p42/44 MAPK, p38 MAPK, and Akt pathways. In our experimental system, resveratrol inhibited the proliferation of PDGF-bb-stimulated RAOSMCs. The contractile morphology and spindle phenotype of the cells were also preserved by resveratrol treatment. Therefore, markers of VSMC differentiation, such as αSMA and calponin, were not inhibited by resveratrol treatment. In other words, resveratrol might prevent morphologic changes from contractile to synthetic phenotype. VSMCs in mature animal vessels exhibit a contractile phenotype (differentiated state) and express multiple contractile proteins, including αSMA, SM22α, and SM-MHC [26, 27]. Calponin and αSMA are characterized in detail as F-actin binding components of smooth muscle thin filaments, and they control actin-based cellular processes by regulating the stability of the actin cytoskeleton [6, 28].

The investigation of signal transduction pathways induced by PDGF-bb showed that resveratrol can inhibit phosphorylation of PDGFR-β, 42/44 MAPK, Akt, and p38MAPK. In particular, Akt/mTOR phosphorylation was preferentially inhibited in PDGF-bb-induced cells treated with resveratrol. It is known that VSMC phenotype is determined by changes in the balance of activation between the Akt pathway, the ERK, and p38MAPK pathways. Therefore, the Akt pathway plays a vital role in maintaining the differentiated phenotype [29].

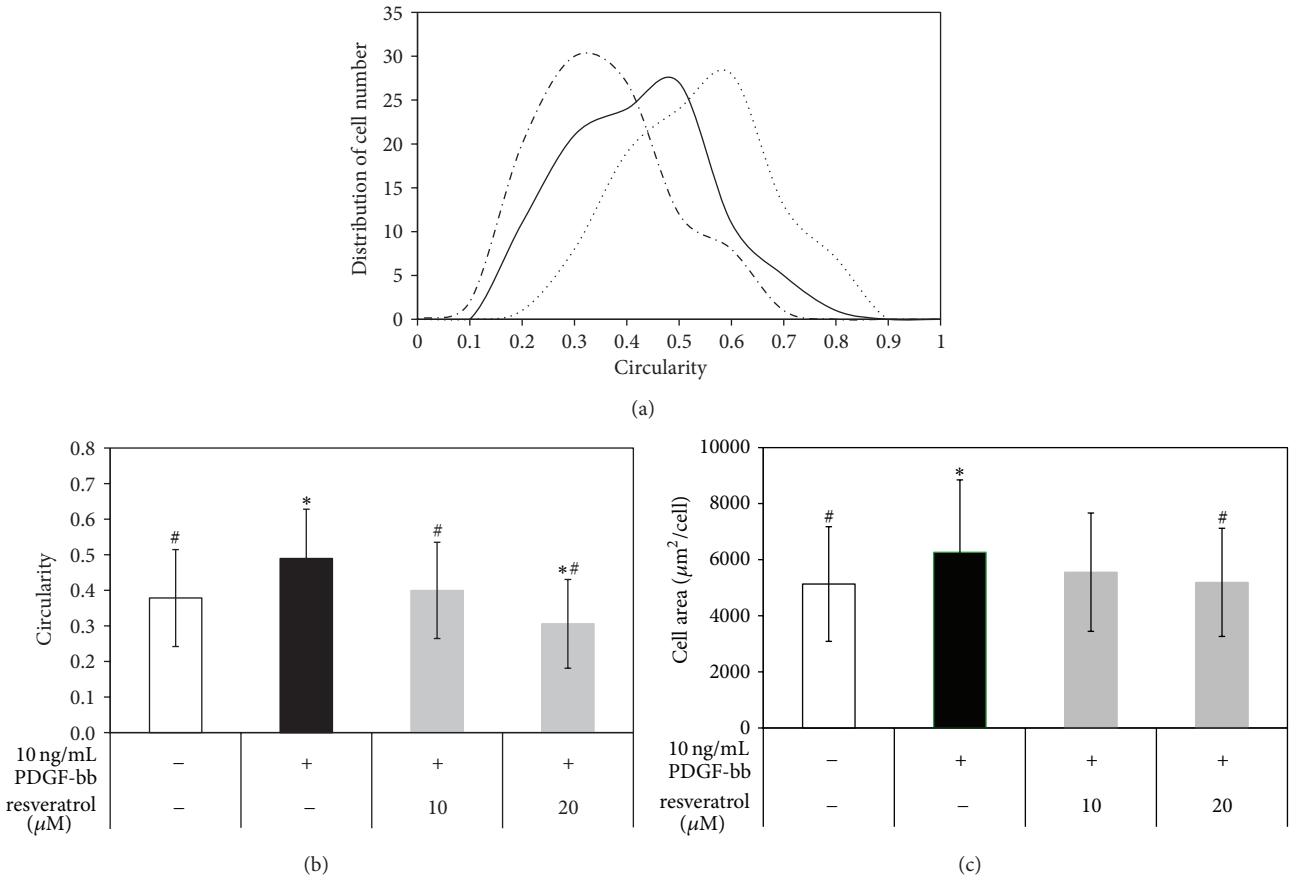

Figure 4: Morphology modulation by resveratrol in PDGF-bb-stimulated RAOSMCs. (a) The distribution of circularity ranged from 0 to 1, for linear to circular, respectively. (—in serum free, —•— in 10 ng/mL PDGF-bb, and • • • • • in 10 ng/mL PDGF-bb with 20 μM resveratrol). (b) The average circularity ±SD was obtained from 100 single cells per each type. $^{*}P < 0.05$ compared with nonstimulated control; $^{\#}P < 0.05$ compared with 10 ng/mL PDGF-bb-stimulated control. (c) The average area (μm^2/cell) ± SD was obtained from 100 single cells of each type. $^{*}P < 0.05$ compared with nonstimulated control; $^{\#}P < 0.05$ compared with 10 ng/mL PDGF-bb-stimulated control.

The phosphoinositol-Akt-mammalian target of the rapamycin-p70S6 kinase (PIK/Akt/mTOR/p70S6K) pathway regulates cell growth and cell differentiation in response to nutrients, growth factors, and cytokines [30, 31]. Pharmacological inhibition with rapamycin was shown to induce contractile morphology, SM2-MHC, and calponin, protein reduction, and collagen synthesis in cultures of synthetic phenotype VSMCs by regulation of the mTOR/p70 S6 K1 pathway [30]. Previous studies have shown that mTOR activation induced SMC proliferation and required the activation of the signaling cascade PI3K/PDK1/Akt, as assessed by the effect of the PI3K inhibitors wortmannin and Ly294002, which block PDK [10, 11, 32]. Thus, resveratrol inhibited SMC phenotypic modulation by changing the balance between the Akt and MAPK pathways via hindering PDGF-bb-induced Akt pathways, but not the ERK and p38MAPK pathways. Furthermore, inhibition of Akt/mTOR pathways by resveratrol in SMC affected not only DNA synthesis, but also expression of phenotype-related proteins. Acute or chronic administration of plant polyphenols in patients has been found to result in the vasoprotective, antiangiogenic, antiatherogenic, vasorelaxant, and antihypertensive effects [33]. Several reports demonstrate resveratrol's efficacy in inhibiting VSMC proliferation [34, 35]. Furthermore, it has been shown that resveratrol specifically blocks the PI3K/PDK1/Akt pathway, thereby inhibiting oxLDL-induced SMC proliferation [14].

In this study, we focused on the effect of resveratrol on phenotypic modulation of RAOSMCs following stimulation with PDGF-bb. From a general point of view, resveratrol exhibits various potentially inhibitory properties on dedifferentiation, including an antiproliferative effect and an ability to modulate important growth signaling pathways.

5. Conclusion

In this study, we investigated the effect of resveratrol on dedifferentiation of RAOSMCs induced by PDGF-bb. Resveratrol inhibited dedifferentiation, phenotypic alterations, and proliferation rate stimulated by PDGF-bb in RAOSMC. In conclusion, our results indicate that this effect was probably mediated via a differential regulation of the balance between Akt, 42/44MAPK, and p38MAPK pathway activations stimulated by PDGF-bb at least in part for the effect of resveratrol. This result suggests that resveratrol may be an inhibitor of the

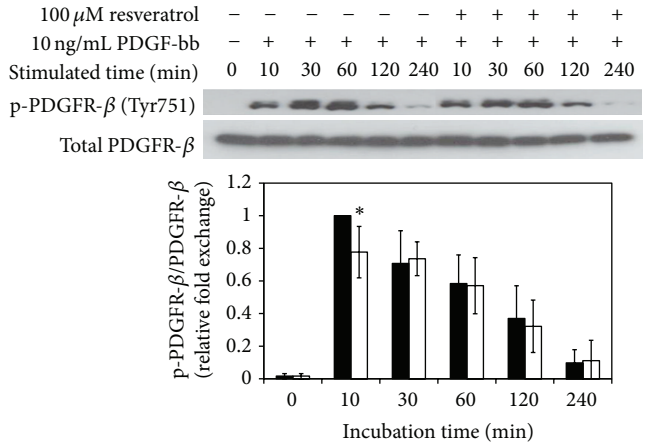

(a)

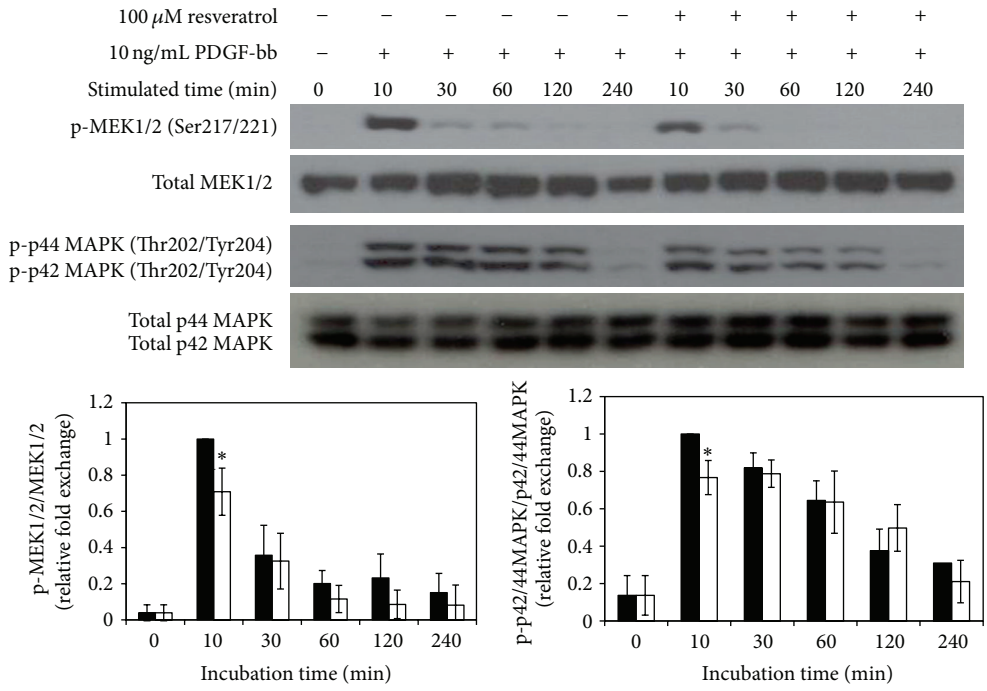

(b)

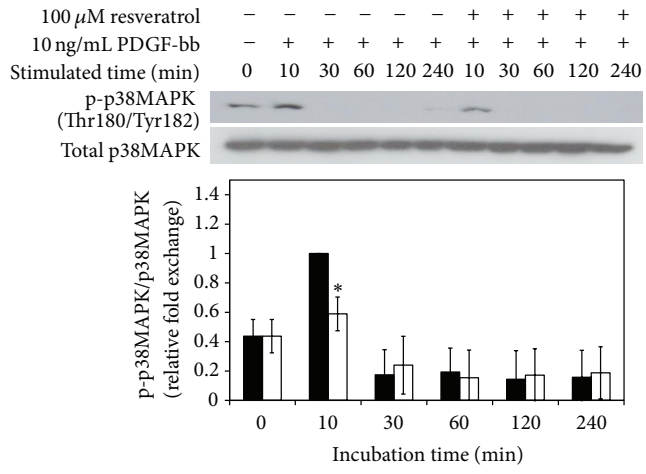

(c)

Figure 5: Continued.

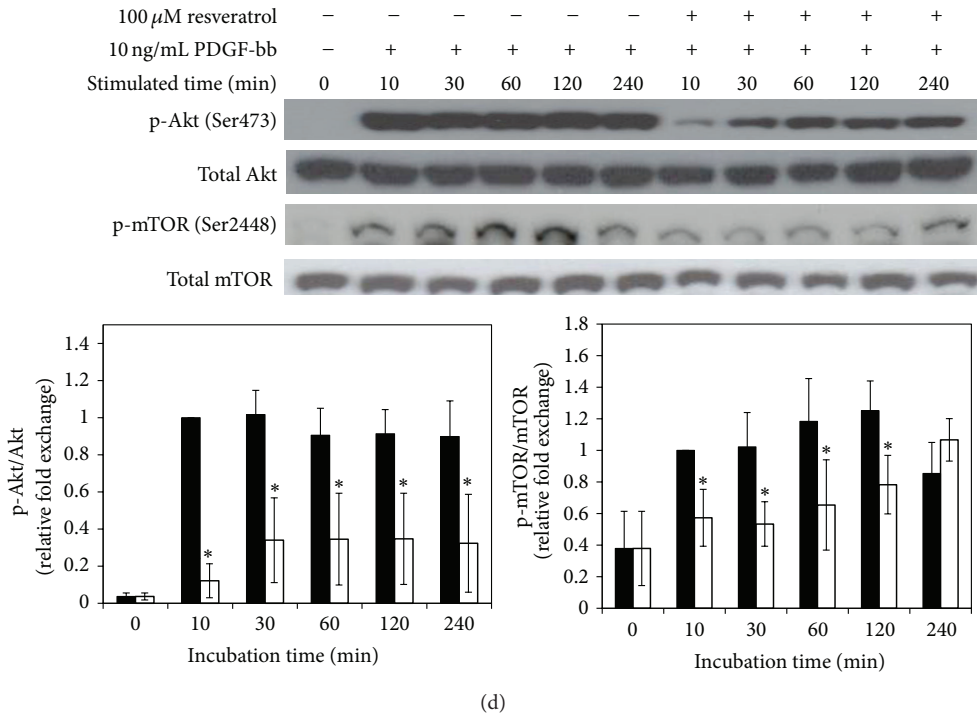

(d)

Figure 5: The effects of resveratrol on modulation of PDGF-bb-stimulated signaling pathways in RAOSMCs. RAOSMCs starved of serum were stimulated with 10 ng/mL PDGF-bb and 100 μM resveratrol for the indicated times (10 m, 30 m, 1 h, 2 h, and 4 h) and lysed. Lysates were immunoblotted with antibodies. After densitometric quantification using the ImageJ program, data were expressed each as the mean ± SD from three independent experiments. Black bar indicates expression by PDGF-bb stimulation. White bar indicates expression by PDGF-bb stimulation with EGCG. (a) The expression of phospho-PDGFR-β in a time-dependent manner. The band intensities were normalized to PDGFR-β expression. (b) The time-dependent expressions of phospho-MEK1/2 and phospho-p42/44MAPK. The band intensities were normalized to MEK1/2 and p42/44MAPK expression. (c) The time-dependent expression of phospho-p38 MAPK. The band intensities were normalized to p38 MAPK expression. (d) The time-dependent expression of phospho-Akt and phospho-mTOR. The band intensities were normalized to Akt and mTOR expression.

phenotype modulation occurring in arterial stenosis and in postangioplasty restenosis following vascular injury.

Conflict of Interests

The authors declare that there is no conflict of interests with any financial organization regarding the commercial identities mentioned in the paper.

Acknowledgment

This study was supported by a grant of the Korea Healthcare Technology R&D Project, Ministry for Health & Welfare, Republic of Korea (A120878).

References

[1] M. G. Davies and P.-O. Hagen, "Pathobiology of intimal hyperplasia," *British Journal of Surgery*, vol. 81, no. 9, pp. 1254–1269, 1994.

[2] W. D. Coats and D. P. Faxon, "The role of the extracellular matrix in arterial remodelling," *Seminars in Interventional Cardiology*, vol. 2, no. 3, pp. 167–176, 1997.

[3] S. M. Schwartz, "Smooth muscle migration in atherosclerosis and restenosis," *The Journal of Clinical Investigation*, vol. 99, no. 12, pp. 2814–2817, 1997.

[4] S. Kenji, H. Ken'ichiro, and N. Wataru, "Molecular mechanism of phenotypic modulation of smooth muscle cells," *Hormone Research*, vol. 50, supplement 2, pp. 15–24, 1998.

[5] E. M. Rzucidlo, K. A. Martin, R. J. Powell, and N. H. Lebanon, "Regulation of vascular smooth muscle cell differentiation," *Journal of Vascular Surgery*, vol. 45, no. 6, pp. 25–32, 2007.

[6] G. T. Rozenblum and M. Gimona, "Calponins: adaptable modular regulators of the actin cytoskeleton," *International Journal of Biochemistry and Cell Biology*, vol. 40, no. 10, pp. 1990–1995, 2008.

[7] M. Sundaresan, Z.-X. Yu, V. J. Ferrans, K. Irani, and T. Finkel, "Requirement for generation of H_2O_2 for platelet-derived growth factor signal transduction," *Science*, vol. 270, no. 5234, pp. 296–299, 1995.

[8] C.-H. Heldin and B. Westermark, "Mechanism of action and *in vivo* role of platelet-derived growth factor," *Physiological Reviews*, vol. 79, no. 4, pp. 1283–1316, 1999.

[9] Y. Zhan, S. Kim, Y. Izumi et al., "Role of JNK, p38, and ERK in platelet-derived growth factor—induced vascular proliferation, migration, and gene expression," *Arteriosclerosis, Thrombosis, and Vascular Biology*, vol. 23, no. 5, pp. 795–801, 2003.

[10] A. Sekulic, C. C. Hudson, J. L. Homme et al., "A direct linkage between the phosphoinositide 3-kinase-AKT signaling pathway and the mammalian target of rapamycin in mitogen-stimulated and transformed cells," *Cancer Research*, vol. 60, no. 13, pp. 3504–3513, 2000.

[11] S. Wullschleger, R. Loewith, and M. N. Hall, "TOR signaling in growth and metabolism," *Cell*, vol. 124, no. 3, pp. 471–484, 2006.

[12] S. Sadruddin and R. Arora, "Resveratrol: biologic and therapeutic implications," *Journal of the CardioMetabolic Syndrome*, vol. 4, no. 2, pp. 102–106, 2009.

[13] X.-B. Wang, J. Huang, J.-G. Zou et al., "Effects of resveratrol on number and activity of endothelial progenitor cells from human peripheral blood," *Clinical and Experimental Pharmacology and Physiology*, vol. 34, no. 11, pp. 1109–1115, 2007.

[14] P. M. Brito, R. Devillard, A. Nègre-Salvayre et al., "Resveratrol inhibits the mTOR mitogenic signaling evoked by oxidized LDL in smooth muscle cells," *Atherosclerosis*, vol. 205, no. 1, pp. 126–134, 2009.

[15] L. Fremont, L. Belguendouz, and S. Delpal, "Antioxidant activity of resveratrol and alcohol-free wine polyphenols related to LDL oxidation and polyunsaturated fatty acids," *Life Sciences*, vol. 64, no. 26, pp. 2511–2521, 1999.

[16] Z. Wang, J. Zou, K. Cao, T.-C. Hsieh, Y. Huang, and J. M. Wu, "Dealcoholized red wine containing known amounts of resveratrol suppresses atherosclerosis in hypercholesterolemic rabbits without affecting plasma lipid levels," *International Journal of Molecular Medicine*, vol. 16, no. 1, pp. 533–540, 2005.

[17] H.-J. Sung, S. G. Eskin, Y. Sakurai, A. Yee, N. Kataoka, and L. V. McIntire, "Oxidative stress produced with cell migration increases synthetic phenotype of vascular smooth muscle cells," *Annals of Biomedical Engineering*, vol. 33, no. 11, pp. 1546–1554, 2005.

[18] S. Li, S. Sims, Y. Jiao, L. H. Chow, and J. G. Pickering, "Evidence from a novel human cell clone that adult vascular smooth muscle cells can convert reversibly between noncontractile and contractile phenotypes," *Circulation Research*, vol. 85, no. 4, pp. 338–348, 1999.

[19] G. K. Owens, "Regulation of differentiation of vascular smooth muscle cells," *Physiological Reviews*, vol. 75, no. 3, pp. 487–517, 1995.

[20] G. K. Owens, M. S. Kumar, and B. R. Wamhoff, "Molecular regulation of vascular smooth muscle cell differentiation in development and disease," *Physiological Reviews*, vol. 84, no. 3, pp. 767–801, 2004.

[21] P. U. Rani, R. Kesavan, R. Ganugula et al., "Ellagic acid inhibits PDGF-BB-induced vascular smooth muscle cell proliferation and prevents atheroma formation in streptozotocin-induced diabetic rats," *Journal of Nutritional Biochemistry*, vol. 24, no. 11, pp. 1830–1839, 2013.

[22] K. K. Griendling and M. Ushio-Fukai, "Redox control of vascular smooth muscle proliferation," *Journal of Laboratory and Clinical Medicine*, vol. 132, no. 1, pp. 9–15, 1998.

[23] Y. Taniyama and K. K. Griendling, "Reactive oxygen species in the vasculature: molecular and cellular mechanisms," *Hypertension*, vol. 42, no. 6, pp. 1075–1081, 2003.

[24] F. Romano, C. Chiarenza, F. Palombi et al., "Platelet-derived growth factor-bb-induced hypertrophy of peritubular smooth muscle cells is mediated by activation of p38 MAP-kinase and of Rho-kinase," *Journal of Cellular Physiology*, vol. 207, no. 1, pp. 123–131, 2006.

[25] H. P. Reusch, S. Zimmermann, M. Schaefer, M. Paul, and K. Moelling, "Regulation of Raf by Akt controls growth and differentiation in vascular smooth muscle cells," *Journal of Biological Chemistry*, vol. 276, no. 36, pp. 33630–33637, 2001.

[26] G. K. Owens and G. Wise, "Regulation of differentiation/maturation in vascular smooth muscle cells by hormones and growth factors," *Agents and Actions Supplements*, vol. 48, pp. 3–24, 1997.

[27] R. S. Blank and G. K. Owens, "Platelet-derived growth factor regulates actin isoform expression and growth state in cultured rat aortic smooth muscle cells," *Journal of Cellular Physiology*, vol. 142, no. 3, pp. 635–642, 1990.

[28] M. Gimona, I. Kaverina, G. P. Resch, E. Vignal, and G. Burgstaller, "Calponin repeats regulate actin filament stability and formation of podosomes in smooth muscle cells," *Molecular Biology of the Cell*, vol. 14, no. 6, pp. 2482–2491, 2003.

[29] K. Hayashi, M. Takahashi, W. Nishida et al., "Phenotypic modulation of vascular smooth muscle cells induced by unsaturated lysophosphatidic acids," *Circulation Research*, vol. 89, no. 3, pp. 251–258, 2001.

[30] M. N. Corradetti and K.-L. Guan, "Upstream of the mammalian target of rapamycin: do all roads pass through mTOR?" *Oncogene*, vol. 25, no. 48, pp. 6347–6360, 2006.

[31] R. C. Braun-Dullaeus, M. J. Mann, U. Seay et al., "Cell cycle protein expression in vascular smooth muscle cells *in vitro* and *in vivo* is regulated through phosphatidylinositol 3-kinase and mammalian target of rapamycin," *Arteriosclerosis, Thrombosis, and Vascular Biology*, vol. 21, no. 7, pp. 1152–1158, 2001.

[32] N. Auge, V. Garcia, F. Maupas-Schwalm, T. Levade, R. Salvayre, and A. Negre-Salvayre, "Oxidized LDL-induced smooth muscle cell proliferation involves the EGF receptor/PI-3 kinase/Akt and the sphingolipid signaling pathways," *Arteriosclerosis, Thrombosis, and Vascular Biology*, vol. 22, no. 12, pp. 1990–1995, 2002.

[33] J.-C. Stoclet, T. Chataigneau, M. Ndiaye et al., "Vascular protection by dietary polyphenols," *European Journal of Pharmacology*, vol. 500, no. 1–3, pp. 299–313, 2004.

[34] A. M. El-Mowafy and R. E. White, "Resveratrol inhibits MAPK activity and nuclear translocation in coronary artery smooth muscle: reversal of endothelin-1 stimulatory effects," *FEBS Letters*, vol. 451, no. 1, pp. 63–67, 1999.

[35] V. P. Ekshyyan, V. Y. Hebert, A. Khandelwal, and T. R. Dugas, "Resveratrol inhibits rat aortic vascular smooth muscle cell proliferation via estrogen receptor dependent nitric oxide production," *Journal of Cardiovascular Pharmacology*, vol. 50, no. 1, pp. 83–93, 2007.

Hindawi Publishing Corporation
Oxidative Medicine and Cellular Longevity
Volume 2014, Article ID 218749, 7 pages
http://dx.doi.org/10.1155/2014/218749

Research Article

Efficacy of a Low Dose of Estrogen on Antioxidant Defenses and Heart Rate Variability

Cristina Campos,[1] Karina Rabello Casali,[2] Dhãniel Baraldi,[1] Adriana Conzatti,[1] Alex Sander da Rosa Araújo,[1] Neelam Khaper,[3] Susana Llesuy,[4] Katya Rigatto,[5] and Adriane Belló-Klein[1]

[1] *Universidade Federal do Rio Grande do Sul, Sarmento Leite, 500 Bairro Farroupilha, 90050-170 Porto Alegre, RS, Brazil*
[2] *Instituto de Cardiologia do Rio Grande do Sul, 90620-001 Porto Alegre, RS, Brazil*
[3] *Medical Sciences Division, Northern Ontario School of Medicine, Lakehead University, Thunder Bay, ON, Canada P7B 5E1*
[4] *Universidad de Buenos Aires, C1053ABJ Buenos Aires, Argentina*
[5] *Universidade Federal de Ciências da Saúde de Porto Alegre, 90050-170 Porto Alegre, RS, Brazil*

Correspondence should be addressed to Adriane Belló-Klein; belklein@ufrgs.br

Received 20 November 2013; Revised 8 January 2014; Accepted 30 January 2014; Published 10 March 2014

Academic Editor: Dalton Valentim Vassallo

This study tested whether a low dose (40% less than the pharmacological dose of 17-β estradiol) would be as effective as the pharmacological dose to improve cardiovascular parameters and decrease cardiac oxidative stress. Female Wistar rats (n = 9/group) were divided in three groups: (1) ovariectomized (Ovx), (2) ovariectomized animals treated for 21 days with low dose (LE; 0.2 mg), and (3) high dose (HE; 0.5 mg) 17-β estradiol subcutaneously. Hemodynamic assessment and spectral analysis for evaluation of autonomic nervous system regulation were performed. Myocardial superoxide dismutase (SOD) and catalase (CAT) activities, redox ratio (GSH/GSSG), total radical-trapping antioxidant potential (TRAP), hydrogen peroxide, and superoxide anion concentrations were measured. HE and LE groups exhibited an improvement in hemodynamic function and heart rate variability. These changes were associated with an increase in the TRAP, GSH/GSSG, SOD, and CAT. A decrease in hydrogen peroxide and superoxide anion was also observed in the treated estrogen groups as compared to the Ovx group. Our results indicate that a low dose of estrogen is just as effective as a high dose into promoting cardiovascular function and reducing oxidative stress, thereby supporting the approach of using low dose of estrogen in clinical settings to minimize the risks associated with estrogen therapy.

1. Introduction

The risk of cardiovascular disease (CVD) increases dramatically in the postmenopausal women as compared to the premenopausal women. Estrogen helps to protect women against CVD during the childbearing years and, after menopause, the CVD can be prevented or at least reduced by estrogen therapy [1–3]. It has been demonstrated that estrogen therapy can reduce many risk factors, improving lipid profile and glucose metabolism [1].

The increased risk of CVD in menopause is also accompanied by oxidative stress, a condition when there is an increase in reactive oxygen species (ROS) levels which may cause oxidative damage to cells [4]. On the other hand, cells have mechanisms to protect from ROS mediated toxicity. Glutathione (GSH) is the major nonenzymatic antioxidant and participates in many cellular reactions of ROS scavenging. In such reactions, GSH is oxidized to form glutathione disulfide (GSSG). An increase in the redox ratio which is represented by GSH/GSSG is indicative of reduced oxidative stress [5]. An impairment in redox balance plays an important role in the reduced nitric oxide bioavailability which may ultimately affect the sympathovagal balance (SVB) [6, 7]. Moreover, some studies have reported a link between menopause and SVB impairment [8, 9] suggesting a role of estrogen in the autonomic nervous control of the cardiovascular system.

Power spectral analysis of heart rate variability (HRV) is a noninvasive method to assess SVB [10]. Alterations in HRV,

which primarily reflect the tonic autonomic modulation, may have substantial clinical implications. Low HRV, which has been shown in postmenopausal women, is associated with an increased risk of CVD [11]. In addition, some studies indicate that menopausal women have a sympathovagal imbalance and that estrogen improves the SVB centrally and peripherally by decreasing sympathetic and increasing parasympathetic tone [12].

Estrogen therapy improves women's quality of life [13] and is widely used for controlling typical menopausal symptoms such as vaginal atrophy, hot flushes, osteoporosis, and sleep disturbances [14]. However, at standard pharmacological doses, several adverse effects, including higher risk of breast cancer, stroke, and venous thromboembolism, outweigh the benefits of estrogen therapy [15].

As cardiovascular diseases are highly prevalent after menopause [16] and estrogen is the most commonly used treatment to reduce menopause symptoms [13], the need to find a safer estrogen dose to control menopause related discomforts has been recommended. Indeed, studies evaluating different regimens of hormone therapy have demonstrated that a low dose of estrogen is associated with a significant decrease in mammographic density [17]. According to Mercuro et al. [18], low doses of estrogen are just as effective as conventional doses to improve the lipid profile and the endothelial function. Moreover, a low dose of estrogen has demonstrated to be effective for the alleviation of climacteric symptoms [19] and it has good tolerability associated with a low incidence of the most common side effects [20].

There have been no studies to date that have tested the effects of low dose of estrogen on oxidative stress and its association with the cardiac autonomic control in ovariectomized rats. Thus, the aim of this study was to test whether the treatment with a low dose of 17-β estradiol to ovariectomized rats could be as effective as a pharmacological dose to reduce the cardiac oxidative stress and improve the SVB.

2. Methods

2.1. Drugs and Reagents. Ketamine hydrochloride was purchased from König Lab S.A., SP, Brazil, and xylazine, from Virbac do Brazil I.P., SP, Brazil. 17-β estradiol and all other drugs/reagents were purchased from Sigma Chemical Co., St. Louis.

2.2. Animals and Groups. In total, 27 female Wistar rats (body weight 200–230 g) from the animal care of the Federal University of Rio Grande do Sul, Brazil, were kept at 20–22°C in a 12 : 12 h dark/light cycle. They were subjected to bilateral ovariectomy under ketamine hydrochloride (80 mg/kg i.p.) and xylazine (16 mg/kg i.p.) anesthesia. After one week following ovariectomy, each ovariectomized animal received subcutaneously (under ketamine and xylazine anesthesia) silastic capsules either filled with 17-β estradiol diluted in sunflower oil (treated groups) or only sunflower oil as a vehicle (ovariectomized control group). Rats were divided into three experimental groups (n = 9, per group): (1) ovariectomized (Ovx) receiving only sunflower oil, (2) animals treated with 40% of the pharmacological (LE; 0.2 mg/pellet for 21 days) dose of estradiol, and (3) animals treated with a pharmacological (HE; 0.5 mg/pellet for 21 days) dose of estradiol [21]. All animals had access to water and regular rodent chow ad libitum. All procedures were approved by the Institutional Animal Care Ethics Committee and the experiments were conducted in accordance with the Guide for the Care and Use of Laboratory Animals (US Department of Health and Human Services, NIH publication number 86-23).

2.3. Hemodynamic Measurements. Under anesthesia (ketamine 80 mg/kg, i.p.; xylazine 16 mg/kg, i.p.), the left carotid artery was cannulated with a PE 50 catheter connected to a strain gauge transducer (Narco Biosystem Pulse Transducer RP-155, Houston, TX, USA) linked to a pressure amplifier (HP 8805C, Hewlett Packard). Pressure readings were recorded on a microcomputer equipped with an analog-to-digital conversion board (WinDaq, 2 kHz sampling frequency; DataQ Instruments, Inc., Akron, OH). The catheter was advanced into the left ventricle (LV) to record the left ventricular systolic pressure (LVSP, mmHg), the left ventricular end-diastolic pressure (LVEDP, mmHg), $+dP/dt$ (mmHg/s), $-dP/dt$ (mmHg/s), and heart rate (HR). After hemodynamic measurements, animals were sacrificed by decapitation for heart and blood collection.

2.4. Autonomic Evaluation. After detecting the pulse intervals, the heart rate was automatically calculated on a beat-to-beat basis as the time interval between two consecutive systolic peaks or pulse interval (PI). All detection was carefully checked to avoid erroneous or missed beats. Sequences of 150–160 beats were randomly chosen and if there was an inconsistent pattern, it was discarded and a new random selection was performed. Frequency domain analysis of HRV was performed with an autoregressive algorithm [22] on the PI interval sequences (tachograms) and on respective systolic sequences (cystograms). The power spectral density was calculated for each time series. In this study, two spectral components were considered: low frequency (LF), from 0.10 to 1.00 Hz and high frequency (HF), from 1.00 to 5.00 Hz. The spectral components were expressed in absolute (abs) and normalized units (nu). Normalization consisted of dividing the power of a given spectral component by the total power, then multiplying the ratio by 100 [23]. All recordings were performed in a sound attenuated room. The ratio of LF/HF, as an index of SVB, was also calculated.

2.5. Plasma Hormone Concentration. Plasma estradiol was measured by electrochemiluminescence (Roche Diagnostics) at the Weinmann Clinical Analysis Laboratory. Briefly, this test employs the principle of competitive assay using a polyclonal antibody against the 17-β estradiol.

2.6. Hydrogen Peroxide Concentration. The assay was based on the horseradish peroxidase- (HRPO-) mediated oxidation of phenol red by H_2O_2, leading to the formation of a compound measureable at 610 nm. Heart slices were incubated for 30 min at 37°C in 10 mmol/L phosphate buffer consisting of

140 mmol/L NaCl and 5 mmol/L dextrose. The supernatants were transferred to tubes with 0.28 mmol/L phenol red and 8.5 U/mL HRPO. After 5 min incubation, 1 mol/L NaOH was added and it was read at 610 nm. The results were expressed in nmol H_2O_2/g tissue [24].

2.7. Determination of Superoxide Anion Concentration. Superoxide anion concentration was determined in heart mitochondrial samples isolated by centrifugations. It was based on the spectrophotometric measurement of the epinephrine oxidation reaction in which superoxide anion is a reactant, leading to the formation of a compound measureable at 480 nm. The results were expressed in mmol/mg protein [25].

2.8. Preparation of Heart Homogenates for Analysis of Antioxidants. Hearts were homogenized in an ultra-Turrax blender using 1 g of tissue for 5 mL of 150 mmol/L potassium chloride added to 20 mmol/L phosphate buffer, pH 7.4. The homogenates were centrifuged at 1000 g for 20 min at −2°C as described elsewhere [26].

2.9. TRAP. Total antioxidant capacity (TRAP) was measured by chemiluminescence using 2,2′-azo-bis(2-amidinopropane) (ABAP, a source of alkyl peroxyl free radicals) and luminol. A mixture consisting of 20 mmol/L ABAP, 40 μmol/L luminol, and 50 mmol/L phosphate buffer (pH 7.4) was incubated to achieve a steady-state luminescence from the free radical-mediated luminol oxidation. A calibration curve was obtained by using different concentrations (between 0.2 and 1 μmol/L) of Trolox (hydrosoluble form of vitamin E). Luminescence was measured in a liquid scintillation counter using the out-of-coincidence mode and the results were expressed in units of Trolox/mg protein [27].

2.10. Determination of Total and Oxidized Glutathione Concentration. To determine oxidized (GSSG) and total glutathione concentration, tissue was homogenized in 2 mol/L perchloric acid and centrifuged at 1000 g for 10 min and 2 mol/L potassium hydroxide was added to the supernatant. The reaction medium contained 100 mmol/L phosphate buffer (pH 7.2), 2 mmol/L NADPH, 0.2 U/mL glutathione reductase, and 70 μmol/L 5,5′ dithiobis (2-nitrobenzoic acid). To determine oxidized glutathione, the supernatant was neutralized with 2 mol/L potassium hydroxide and inhibited by the addition of 5 μmol/L N-ethylmaleimide and absorbance was read at 420 nm [28]. Reduced glutathione (GSH) values were determined from the total and GSSG concentration. The redox status was represented by the GSH/GSSG ratio.

2.11. Determination of Antioxidant Enzyme Activities. Superoxide dismutase activity was expressed as units per milligram of protein and is based on the inhibition of superoxide radical reaction with pyrogallol [29]. Catalase activity was determined in heart homogenates by following the decrease in absorption of hydrogen peroxide. It was expressed as pmol/mg protein [30]. Protein was measured in heart homogenates, using bovine serum albumin as described by Lowry et al. [31].

Table 1: Morphometrics data.

	Ovx ($N = 9$)	LE ($N = 9$)	HE ($N = 9$)
Uterine weight (g)	0.15 ± 0.01	0.63 ± 0.02*	0.89 ± 0.13*†
Body weight (g)	234 ± 11	209 ± 9*	210 ± 7*

Data are mean ± SD. Ovx: ovariectomized group; HE: high dose estrogen-treated group; LE: low dose estrogen-treated group. *$P < 0.05$ versus Ovx; †$P < 0.05$ versus LE.

Table 2: Left ventricular hemodynamic parameters.

	Ovx ($N = 5$)	LE ($N = 5$)	HE ($N = 5$)
LVEDP (mmHg)	12.17 ± 4.54	5.10 ± 1.98*	7.95 ± 2.21*
LVSP (mmHg)	101.71 ± 12.78	120.91 ± 20.71	110.40 ± 7.51
HR (bpm)	212 ± 12.78	221 ± 22.59	183.81 ± 20.83
+dP/dt (mmHg/s)	5809 ± 924	6435 ± 549	5505 ± 450
−dP/dt (mmHg/s)	−3946 ± 786	−5262 ± 890	−4098 ± 251

Data are mean ± SD. Ovx: ovariectomized group; HE: high dose estrogen-treated group; LE: low dose estrogen-treated group. *$P < 0.05$ versus Ovx.

2.12. Statistical Analysis. Data are shown as mean ± standard deviation. Statistical analyses were performed using one-way ANOVA followed by Student Newman-Keuls post hoc test. The Pearson correlation was used to assess the association among variables. $P < 0.05$ was considered significant.

3. Results

3.1. Ovariectomy and Estradiol Therapy. As expected, the ovariectomy decreased plasma estrogen concentration and 17-β estradiol treatment increased its concentration (LE = 587 ± 19 pg/L, HE = 1813 ± 37 pg/L versus Ovx = 58 ± 6 pg/L). This result is in consonance with Paigel et al. [32], who observed serum estrogen levels in ovariectomized rats similar to those observed by us. Moreover, in ovary-intact animals, Paigel et al. [32] found estrogen serum concentration of about 120 pg/L. The 17-β estradiol treatment also significantly ($P < 0.001$) decreased the body weight and increased the uterine weight (Table 1), confirming the effectiveness of hormonal treatment.

3.2. Hemodynamic Parameters. The LVEDP, which is a diastolic function, was significantly ($P < 0.05$) decreased in LE (by 60%) and HE (by 35%) groups when compared to Ovx animals. Moreover, no changes were found in $+dP/dt$, a cardiac contractility index, and $-dP/dt$, a cardiac relaxation index, LVSP, and HR, among any of the groups (Table 2).

3.3. Autonomic Evaluations. Hfabs, which represents the parasympathetic drive, and HRV were significantly higher ($P < 0.05$) in both the HE and LE groups as compared to the Ovx group. LFabs, LFnu, HFnu, and LF/HF ratio did not show any statistically significant differences with estrogen treatment (Table 3).

Table 3: Power spectral analysis.

	Ovx ($N = 5$)	LE ($N = 5$)	HE ($N = 5$)
HRV (ms^2)	14.34 ± 3.56	39.98 ± 11.00*	69.62 ± 27.32*
LFabs (ms^2)	2.49 ± 1.53	5.03 ± 1.89	8.09 ± 7.04
HFabs (ms^2)	9.78 ± 2.84	28.04 ± 9.718*	53.35 ± 29.96*
LFnu	20.22 ± 5.20	16.67 ± 5.12	11.05 ± 3.03
HFnu	79.77 ± 5.14	83.32 ± 5.10	88.95 ± 15.74
LF/HF	0.25 ± 0.07	0.2 ± 0.07	0.12 ± 0.08

Data are mean ± SD. Ovx: ovariectomized group; HE: high dose estrogen-treated group; LE: low dose estrogen-treated group; HRV: heart rate variability; LFabs: absolute low frequency; HFabs: absolute high frequency; LFnu: normalized low frequency; HFnu: normalized high frequency. *$P < 0.05$ versus Ovx.

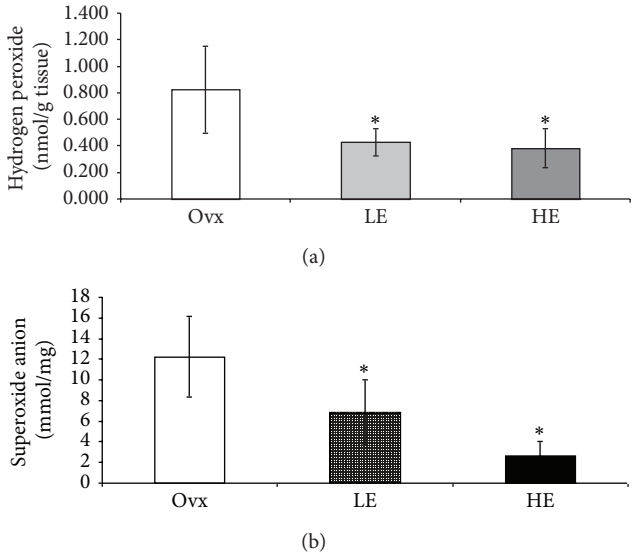

Figure 1: (a) Hydrogen peroxide concentration in myocardium (in nmol/g tissue) and (b) superoxide anion concentration in myocardium (in mmol/mg protein). Data are mean ± SD. $N = 9$ per group. Ovariectomized group = Ovx; ovariectomized group treated for 21 days with low dose of estrogen = LE; ovariectomized group treated for 21 days with high dose of estrogen = HE. *$P < 0.05$ versus Ovx.

3.4. Reactive Oxygen Species Concentrations. Cardiac H_2O_2 concentration (in nmol/g tissue) was significantly decreased ($P < 0.05$) in estrogen groups as compared to the Ovx group (LE = 0.43 ± 0.10; HE = 0.38 ± 0.14 versus Ovx = 0.83 ± 0.32 (Figure 1(a)). Similarly, the cardiac superoxide anion concentration (mmol/mg protein) was significantly ($P < 0.05$) decreased in the treated groups (LE = 6.87 ± 3.13; HE = 2.65 ± 1.37) as compared to the Ovx group (Ovx = 12.22 ± 3.90) (Figure 1(b)).

3.5. TRAP, Glutathione Concentration, and the Redox Ratio. Total antioxidant capacity was significantly higher in estrogen treated groups as compared to the Ovx group. Moreover, a strong positive correlation between TRAP and HRV ($r = 0.8922$; $P < 0.01$) was also observed. GSSG levels decreased in the HE group as compared to Ovx group. The redox

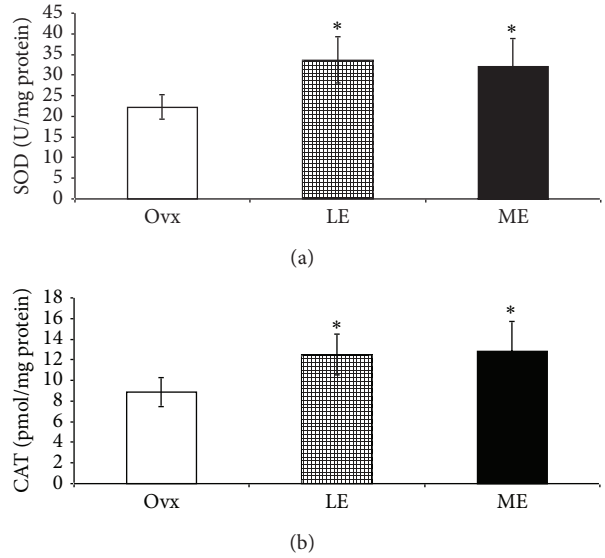

Figure 2: (a) Superoxide dismutase activity (U/mg protein) and (b) catalase activity (pmol/mg protein). Data are mean ± SD. $N = 9$ per group. Ovariectomized group = Ovx; ovariectomized group treated for 21 days with low dose of estrogen = LE; ovariectomized group treated for 21 days with high dose of estrogen = HE. *$P < 0.05$ versus Ovx.

(GSH/GSSG) ratio, which is an index of oxidative stress, and GSH were significantly ($P < 0.05$) higher in both the estrogen treated groups when compared to the Ovx group (Table 4).

3.6. Antioxidant Enzyme Activities. SOD and CAT activities were significantly higher in estrogen treated groups (SOD in U/mg protein: LE = 33.65 ± 5.54; HE = 32.10 ± 6.80; CAT in pmol/mg protein: 12.5 ± 2.0; 12.8 ± 2.9) as compared to the Ovx group (SOD: 22.24 ± 3.00; CAT: 8.9 ± 1.4), and there was no difference between HE and LE groups (Figures 2(a) and 2(b)).

4. Discussion

The present study showed for the first time that a low dose of estrogen is just as effective as a high dose to improve the antioxidant reserve and reduces cardiac oxidative stress. This was associated with a lower LVEDP and higher HRV, which signifies reduced cardiovascular risk.

In this study, we reported a significant decrease in LVEDP in both estrogen-treated groups. This result is in agreement with a study from Bhuiyan et al. [33] who demonstrated similar values of LVEDP in ovariectomized rats. Moreover, we did not observe significant differences in $+dP/dt$, an index of myocardial contractility, or $-dP/dt$, an index of myocardial relaxation, neither in LVSP and HR. Furthermore, our study also is in consonance with Nekooeian and Pang [34] who documented a decrease in LVEDP in rats treated with a pharmacological dose of estrogen. This result suggests a reduction in afterload with maintained systolic function. Indeed, in another study we observed that estrogen therapy induces an increase in aortic nitric oxide bioavailability,

Table 4: Myocardial nonenzymatic antioxidant defenses.

	Ovx ($N = 9$)	LE ($N = 9$)	HE ($N = 9$)
TRAP (units of Trolox/mg protein)	25.50 ± 7.96	57.60 ± 24.13*	53.55 ± 16.15*
Total GSH (nmol/mg protein)	0.18 ± 0.08	0.32 ± 0.06*	0.28 ± 0.14*
GSSG (nmol/mg protein)	0.026 ± 0.008	0.022 ± 0.005	0.014 ± 0.005*
GSH/GSSG	5.98 ± 2.45	13.57 ± 2.23*	19.55 ± 9.03*

Data are mean ± SD. Ovx: ovariectomized group; HE: high dose estrogen-treated group; LE: low dose estrogen-treated group. * $P < 0.05$ versus Ovx.

resulting in an increase in vasodilation and blood pressure reduction [7]. Estradiol has been reported to play a role in mediating a reduction in blood pressure in hypertensive female animal models [7, 35, 36]. Moreover, since nitric oxide is reported to increase diastolic distensibility [37], estrogen treatment could prevent the increase of LVEDP by increasing nitric oxide synthase activity in the heart as reported by others [38].

We did not find changes in LFa, LFnu, HFnu, and LF/HF ratio in the two treated groups. These results are consistent with Schuchert et al. [39] who have also demonstrated no changes in these parameters after estrogen treatment. On the other hand, HFabs, an important index of cardiac parasympathetic modulation [23], was significantly improved after estrogen treatment representing reduced cardiovascular risk [40]. HRV was also increased in the estrogen treated groups. This result is in agreement with Liu et al. [41] who have reported that estrogen therapy is able to improve cardiac autonomic control. Although no changes were found in HR, our results demonstrated that there was a significant increase in HRV after estrogen treatment. This result highlights the effectiveness of estrogen, even in a low dose, to increase HRV and potentially lower the risk factors for cardiovascular complications [42]. More importantly, in our current study, we also found a positive correlation between HRV and TRAP ($r = 0.8922$; $P < 0.01$), suggesting that an increase in the antioxidant capacity might contribute to the improvement in cardiac autonomic control. This association supports the hypothesis that estrogen administration increases nonenzymatic antioxidants, which improves cardiac autonomic control and reduces oxidative stress. According to Semen et al. [43], a decrease in oxidative stress results in an improved HRV. It has also been reported that estrogen therapy leads to an increase in total serum antioxidant capacity resulting in an improvement in the antioxidant status in women [44]. Accordingly, in the treated groups, we have observed an increase in TRAP that represents an index of nonenzymatic antioxidants, especially the hydrosoluble ones. One possible explanation to this preservation in the nonenzymatic antioxidants could be the enhanced antioxidant enzyme activity. In fact, SOD and CAT activities were significantly higher after estrogen treatment. These results are in agreement with others who have reported that estradiol has antioxidant properties whereby it increases CAT [45] and SOD activities and decreases NADPH oxidase enzyme activity and superoxide production [7, 45–47]. In the present study a significant decrease in cardiac concentrations of superoxide anion and hydrogen peroxide in animals treated with estrogen was also documented. These results are in consonance with a study of Lam et al. [48] who demonstrated a significant decrease in superoxide anion production in aortas from ovariectomized rats treated with estrogen. According to our results, the low dose was also able to decrease these ROS concentrations. Additionally, it is widely recognized that estrogen exhibits protective antioxidant effects through the phenolic hydroxyl group of 17-β estradiol that can act as a ROS scavenger [49]. Our findings do suggest that estrogen, even in a low dose, is able to improve the antioxidant defenses and decrease ROS concentrations.

Indeed, GSH/GSSG ratio was significantly increased and GSSG was decreased in our treated groups. These results indicate that there was a reduction in oxidative stress after estrogen treatment. Our data are in agreement with Baeza et al. [50], who also demonstrated that estrogen in a conventional dose was able to decrease oxidative stress in liver, heart, and kidney from ovariectomized rats.

This scenario, where antioxidants are increased and ROS concentration is decreased, contributes to a more favorable redox balance.

5. Conclusion

In conclusion, based on our results, estrogen therapy, even in a low dose, reduced cardiac ROS concentration and increased enzymatic and nonenzymatic antioxidants in ovariectomized rats. This was reflected in improved left ventricle function and cardiac autonomic control. Once these cardioprotective effects were similar in low and high dose of estrogen, it is reasonable to recommend low doses in clinical settings to avoid undesirable side effects associated with the high dose.

Conflict of Interests

The authors declare that there is no conflict of interests that could be perceived as prejudicing the impartiality of the research reported.

Acknowledgment

The authors would like to thank the Weinmann Clinical Analysis Laboratory for performing the hormone measurements.

References

[1] E. Murphy, "Estrogen signaling and cardiovascular disease," *Circulation Research*, vol. 109, no. 6, pp. 687–696, 2011.

[2] J. Hsia, R. D. Langer, J. E. Manson et al., "Conjugated equine estrogens and coronary heart disease: the women's health initiative," *Archives of Internal Medicine*, vol. 166, no. 3, pp. 357–365, 2006.

[3] J. E. Rossouw, R. L. Prentice, J. E. Manson et al., "Postmenopausal hormone therapy and risk of cardiovascular disease by age and years since menopause," *Journal of the American Medical Association*, vol. 297, no. 13, pp. 1465–1477, 2007.

[4] C. Vassalle, A. Mercuri, and S. Maffei, "Oxidative status and cardiovascular risk in women: keeping pink at heart," *World Journal of Cardiology*, vol. 1, pp. 26–30, 2009.

[5] G. Wu, Y. Z. Fang, S. Yang, J. R. Lupton, and N. D. Turner, "Glutathione metabolism and its implications for health," *Journal of Nutrition*, vol. 134, no. 3, pp. 489–492, 2004.

[6] B. Xue, M. Singh, F. Guo, M. Hay, and A. K. Johnson, "Protective actions of estrogen on angiotensin II-induced hypertension: role of central nitric oxide," *The American Journal of Physiology—Heart and Circulatory Physiology*, vol. 297, no. 5, pp. H1638–H1646, 2009.

[7] C. Campos, C. L. Sartorio, K. R. Casali et al., "Low dose estrogen is as effective as high dose treatment in rats with postmenopausal hypertension," *Journal of Cardiovascular Pharmacology*, vol. 63, no. 2, pp. 144–151, 2014.

[8] S. S. Moodithaya and S. T. Avadhany, "Comparison of cardiac autonomic activity between pre and post menopausal women using heart rate variability," *Indian Journal of Physiology and Pharmacology*, vol. 53, no. 3, pp. 227–234, 2009.

[9] D. Kaya, S. Cevrioglu, E. Onrat, I. V. Fenkci, and M. Yilmazer, "Single dose nasal 17beta-estradiol administration reduces sympathovagal balance to the heart in postmenopausal women," *Journal of Obstetrics and Gynaecology Research*, vol. 29, no. 6, pp. 406–411, 2003.

[10] J. S. Petrofsky, E. Lohman, and T. Lohman, "A device to evaluate motor and autonomic impairment," *Medical Engineering and Physics*, vol. 31, no. 6, pp. 705–712, 2009.

[11] G. Mercuro, A. Podda, L. Pitzalis et al., "Evidence of a role of endogenous estrogen in the modulation of autonomic nervous system," *The American Journal of Cardiology*, vol. 85, no. 6, pp. 787–789, 2000.

[12] P. M. McCabe, S. W. Porges, and C. S. Carter, "Heart period variability during estrogen exposure and withdrawal in female rats," *Physiology and Behavior*, vol. 26, no. 3, pp. 535–538, 1981.

[13] A. Yildirir, "Postmenopausal hormone replacement therapy and cardiovascular system," *Turk Kardiyoloji Dernegi Arsivi*, vol. 38, supplement 1, pp. 32–40, 2010.

[14] S. Rozenberg, J. Vandromme, and C. Antoine, "Reactualisation of hormonal treatment at the menopause in 2011," *Revue Medicale de Bruxelles*, vol. 32, no. 4, pp. 239–242, 2011.

[15] H. N. Hodis and W. J. Mack, "Postmenopausal hormone therapy in clinical perspective," *Menopause*, vol. 14, no. 5, pp. 944–957, 2007.

[16] K. A. Matthews, E. Meilahn, L. H. Kuller, S. F. Kelsey, A. W. Caggiula, and R. R. Wing, "Menopause and risk factors for coronary heart disease," *The New England Journal of Medicine*, vol. 321, no. 10, pp. 641–646, 1989.

[17] P. H. Wang, H. C. Horng, M. H. Cheng, H. T. Chao, and K. C. Chao, "Standard and low-dose hormone therapy for postmenopausal women—focus on the breast," *Taiwanese Journal of Obstetrics and Gynecology*, vol. 46, no. 2, pp. 127–134, 2007.

[18] G. Mercuro, C. Vitale, M. Fini, S. Zoncu, F. Leonardo, and G. M. C. Rosano, "Lipid profiles and endothelial function with low-dose hormone replacement therapy in postmenopausal women at risk for coronary artery disease: a randomized trial," *International Journal of Cardiology*, vol. 89, no. 2-3, pp. 257–265, 2003.

[19] R. Schürmann, T. Holler, and N. Benda, "Estradiol and drospirenone for climacteric symptoms in postmenopausal women: a double-blind, randomized, placebo-controlled study of the safety and efficacy of three dose regimens," *Climacteric*, vol. 7, no. 2, pp. 189–196, 2004.

[20] P. H. van de Weijer, L. A. Mattsson, and O. Ylikorkala, "Benefits and risks of long-term low-dose oral continuous combined hormone therapy," *Maturitas*, vol. 56, no. 3, pp. 231–248, 2007.

[21] S. E. Campbell and M. A. Febbraio, "Effect of the ovarian hormones on GLUT4 expression and contraction-stimulated glucose uptake," *The American Journal of Physiology—Endocrinology and Metabolism*, vol. 282, no. 5, pp. E1139–E1146, 2002.

[22] A. Malliani, M. Pagani, F. Lombardi, and S. Cerutti, "Cardiovascular neural regulation explored in the frequency domain," *Circulation*, vol. 84, no. 2, pp. 482–492, 1991.

[23] N. Montano, T. G. Ruscone, A. Porta, F. Lombardi, M. Pagani, and A. Malliani, "Power spectrum analysis of heart rate variability to assess the changes in sympathovagal balance during graded orthostatic tilt," *Circulation*, vol. 90, no. 4 I, pp. 1826–1831, 1994.

[24] E. Pick and Y. Keisari, "A simple colorimetric method for the measurement of hydrogen peroxide produced by cells in culture," *Journal of Immunological Methods*, vol. 38, no. 1-2, pp. 161–170, 1980.

[25] A. Boveris, "Determination of the production of superoxide radicals and hydrogen peroxide in mitochondria," *Methods in Enzymology*, vol. 105, pp. 429–435, 1984.

[26] S. F. Llesuy, J. Milei, and H. Molina, "Comparison of lipid peroxidation and myocardial damage induced by adriamycin and 4′-epiadriamycin in mice," *Tumori*, vol. 71, no. 3, pp. 241–249, 1985.

[27] P. Evelson, M. Travacio, M. Repetto, J. Escobar, S. Llesuy, and E. A. Lissi, "Evaluation of total reactive antioxidant potential (TRAP) of tissue homogenates and their cytosols," *Archives of Biochemistry and Biophysics*, vol. 388, no. 2, pp. 261–266, 2001.

[28] T. P. Akerboom and H. Sies, "Assay of glutathione, glutathione disulfide, and glutathione mixed disulfides in biological samples," *Methods in Enzymology*, vol. 77, no. C, pp. 373–382, 1981.

[29] S. L. Marklund, "Superoxide dismutase isoenzymes in tissues and plasma from New Zealand black mice, nude mice and normal BALB/c mice," *Mutation Research*, vol. 148, no. 1-2, pp. 129–134, 1985.

[30] H. Aebi, "Catalase in vitro," *Methods in Enzymology*, vol. 105, no. C, pp. 121–126, 1984.

[31] O. H. Lowry, N. J. Rosebrough, A. L. Farr, and R. J. Randall, "Protein measurement with the Folin phenol reagent," *The Journal of biological chemistry*, vol. 193, no. 1, pp. 265–275, 1951.

[32] A. S. Paigel, R. F. Ribeiro Junior, A. A. Fernandes, G. P. Targueta, D. V. Vassallo, and I. Stefanon, "Myocardial contractility is preserved early but reduced late after ovariectomy in young female rats," *Reproductive Biology and Endocrinology*, vol. 9, article 54, 2011.

[33] M. S. Bhuiyan, N. Shioda, and K. Fukunaga, "Ovariectomy augments pressure overload-induced hypertrophy associated

with changes in Akt and nitric oxide synthase signaling pathways in female rats," *The American Journal of Physiology—Endocrinology and Metabolism*, vol. 293, no. 6, pp. E1606–E1614, 2007.

[34] A. A. Nekooeian and C. C. Y. Pang, "Estrogen restores role of basal nitric oxide in control of vascular tone in rats with chronic heart failure," *The American Journal of Physiology—Heart and Circulatory Physiology*, vol. 274, no. 6, pp. H2094–H2099, 1998.

[35] Z. Wu, C. Maric, D. M. Roesch, W. Zheng, J. G. Verbalis, and K. Sandberg, "Estrogen regulates adrenal angiotensin AT1 receptors by modulating AT1 receptor translation," *Endocrinology*, vol. 144, no. 7, pp. 3251–3261, 2003.

[36] C. Hinojosa-Laborde, D. L. Lange, and J. R. Haywood, "Role of female sex hormones in the development and reversal of Dahl hypertension," *Hypertension*, vol. 35, no. 1, pp. 484–489, 2000.

[37] B. D. Prendergast, V. F. Sagach, and A. M. Shah, "Basal release of nitric oxide augments the Frank-Starling response in the isolated heart," *Circulation*, vol. 96, no. 4, pp. 1320–1329, 1997.

[38] S. Nuedling, S. Kahlert, K. Loebbert et al., "17β-estradiol stimulates expression of endothelial and inducible NO synthase in rat myocardium in-vitro and in-vivo," *Cardiovascular Research*, vol. 43, no. 3, pp. 666–674, 1999.

[39] A. Schuchert, M. Liebau, G. Behrens, A. O. Mueck, and T. Meinertz, "Are the acute effects of transdermal estradiol in postmenopausal women with coronary artery disease related to changes of the autonomic tone?" *Zeitschrift fur Kardiologie*, vol. 91, no. 2, pp. 156–160, 2002.

[40] F. M. Abboud, S. C. Harwani, and M. W. Chapleau, "Autonomic neural regulation of the immune system: implications for hypertension and cardiovascular disease," *Hypertension*, vol. 59, no. 4, pp. 755–762, 2012.

[41] C. C. Liu, T. B. J. Kuo, and C. C. H. Yang, "Effects of estrogen on gender-related autonomic differences in humans," *The American Journal of Physiology—Heart and Circulatory Physiology*, vol. 285, no. 5, pp. H2188–H2193, 2003.

[42] M. W. Gillman, W. B. Kannel, A. Belanger, and R. B. D'Agostino, "Influence of heart rate on mortality among persons with hypertension: the Framingham Study," *The American Heart Journal*, vol. 125, no. 4, pp. 1148–1154, 1993.

[43] K. O. Semen, O. P. Yelisyeyeva, D. V. Kaminskyy et al., "Interval hypoxic training in complex treatment of Helicobacter pylori-associated peptic ulcer disease," *Acta Biochimica Polonica*, vol. 57, no. 2, pp. 199–208, 2010.

[44] M. Darabi, M. Ani, A. Movahedian, E. Zarean, M. Panjehpour, and M. Rabbani, "Effect of hormone replacement therapy on total serum anti-oxidant potential and oxidized ldl/ß2-glycoprotein i complexes in postmenopausal women," *Endocrine Journal*, vol. 57, no. 12, pp. 1029–1034, 2010.

[45] M. A. Gómez-Zubeldia, S. Corrales, J. Arbués, A. G. Nogales, and J. C. Millán, "Influence of estradiol and gestagens on oxidative stress in the rat uterus," *Gynecologic Oncology*, vol. 86, no. 3, pp. 250–258, 2002.

[46] H. Ji, W. Zheng, S. Menini et al., "Female protection in progressive renal disease is associated with estradiol attenuation of superoxide production," *Gender Medicine*, vol. 4, no. 1, pp. 56–71, 2007.

[47] A. A. Miller, G. R. Drummond, A. E. Mast, H. H. H. W. Schmidt, and C. G. Sobey, "Effect of gender on NADPH-oxidase activity, expression, and function in the cerebral circulation: role of estrogen," *Stroke*, vol. 38, no. 7, pp. 2142–2149, 2007.

[48] K. K. Lam, Y. M. Lee, G. Hsiao, S. Y. Chen, and M. H. Yen, "Estrogen therapy replenishes vascular tetrahydrobiopterin and reduces oxidative stress in ovariectomized rats," *Menopause*, vol. 13, no. 2, pp. 294–302, 2006.

[49] C. Behl, T. Skutella, F. Lezoualc'h et al., "Neuroprotection against oxidative stress by estrogens: structure-activity relationship," *Molecular Pharmacology*, vol. 51, no. 4, pp. 535–541, 1997.

[50] I. Baeza, J. Fdez-Tresguerres, C. Ariznavarreta, and M. De La Fuente, "Effects of growth hormone, melatonin, oestrogens and phytoestrogens on the oxidized glutathione (GSSG)/reduced glutathione (GSH) ratio and lipid peroxidation in aged ovariectomized rats," *Biogerontology*, vol. 11, no. 6, pp. 687–701, 2010.

Hindawi Publishing Corporation
Oxidative Medicine and Cellular Longevity
Volume 2014, Article ID 690953, 7 pages
http://dx.doi.org/10.1155/2014/690953

Research Article

Human Serum Albumin Cys^{34} Oxidative Modifications following Infiltration in the Carotid Atherosclerotic Plaque

Antonio Junior Lepedda,[1] Angelo Zinellu,[1] Gabriele Nieddu,[1] Pierina De Muro,[1] Ciriaco Carru,[1] Rita Spirito,[2] Anna Guarino,[2] Franco Piredda,[3] and Marilena Formato[1]

[1] *Dipartimento di Scienze Biomediche, University of Sassari, Via Muroni 25, 07100 Sassari, Italy*
[2] *Centro Cardiologico "F. Monzino", IRCCS, 20138 Milano, Italy*
[3] *Servizio di Chirurgia Vascolare, Clinica Chirurgica Generale, University of Sassari, 07100 Sassari, Italy*

Correspondence should be addressed to Antonio Junior Lepedda; ajlepedda@uniss.it and Marilena Formato; formato@uniss.it

Received 20 November 2013; Accepted 27 January 2014; Published 6 March 2014

Academic Editor: Constantinos Pantos

Objectives. To evaluate if the prooxidant environment present in atherosclerotic plaque may oxidatively modify filtered albumin. *Methods.* Fluorescein-5-maleimide labelled plasma samples and plaque extracts from 27 patients who had undergone carotid endarterectomy were analysed through nonreducing SDS-PAGE for albumin-Cys^{34} oxidation. Furthermore, degree and pattern of S-thiolation in both circulating and plaque-filtered albumin were assayed. *Results.* Albumin filtered in the atherosclerotic plaque showed higher levels of Cys^{34} oxidative modifications than the corresponding circulating form as well as different patterns of S-thiolation. *Conclusions.* Data indicate that the circulating albumin, once filtered in plaque, undergoes Cys^{34} oxidative modifications and demonstrate for the first time that albumin is a homocysteine and cysteinylglycine vehicle inside the plaque environment.

1. Introduction

Human serum albumin (HSA) is the most abundant multifunctional plasma protein (about 60% of total protein content). It is a small globular protein of 66,438 Da that accounts for both antioxidant functions such as ROS/RNS scavenging, extracellular redox balance, and redox active transition metal ion binding and transport functions for many molecules such as fatty acids, nitric oxide, hemin and drugs [1, 2]. Paradoxically, for cycling transition metal ions such as iron and copper from less reactive (ferric/cupric) to more prooxidant (ferrous/cuprious) states, albumin can also display prooxidant properties [3]. Furthermore, albumin acts as a strong inhibitor of apoptosis in cultured macrophages, neutrophils, lymphocytes, and endothelial cells [4–7]. In its primary structure, it contains 34 cysteine residues that contribute with 17 disulfide bridges to overall tertiary structure and one redox active free cysteine residue (Cys^{34}), responsible for many functions described above [1, 2]. It has been reported that this highly reactive residue, which accounts for 80% (500 μmol/L) of total thiols in plasma, is the preferential plasma scavenger of oxygen and nitrogen reactive species, having an unexpectedly low pKa compared to that of cysteine and glutathione [8].

HSA is present primarily in the reduced form (mercaptalbumin), although about 30–40% could be variably oxidized (nonmercaptalbumin), both reversibly as mixed disulfide with low molecular weight thiols [9], S-nitroso Cys [10], or sulfenic acid and irreversibly as sulfinic or sulfonic acid [11]. Furthermore, recently, it has been described that albumin, through nucleophilic residues and in particular Cys^{34}, is the main plasma target of reactive carbonyl species such as 4-hydroxy-trans-2-nonenal, therefore acting as an endogenous detoxifying agent for these proatherogenic species [12].

Although a large number of clinical studies have associated both the albumin levels and the oxidation state of Cys^{34} to various clinical conditions such as aging [13], renal disease [14], hepatic disease [15], diabetes [16], and coronary artery disease [17–19], little is known about its pathophysiological significance.

Albumin S-thiolation by low molecular weight (LMW) thiols, such as cysteine (Cys), homocysteine (Hcy), cysteinylglycine (Cys-Gly), glutamylcysteine (Glu-Cys), and glutathione (GSH), is the most common Cys^{34} oxidative modification. Even though high plasma levels of homocysteine are known to be an important risk factor in arterial disease, the pathophysiological processes leading to arterial injury have not been fully understood yet. It has been reported that homocysteine promotes vascular endothelial dysfunctions [20], stimulates the proliferation of vascular smooth muscle cells [21], and induces extracellular matrix remodelling through activation of latent metalloproteinases [22, 23]. In this regard, also the activation of the pro-MMP-1, -8, and -9 by S-glutathionylation, via the so-called cysteine switch mechanism, has been described [24]. One interesting hypothesis on the molecular mechanisms of homocysteine action on vascular cells was proposed by Sengupta et al. [25], who suggested that albumin could be homocysteine vehicle inside the cells by some different described endocytic pathways [26–29].

We have previously demonstrated that LDL apolipoprotein B-100 is able to bind all plasma thiols [30–32] and that human carotid atherosclerotic plaques contain all LMW thiols present in plasma but with a different distribution [33]. Recently, by means of a proteomic approach on human carotid atherosclerotic plaques, we evidenced that the majority of extracted proteins were of plasma origin (about 70% of total proteins), with albumin being the most represented, and identified a panel of proteins differentially expressed/oxidized in stable and unstable lesions [34, 35].

The aim of this work was to evaluate if the prooxidant environment present in atherosclerotic plaque could oxidatively modify the filtered albumin. In particular we analysed fluorescein-5-maleimide labelled plasma and plaque extracts by nonreducing SDS-PAGE for Cys^{34} oxidation and assayed degree and pattern of HSA S-thiolation by applying a highly sensitive quantitative method recently developed by our research group [36].

2. Materials and Methods

2.1. Sample Collection. Twenty-seven atherosclerotic plaque specimens were collected from patients undergoing carotid endarterectomy and stored at −80°C until analysis. Blood samples were collected into Vacutainer tubes containing EDTA and immediately processed. After centrifugation at 2,000 g for 10 minutes at 4°C, plasma was separated and stored at −80°C until analysis. Informed consent was obtained before enrolment. The study was approved by the local Ethical Committees of the University of Sassari and of Centro Cardiologico "F. Monzino," IRCCS, in accordance with institution guidelines and conformed to the principles outlined in the Declaration of Helsinki.

2.2. Plaque Proteins Extraction. Plaque segments were thawed at 4°C, washed in phosphate buffered saline to remove residual blood, weighed, and finely minced with a tissue slicer blade. Protein extraction was conducted in a buffer containing 6 mol/L guanidinium chloride, 50 mmol/L sodium acetate, 100 μmol/L 4-amidinophenylmethanesulfonyl fluoride, 2 μg/mL Kallikrein inactivator, and 50 μmol/L leupeptin (pH 7) at a ratio of 7 mL of extraction buffer for 1 g of wet weight tissue, under continuous shaking for 1 hour at room temperature. The resulting suspension was centrifuged at 65,000 g in a TL-100 centrifuge (Beckman Coulter, Brea, USA) for 30 minutes at 20°C. Extracts were delipidated [37] and resolubilized in 250 mmol/L Tris, 4% SDS, pH 7. Protein concentration was quantified with the DC Protein Assay Kit (Bio-Rad, Hercules, USA) using bovine serum albumin as a standard.

2.3. Fluoro-Tagging of Protein Reduced Sulfhydryl Groups. To evaluate HSA-Cys^{34} residue oxidation, we analysed fluorescein-5-maleimide (F5M) labelled plasma samples and plaque extracts by nonreducing SDS-PAGE, followed by fluorescence image acquisition and Coomassie Brilliant Blue G250 staining [35]. A calibration curve with commercial bovine serum albumin, ranging from 0.04 to 1.0 μg, was set up. Both standards and samples were incubated with phosphate buffered saline containing 25-fold molar excess of F5M for two hours in the dark at room temperature following the manufacturer instructions (PIERCE Biotechnology, Rockford, USA). The fluorescent probe used is known to be effective for labelling reduced protein sulfhydryl groups at pH 6.5–7.5 forming a stable thioether bond [38].

2.4. Nonreducing SDS-PAGE. After F5M labelling both standards and samples were solubilised with Laemmli buffer 4X containing 250 mmol/L Tris, 8% SDS, 40% glycerol, 0.0008% bromophenol blue, and pH 6.8 at 60°C for 30 minutes. 4 μL of each of derivatized standards and samples (about 1 μg and 20 μg of total proteins for plasma and plaque extracts, resp.), in duplicate, was resolved by Tris-glycine SDS-PAGE in 0.75 mm thick 10% T, 3% C running gel with a 5% T, 3% C stacking gel, in a Mini-Protean Tetra cell vertical slab gel electrophoresis apparatus (Bio-Rad, Hercules, USA). Electrophoresis was carried out in the dark at 50 V for 15 minutes and subsequently at 150 V until the bromophenol dye front reached the lower limit of the gel. Fluorescence images of resolved proteins were acquired by using the Gel Doc XR system (Bio-Rad). Subsequently, gels were stained with Coomassie Brilliant Blue G250 (CBB) and acquired by using GS-800 calibrated densitometer (Bio-Rad, Hercules, USA) at 63 μm resolution. Gel images were analysed using Quantity One 4.6.3 software (Bio-Rad, Hercules, USA). HSA-fluorescence intensity data were normalized for HSA content.

Precision tests were performed as follows: intra-assay CV was evaluated by measuring fluorescent band intensity/μg_{HSA} in the same sample, independently prepared ten times and loaded in the same gel, while inter-assay CV was determined by carrying out the measure on ten consecutive days.

2.5. HSA-Bound LMW Thiols Analysis. Levels of Cys^{34}-bound LMW thiols were evaluated as described previously [36]. Briefly, circulating and plaque-resident HSA were resolved by nonreducing SDS-PAGE. Then, HSA

Table 1: Levels of HSA-bound LMW thiols in plasma and plaque assayed by CE-LIF analysis.

HSA-bound thiols	Plasma (pmol/nmol HSA)	Plaque (pmol/nmol HSA)	Plaque versus plasma P value*
Cys-Gly	37.5 ± 24.5	5.1 ± 5.6	**<0.001**
Hcy	23.2 ± 8.7	9.8 ± 12.8	**<0.001**
Cys	402.2 ± 150.1	324.2 ± 329.0	0.227
GSH	3.4 ± 1.9	9.6 ± 6.5	**<0.001**
Glu-Cys	1.5 ± 0.9	1.8 ± 1.2	0.347
TOTAL Thiol	468.8 ± 165.2	351.1 ± 345.6	0.097

Values are mean ± SD.
Significant differences are reported in bold ($P < 0.05$).
*Paired Student's t-test.

bands were excised from the gel, destained and LMW thiols extracted by incubating dried bands with 1% tri-n-butylphosphine in aqueous solution (10% tri-n-butylphosphine stock solution in N,N-dimethylformamide). After 5-iodoacetamidofluorescein (5-IAF) derivatization, LMW thiols were resolved by using a P/ACE 5510 CE system with 488 nm Argon ion laser (CE-LIF) (Beckman Coulter, Brea, USA).

2.6. Statistical Analysis. Differences between circulating human serum albumin and the corresponding plaque-filtered form were evaluated by using the paired Student's t-test. Both levels and distribution of LMW thiols in the two forms have been analysed by using Pearson's Product Moment Correlation test.

3. Results

Preliminarily, we set up calibration curves and performed precision tests on the adopted method for evaluating HSA Cys^{34} total oxidation (Figure 1). Fluorescein-5-maleimide is a reagent effective for labelling free sulfhydryl-containing molecules since, at pH 7, the maleimide group is ~1,000 times more reactive toward a free sulfhydryl than to an amine [38]. Intra- and inter-assay CVs were 2.48% and 4.40%, respectively. Analyses evidenced deep differences between the circulating form of HSA and the corresponding filtered in plaque, the latter being about 2.8-fold less fluorescent with a P value < 0.001 (Figure 2).

CE-LIF analyses evidenced no differences in total levels of HSA-bound LMW thiols (35% versus 47% of thiolation, $P = 0.097$) but a significant reduction of Cys-Gly (~7-fold) and Hcy (~2-fold) as well as an increase of GSH (~2.8-fold) in plaque-filtered HSA compared to the circulating form (Table 1 and Figure 3) that reflect distinct patterns of thiolation (Table 2 and Figure 4). Overall, results on Cys^{34} thiolation highlight that, once filtered into the plaque environment, HSA releases 15.8 ± 10.9 and 32.4 ± 24.9 pmoL/nmoL HSA of HCy and Cys-Gly, respectively (corresponding to 16.2 ± 11.2 and 32.8 ± 23.9 nmoL/g extracted proteins for HCy and Cys-Gly, resp.), which is noteworthy considering the high HSA levels in plaque extracts (971.7 ± 536.9 nmoL/g extracted proteins). Pearson's correlation tests showed no correlation between LMW thiols bound to circulating HSA and the corresponding plaque-filtered form (Table 3).

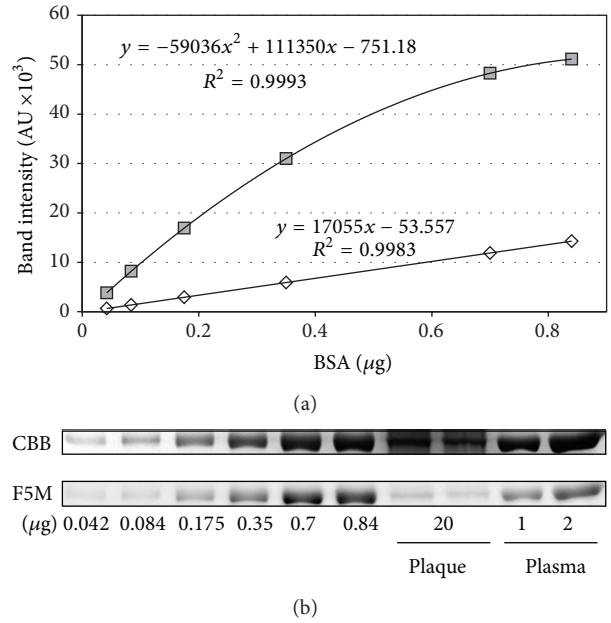

Figure 1: Calibration curves (a) showing a fluorescence linear response of fluorescein-5-maleimide (F5M) labelled BSA over the tested range (0.04–1.0 μg) with a determination coefficient R^2 = 0.998, and a Coomassie Brilliant Blue G-250 (CBB) second order polynomial response with $R^2 = 0.999$ obtained by image analysis on 1D gels (b). AU: arbitrary units; BSA: bovine serum albumin.

4. Discussion

It is generally held that atherosclerotic plaques are characterized by a proinflammatory and prooxidant environment [39]. Previously, by applying proteomics to the study of carotid plaque vulnerability, we identified a panel of proteins differentially expressed in stable/unstable lesions, with prooxidant and proinflammatory potentials, according to our current understanding of the molecular basis of the atherosclerotic process [34]. Furthermore, the study evidenced that about 70% of extractable proteins from plaques were of plasma origin, with albumin being the most represented [34]. Recently,

Table 2: Distribution of HSA-bound LMW thiols in plasma and plaque.

HSA-bound thiols	Plasma (%)	Plaque (%)	Plaque versus plasma P value*
Cys-Gly	8.01 ± 4.22	1.61 ± 1.26	**<0.001**
Hcy	5.10 ± 1.69	2.52 ± 1.07	**<0.001**
Cys	85.84 ± 5.15	89.78 ± 5.80	**<0.001**
GSH	0.73 ± 0.33	5.29 ± 5.55	**<0.001**
Glu-Cys	0.32 ± 0.15	0.79 ± 0.54	**<0.001**

Values are mean ± SD.
Significant differences are reported in bold ($P < 0.05$).
*Paired Student's t-test.

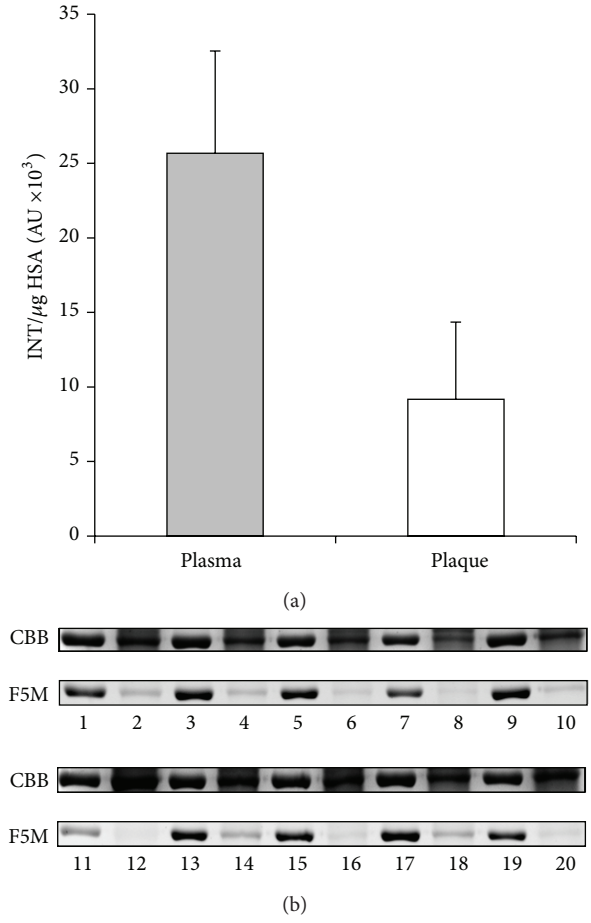

Figure 2: Degree of HSA-Cys^{34} labelling by F5M in plasma and in the corresponding plaque extracts expressed as fluorescent band intensity normalized for μg of HSA (a) obtained by image analysis of 1D gels. Circulating HSA (lanes 1, 3, ...) and the corresponding plaque-filtered form (lanes 2, 4, ...) from 10 representative patients are reported (b). CBB: Coomassie Brilliant Blue; F5M: fluorescein-5 maleimide.

Table 3: Pearson's correlations between HSA-bound LMW-thiols levels in plasma and in plaque.

HSA-bound thiols	Correlation coefficient	P value
Cys-Gly	0.049	0.812
Hcy	−0.144	0.482
Cys	0.275	0.174
GSH	0.269	0.183
Glu-Cys	0.005	0.980

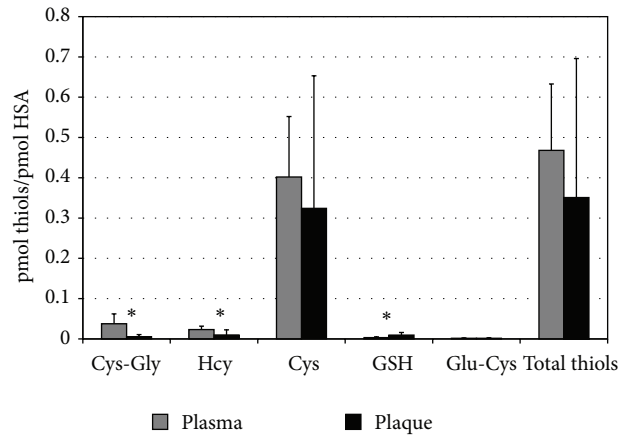

Figure 3: Levels of LMW thiols extracted from both circulating and plaque-filtered HSA, expressed as pmoles per pmoles of albumin, obtained by CE-LIF analysis. *Significant differences between the two HSA forms ($P < 0.001$). Cys-Gly: cysteine-glycine. HCy: homocysteine. Cys: cysteine. GSH: glutathione. Glu-Cys: glutamyl-cysteine.

we focused on some protein oxidative modifications, which might occur in the plaque environment, observing a higher degree of protein sulfhydryl oxidation of both plasma-derived and topically expressed proteins in unstable plaques, partly due to higher levels of S-thiolation [35]. *In situ* oxidative events may have important functional consequences on protein metabolic fate as well as on their bioactivity and antigenic properties. Therefore, in this study, we evaluated albumin Cys^{34} oxidation/thiolation that could follow its subendothelial infiltration in atherosclerotic plaque.

The degree of Cys^{34} oxidation was evaluated by fluorescein-5-maleimide labelling of plasma and plaque extracts. Samples were resolved by nonreducing SDS-PAGE and analysed for fluorescent band intensity after normalization for HSA quantity. The Cys^{34} residue of plaque-filtered HSA was almost 3 times more oxidized with respect to the corresponding circulating form, indicating that the latter, once filtered in plaque, is subjected to Cys^{34} oxidative modifications, probably due to the strong prooxidant environment.

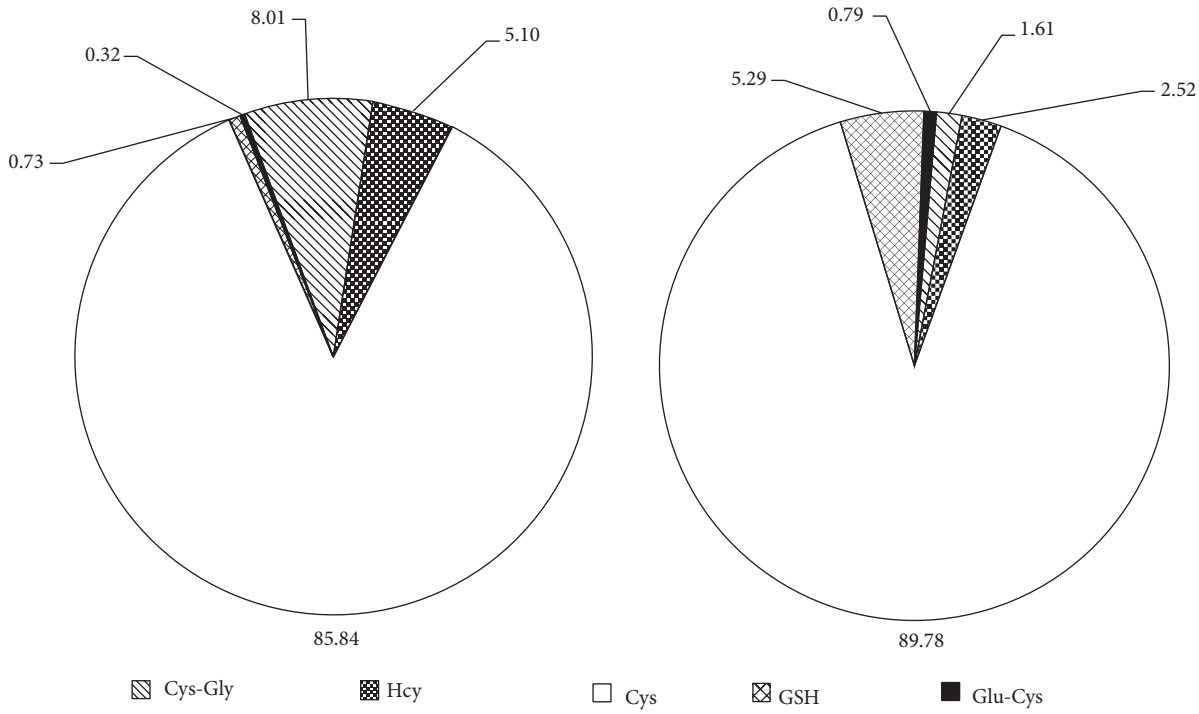

Figure 4: Pattern of S-thiolation of circulating (a) and filtered HSA (b).

Degree and pattern of protein S-thiolation are the result of both reactivity and levels of LMW-thiols and of protein-SH groups microenvironment. S-Thiolation of circulating albumin by LMW thiols is the most prevalent Cys^{34} oxidative modification. Although the proinflammatory mechanisms mediated by LMW thiols are not yet completely understood, one interesting hypothesis suggests that albumin could be an homocysteine vehicle inside the cells where it could exert its noxious effects. In particular, after proteolysis in lysosomes, both Hcy and the other LMW thiols could be released into the cytosol, where they may alter the intracellular redox potential or modify intracellular proteins resulting in cellular dysfunction [25].

We evaluated albumin Cys^{34} thiolation in plasma samples and in the corresponding plaque extracts by a new approach consisting of a preanalytical HSA purification by nonreducing SDS-PAGE, *in gel* extraction of LMW thiols and analysis by CE-LIF [36]. Although no differences in total HSA-bound LMW thiols levels between the circulating and filtered forms were found, the obtained results evidenced pattern of thiolation specific for the vascular compartment in which HSA resides. In confirmation of these findings, Pearson's test indicated no correlation between levels of LMW thiols bound to the two forms. Interestingly, GSH was significantly higher while both Cys-Gly and Hcy were lower in plaque-filtered HSA. Our data demonstrates, for the first time, that, once filtered, albumin releases significant amounts of Hcy and Cys-Gly in the plaque environment corresponding to 16.2 ± 11.2 and 32.8 ± 23.9 nmoL/g extracted proteins, respectively. Compared to our previous data on total and protein-bound intraplaque LMW thiols [33], such levels represent the bulk of free Hcy and Cys-Gly inside the plaque environment. The different equilibrium in the LMW thiols bound to filtered albumin, with respect to the circulating form, could be partly explained by the high intraplaque GSH levels [33]. We hypothesize that, after being filtered into the carotid subendothelial space, albumin is subjected to Cys^{34}-glutathionylation leading to the release of both Hcy and Cys-Gly in the plaque environment. The high intraplaque GSH levels are probably due to cell lysis during apoptotic and/or necrotic events, as suggested by the positive correlation between haemoglobin and GSH levels previously described in carotid plaque extracts [33]. In this regard, haemoglobin represented about 2.6% of total extracted proteins [34], suggesting the relevance of red blood cell lysis in the elevated levels of intraplaque GSH. We have previously demonstrated that circulating LDL apolipoprotein B-100 is able to bind all plasma thiols [30–32]. After infiltration in subendothelial space, oxidative events could lead to proatherogenic LDL isoforms more susceptible to internalization by macrophages. Together with our previous report [33], the present results highlight *in situ* oxidative modifications of plaque extractable protein sulfhydryl groups that could play noteworthy roles in atherosclerotic plaque development and deserve further investigations. Since no differences in the degree of total Cys^{34} thiolation between the two forms of albumin have been detected, the higher degree of oxidation observed could be ascribed to other oxidative modifications driven by ROS, RNS, and reactive electrophilic aldehydes [10–12].

5. Conclusions

By comparing circulating and plaque-filtered HSA, we evidenced that the prooxidant environment present in atherosclerotic plaque could modify filtered proteins also by protein-SH group oxidation, probably contributing to plaque progression. Moreover, the results showed patterns of HSA thiolation specific for the filtered form and demonstrated, for the first time, that albumin is a homocysteine and cysteinylglycine vehicle inside the plaque environment. In this respect, the contribution of GSH to the intra-plaque protein-bound LMW thiols equilibrium seems to be of particular importance. For the first time, such a modification in a plasma protein largely filtered in carotid plaque has been described.

Conflict of Interests

The authors declare that there is no conflict of interests regarding the publication of this paper.

Acknowledgments

The authors thank Dr. Giustina Casu Finlayson for the English language revision. This study was supported by Regione Autonoma della Sardegna (Grant no. CRP-26789 and P.O.R. Sardegna F.S.E. 2007/2013, Asse IV Capitale Umano - Obiettivo competitività regionale e occupazione, Asse IV Capitale umano, Linea di Attività l.3.1) and by "Fondazione Banco di Sardegna" (Sassari, Italy).

References

[1] G. J. Quinlan, G. S. Martin, and T. W. Evans, "Albumin: biochemical properties and therapeutic potential," *Hepatology*, vol. 41, no. 6, pp. 1211–1219, 2005.

[2] T. Peters, *All about Albumin: Biochemistry, Genetics, and Medical Applications*, Academic Press, San Diego, Calif, USA, 1996.

[3] Y. A. Gryzunov, A. Arroyo, J.-L. Vigne et al., "Binding of fatty acids facilitates oxidation of cysteine-34 and converts copper-albumin complexes from antioxidants to prooxidants," *Archives of Biochemistry and Biophysics*, vol. 413, no. 1, pp. 53–66, 2003.

[4] J. Iglesias, V. E. Abernethy, Z. Wang, W. Lieberthal, J. S. Koh, and J. S. Levine, "Albumin is a major serum survival factor for renal tubular cells and macrophages through scavenging of ROS," *The American Journal of Physiology*, vol. 277, no. 5, part 2, pp. F711–F722, 1999.

[5] E. C. Moran, A. S. Kamiguti, J. C. Cawley, and A. R. Pettitt, "Cytoprotective antioxidant activity of serum albumin and autocrine catalase in chronic lymphocytic leukaemia," *British Journal of Haematology*, vol. 116, no. 2, pp. 316–328, 2002.

[6] F. Kouoh, B. Gressier, M. Luyckx et al., "Antioxidant properties of albumin: effect on oxidative metabolism of human neutrophil granulocytes," *Farmaco*, vol. 54, no. 10, pp. 695–699, 1999.

[7] C. Bolitho, P. Bayl, J. Y. Hou et al., "The anti-apoptotic activity of albumin for endothelium is mediated by a partially cryptic protein domain and reduced by inhibitors of G-coupled protein and PI-3 kinase, but is independent of radical scavenging or bound lipid," *Journal of Vascular Research*, vol. 44, no. 4, pp. 313–324, 2007.

[8] L. Turell, R. Radi, and B. Alvarez, "The thiol pool in human plasma: the central contribution of albumin to redox processes," *Free Radical Biology and Medicine*, vol. 65, pp. 244–253, 2013.

[9] Y. Ogasawara, Y. Mukai, T. Togawa, T. Suzuki, S. Tanabe, and K. Ishii, "Determination of plasma thiol bound to albumin using affinity chromatography and high-performance liquid chromatography with fluorescence detection: ratio of cysteinyl albumin as a possible biomarker of oxidative stress," *Journal of Chromatography B*, vol. 845, no. 1, pp. 157–163, 2007.

[10] J. S. Stamler, O. Jaraki, J. Osborne et al., "Nitric oxide circulates in mammalian plasma primarily as an S-nitroso adduct of serum albumin," *Proceedings of the National Academy of Sciences of the United States of America*, vol. 89, no. 16, pp. 7674–7677, 1992.

[11] S. Carballal, B. Alvarez, L. Turell, H. Botti, B. A. Freeman, and R. Radi, "Sulfenic acid in human serum albumin," *Amino Acids*, vol. 32, no. 4, pp. 543–551, 2007.

[12] G. Aldini, G. Vistoli, L. Regazzoni et al., "Albumin is the main nucleophilic target of human plasma: a protective role against pro-atherogenic electrophilic reactive carbonyl species?" *Chemical Research in Toxicology*, vol. 21, no. 4, pp. 824–835, 2008.

[13] W. Dröge, "The plasma redox state and ageing," *Ageing Research Reviews*, vol. 1, no. 2, pp. 257–278, 2002.

[14] A. Soejima, N. Matsuzawa, T. Hayashi et al., "Alteration of redox state of human serum albumin before and after hemodialysis," *Blood Purification*, vol. 22, no. 6, pp. 525–529, 2004.

[15] A. Watanabe, S. Matsuzaki, H. Moriwaki, K. Suzuki, and S. Nishiguchi, "Problems in serum albumin measurement and clinical significance of albumin microheterogeneity in cirrhotics," *Nutrition*, vol. 20, no. 4, pp. 351–357, 2004.

[16] E. Suzuki, K. Yasuda, N. Takeda et al., "Increased oxidized form of human serum albumin in patients with diabetes mellitus," *Diabetes Research and Clinical Practice*, vol. 18, no. 3, pp. 153–158, 1992.

[17] K. Kadota, Y. Yui, R. Hattori, Y. Murohara, and C. Kawai, "Decreased sulfhydryl groups of serum albumin in coronary artery disease," *Japanese Circulation Journal*, vol. 55, no. 10, pp. 937–941, 1991.

[18] L. Djoussé, K. J. Rothman, L. A. Cupples, D. Levy, and R. C. Ellison, "Serum albumin and risk of myocardial infarction and all-cause mortality in the framingham offspring study," *Circulation*, vol. 106, no. 23, pp. 2919–2924, 2002.

[19] M. Schillinger, M. Exner, W. Mlekusch et al., "Serum albumin predicts cardiac adverse events in patients with advanced atherosclerosis—interrelation with traditional cardiovascular risk factors," *Thrombosis and Haemostasis*, vol. 91, no. 3, pp. 610–618, 2004.

[20] R. C. Austin, S. R. Lentz, and G. H. Werstuck, "Role of hyperhomocysteinemia in endothelial dysfunction and atherothrombotic disease," *Cell Death & Differentiation*, vol. 11, supplement 1, pp. S56–S64, 2004.

[21] J.-C. Tsai, M. A. Perrella, M. Yoshizumi et al., "Promotion of vascular smooth muscle cell growth by homocysteine: a link to atherosclerosis," *Proceedings of the National Academy of Sciences of the United States of America*, vol. 91, no. 14, pp. 6369–6373, 1994.

[22] A. Bescond, T. Augier, C. Chareyre, D. Garçon, W. Hornebeck, and P. Charpiot, "Influence of homocysteine on matrix metalloproteinase-2: activation and activity," *Biochemical and Biophysical Research Communications*, vol. 263, no. 2, pp. 498–503, 1999.

[23] S. C. Tyagi, L. M. Smiley, V. S. Mujumdar, B. Clonts, and J. L. Parker, "Reduction-oxidation (Redox) and vascular tissue level of homocyst(e)ine in human coronary atherosclerotic lesions and role in extracellular matrix remodeling and vascular tone," *Molecular and Cellular Biochemistry*, vol. 181, no. 1-2, pp. 107–116, 1998.

[24] T. Okamoto, T. Akaike, T. Sawa, Y. Miyamoto, A. van der Vliet, and H. Maeda, "Activation of matrix metalloproteinases by peroxynitrite-induced protein S-glutathiolation via disulfide S-oxide formation," *The Journal of Biological Chemistry*, vol. 276, no. 31, pp. 29596–29602, 2001.

[25] S. Sengupta, H. Chen, T. Togawa et al., "Albumin thiolate anion is an intermediate in the formation of albumin-S-S-homocysteine," *The Journal of Biological Chemistry*, vol. 276, no. 32, pp. 30111–30117, 2001.

[26] J. E. Schnitzer and P. Oh, "Albondin-mediated capillary permeability to albumin. Differential role of receptors in endothelial transcytosis and endocytosis of native and modified albumins," *The Journal of Biological Chemistry*, vol. 269, no. 8, pp. 6072–6082, 1994.

[27] C. Tiruppathi, A. Finnegan, and A. B. Malik, "Isolation and characterization of a cell surface albumin-binding protein from vascular endothelial cells," *Proceedings of the National Academy of Sciences of the United States of America*, vol. 93, no. 1, pp. 250–254, 1996.

[28] J. E. Schnitzer, A. Sung, R. Horvat, and J. Bravo, "Preferential interaction of albumin-binding proteins, gp30 and gp18, with conformationally modified albumins. Presence in many cells and tissues with a possible role in catabolism," *The Journal of Biological Chemistry*, vol. 267, no. 34, pp. 24544–24553, 1992.

[29] J. E. Schnitzer and J. Bravo, "High affinity binding, endocytosis, and degradation of conformationally modified albumins. Potential role of gp30 and gp18 as novel scavenger receptors," *The Journal of Biological Chemistry*, vol. 268, no. 10, pp. 7562–7570, 1993.

[30] A. Zinellu, S. Sotgia, L. Deiana, and C. Carru, "Quantification of thiol-containing amino acids linked by disulfides to LDL," *Clinical Chemistry*, vol. 51, no. 3, pp. 658–660, 2005.

[31] A. Zinellu, S. Sotgia, E. Zinellu et al., "Distribution of low-density lipoprotein-bound low-molecular-weight thiols: a new analytical approach," *Electrophoresis*, vol. 27, no. 13, pp. 2575–2581, 2006.

[32] A. Zinellu, E. Zinellu, S. Sotgia et al., "Factors affecting S-homocysteinylation of LDL apoprotein B," *Clinical Chemistry*, vol. 52, no. 11, pp. 2054–2059, 2006.

[33] A. Zinellu, A. Lepedda Jr., S. Sotgia et al., "Evaluation of low molecular mass thiols content in carotid atherosclerotic plaques," *Clinical Biochemistry*, vol. 42, no. 9, pp. 796–801, 2009.

[34] A. J. Lepedda, A. Cigliano, G. M. Cherchi et al., "A proteomic approach to differentiate histologically classified stable and unstable plaques from human carotid arteries," *Atherosclerosis*, vol. 203, no. 1, pp. 112–118, 2009.

[35] A. J. Lepedda, A. Zinellu, G. Nieddu et al., "Protein sulfhydryl group oxidation and mixed-disulfide modifications in stable and unstable human carotid plaques," *Oxidative Medicine and Cellular Longevity*, vol. 2013, Article ID 403973, 8 pages, 2013.

[36] A. Zinellu, A. Lepedda Jr., S. Sotgia et al., "Albumin-bound low molecular weight thiols analysis in plasma and carotid plaques by CE," *Journal of Separation Science*, vol. 33, no. 1, pp. 126–131, 2010.

[37] R. Mastro and M. Hall, "Protein delipidation and precipitation by tri-n-butylphosphate, acetone, and methanol treatment for isoelectric focusing and two-dimensional gel electrophoresis," *Analytical Biochemistry*, vol. 273, no. 2, pp. 313–315, 1999.

[38] D. J. Bigelow and G. Inesi, "Frequency-domain fluorescence spectroscopy resolves the location of maleimide-directed spectroscopic probes within the tertiary structure of the Ca-ATPase of sarcoplasmic reticulum," *Biochemistry*, vol. 30, no. 8, pp. 2113–2125, 1991.

[39] P. Libby, "Inflammation in atherosclerosis," *Arteriosclerosis, Thrombosis, and Vascular Biology*, vol. 32, no. 9, pp. 2045–2051, 2012.

Hindawi Publishing Corporation
Oxidative Medicine and Cellular Longevity
Volume 2014, Article ID 123963, 11 pages
http://dx.doi.org/10.1155/2014/123963

Research Article

Sulforaphane Attenuation of Type 2 Diabetes-Induced Aortic Damage Was Associated with the Upregulation of Nrf2 Expression and Function

Yonggang Wang,[1,2] Zhiguo Zhang,[1,2] Wanqing Sun,[1] Yi Tan,[2,3,4] Yucheng Liu,[2] Yang Zheng,[1] Quan Liu,[1] Lu Cai,[2,3,4] and Jian Sun[1]

[1] *Cardiovascular Center at the First Hospital of Jilin University, 71 Xinmin Street, Changchun 130021, China*
[2] *Kosair Children's Hospital Research Institute, Department of Pediatrics, University of Louisville, Louisville, KY 40202, USA*
[3] *The Chinese-American Research Institute, Wenzhou Medical University, Wenzhou 325035, China*
[4] *Departments of Radiation Oncology, Pharmacology and Toxicology, University of Louisville, Louisville, KY 40292, USA*

Correspondence should be addressed to Lu Cai; l0cai001@louisville.edu and Jian Sun; sunjianemail@126.com

Received 3 November 2013; Revised 11 December 2013; Accepted 6 January 2014; Published 23 February 2014

Academic Editor: Adriane Belló-Klein

Type 2 diabetes mellitus (T2DM) significantly increases risk for vascular complications. Diabetes-induced aorta pathological changes are predominantly attributed to oxidative stress. Nuclear factor E2-related factor-2 (Nrf2) is a transcription factor orchestrating antioxidant and cytoprotective responses to oxidative stress. Sulforaphane protects against oxidative damage by increasing Nrf2 expression and its downstream target genes. Here we explored the protective effect of sulforaphane on T2DM-induced aortic pathogenic changes in C57BL/6J mice which were fed with high-fat diet for 3 months, followed by a treatment with streptozotocin at 100 mg/kg body weight. Diabetic and nondiabetic mice were randomly divided into groups with and without 4-month sulforaphane treatment. Aorta of T2DM mice exhibited significant increases in the wall thickness and structural derangement, along with significant increases in fibrosis (connective tissue growth factor and transforming growth factor), inflammation (tumor necrosis factor-α and vascular cell adhesion molecule 1), oxidative/nitrative stress (3-nitrotyrosine and 4-hydroxy-2-nonenal), apoptosis, and cell proliferation. However, these pathological changes were significantly attenuated by sulforaphane treatment that was associated with a significant upregulation of Nrf2 expression and function. These results suggest that sulforaphane is able to upregulate aortic Nrf2 expression and function and to protect the aorta from T2DM-induced pathological changes.

1. Introduction

Type 2 diabetes mellitus (T2DM) is a growing public health problem, associated with a substantial burden of morbidity and mortality [1]. Youth with T2DM had higher rates of all complications than nondiabetes subjects, and an overall 6.15-fold increased risk of any vascular disease [2]. Individuals with T2DM have a unique propensity towards microvascular and macrovascular diseases [3]. The macrovascular disorders include atherosclerosis, coronary artery disease, and peripheral vascular diseases. Although application of drugs and changing life style had been widely promoted to control the complications, unfortunately, the preventive of the development and progression of vascular complications in the diabetic patients remains unoptimistic [4]. Therefore, an effective approach to prevent and/or delay the development and progression of diabetic vascular complications urgently needs to be developed.

Impaired endothelial function is considered as a major diabetic vascular alteration, which may be mainly derived from diabetes-induced overexpression of inflammation. Diabetic inflammation in the vascular endothelium leads to continuous infiltration and accumulation of leukocytes at sites of endothelial cell injury. Consistent with our previous studies, vascular inflammatory response was increased in diabetic mice reflect by increased expression of tumor necrosis factor-alpha (TNF-α) and vascular cell adhesion molecule 1 (VCAM-1) [5, 6]. It is known that inflammation and oxidative

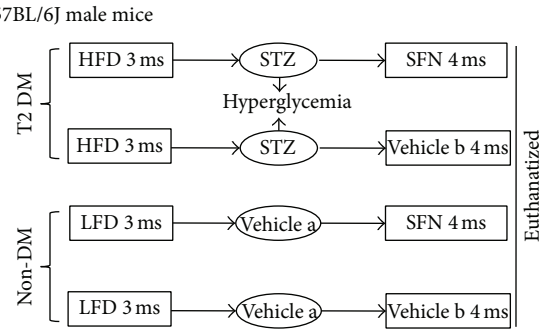

Figure 1: Schematic illustration for the animal experimental design.

stress are reciprocal cause and outcomes [7]. There was also increasing evidence indicating that the increased production of reactive oxygen and/or nitrogen species (ROS and/or RNS) is the major pathogenic factor responsible for the development and progression of vascular complications in diabetic patients, although several other mechanisms are also proposed [8–10]. Clinical trials with single antioxidants or a few have shown ineffective intervention in diabetic patients [6, 9–11]; therefore, upregulation of multiple endogenous antioxidants may be a better approach for the prevention of diabetic vascular complications. Transcription factor nuclear factor E2-related factor-2 (Nrf2) has been shown to play a pivotal role in cellular preventing against oxidative stress and damage *in vitro* and *in vivo* [12, 13]. Under physiological conditions, Nrf2 generally localizes in the cytoplasm and binds to its inhibitor Kelch-like ECH-associated protein 1 (Keap1) [14]; however, under oxidative or electrophilic stress conditions, Nrf2 detaches from Keap1 and translocates into the nucleus to bind to antioxidant-responsive elements (ARE) in the promoter region of its downstream genes, such as NADPH quinoneoxidoreductase (NQO1), heme oxygenase-1 (HO-1), glutathione S-transferase (GST), superoxide dismutase (SOD), catalase (CAT), and other genes regulating the responses to oxidative stress [15, 16]. The Nrf2-ARE pathway is important in the cellular detoxification, antioxidant, and anti-inflammatory system to protect the cell and tissue from oxidative stress [17, 18]. Therefore, Nrf2 is widely appreciated for its potential prevention of and/or therapy for diabetic vascular complications [5, 19].

Sulforaphane (SFN) is an isothiocyanate that is found in cruciferous vegetables and has a strong cytoprotective function against oxidative stress. This beneficial effect was mediated by its direct interaction with Keap1, resulting in the disruption of Nrf2—Keap1 interaction. Released Nrf2 from Keap1 enters into the nucleus to induce the expression of Nrf2 downstream antioxidant genes [14]. Evidence has confirmed the specific cysteine residues of Keap1 that act as "sensors" to be modified by SFN [20]. SFN as a Nrf2 activator [21] has been reported to prevent oxidative damage [22] and cardiovascular diseases [23]. SFN has garnered particular interests as an indirect antioxidant due to its extraordinary ability to induce expression of endogenous, multiple enzymes via the upregulation of Nrf2 function [24]. Our previous study has found that SFN had a beneficial effect on type 1 diabetic vascular complications [5]. However, there was no report yet whether SFN can prevent the development of aortic pathogenesis alterations in T2DM.

To this end, we used a type 2 diabetic mouse model to verify the protective function of SFN against diabetic aortic damage and dissect the underlying mechanisms. The experimental design was illustrated in Figure 1. Type 2 diabetic and age-matched control mice were treated with SFN for 4 months. At the end of 4 months treatment of SFN mice were euthanized for collecting tissues to perform the experimental measurements.

2. Materials and Methods

2.1. Animals. C57BL/6J male mice, 8–10 weeks of age, were purchased from the Jackson Laboratory (Bar Harbor, Maine) and housed at the University of Louisville Research Resources Center at 22°C with a 12 h light/dark cycle with free access to food and tap water. All experimental procedures for these animals were approved by the Institutional Animal Care and Use Committee of the University of Louisville, which is compliant with the Guide for the Care and Use of Laboratory Animals published by the US National Institutes of Health (NIH Publication number 85–23, revised 1996).

2.2. Type 2 Diabetes Model. To establish type 2 diabetic model, mice were fed with high-fat diet (HFD, Research Diets 12492, 60% kcal from fat) for 3 months, which made these mice become significantly obese (44.6 ± 2.9 g for HFD versus 32.4 ± 1.5 g for control, $P < 0.05$). Insulin resistance was also induced, shown by the increased area size under curves for both *Intraperitoneal (IP) glucose tolerance test (IPGTT)* (35493.28 ± 5270.90 for HFD versus 25114.82 ± 4630.55 for control, $P < 0.05$) and *IP insulin tolerance test (IPITT)* (15403.26 ± 3252.76 for HFD versus 9790.5 ± 3462.36 for control, $P < 0.05$). These insulin resistant mice were randomly injected intraperitoneally with STZ (Sigma-Aldich, St. Louis, MO, dissolved in 0.1 M sodium citrate (pH4.5, Vehicle a, Figure 1)) at 100 mg/kg body weight once [25, 26]. Five days after STZ injection, mice with hyperglycemia (blood glucose levels ≥ 250 mg/dL, blood sample collected from the tail vein measured using a Free Style Lite glucometer (Abbott Diabetes Care, Alameda, CA)) were defined as diabetic. In parallel, age-matched control mice were given low-fat diet (LFD, Research Diets 12450B, 10% kcal from fat) for 3 month, followed by an injection of the same volume of sodium citrate buffer when HFD-fed mice were received STZ injection. Both diabetic and control mice continually received HFD or LFD feeding for additional 4 months (Figure 1). During this 4-month period, both diabetic and control mice were further divided into two groups, with and without SFN treatment (Sigma-Aldich), which were given SFN at 0.5 mg/kg subcutaneously for five days per week. Dose of SFN used was based on our previous study [27].

At the end of the additional 4 months, these diabetic mice remained showing the significantly increased insulin resistance (29230 ± 3173.43 for HFD versus 7947.50 ± 1209.02 for control, $P < 0.05$) and blood glucose (324.66 ± 51.07 for HFD versus 116.00 ± 11.04 for control, $P < 0.05$), insulin

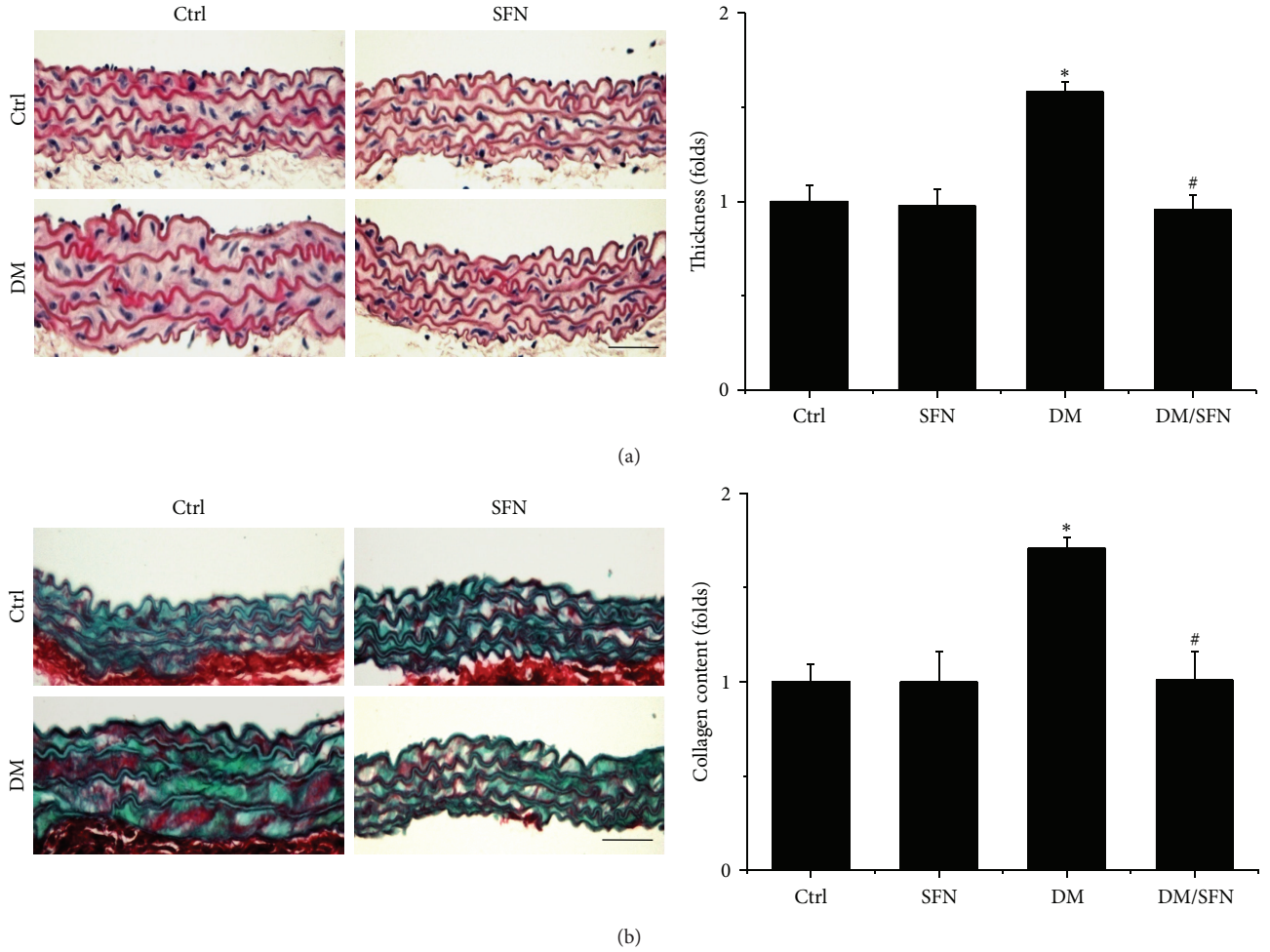

FIGURE 2: Protective effect of SFN on diabetes-induced aortic pathological changes. The pathogenic changes of aortas were examined by H&E staining (a) and the accumulation of collagen was detected by Sirius-red staining (b), followed by semiquantitative analysis. Data were presented as means ± SD ($n = 6$); $^{*}P < 0.05$ versus corresponding Ctrl; $^{\#}P < 0.05$ versus corresponding DM. Bar = 50 μM.

(0.8293 ± 0.13 for HFD versus 0.55 ± 0.05 for control, $P < 0.05$), triglyceride (395.05 ± 64.43 for HFD versus 48.48 ± 4.80 for control, $P < 0.05$), and cholesterol (139.12 ± 6.53 for HFD versus 80.39 ± 15.56 for control, $P < 0.05$) levels; all of which are typical magnifications, suggesting the induction of T2DM. In summary, there were four groups of mice ($n = 6$ at least per group): LFD control (Ctrl), LFD/SFN (SFN), type 2 diabetes (DM), and DM plus SFN (DM/SFN). At the end of 4 months of SFN treatment, mice were euthanatized for experimental measurements. Since SFN was dissolved in 1% dimethyl sulfoxide (DMSO) and diluted in PBS, mice serving as controls were also subcutaneously given the same volume of PBS containing 1% DMSO (Vehicle b, Figure 1), based on our own and other studies [27–29].

2.3. Aorta Preparation and Histopathological Examination. After mice were anesthetized with 2,2,2-tribromoethanol (commercial name: avertin) at 4–6 mg/kg body weight, thoraxes were opened and the descending thoracic aortas were isolated carefully without rips or cuts. Aortic tissues were fixed in 10% buffered formalin overnight. The fixed tissues were cut into ringed segments (approx. 2-3 mm in length) so they can be dehydrated in graded alcohol series, clean with xylene, embedded in paraffin, and sectioned at 5 μm thickness for pathological and immunohistochemical or immunofluorescent staining. Histological evaluation of aorta was performed by H&E staining. The thickness of aorta was evaluated by measuring the width of tunica media using Image Pro Plus 6.0 software. For immunohistochemical or immunofluorescent staining, paraffin sections from aortic tissues were dewaxed, incubated with 1x Target Retrieval Solution (Dako, Carpinteria, CA) in a microwave oven for 15 min at 98°C for antigen retrieval, followed by 3% hydrogen peroxide for 10 min at room temperature and 5% bovine serum albumin for 60 min, respectively. These sections were then incubated with primary antibodies against connective tissue growth factor (CTGF) at 1 : 100 dilution (BD Bioscience, San Jose, CA) and transforming growth factor (TGF-β1) at 1 : 100 dilution (Santa Cruz Biotechnology, Santa Cruz, CA, USA), tumor necrosis factor-alpha (TNF-α) at 1 : 50 dilution (Abcam, Cambridge, MA), vascular cell adhesion molecule 1 (VCAM-1) at 1 : 100 dilution (Santa Cruz

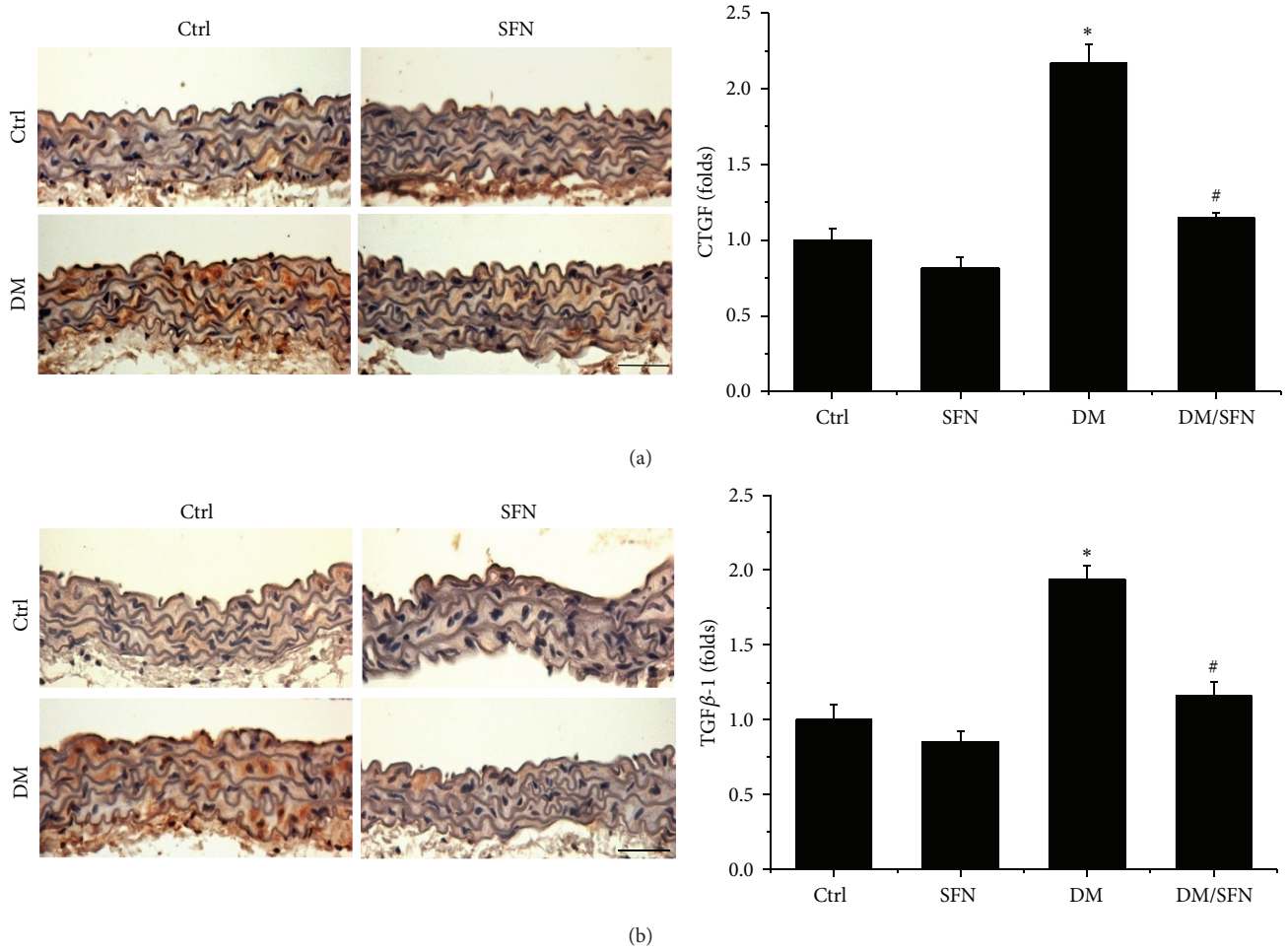

Figure 3: Protective effect of SFN on diabetes-induced aortic fibrosis. Aortic fibrosis was examined by immunohistochemical staining for the expression of CTGF (a) and TGF-β1 (b), followed by semiquantitative analysis. Data were presented as means ± SD ($n = 6$); $^{*}P < 0.05$ versus corresponding Ctrl; $^{\#}P < 0.05$ versus corresponding DM. Bar = 50 μM.

Biotechnology, Santa Cruz, CA, USA), 3-nitrotyrosine (3-NT) at 1 : 400 dilution (Millipore, Billerica, CA), 4-hydroxy-2-nonenal (4-HNE) at 1 : 400 dilution (Alpha Diagnostic International, San Antonio, TX), Nrf2 at 1 : 50 dilution, and Cu-Zn super oxide dismutase-1 (SOD-1) at 1 : 400 dilution (both from Santa Cruz Biotechnology, Santa Cruz, CA, USA) over night at 4°C. Afterwards sections were washed with PBS, and incubated with horseradish peroxidase conjugated secondary antibody (1 : 100–400 dilutions with PBS) or Cy3-coupled donkey anti-rabbit or anti-goat IgG secondary antibody (1 : 200 dilution with PBS) for 1 h at room temperature. For color development purposes, immunohistochemical staining sections were treated with peroxidase substrate DAB kit (Vector Laboratories, Inc. Burlingame, CA) and counterstained the nuclei with hematoxylin, while immunofluorescent staining sections were stained with DAPI at 1 : 1000 dilution to localize the nucleus.

For quantitative analysis of these immunohistochemical and immunofluorescent staining, the Nikon Eclipse E600 microscopy system was used and 3 sections at interval of 10 sections from each aorta (per mouse) were selected and at least five high-power fields randomly sections were randomly recaptured. Image Pro Plus 6.0 software was used to translate the interesting area staining density into an integrated optical density (IOD) that was divided by the area size of interest to reflect the staining intensity, and the ratio of IOD/area size in experimental group was presented as a fold relative to that of control.

2.4. Sirius-Red Staining for Collagen. Aortic fibrosis was detected by Sirius-red staining of collagen, as described in our previous study [6]. Briefly sections were stained with 0.1% Sirius-red F3BA and 0.25% Fast Green FCF. The stained sections were then assessed for the presence of collagen using a Nikon Eclipse E600 microscopy system.

2.5. Terminal Deoxynucleotidyl-Transferase-Mediated dUTP Nick-End Labeling (TUNEL) Staining. TUNEL staining was performed with formalin-fixed, paraffin-embedded sections using peroxidase *in situ* Apoptosis Detection Kit S7100 (Millipore, Billerica, MA), according to the manufacture's instruction. The positively stained apoptotic cells were counted randomly in five microscopic fields at least for each of the three slides from each mouse under light microscopy. The

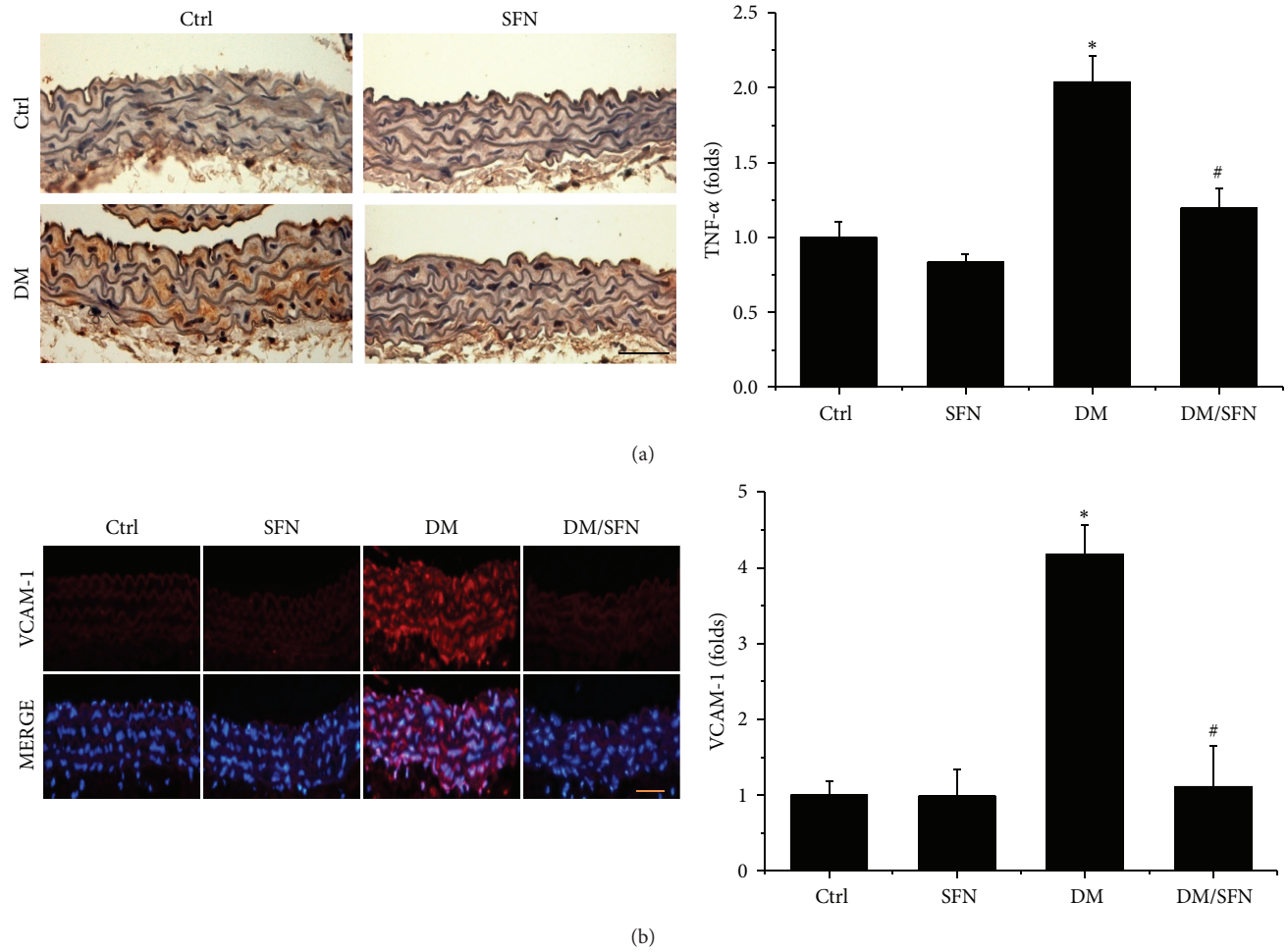

Figure 4: Protective effect of SFN on diabetes-induced aortic inflammation. Aortic inflammation was examined by immunohistochemical staining for the expression of TNF-α (a) and immunofluorescent staining for the expression of VCAM-1 (red) (b), followed by semiquantitative analysis. Data were presented as means ± SD ($n = 6$); $^{*}P < 0.05$ versus corresponding Ctrl; $^{\#}P < 0.05$ versus corresponding DM. Bar = 50 μM.

percentage of TUNEL positive cells relative to 100 nuclei was presented.

2.6. Proliferating Cell Nuclear Antigen (PCNA) Staining. The PCNA staining kit (Invitrogen, Camarillo, CA) was used for staining proliferating cells, according to the manufacture's instruction. The positively stained proliferating cells were counted randomly in five microscopic fields at least for each of the three slides per mouse under light microscopy. The percentage of PCNA positive cells relative to 100 nuclei was presented.

2.7. Real-Time qPCR. Aortas were frozen with liquid nitrogen and stored at −80°C. Total RNA was extracted using the TRIzol Reagent (Invitrogen, USA). RNA concentrations and purity were quantified using a Nanodrop ND-1000 spectrophotometer. First-strand complimentary DNA (cDNA) was synthesized from total RNA according to manufacturer's protocol from the RNA PCR kit (Promega, Madison, WI). Reverse transcription was performed using 0.5 μg of total RNA in 12.5 μL of the solution containing 4 μL 25 mM $MgCl_2$, 4 μL AMV reverse transcriptase 5x buffer, 2 μL dNTP, 0.5 μL RNase inhibitor, 1 μL of AMV reverse transcriptase, and 1 μL of oligodT primer, which were added with nuclease-free water to make a final volume of 20 μL. Reaction system was run at 42°C for 50 min and 95°C for 5 min. Primers of Nrf2, SOD-1, HO-1, and GAPDH were purchased from Applied Biosystems (Carlsbad, CA). Real-time quantitative PCR (qPCR) was carried out in a 20 μL reaction buffer that included 10 μL of TaqMan Universal PCR Master Mix, 1 μL of primer, and 9 μL of cDNA with the ABI 7300 Real-Time PCR system. The fluorescence intensity of each sample was measured at each temperature change to monitor amplification of the target gene. The comparative cycle time (CT) was used to determine fold differences between samples.

2.8. Statistical Analysis. Data were presented as mean ± SD ($n = 6$). Comparisons were performed by two-way ANOVA for the different groups. When there was significant difference among groups, the repetitive comparing Tukey's test was used to further analyse with Origin 7.5 Lab data analysis and

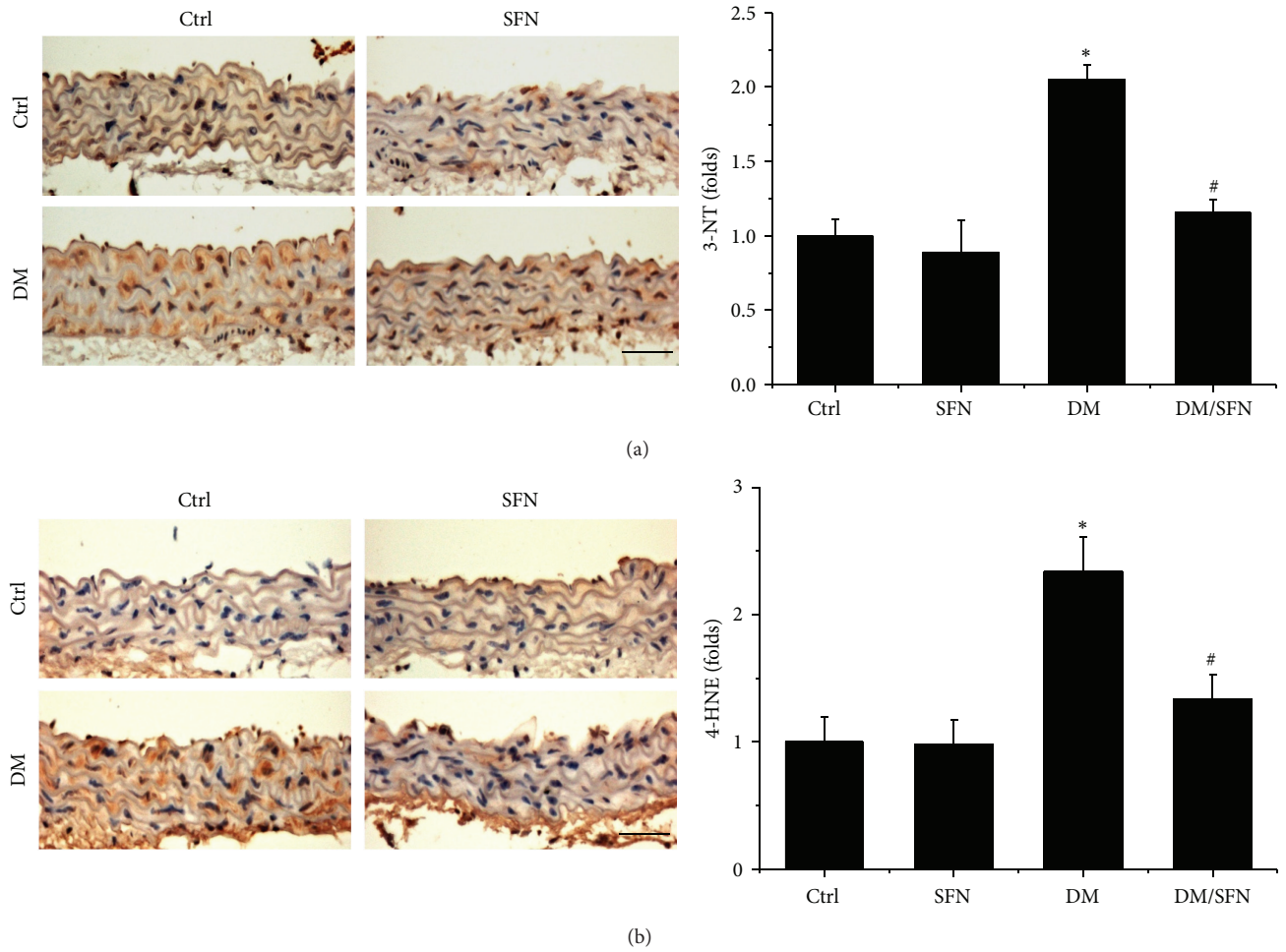

Figure 5: Protective effect of SFN on diabetes-induced aortic oxidative damage. Aortic oxidative damage was examined by immunohistochemical staining for the accumulation of 3-NT (a) and 4-HNE (b), followed by semiquantitative analysis. Data were presented as means ± SD ($n = 6$); $^{*}P < 0.05$ versus corresponding Ctrl; $^{\#}P < 0.05$ versus corresponding DM. Bar = 50 μM.

graphing software. $P < 0.05$ was considered as statistical significance.

3. Result

3.1. SFN Prevented T2DM-Induced Aortic Pathological Changes and Fibrosis. At the end of experiment, aortas were examined pathologically by H&E staining, which displayed significantly increase of the tunica media thickness in T2DM mice (Figure 2(a)). Sirius-red staining also revealed an increased collagen accumulation in tunica media of aortas in T2DM group (Figure 2(b)). However, all these pathological changes observed in the aortas of T2DM mice were completely prevented by the 4-month SFN treatment.

To further detect the preventive effect of SFN on T2DM-induced aortic fibrosis, immunohistochemical staining showed the increased expression of profibrotic mediators, CTGF (Figure 3(a)), and TGF-β1 (Figure 3(b)), in aortic tunica media of diabetic mice. Supplementation with SFN completely prevented these fibrotic responses in the aortas of type 2 diabetic plus SFN mice (DM/SFN group).

3.2. SFN Prevented T2DM-Induced Aortic Inflammation and Oxidative Damage. On account of the fact that both inflammation and oxidative damage are primary risk factors for the vascular endothelium remodeling, the expression of TNF-α (Figure 4(a)) and VCAM-1 (Figure 4(b)) was examined with immunohistochemical and immunofluorescent staining, which showed a significant increase in aortic tunica media of T2DM mice, an effect that was completely prevented by 4-month SFN treatment.

Considering that inflammation and oxidative stress are reciprocal cause and outcomes, oxidative and nitrative damage was examined by immunohistochemical staining for increased accumulation of 3-NT (Figure 5(a)) and 4-HNE (Figure 5(b)), which was found to be significantly increased in the aortic tunica media of T2DM mice. However, treatment with SFN for 4 months completely prevented the oxidative damage (Figures 5(a) and 5(b)).

3.3. SFN Prevented T2DM-Induced Aortic Apoptotic Cell Death and Proliferation. We recently reported the induction of apoptotic cell death and cell proliferation in the aortas of

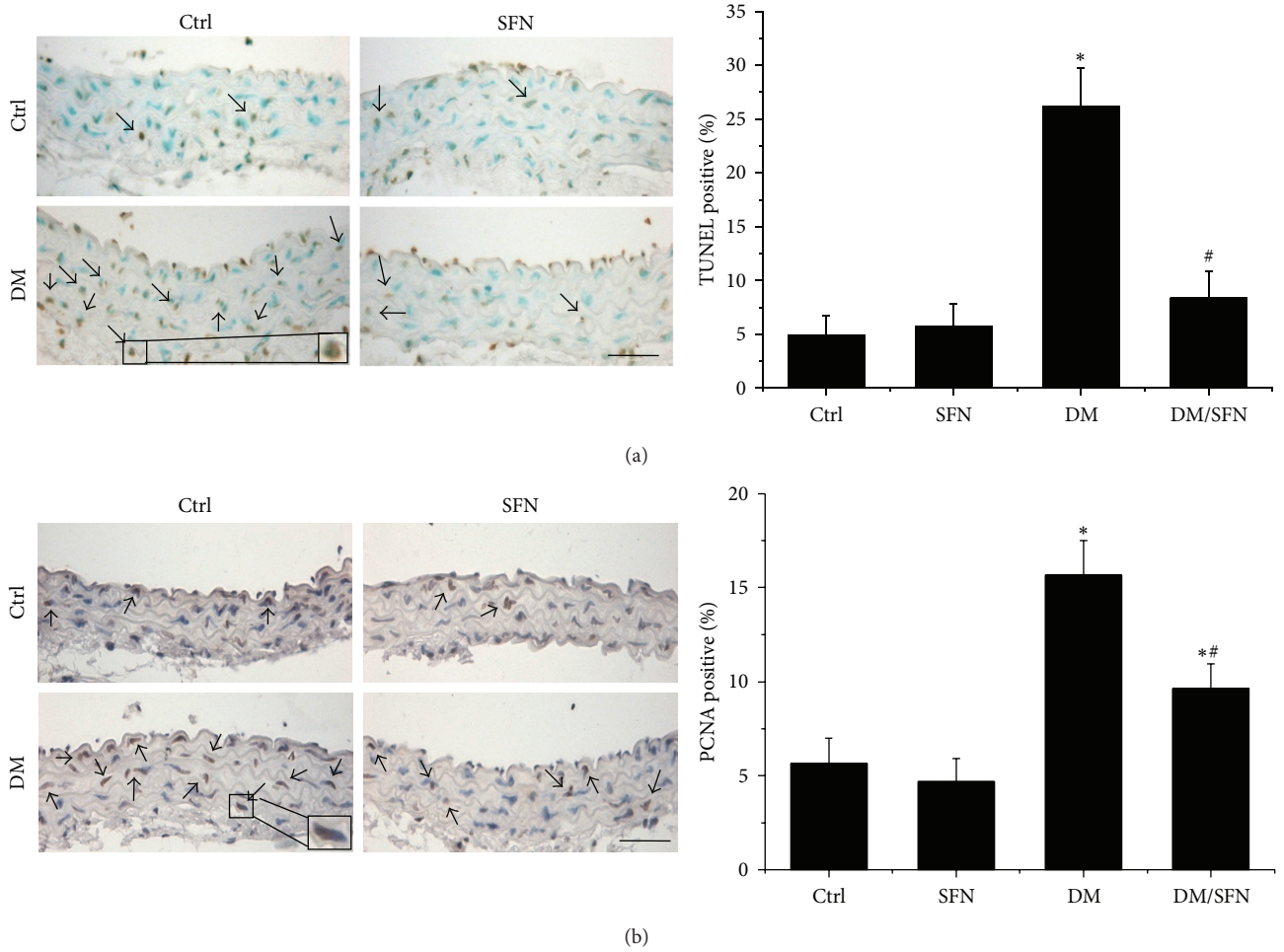

Figure 6: Diabetes-induced aortic apoptosis and proliferation increased. The apoptotic cell was examined by TUNEL staining (a) and the proliferation of aortic tunica media was examined by PCNA staining (b), followed by semiquantitative analysis. Data were presented as means ± SD ($n = 6$). $^{*}P < 0.05$ versus corresponding Ctrl; $^{\#}P < 0.05$ versus corresponding DM. Bar = 50 μM.

T2DM mice [6]. The next study was conducted to further examine the effect of SFN on the cell death and proliferation by TUNEL staining (Figure 6(a)) and PCNA staining (Figure 6(b)), which showed significant increases of apoptotic cell death and proliferation in the aortas of T2DM mice, but not in the aortas of diabetic mice with SFN administration (DM/SFN group).

3.4. SFN Upregulated the Expression of Nrf2 and Its Downstream Genes. The above results showed that SFN protected diabetic induction of aortic fibrosis, inflammation, and oxidative damage. Considering that oxidative stress has been extensively considered as the pivotal mediator for various cardiovascular complications of diabetic patients, we assume that the above pathological changes in the aortas of T2DM mice may predominantly attribute to the increased oxidative stress. The protective effect of SFN on diabetes-induced aortic pathogenesis may be mediated by upregulation of endogenous antioxidants. SFN is an Nrf2 activator [21], therefore, whether SFN protects the aorta from diabetes by activating Nrf2 was examined first by measuring the expression and transcription of Nrf2. Immunofluorescent staining showed that diabetes significantly decreased Nrf2 protein (Figures 7(a) and 7(b)) expression in the aorta of T2DM compared to control. Similarly, the Nrf2-downstream gene SOD-1 protein (Figures 8(a) and 8(b)) expression also decreased in the aorta of T2DM compared to control. Furthermore, diabetes also significantly downregulated the mRNA expression of Nrf2 (Figure 7(c)) and its downstream antioxidant genes SOD-1 (Figure 8(c)) and HO-1 (Figure 8(d)) in the aorta of T2DM compared to control. Although 4 months of SFN treatment significantly increased Nrf2 and its downstream antioxidant genes at both protein and mRNA levels in non-DM and T2DM mice.

4. Discussion

We have provided the first experimental evidence to show the significant protective effect of SFN on the aorta against T2DM-induced damage. Significant increase of aortic wall thickness, fibrosis, inflammation, oxidative damage, apoptosis and proliferation was developed in type 2 diabetic mice,

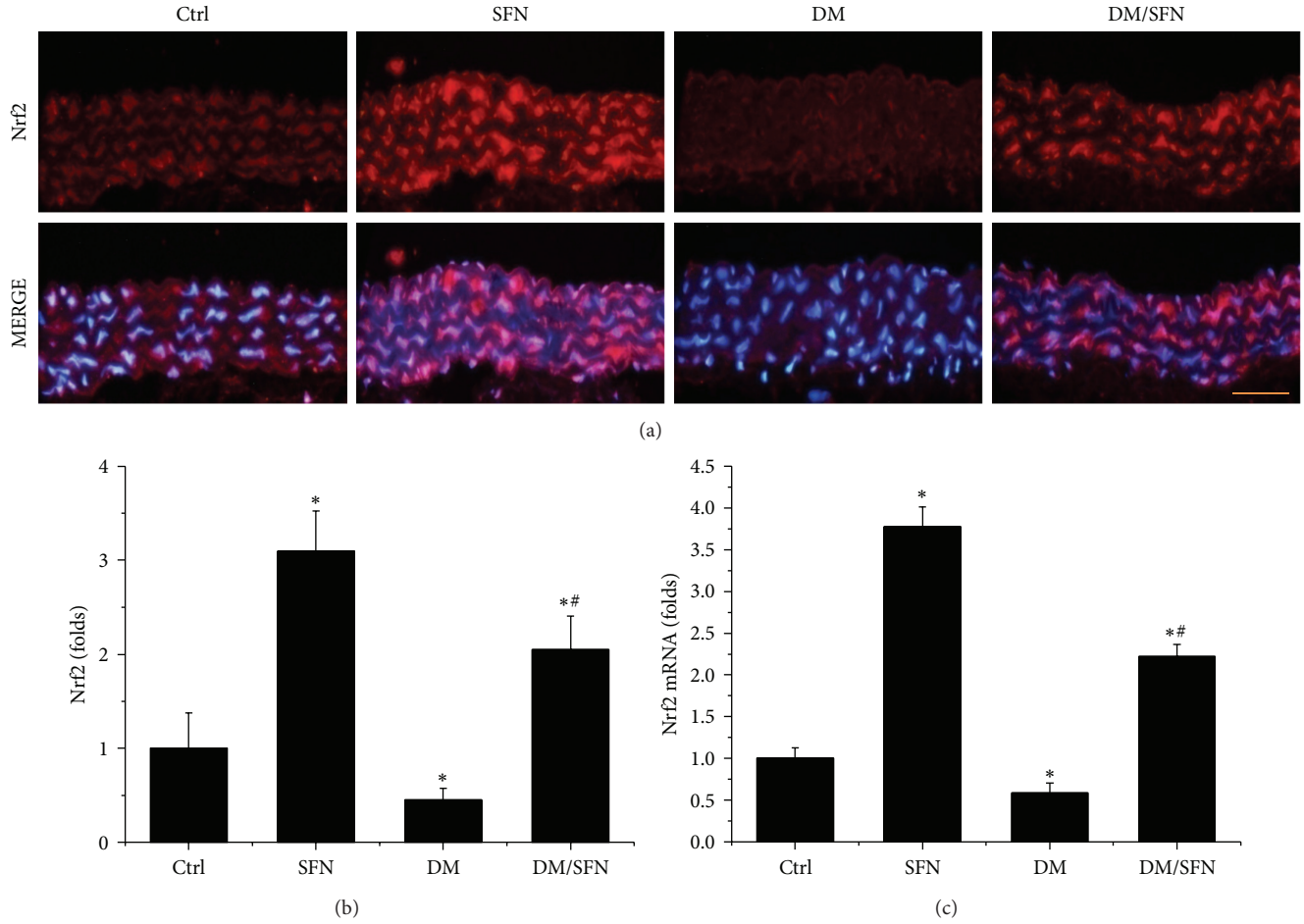

Figure 7: Effects of SFN on aortic expression of Nrf2. Aortic expression of Nrf2 was examined by immunofluorescent staining for its protein expression (red) (a) with semiquantitative analysis (b) and real-time PCR for its mRNA level (c). Data were presented as means ± SD ($n = 6$). $^{*}P < 0.05$ versus corresponding Ctrl; $^{\#}P < 0.05$ versus corresponding DM. Bar = 50 μM.

and these pathological changes were significantly prevented by treatment with SFN, which is associated with the upregulation of aortic Nrf2 expression and transcription.

Chronic inflammation plays an important role for the development of various chronic pathogeneses, including diabetes [30–33]. The effects of chronic inflammation include induction of oxidative stress, apoptotic cell death, and abnormal cell proliferation, all of which could contribute to the tissue structural and functional abnormalities [30–33]. In the present study we demonstrated the diabetic induction of aortic inflammation, shown by increased expression of TNF-α (Figure 4(a)), VACM-1 (Figure 4(b)) in the aorta of T2DM, which was accompanied with increased aortic oxidative stress (3-NT (Figure 5(a)) and 4-HNE (Figure 5(b))), apoptotic cell death (TUNEL (Figure 6(a))), cell proliferation (PCNA (Figure 6(b))), and remodeling (CTGF (Figure 3(a)) and TGF-β1 (Figure 3(b))) in T2DM group. All these pathogenic alterations were prevented by SFN administration. These findings are consistent with the classic concept that inflammation and oxidative stress are reciprocal cause and outcomes [7], both of which are main pathogenic factors for the development of various cardiovascular diseases under stress conditions.

It is known that Nrf2 expression and transcription *in vitro* and *in vivo* are increased in response to oxidative stress [34–36]. Ungvari et al. found that HFD increased endothelia ROS levels and endothelial dysfunctions were significantly severer in Nrf2-KO mice than in wild-type mice [37], indicating that adaptive upregulation of Nrf2-driven antioxidant systems effectively attenuates cellular oxidative stress under diabetic conditions [37]. There are a few studies recently, indicating the protective effect by activation of Nrf2 with various compounds on the aortas under various pathological conditions [6, 38, 39]. Here we have found that SFN treatment also significantly increased Nrf2 expression and function (Figure 7), which indicates that SFN prevents diabetes-induced aortic pathogenesis that may be associated with the upregulation of Nrf2.

In previous studies from our group and others, Nrf2 was found to play a critical role in preventing diabetes-induced aortic damage [5, 6, 19] and cardiac or renal damage [40–43]. We found that Nrf2 expression in the aorta was significantly upregulated at 3 months without significant aortic damage, but significantly downregulated at 6 months along with significant aortic damage in type 1 diabetic mouse model [5].

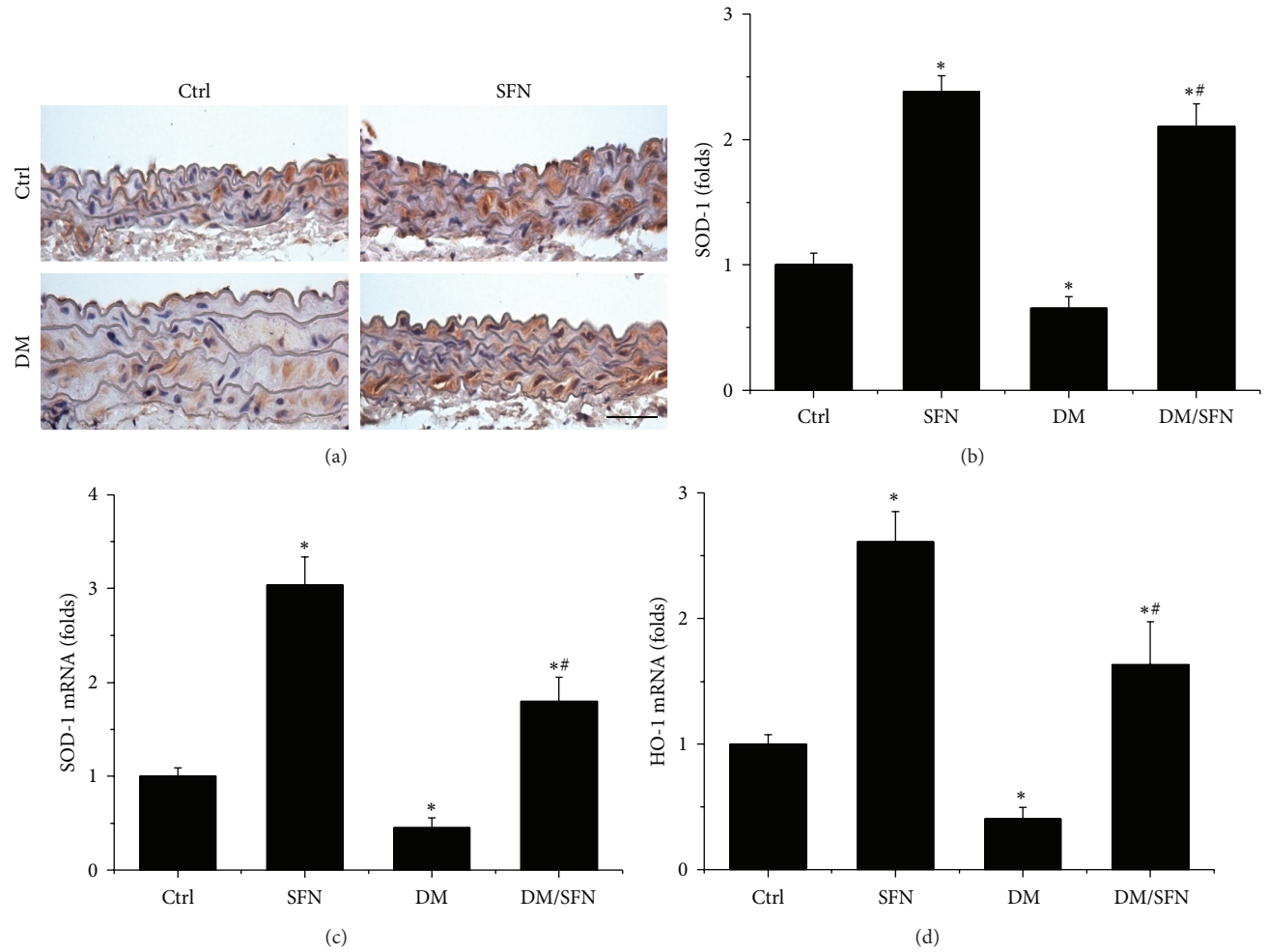

Figure 8: Effects of SFN on aortic expression of Nrf2 downstream genes. Aortic expression of Nrf2 downstream genes SOD-1 expression was examined by immunohistochemical staining for protein expression (a) in aortic tunica media with semiquantitative analysis (b) and real-time PCR at mRNA level SOD-1 (c) and HO-1 (d). Data were presented as means ± SD ($n = 6$). $^{*}P < 0.05$ versus corresponding Ctrl; $^{\#}P < 0.05$ versus corresponding DM. Bar = 50 μM.

Similarly, aortic expression of Nrf2-driven antioxidant enzymes markedly increases in young mice fed a HFD, but tend to decrease or only mild increase in middle-aged mice fed a HFD, despite the fact that vascular oxidative stress is more severe in HFD-fed middle-aged mice than in young mice [44]. Consistent with these previous studies, we found the significant reduction of Nrf2 expression at both protein and mRNA levels in the aorta of type 2 diabetic mice at 4 months (Figure 7), along with significant downregulation of its transcription function that is reflected by the expression of its downstream antioxidant genes SOD-1 and HO-1 (Figure 8), which were accompanied by significant aortic damage. Most importantly, SFN-treated type 2 diabetic mice showed a significant increase of aortic Nrf2 expression and function. The upregulated Nrf2 and its downstream antioxidant genes in SFN-treated type 2 diabetic mice efficiently reduced diabetes-induced oxidative damage, inflammation, apoptosis, proliferation, and remodeling and eventually significantly prevented the aortic pathological and structural changes.

5. Conclusions

In summary, to our knowledge, this is the first study to investigate the protective effects of SFN against T2DM-induced aortic pathological changes. We found that treatment with SFN can completely reverse and/or prevent the progression of diabetes-induced aortic fibrosis, inflammation, oxidative damage, apoptosis, and proliferation in T2DM mice. Mechanism responsible for the preventive effect of SFN is related to upregulation of Nrf2 expression and function to afford potent antioxidant effect. Considering the fact that SFN is a molecule able to be obtained from cruciferous vegetables such as broccoli, cauliflower, or cabbages [24], our findings would be very important for patients with T2DM consider intaking foods rich with SFN for preventing vascular complications.

Conflict of Interests

There is no conflict of interests to be declared by the authors.

Authors' Contribution

Yonggang Wang, Zhigou Zhang, Wanqing Sun, and Yucheng Liu performed the experiments, which were initiated and designed by Jian Sun, Yang Zheng, Quan Liu, and Lu Cai. Lu Cai and Yi Tan were the critical supervisor of the experimental performance and, were critically involved in drafting, writing, and revising the paper. All the authors reviewed the final version of paper.

Acknowledgments

This study was supported in part by the Basic Research Award from American Diabetes Association (1-11-BA-17, to Lu Cai) and the regular grants from National Natural Science Foundation of China (no. 81273509, to Yi Tan; no. 81370318, to Yang Zheng).

References

[1] I. D. Atlas, *The Global Burden*, International Diabetes Federation, Brussels, Belgium, 4th edition, 2009.

[2] A. B. Dart, P. J. Martens, C. Rigatto et al., "Earlier onset of complications in youth with type 2 diabetes," *Diabetes Care*, 2013.

[3] K. Khavandi, H. Amer, B. Ibrahim et al., "Strategies for preventing type 2 diabetes: an update for clinicians," *Therapeutic Advances in Chronic Disease*, vol. 4, no. 5, pp. 242–261, 2013.

[4] L. Cai and Y. J. Kang, "Oxidative stress and diabetic cardiomyopathy: a brief review," *Cardiovascular Toxicology*, vol. 1, no. 3, pp. 181–193, 2001.

[5] X. Miao, Y. Bai, W. Sun et al., "Sulforaphane prevention of diabetes-induced aortic damage was associated with the up-regulation of Nrf2 and its down-stream antioxidants," *Nutrition & Metabolism*, vol. 9, no. 1, p. 84, 2012.

[6] X. Miao, Y. Wang, J. Sun et al., "Zinc protects against diabetes-induced pathogenic changes in the aorta: roles of metallothionein and nuclear factor (erythroid-derived 2)-like 2," *Cardiovascular Diabetology*, vol. 12, p. 54, 2013.

[7] S. Gupta, J. K. Gambhir, O. Kalra et al., "Association of biomarkers of inflammation and oxidative stress with the risk of chronic kidney disease in Type 2 diabetes mellitus in North Indian population," *Journal of Diabetes and Its Complications*, vol. 27, no. 6, pp. 548–552, 2013.

[8] G. L. King and M. R. Loeken, "Hyperglycemia-induced oxidative stress in diabetic complications," *Histochemistry and Cell Biology*, vol. 122, no. 4, pp. 333–338, 2004.

[9] I. K. Jeong and G. L. King, "New perspectives on diabetic vascular complications: the loss of endogenous protective factors induced by hyperglycemia," *Diabetes & Metabolism Journal*, vol. 35, no. 1, pp. 8–11, 2011.

[10] F. A. Matough, S. B. Budin, Z. A. Hamid, N. Alwahaibi, and J. Mohamed, "The role of oxidative stress and antioxidants in diabetic complications," *Sultan Qaboos University Medical Journal*, vol. 12, no. 1, pp. 556–569, 2012.

[11] L. Cai, "Diabetic cardiomyopathy and its prevention by metallothionein: experimental evidence, possible mechanisms and clinical implications," *Current Medicinal Chemistry*, vol. 14, no. 20, pp. 2193–2203, 2007.

[12] J.-M. Lee and J. A. Johnson, "An important role of Nrf2-ARE pathway in the cellular defense mechanism," *Journal of Biochemistry and Molecular Biology*, vol. 37, no. 2, pp. 139–143, 2004.

[13] V. O. Tkachev, E. B. Menshchikova, and N. K. Zenkov, "Mechanism of the Nrf2/Keap1/ARE signaling system," *Biochemistry*, vol. 76, no. 4, pp. 407–422, 2011.

[14] M. McMahon, K. Itoh, M. Yamamoto, and J. D. Hayes, "Keap1-dependent proteasomal degradation of transcription factor Nrf2 contributes to the negative regulation of antioxidant response element-driven gene expression," *Journal of Biological Chemistry*, vol. 278, no. 24, pp. 21592–21600, 2003.

[15] R. K. Thimmulappa, K. H. Mai, S. Srisuma, T. W. Kensler, M. Yamamoto, and S. Biswal, "Identification of Nrf2-regulated genes induced by the chemopreventive agent sulforaphane by oligonucleotide microarray," *Cancer Research*, vol. 62, no. 18, pp. 5196–5203, 2002.

[16] W. Li and A.-N. Kong, "Molecular mechanisms of Nrf2-mediated antioxidant response," *Molecular Carcinogenesis*, vol. 48, no. 2, pp. 91–104, 2009.

[17] G. P. Sykiotis, I. G. Habeos, A. V. Samuelson, and D. Bohmann, "The role of the antioxidant and longevity-promoting Nrf2 pathway in metabolic regulation," *Current Opinion in Clinical Nutrition and Metabolic Care*, vol. 14, no. 1, pp. 41–48, 2011.

[18] E. L. Donovan, J. M. McCord, D. J. Reuland et al., "Phytochemical activation of Nrf2 protects human coronary artery endothelial cells against an oxidative challenge," *Oxidative Medicine and Cellular Longevity*, vol. 2012, Article ID 132931, 9 pages, 2012.

[19] X. Miao, W. Cui, W. Sun et al., "Therapeutic effect of MG132 on the aortic oxidative damage and inflammatory response in OVE26 type 1 diabetic mice," *Oxidative Medicine and Cellular Longevity*, vol. 2013, Article ID 879516, 12 pages, 2013.

[20] A. T. Dinkova-Kostova, W. D. Holtzclaw, R. N. Cole et al., "Direct evidence that sulfhydryl groups of Keap1 are the sensors regulating induction of phase 2 enzymes that protect against carcinogens and oxidants," *Proceedings of the National Academy of Sciences of the United States of America*, vol. 99, no. 18, pp. 11908–11913, 2002.

[21] Y.-S. Keum, "Regulation of the Keap1/Nrf2 system by chemopreventive sulforaphane: implications of posttranslational modifications," *Annals of the New York Academy of Sciences*, vol. 1229, no. 1, pp. 184–189, 2011.

[22] C. E. Guerrero-Beltrán, M. Calderón-Oliver, J. Pedraza-Chaverri, and Y. I. Chirino, "Protective effect of sulforaphane against oxidative stress: recent advances," *Experimental and Toxicologic Pathology*, vol. 64, no. 5, pp. 503–508, 2012.

[23] P. C. Evans, "The influence of sulforaphane on vascular health and its relevance to nutritional approaches to prevent cardiovascular disease," *EPMA Journal*, vol. 2, no. 1, pp. 9–14, 2011.

[24] J. W. Fahey and P. Talalay, "Antioxidant functions of sulforaphane: a potent inducer of phase II detoxication enzymes," *Food and Chemical Toxicology*, vol. 37, no. 9-10, pp. 973–979, 1999.

[25] J. Mu, J. Woods, Y.-P. Zhou et al., "Chronic inhibition of dipeptidyl peptidase-4 with a sitagliptin analog preserves pancreatic β-cell mass and function in a rodent model of type 2 diabetes," *Diabetes*, vol. 55, no. 6, pp. 1695–1704, 2006.

[26] Y. Zhao, Y. Tan, S. Xi et al., "A novel mechanism by which SDF-1beta protects cardiac cells from palmitate-induced endoplasmic reticulum stress and apoptosis via CXCR7 and AMPK/p38 MAPK-mediated interleukin-6 generation," *Diabetes*, vol. 62, no. 7, pp. 2545–2558, 2013.

[27] Y. Bai, W. Cui, Y. Xin et al., "Prevention by sulforaphane of diabetic cardiomyopathy is associated with up-regulation of Nrf2 expression and transcription activation," *Journal of Molecular and Cellular Cardiology*, vol. 57C, pp. 82–95, 2013.

[28] A. Qazi, J. Pal, M. Maitah et al., "Anticancer activity of a broccoli derivative, sulforaphane, in barrett adenocarcinoma: potential use in chemoprevention and as adjuvant in chemotherapy," *Translational Oncology*, vol. 3, no. 6, pp. 389–399, 2010.

[29] K. Mahéo, F. Morel, S. Langouët et al., "Inhibition of cytochromes P-450 and induction of glutathione S- transferases by sulforaphane in primary human and rat hepatocytes," *Cancer Research*, vol. 57, no. 17, pp. 3649–3652, 1997.

[30] D. I. Simon, "Inflammation and vascular injury: basic discovery to drug development," *Circulation Journal*, vol. 76, no. 8, pp. 1811–1818, 2012.

[31] N. Ishigami, K. Isoda, T. Adachi et al., "Deficiency of CuZn superoxide dismutase promotes inflammation and alters medial structure following vascular injury," *Journal of Atherosclerosis and Thrombosis*, vol. 18, no. 11, pp. 1009–1017, 2011.

[32] V. O. Puntmann, P. C. Taylor, and M. Mayr, "Coupling vascular and myocardial inflammatory injury into a common phenotype of cardiovascular dysfunction: systemic inflammation and aging—a mini-review," *Gerontology*, vol. 57, no. 4, pp. 295–303, 2011.

[33] C. Davis, J. Fischer, K. Ley, and I. J. Sarembock, "The role of inflammation in vascular injury and repair," *Journal of Thrombosis and Haemostasis*, vol. 1, no. 8, pp. 1699–1709, 2003.

[34] P. Palsamy and S. Subramanian, "Resveratrol protects diabetic kidney by attenuating hyperglycemia-mediated oxidative stress and renal inflammatory cytokines via Nrf2-Keap1 signaling," *Biochimica et Biophysica Acta*, vol. 1812, no. 7, pp. 719–731, 2011.

[35] Y. Tan, T. Ichikawa, J. Li et al., "Diabetic downregulation of Nrf2 activity via ERK contributes to oxidative stress-induced insulin resistance in cardiac cells in vitro and in vivo," *Diabetes*, vol. 60, no. 2, pp. 625–633, 2011.

[36] Y.-C. Yang, C.-K. Lii, A.-H. Lin et al., "Induction of glutathione synthesis and heme oxygenase 1 by the flavonoids butein and phloretin is mediated through the ERK/Nrf2 pathway and protects against oxidative stress," *Free Radical Biology and Medicine*, vol. 51, no. 11, pp. 2073–2081, 2011.

[37] Z. Ungvari, L. Bailey-Downs, T. Gautam et al., "Adaptive induction of NF-E2-related factor-2-driven antioxidant genes in endothelial cells in response to hyperglycemia," *American Journal of Physiology—Heart and Circulatory Physiology*, vol. 300, no. 4, pp. H1133–H1140, 2011.

[38] A. Ishikado, K. Morino, Y. Nishio et al., "4-Hydroxy hexenal derived from docosahexaenoic acid protects endothelial cells via Nrf2 activation," *PloS One*, vol. 8, no. 7, Article ID e69415, 2013.

[39] P. R. Avila, S. O. Marques, T. F. Luciano et al., "Resveratrol and fish oil reduce catecholamine-induced mortality in obese rats: role of oxidative stress in the myocardium and aorta," *The British Journal of Nutrition*, vol. 110, no. 9, pp. 1580–1590, 2013.

[40] X. He, H. Kan, L. Cai, and Q. Ma, "Nrf2 is critical in defense against high glucose-induced oxidative damage in cardiomyocytes," *Journal of Molecular and Cellular Cardiology*, vol. 46, no. 1, pp. 47–58, 2009.

[41] T. Jiang, Z. Huang, Y. Lin, Z. Zhang, D. Fang, and D. D. Zhang, "The protective role of Nrf2 in streptozotocin-induced diabetic nephropathy," *Diabetes*, vol. 59, no. 4, pp. 850–860, 2010.

[42] J. B. De Haan, "Nrf2 activators as attractive therapeutics for diabetic nephropathy," *Diabetes*, vol. 60, no. 11, pp. 2683–2684, 2011.

[43] W. Cui, B. Li, Y. Bai et al., "Potential role for Nrf2 activation in the therapeutic effect of MG132 on diabetic nephropathy in OVE26 diabetic mice," *American Journal of Physiology*, vol. 304, no. 1, pp. E87–E99, 2013.

[44] A. R. Collins, C. J. Lyon, X. Xia et al., "Age-accelerated atherosclerosis correlates with failure to upregulate antioxidant genes," *Circulation Research*, vol. 104, no. 6, pp. e42–e54, 2009.

Hindawi Publishing Corporation
Oxidative Medicine and Cellular Longevity
Volume 2014, Article ID 290381, 15 pages
http://dx.doi.org/10.1155/2014/290381

Research Article

Enhancement of Cellular Antioxidant-Defence Preserves Diastolic Dysfunction via Regulation of Both Diastolic Zn^{2+} and Ca^{2+} and Prevention of RyR2-Leak in Hyperglycemic Cardiomyocytes

Erkan Tuncay, Esma N. Okatan, Aysegul Toy, and Belma Turan

Department of Biophysics, Faculty of Medicine, Ankara University, Ankara 06100, Turkey

Correspondence should be addressed to Belma Turan; belma.turan@medicine.ankara.edu.tr

Received 24 September 2013; Accepted 17 December 2013; Published 13 February 2014

Academic Editor: Susana Llesuy

We examined whether cellular antioxidant-defence enhancement preserves diastolic dysfunction via regulation of both diastolic intracellular free Zn^{2+} and Ca^{2+} levels ($[Zn^{2+}]_i$ and $[Ca^{2+}]_i$) levels *N*-acetyl cysteine (NAC) treatment (4 weeks) of diabetic rats preserved altered cellular redox state and also prevented diabetes-induced tissue damage and diastolic dysfunction with marked normalizations in the resting $[Zn^{2+}]_i$ and $[Ca^{2+}]_i$. The kinetic parameters of transient changes in Zn^{2+} and Ca^{2+} under electrical stimulation and the spatiotemporal properties of Zn^{2+} and Ca^{2+} sparks in resting cells are found to be normal in the treated diabetic group. Biochemical analysis demonstrated that the NAC treatment also antagonized hyperphosphorylation of cardiac ryanodine receptors (RyR2) and significantly restored depleted protein levels of both RyR2 and calstabin2. Incubation of cardiomyocytes with 10 μM $ZnCl_2$ exerted hyperphosphorylation in RyR2 as well as higher phosphorphorylations in both PKA and CaMKII in a concentration-dependent manner, similar to hyperglycemia. Our present data also showed that a subcellular oxidative stress marker, NF-κB, can be activated if the cells are exposed directly to Zn^{2+}. We thus for the first time report that an enhancement of antioxidant defence in diabetics via directly targeting heart seems to prevent diastolic dysfunction due to modulation of RyR2 macromolecular-complex thereby leading to normalized $[Ca^{2+}]_i$ and $[Zn^{2+}]_i$ in cardiomyocytes.

1. Introduction

Diabetic cardiomyopathy was first recognized by Rubler et al. [1] in diabetic humans with congestive heart failure without any evidence of coronary atherosclerosis. It is well accepted that chronic hyperglycemia is an important risk factor for myocardial infarction, and importantly, both acute and chronic hyperglycemia trigger several biochemical and electrophysiological changes resulting in an impaired cardiac contractile function [2]. Hypoglycemia first initiates repeated acute changes in cellular metabolism and then followed by cumulative long-term changes in macromolecules. The long-term changes include mainly a big amount of increases in the production of reactive oxygen species, ROS, which then induce a diabetic tissue/cell damage in several target organs including the heart [3–5]. Although oxidants are produced also in healthy tissues, increased oxidative stress plays an important role in the development of a number of diseases such as cardiovascular system disorders [6].

Accumulated evidence indicates that oxidative stress has closely been associated with diabetes and its complication including diabetic cardiomyopathy. Increased oxidative stress results also from a reduction of antioxidants/antioxidant defence system, thereby contributing to the initiation and progression of cardiac dysfunction [7]. Hyperglycemia-induced oxidative stress can also result in formation of misfolded or damaged proteins as well as changes in cellular redox status, which is closely modulated by reductants or antioxidant molecules as well as enzymes [8, 9]. Therefore, an imperfection in the cellular defence systems leads to development over time of oxidatively damaged cellular macromolecules and consequently, in part, dyshomeostasis

in intracellular free Ca^{2+} [10]. In addition, it has been also shown that intracellular free Zn^{2+} level can increase rapidly in cardiomyocytes due to the mobilization of Zn^{2+} from intracellular stores mostly by ROS [11, 12].

Zinc, being an essential trace element, is vital in maintaining normal physiology and cellular functions in many cell types. Intracellularly, it is mostly bound to metalloproteins and plays a key role as an activating cofactor for many enzymes. On the cellular level, it has been demonstrated that the intracellular Zn^{2+} homeostasis is involved in signal transduction, in which Zn^{2+} acts as an intracellular mediator, similar to Ca^{2+} [13, 14]. Total Zn^{2+} in eukaryotic cells (up to 200 μM) is not too different from the Ca^{2+} one with 30% localized in the nucleus, 50% in the cytosol and organelles, and the remainder associated with the proteins [15]. In cardiomyocytes, the intracellular free Zn^{2+} concentration ($[Zn^{2+}]_i$) is measured to be less than one nanomolar under physiological conditions [11, 16], similar to the one reported in HT-29 cells [17], that is, some 100-fold less than that of intracellular free Ca^{2+}. Moreover, oxidants caused about 30-fold increase in intracellular free Zn^{2+} but only 2-fold in intracellular free Ca^{2+} in freshly isolated cardiomyocytes [11].

Zinc, a redox-inactive metal, has been long viewed as a component of the antioxidant network, and growing evidence points to its involvement in redox-regulated signaling via a direct or indirect regulation [18, 19]. Although there are a number of findings on cell/tissue dysfunction and its association with cellular oxidative stress level, redox signaling, and intracellular free Zn^{2+} level, very little is known about the contribution as well as the intracellular control of free Zn^{2+} in cardiomyocytes under physiological and pathophysiological conditions. Ca^{2+} release from intracellular stores mainly from sarcoplasmic reticulum (SR) via ryanodine receptors (RyR2) plays an important role in the regulation of cardiac function. Changes in the channel regulation are demonstrated to cause diastolic Ca^{2+} leakage from SR, which underlies many cardiac dysfunctions including diabetic cardiomyopathy [20]. Since redox modifications of RyR2 with direct and/or indirect action of oxidants contribute to SR Ca^{2+} leak in cardiomyocytes under many diseased-heart models [21–24], RyR2s are modulated with sulfhydryl oxidation in cardiomyocytes biphasically [25], high glucose attenuates protein S-nitrosylation via superoxide production [26], and nitric oxide (NO) mediates intracytoplasmic and intranuclear Zn^{2+} release [27], we aimed to test a hypothesis that the intracellular free Zn^{2+} changes, via increased oxidative stress and/or defective antioxidant defence system, play an important role in the development of diabetes-related alterations in RyR2 function. Under published data, we hypothesized that alterations in phosphorylation status of RyR2 are not the only type of biochemical modification in diabetic heart [20]. Shortly, diabetes is accompanied by increased oxidative stress and defective antioxidant defence system [28, 29] via increased ROS/RNS production, which can cause changes in RyR2 function as well as release of Zn^{2+} from intracellular stores [11, 12]. Accordingly, the goal of the present study was to test whether intracellular Zn^{2+} release besides Ca^{2+} release due to an increased oxidative stress/defective antioxidant defence system in cardiomyocytes under hyperglycemia mediates in part RyR2 leak and consequently diastolic dysfunction in heart from streptozotocin (STZ)-diabetic rats by using *N*-acetyl cysteine (NAC), under *in vivo* and *in vitro* approaches.

2. Materials and Methods

2.1. Experimental Rats and Diabetes Model. Male Wistar rats were used (200–250 g). Diabetes was induced in diabetic group as previously described [20]. One week after injection of STZ, blood glucose level was measured and rats with at least 3-fold higher level of blood glucose than preinjection level were used in the experiments as diabetic animals (DM group). Diabetic animals, 4 weeks after diabetes confirmation, received either *N*-acetyl cysteine (NAC; 150 mg/kg, daily and intragastrically, DM + NAC group) or vehicle (saline) for 4 weeks in an identical fashion, while nondiabetic rats (CON group) received saline alone. All rats had free access to standard chow and water. All animals were handled in accordance to the Guide for the Care and Use of Laboratory Animals published by the US National Institutes of Health (NIH publication number 85-23, revised 1996). The protocol was approved by the Ankara University Experimental Animals Ethics Committee, and approval reference number is 2011-115-449.

2.2. Assessment of Oxidative Stress/Antioxidant Status in Plasma and Heart Homogenates. Lipid peroxides, derived from polyunsaturated fatty acids, are unstable and decompose to form a complex series of compounds, which include reactive carbonyl compounds, such as MDA. Plasma lipid peroxidation was determined by measuring malondialdehyde (MDA) level with thiobarbituric acid reactive substances (TBARS) assay kit (Cayman Chemical Company). The MDA-TBA adduct was formed under high temperature and acidic condition was measured colorimetrically at 530–540 nm.

Plasma glutathione status was determined by measuring reduced glutathione (GSH) and oxidized glutathione (GSSG) levels, carried out with glutathione assay kit (Cayman Chemical Company) containing 2-(N-morpholino)ethanesulfonic acid buffer, GSSG standard, enzyme mixture, and 5,5′-dithiobis(2-nitrobenzoate). Levels of GSH and GSSG were calculated using reduced glutathione standard and the results were expressed as μmol/L. Detection limits for GSH and GSSG were 0.1 μmol/L and 0.001 μmol/L, respectively, while intraassay coefficients of variation for GSH and GSSG were 0.96% and 6.45%, respectively.

To prepare heart homogenates, first frozen hearts were pulverized at liquid N_2 temperature and then homogenized [30]. Protein contents in homogenates were analyzed by using the Bradford method (Bio-Rad). Bovine serum albumin was used as a protein standard. Protein oxidation level in heart homogenates was determined as described previously [31].

Total sulfhydryl (SH) and acid-soluble sulfhydryl (total thiol and free thiol) groups of proteins were estimated with Ellman's reagent as described previously [31]. Shortly,

heart homogenates were thawed and lysed in 0.2 M Tris/HCl buffer, pH 8.1, containing 2% sodium dodecylsulfate. For determination of total SH groups, 0.05 mL of aliquots of cell lysates was mixed with 0.8 mL of distilled water and 0.1 mL of 2 mM 5,5′-dithiobis-(2-nitrobenzoic acid). Absorbances of the supernatants were read at 412 nm (Shimadzu UV-120-02 spectrophotometer). After correction of the absorbances with sample and reagent blanks, levels of SH groups in each sample were calculated employing an extinction coefficient of 1.31 $mM^{-1} \cdot mm^{-1}$. To determine level of acid-soluble SH groups, 0.7 mL aliquots of heart homogenate lysates were mixed with 0.35 mL of 20% trichloroacetic acid (TCA) and final precipitates were washed with 0.2 mL of 20% TCA in a similar manner and the supernatants were combined and brought to pH 8 with NaOH. The total SH levels of the supernatants were measured as described above for free SH measurement.

2.3. Electron Microscopy. Histological examination was performed as described elsewhere. For electron microscopy evaluation, samples were fixed in 2.5% glutaraldehyde in phosphate buffer for 2–4 h at 4°C and postfixed in 1% osmium tetroxide. Following samples dehydration through graded alcohol concentrations (50%, 75%, 96%, and 100%), the heart tissues were embedded into Araldite 6005. The embedded samples were sliced at a thickness of 4–6 μm using a Leitz-1512 microtome. Sections were stained with uranyl acetate-lead citrate for examination by using a Leo 906 E transmission electron microscopy.

2.4. Isolated Langendorff-Perfused Hearts. Hearts were isolated and perfused as described previously [30]. Briefly, isolated hearts were electrically stimulated (DCS, Harvard Instruments) at 300 beats/min by a square wave of twice the threshold voltage of 1.5 ms duration. Hearts were perfused for a total of 50–60 min and functional parameters were determined at 40 min. The left ventricular end-diastolic pressure (LVEDP) changes of isolated hearts were measured.

2.5. Isolation of Ventricular Cardiomyocytes. Cell isolation was performed as described elsewhere [31]. Briefly, rats were anaesthetized using sodium pentobarbital (30 mg/kg, intraperitoneal) and ventricles were removed from rapidly excised hearts and minced into small pieces and gently passed through a nylon mesh. Following collagenase digestion, dissociated cardiomyocytes were washed with collagenase-free solution. Subsequently Ca^{2+} in the medium was gradually increased to a final concentration of 1.3 mM. Cells were kept in this solution at 37°C and only Ca^{2+} tolerant cells were used in the experiments.

2.6. Measurement of Cytosolic Zn^{2+} and Ca^{2+} in Resting and Electrically Stimulated Cells. Fluorescence changes were recorded using microspectrophotometer and FELIX software (PTI, Lawrenceville, NJ, USA) as described previously [12]. Cardiomyocytes were loaded with cell-permeable acetoxymethoxy derivatives of FluoZin-3 or Fluo-3 (FluoZin-3-AM or Fluo-3 AM; 35–40 min incubation) and excited at 0.2 Hz by field stimulation using two platinum electrodes positioned on either side of the recording chamber. The basal levels of $[Zn^{2+}]_i$ and $[Ca^{2+}]_i$ were measured from Fura-2 loaded (4 μM Fura-2 AM) cardiomyocytes at room temperature as described previously [11]. The transient fluorescence changes under electrical stimulation, which are estimated from the difference between peak and basal levels, were detected. All experiments were performed at room temperature. Cells were superfused continuously with HEPES-buffered solution as used for confocal imaging. Cells were excited at 488 nm for FluoZin-3 and at 480 nm for Fluo-3, and emissions were recorded at 520 and 515 nm, respectively. Cells showing a significant fluorescence decrease during the 5 min equilibration period were eliminated. The amplitude of Zn^{2+} or Ca^{2+} transients was stable within 10% during experimental period.

2.7. Confocal Measurement of Zn^{2+}- and Ca^{2+}-Sparks. Short-lived, tiny, and localized light emissions (named sparks) were recorded from different cardiomyocytes after 35–40 min incubation with FluoZin-3-AM or Fluo-3 AM, respectively, as described previously [12]. Loaded cells were transferred to the experimental chamber mounted on the stage of a Leica TCS SP5 laser scanning microscope. Experiments were conducted on quiescent cardiomyocytes. FluoZin-3 or Fluo-3 was excited at either 485 or 506 nm, and emission was collected at either 535 or 526 nm, respectively. In some experiments, recordings were obtained with HEPES-buffered solution supplemented with either zinc ionophore pyrithione (ZnPT; 1 or 10 μM), with the subsequent addition of 50 mM N,N,N′,N′-tetrakis(2-pyridylmethyl) ethylenediamine (TPEN) to bring the intracellular free Zn^{2+} level to zero. Experiments were performed at room temperature.

Sparks were initially detected with ImageJ (SparkMaster, plug-in) which is an open access programme (http://rsb.info.nih.gov/ij) and then were manually selected. The parameters of fluorescence changes such as peak amplitude ($\Delta F/F_0$, where $\Delta F = F - F_0$; F was identified as local maximum elevation of fluorescence intensity over basal level, F_0), time to peak (TP), frequency, full duration at half-maximum, or rise time (FDHM) were calculated automatically by using ImageJ programme.

2.8. Western Blot Analysis. For preparation of tissue homogenates, frozen heart samples from left ventricle were crushed at liquid N_2 temperature and then homogenized to measure the phosphorylation and protein levels of contractile machinery complex as described previously [20] (CaMKII, phospho-CaMKII-Thr286, PKA, phospho-PKA-Thr198, FKBP12.6, RyR2, phospho-RyR2-Ser^{2808}, phospho-NFκB, NFκB, and β-actin were identified using specific antibodies with recommended dilutions of either Santa Cruz biotechnology (USA) or Badrilla Ltd. (UK) companies). Density analysis of protein bands was performed using ImageJ programme.

Similar Western blot analysis was also performed in the diabetic rat cardiomyocytes from left ventricle incubated with *N*-acetyl cysteine (NAC; 1 mM) for 1 h at 37°C.

2.9. Chemicals and Data Analysis. Unless otherwise stated, all chemicals used were purchased from Sigma (Sigma-Aldrich Chemie, Steinheim, Germany).

Groups were tested and compared using one-way ANOVA and Tukey post hoc test. Values of $P < 0.05$ were taken as statistically significant. Significance levels are given in the text, and data are presented as means ± SEM.

3. Results

3.1. General Characteristics of the Experimental Animals. A single administration of streptozotocin, STZ, to rats induced diabetic symptoms compared to the aged-matched controls including body weight loss (199 ± 14 g versus 279 ± 13 g; number of rats 32 versus 24) and marked increase in blood glucose level (425 ± 25 mg/dL versus 109 ± 13 mg/dL). The rats from an antioxidant *N*-acetyl cysteine (NAC)-treated diabetic group (DM + NAC group) gained body weight similar to the controls (281 ± 17 g versus 279 ± 13 g; $n = 11$ rats) although they had high blood glucose level at the end of the experimental period (438 ± 33 mg/dL versus 109 ± 13 mg/dL) (Figure 1). In order to demonstrate whether there is hypertrophy in the diabetic rat hearts and to avoid the possible insensitive heart to body weight ratio measurement, we measured the cell capacitance in the isolated cardiomyocytes and compared the values between the groups. In STZ-induced diabetic rat heart during 7-8 weeks, hypertrophy has not been measured (data not shown).

3.2. Ultrastructure, Oxidative Stress, and Redox Status in Diabetic Rat Heart. The extent of hyperglycemia-induced oxidative stress, lipid peroxidation level evaluated by MDA analysis in the heart homogenate, was significantly decreased in *N*-acetyl cysteine (NAC)-treated diabetic group (298 ± 47 μmol/mg protein) when compared to untreated diabetic group (917 ± 36 μmol/mg protein), which was also significantly higher compared to that of the control group (324 ± 31 μmol/mg protein), suggesting both increased oxidative stress and an antioxidant role of NAC during hyperglycemic stress in heart. The extent of altered redox status in the heart was detected by measuring a ratio of GSH to GSSG (GSH/GSSG). This ratio was found to be significantly lower in the diabetic group (27 ± 3) when compared to both the controls (41 ± 4) and NAC-treated diabetics (48 ± 9), suggesting the altered cellular redox status in the heart during hyperglycemic stress. Furthermore, we found that the oxidation level of protein-SH (thiol) was significantly higher in diabetic rat heart homogenate (free thiol level: 1.3 ± 0.3 μmol/mg wet wt) compared to that of the control (free thiol level: 2.8 ± 0.2 μmol/mg wet wt) (Figure 1). Free protein-thiol level in the homogenate from NAC-treated diabetic group (2.7 ± 0.3 μmol/mg wet wt) was found to be significantly lower compared to that of untreated diabetic group. Furthermore, total protein-thiol level was not affected by either diabetes or NAC treatment (data not shown). We, therefore, demonstrated that there is marked increase in oxidative stress in the heart of diabetics besides a high circulatory level of lipid peroxidation [32] from STZ-induced diabetic rat, and it can be controlled to normal level by NAC treatment, which is confirmed also with previously published data [33–35].

Although diabetic rats did not show abnormal behaviour or any sign of heart failure as well as any signs of any tissue necrosis, as shown previously [36], the ultrastructure of diabetic rat heart showed various morphological changes including a loss in cardiomyocyte diameter, alterations in myofilaments and Z-lines of myofibers, myofibrillar degeneration, and destruction and loss of myofibrils over sarcomere lengths when compared to control hearts (Figures 2(a) and 2(b)). In the diabetic group most of the mitochondria of the cardiomyocytes showed loss of cristae and granular matrix and also increased numbers of lipid droplets (Figure 2(b)). NAC treatment normalized fully these alterations in the myofilaments (Figure 2(c)).

For quantification of electron microscopy findings among diabetic and nondiabetic rat hearts, we investigated only the lipid droplets and observed basically that the number and size of the lipid droplets in the diabetic group were significantly higher than that of the control group (~40% and ~15% for diabetic versus control group) while these changes have fully disappeared in the NAC-treated group. The lipid quantification of cardiac tissue was performed by using oil red O staining which revealed severe lipid accumulation in the heart. The lipid contents were expressed as lipid area normalized to total investigated tissue area.

3.3. Cardiac Function of Diabetic Rat Heart. We, previously, showed that STZ injection in rats either short- (4-5 weeks) or long-period (8–12 weeks) experimental durations induced marked several alterations in electrical and mechanical parameters of heart [12, 29, 37, 38]. Left ventricular systolic and diastolic dysfunctions are among these alterations. In the present study, since we aimed to investigate a possible contribution of intracellular free Zn^{2+} release besides that of Ca^{2+} release due to an increased oxidative stress under hyperglycemia, we first examined diastolic function of heart from diabetic rat and compared it to those of control and *N*-acetyl cysteine (NAC)-treated rats. Rats following 5-6 weeks of STZ injection developed increased diastolic dysfunction (Figure 3(a)), as evidenced by about 80% increase in left ventircular end diastolic pressure (LVEDP). NAC treatment of diabetic rats for 4 weeks induced a full normalization in LVEDP.

3.4. Basal Levels of Intracellular Free Zn^{2+} and Ca^{2+} in Cardimyocytes from Diabetic Rats. To identify and compare basal intracellular free Zn^{2+} level in diabetic rat cardiomyocytes with that of the control, we used a ratiometric fluorescence dye, Fura-2 AM. In order to compare the individual data, we normalized the initial fluorescence values to obtain a common ratio in all cardiomyocytes, and then we used TPEN responses for minimum and maximum fluorescence changes ($\Delta F_{340/380}$). The original fluorescence changes for basal $[Zn^{2+}]_i$ level are given in Figure 3(b). The data are given as percentage changes in order to compare diabetic and *N*-acetyl cysteine (NAC)-treated diabetic groups with the

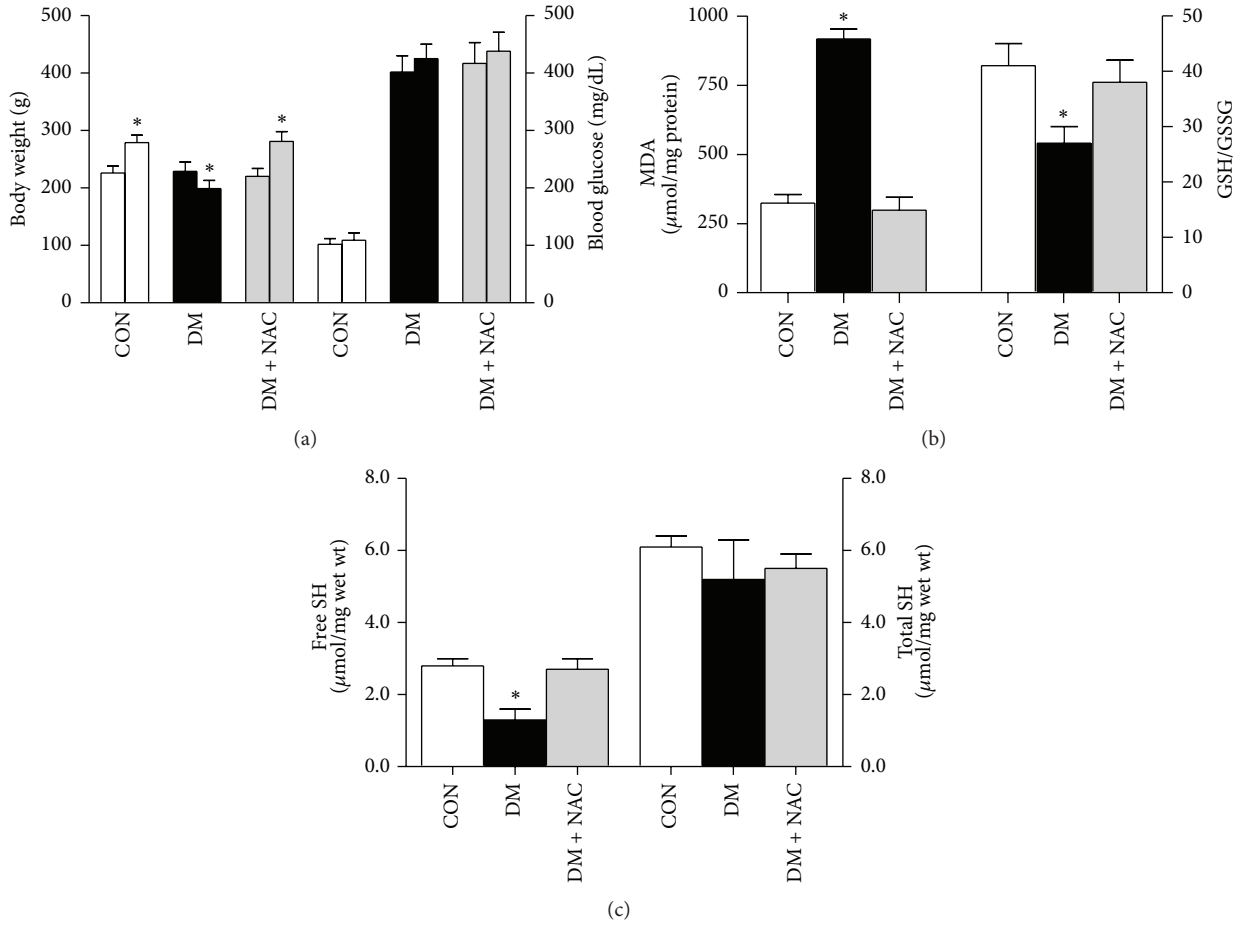

Figure 1: Body weight, blood glucose, and oxidative stress markers of normal rats (CON group) and diabetic (DM) rats treated with *N*-acetyl cysteine (DM+NAC group) or untreated DM rats. (a) Body weight (left) and blood glucose levels (right) in the rats both at the beginning (first column) and 5th week end (second column) of experimental period. (b) The levels of lipid peroxidation marker malondialdehyde, MDA, (left) and the reduced glutathione to oxidized glutathione (GSH/GSSG) ratio (right), and (c) total (right) and free (left) thiol (SH) levels measured in heart homogenates. Bar graphs represent mean ± SEM values and number of rats in groups; $n_{CON} = 8$, $n_{DM} = 7$, and $n_{DM+NAC} = 6$, respectively. Significant at $^*P < 0.05$, due to comparison between 1st and 5th weeks.

control group. As can be seen in Figure 3(b), the addition of the membrane-permeant Zn^{2+} chelator TPEN (50 μM) caused a rapid decrease in fluorescence ratio ($\Delta F_{340/380}$) to a level lower than that of initial value, verifying that the initial observed fluorescence ratio is attributable to intracellular basal free Zn^{2+} level. This decrease is bigger in the diabetic group compared to that of the control group while it is almost the same level in the NAC-treated diabetic group and the control group as well. As can be seen in the same bar graphs, the fluorescence change with respect to the basal level of intracellular free Ca^{2+} is significantly higher in the diabetic cardiomyocytes compared to those of both the control and NAC-treated diabetic groups. The present data demonstrate that both increased intracellular basal free Zn^{2+} and Ca^{2+} levels are dependent on increased oxidative stress and decreased antioxidant-defence system in the hyperglycemic rats.

To test directly whether increased oxidative stress can induce simultaneous increases in basal levels of both intracellular free Zn^{2+} and Ca^{2+} of diabetic rat cardiomyocytes, we incubated cardiomyocytes from diabetic rats with NAC (1 mM, for 1 h at 37°C) before loading the cells with Fura-2 AM. As can be seen from Figure 3(c), NAC incubation of diabetic cardiomyocytes (+NAC group) induced a similar change in the fluorescence ratios related to basal levels of both intracellular free Zn^{2+} and Ca^{2+}. These groups of experiments confirm also that diabetes can induce significant increases not only in basal Ca^{2+} level but also in basal Zn^{2+} level, at most, due to increased reactive oxygen species, ROS.

3.5. Local Intracellular Releases of Both Zn^{2+} and Ca^{2+} in Diabetic Rat Cardiomyocytes. Recently, we have demonstrated that there are local tiny Zn^{2+} releases (named as Zn^{2+} sparks) in resting quiescent cardiomyocytes isolated from 3-month-old male rats and loaded with a Zn^{2+}-specific fluorescence dye, FluZin-3, which can be visualized in a similar manner to known Ca^{2+} sparks [12]. The contributions of elementary Zn^{2+} release similar to Ca^{2+} release, either Zn^{2+} or Ca^{2+} sparks, to increased basal levels of both Zn^{2+} and Ca^{2+}

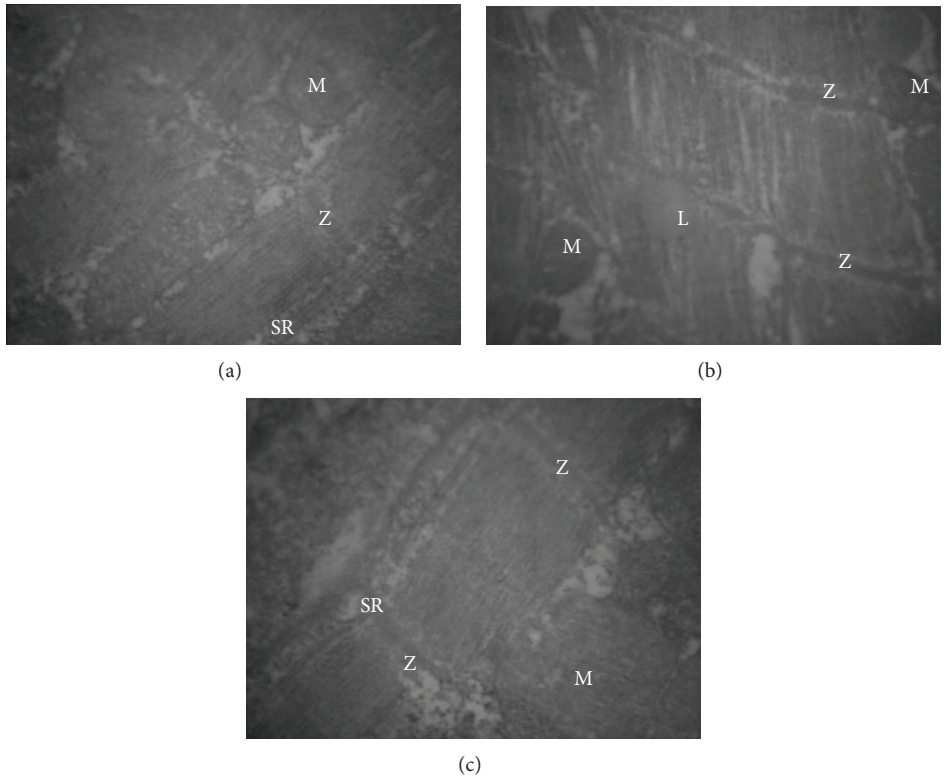

Figure 2: Morphological findings in experimental rat hearts. Micrographs of left ventricular cross section through control (CON), diabetic (DM), and *N*-acetyl cysteine (NAC)-treated diabetic (DM + NAC group; 150 mg/kg, daily and intragastrically, for 4 weeks) groups, respectively, obtained by electron microscopy. (a) There is no sign of any tissue necrosis in CON group. Marked alterations in myofilaments and sarcoplasmic reticulum (SR), destruction in Z-lines (Z), loss of cristae and granular matrix in mitochondria (M), and also increased numbers of lipid droplets (L) are seen in DM group (b) while these alterations have almost disappeared with NAC treatment (c); magnifications are ×12, 390, ×10, 000, and ×12, 990 for (a), (b), and (c), respectively.

(mentioned in previous section) and altered Zn^{2+}/Ca^{2+} contents of SR (of which, in part, present a function of SR Ca^{2+} release channels, RyR2) were examined and monitored the differences in parameters of these sparks among the diabetic and control groups. Representative line-scan images of of both type of sparks from control (CON group), diabetic (DM group), and *N*-acetyl cysteine (NAC)-treated diabetic (DM + NAC group) rats (individual Zn^{2+} or Ca^{2+} sparks images as x versus t) are displayed in Figure 4(a). The maximum fluorescence intensity, determined as $\Delta F/F_0$ at the peak of either Zn^{2+} or Ca^{2+} sparks (Figure 4(b); left and right, resp.), and spontaneous Zn^{2+}/Ca^{2+}-spark frequencies (Figure 4(c); left and right, resp.) were calculated from individual gamma distribution function fits. The maximum FluoZin-3 intensity as well as Fluo-3 intensity was not significantly different among the DM and CON groups. On the other hand, we observed marked increases in their occurrence frequency of both fluorescences during diabetes. Furthermore, time to peak (TP) of maximum FluoZin-3 intensity was found to be similar among the DM and CON groups; TP value for maximum Fluo-3 was markedly prolonged in DM group compared to that of the CON group (Figure 4(d); left and right, resp.). Moreover, the full duration at half-maximum (FDHM) of both FluoZin-3 and Fluo-3 was also found to be significantly prolonged in DM group with respect to age-matched CON group (Figure 4(e); left and right, resp.). *N*-acetyl cysteine (NAC)-treatment of the diabetic rats (DM + NAC group) for 4 weeks significantly prevented diabetes-induced all changes in both Zn^{2+} and Ca^{2+} sparks parameters.

Of note, as shown in Figures 4(b)–4(e), essentially similar results on the parameters of both Zn^{2+} and Ca^{2+}-sparks were obtained in cardiomyocytes isolated from diabetic rats after 1 h incubation with 1 mM NAC at 37°C (+NAC group).

3.6. Regulation of Both Zn^{2+} and Ca^{2+} Transients with an Antioxidant, N-Acetyl Cysteine. To further understand the effects of both diabetes and NAC treatment of diabetes on the distributions of both intracellular free Zn^{2+} and Ca^{2+} changes in isolated cardiomyocytes, we performed some additional experiments to monitor intracellular transient changes of either intracellular free Zn^{2+} or Ca^{2+} elicited by electrical-field stimulation. Figure 5(a) (left) shows original recordings of Zn^{2+} and Ca^{2+} transients elicited in control, diabetic, and *N*-acetyl cysteine (NAC)-treated (4 weeks) diabetic rat cardiomyocytes as well as NAC-incubated diabetic cardiomyocytes for 1 h with 1 mM NAC at 37°C. The averaged peak fluorescence amplitudes of both FluoZin-3 and Fluo-3 as F/F_0 were significantly smaller in diabetic cells than

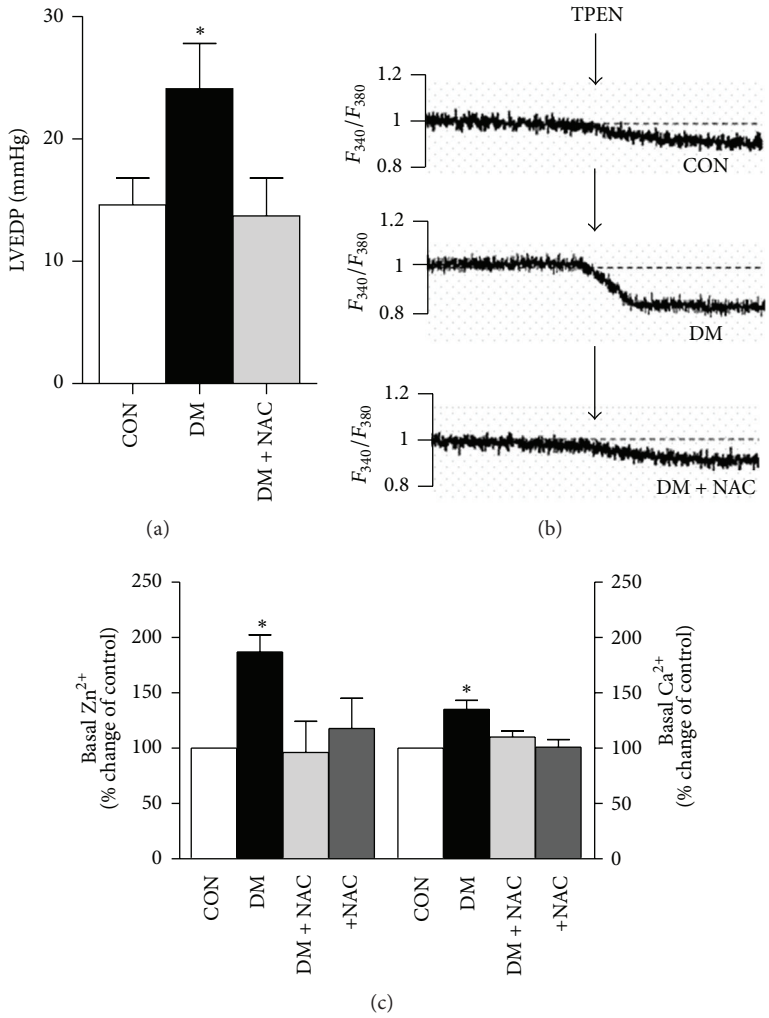

FIGURE 3: *N*-acetyl cysteine (NAC) treatment normalizes diastolic function of the heart due to normalization of increased levels of basal Ca^{2+} and Zn^{2+}. (a) Left ventricular end diastolic pressure, LVEDP, changes among the groups are given for controls (CON), diabetics (DM), and NAC-treated diabetics (DM + NAC group; 150 mg/kg, daily and intragastrically, for 4 weeks). (b) Representative traces showing how basal levels of intracellular free Ca^{2+} and Zn^{2+} can be demonstrated by using fluorescence changes following TPEN application in cardiomyocytes loaded with Furo-AM. The average values of basal intracellular free Zn^{2+} (left) and Ca^{2+} (right) are given in (c). Bar graphs represent mean ± SEM values. In here, a fourth group is NAC-incubated diabetic cells (+NAC; 1 mM, for 1 h at 37°C). The numbers of animals/cells for each group as well as for each protocol, at least used, are the following; $n_{CON} = 5$, $n_{cell} = 15$; $n_{DM} = 5$, $n_{cell} = 20$; $n_{DM+NAC} = 4$, $n_{cell} = 12$; $n_{+NAC} = 5$, $n_{cell} = 19$ for CON, DM, DM + NAC, and +NAC groups, respectively. Significant at $^*P < 0.05$ versus CON group.

in control cells (Figure 5(a), right) while their amplitudes in either NAC-treated diabetic rat cardiomyocytes or NAC-incubated diabetic cardiomyocytes were found to be similar to those of the controls. The time to peak amplitude (TP) and the half-time for recovery (DT_{50}) of transient changes of FluoZin-3 were found to be similar between diabetic and control groups as well as NAC-treated or NAC-incubated diabetics (Figure 5(b)). In addition, the similar parameters of transient changes of Fluo-3 were significantly prolonged in diabetic groups compared to that of the controls. These changes were also significantly prevented with either NAC treatment of diabetic rats or NAC incubation of diabetic cardiomyocytes for 1 h with 1 mM at 37°C (Figure 5(c)).

3.7. Biochemical Analysis of Cardiac Ryanodine Receptors, RyR2 and Calstabin2. It has been previously shown that the mechanisms underlying the dysfunction of RyR2 in diabetes include, in part, a hyperphosphorylation of RyR2 due to both high phosphorylation levels of both protein kinase A (PKA) and Ca^{2+}-calmodulin kinase II (CaMKII) under hyperglycemia [12]. The phosphorylation level of RyR2 in diabetic and control rat left ventricular heart tissue was evaluated by using specific antibodies directed against RyR2 and phosphorylated RyR2 (Figure 6(a), left). Total RyR2 in the diabetic group was about 64% less than that of the control group as estimated from the Western blot bands. From the band-intensity analysis, there was a strong evidence for the

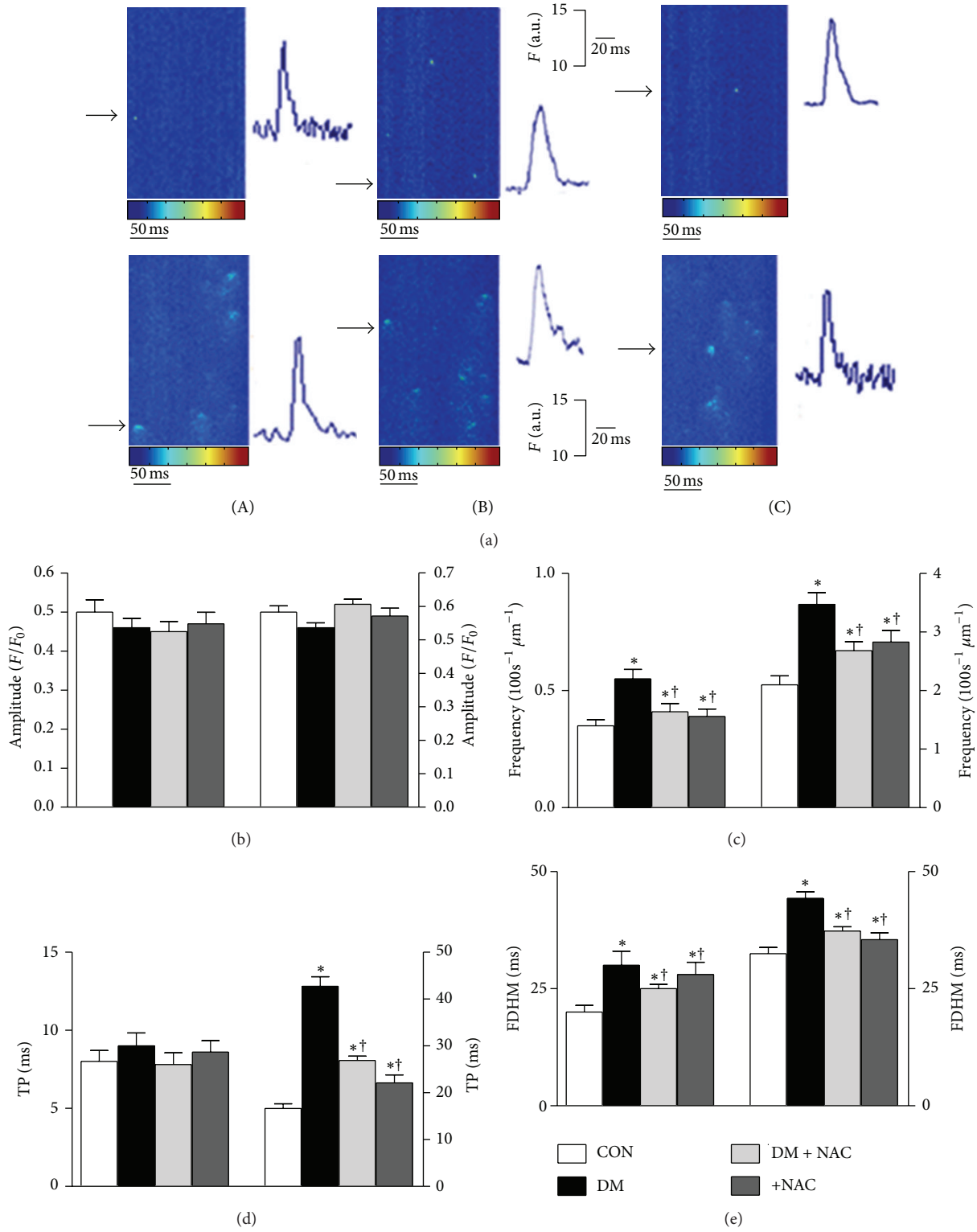

FIGURE 4: *N*-acetyl cysteine (NAC) treatment/incubation of diabetic rats/diabetic cells ameliorates altered parameters of both Ca^{2+} and Zn^{2+} sparks. (a) Representative line-scan images of freshly isolated cardiomyocytes (CON: control group, DM: diabetic group, DM + NAC: *N*-acetyl cysteine-treated DM group (150 mg/kg, daily and intragastrically, for 4 weeks), and +NAC: NAC-incubated diabetic cells; 1 mM, for 1 h at 37°C). The peak intensity and frequency of either FluoZin-3 (left) or Fluo-3 (right) recorded in the groups are given in (b) and (c), respectively. Time to peak amplitude (TP) and full duration at half-maximum (FDHM) of both fluorescence changes are given in (d) and (e), respectively. Bar graphs represent mean ± SEM values (n_{rat} = 5, n_{cell} = 44, n_{spark} = 150; n_{rat} = 5, n_{cell} = 55, n_{spark} = 165; n_{rat} = 5, n_{cell} = 38, n_{spark} = 135 in CON, DM, DM + NAC, and +NAC, resp.). Significant at $^{*}P < 0.05$ versus CON; $^{\dagger}P < 0.05$ versus DM.

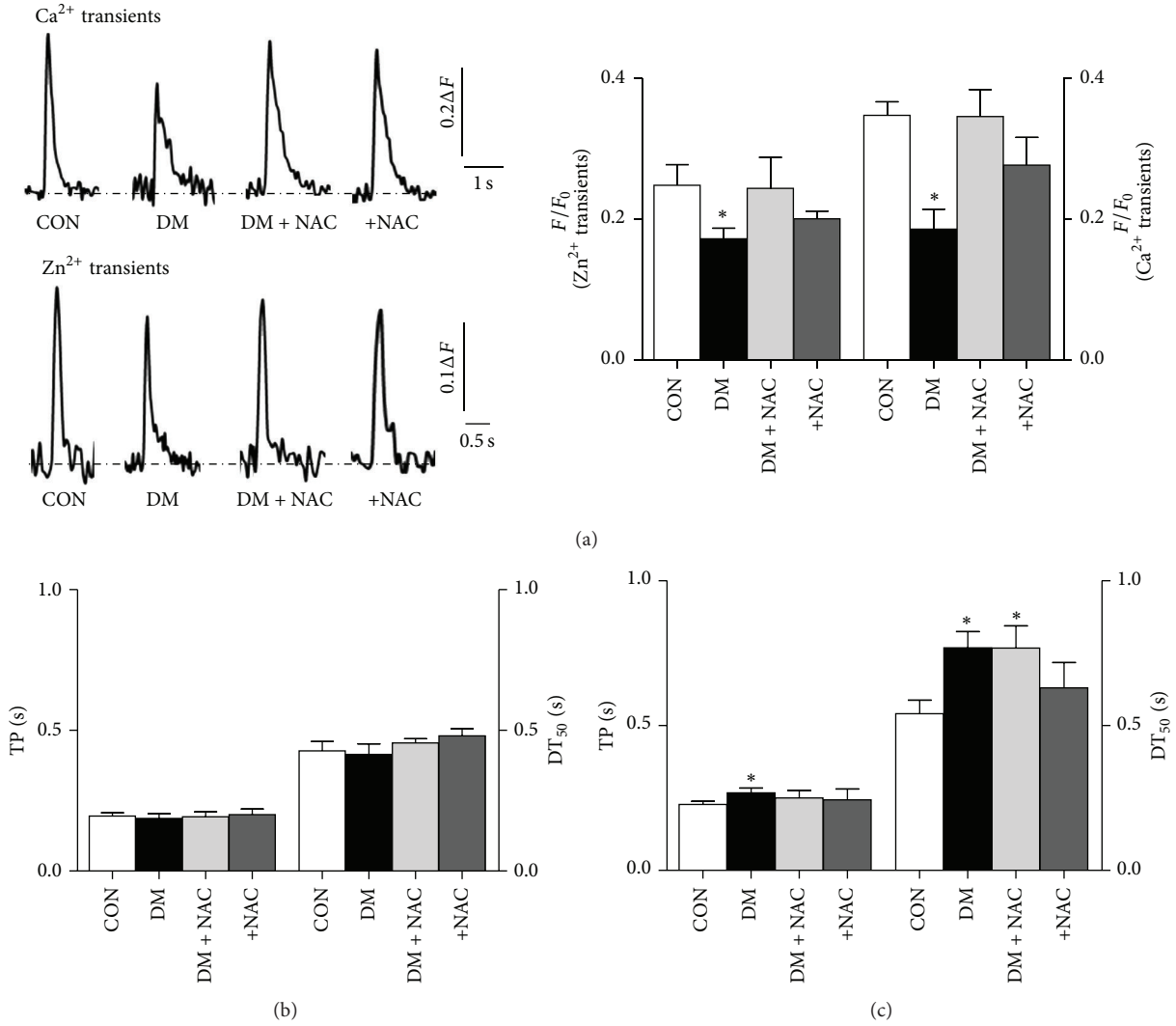

Figure 5: Altered intracellular global either Ca^{2+} or Zn^{2+} changes in cardiomyocytes are normalized with either *N*-acetyl cysteine (NAC)-treatment of diabetic rats or NAC-incubation in diabetic cardiomyocytes. (a) *Inset:* representative Ca^{2+} or Zn^{2+} transients in freshly isolated cardiomyocytes loaded with either FluoZin-3 (low) or Fluo-3 (up) and field-stimulated at 0.2 Hz (left). The peak amplitude of the fluorescences related to either global Ca^{2+} or Zn^{2+} (the transient changes) is given as F/F_0. The effect of NAC treatment of diabetic rats (DM + NAC group: 150 mg/kg, daily and intragastrically, for 4 weeks) or NAC incubation of diabetic cardiomyocytes (+NAC group; 1 mM, for 1 h at 37°C) on the time to peak fluorescence, TP (left), and half-decay time, DT_{50} (right), of fluorescences either FluoZin-3 (b) or Fluo-3 (c). Bars represent mean ± SEM for controls (CON; $n_{rat} = 5$, $n_{cell} = 21$) and diabetics (DM; $n_{rat} = 5$, $n_{cell} = 28$) as well as DM + NAC ($n_{rat} = 6$, $n_{cell} = 34$) and +NAC ($n_{rat} = 4$, $n_{cell} = 22$) groups, respectively. Significant at $^{*}P < 0.05$ versus CON.

RyR2 phosphorylation in diabetic rat heart homogenates while no detectable band in the heart homogenates of the control group. The amount of calstabin2 (FKBP12.6) was decreased by 40% in the diabetic rat heart compared to that of the control (Figure 6(a), right). There was no significant difference in the protein levels of actin in diabetic and control groups (Figure 6(a), right). In addition, these parameters were found to be markedly prevented by NAC treatment of diabetic rats for 4 weeks.

For an assessment of a direct action of antioxidant NAC, we first incubated freshly isolated cardiomyocytes from diabetic rats with 1 mM NAC for 1 h at 37°C and then performed the similar Western blot analysis for pRyR2, RyR2, FKBP12.6. Incubation of diabetic cardiomyocytes with 1 mM NAC significantly declined hyperphosphorylation level in RyR2, while there was no effect of its depressed protein level (Figure 6(b), left). Similarly, NAC incubation did not affect the decreased FKBP12.6 protein level in diabetic cardiomyocytes (Figure 6(b), right).

3.8. Direct Effects of External Zn^{2+} on RyR2 Macromolecular-Complex of Ventricular Heart Tissue. The intracellular free Zn^{2+} distribution is linked to redox metabolism despite Zn^{2+} itself not being redox-active and generally Zn^{2+}-proteins being redox-inert [39, 40]. Therefore, since we previously

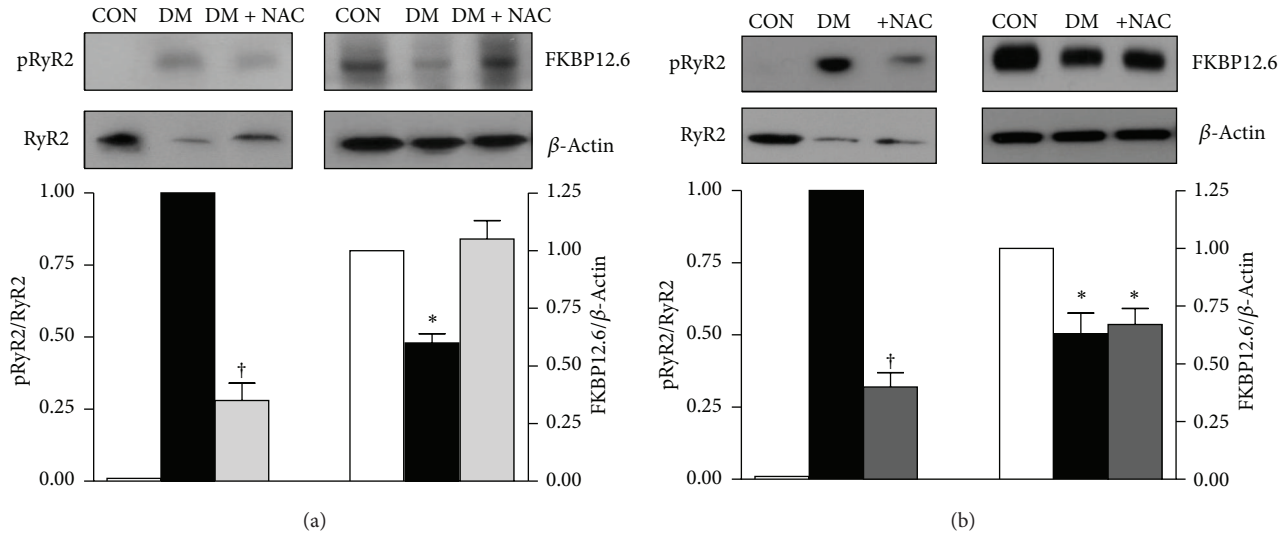

Figure 6: Effect of *N*-acetyl cysteine (NAC) treatment of diabetic rats or NAC incubation of diabetic cardiomyocytes on hyperphosphorylation and protein levels of SR Ca^{2+} release channel (RyR2) and its accessory proteins. (a) *Top*: representative Western blot images for phospho-RyR2-Ser^{2808} (pRyR2; upper left band), and FK-binding protein, calstabin2 (FKBP; upper right band), RyR2 (lower left band), and β-actin (lower right band). *Bottom*: quantification for the ratio of pRyR2 to RyR2 and FKBP to β-actin. Data presented in (a) are obtained from control (CON), diabetic (DM), and NAC-treated diabetic (DM + NAC; 150 mg/kg, daily and intragastrically, for 4 weeks) rat heart homogenates. (b) *Top*: representative Western blotting for phospho-RyR2-Ser^{2808} (pRyR2; upper left band), calstabin2, (FKBP; upper right band), RyR2 (lower left band), and β-actin (lower right band). *Bottom*: quantification for the ratio of pRyR2 to RyR2 and FKBP to β-actin. Data presented in (b) are obtained from controls (CON), diabetics (DM), and NAC-incubated diabetic cardiomyocytes (+NAC group: 1 mM, for 1 h at 37°C). Bar graphs represent mean ± SEM (n_{rats} = 6–8 for each protocol/group). Significant at $^{*}P < 0.05$ versus CON and $^{\dagger}P < 0.05$ versus DM.

have shown a mediation of rapid, large, and selective elevation of intracellular free Zn^{2+} through the modulation of the redox status of intracellular protein thiols, in here, we aimed to examine the effects of external $ZnCl_2$ incubation (10 μM) of heart homogenates from both control and diabetic groups rats for 20–30 min at 37°C on members of RyR2-macromolecular complex. As can be seen from Figures 7(a) and 7(b), total protein levels of RyR2 and its accessory proteins, FKBP12.6, PKA, and CaMKII, were not affected with either 1 μM (data not shown) or 10 μM $ZnCl_2$ incubation of left ventricular heart homogenates from both group rats. However, we measured significantly increased phosphorylation levels of RyR2, PKA, and CaMKII with these two $ZnCl_2$ incubations in a concentration-dependent manner. The last data further support the hypothesis that Zn^{2+} disbalance results in a signaling disbalance caused by a local surplus of Zn^{2+} interfering with cellular signaling networks.

3.9. Relation between Intracellular Zn^{2+} and Nuclear Factor Kappa B (NF-κB) Activation. There are multiple studies with different conclusions regarding whether NF-κB is protective or detrimental for heart function although its important role in cardiac pathology [41, 42] has been demonstrated. This disagreement is not surprising considering the complexity of NF-κB signaling that involves multiple components and regulation at several steps. Furthermore, NF-κB is a pleiotropic transcription factor that receives signals from multiple pathways including different important modulators of cardiac remodeling. To asses a possible direct role of intracellular Zn^{2+} on NF-κB, we tested the effect of external $ZnCl_2$ incubation (10 μM) of heart homogenates from both control and diabetic groups rats for 20–30 min at 37°C, similar to previous section. As can be seen from Figures 7(a) and 7(b), total protein level of NF-κB was not affected with 10 μM $ZnCl_2$ incubation of left ventricular heart homogenates from both control and diabetic group rats. However, the activation levels of NF-κB in both group rat heart homogenates were significantly increased (~3-fold in both groups) after $ZnCl_2$ incubations. This last data further supports the hypothesis that although cardiac remodeling is associated with increased oxidative stress, inflammation, and activation of hormonal systems under hyperglycemia, increased intracellular $ZnCl_2$-mediated NF-κB activation seems to be a distinct fact among the others under high Zn^{2+} exposure of heart.

4. Discussion

This study on *N*-acetyl cysteine (NAC) effect in STZ-induced diabetes in rats reports a significant role of cellular antioxidant-defence enhancement on preservation of diastolic dysfunction via regulation of not only diastolic Zn^{2+} but also diastolic Ca^{2+} due to a prevention of RyR2-leak in diabetic rat heart. At first, we confirmed a defective intracellular Zn^{2+} signaling, besides previously shown Ca^{2+} signaling [20], in part, due to increased oxidative stress/depressed antioxidant defence in diabetic cardiomyocytes, with lower amplitude of Zn^{2+} transients as well as markedly increased diastolic

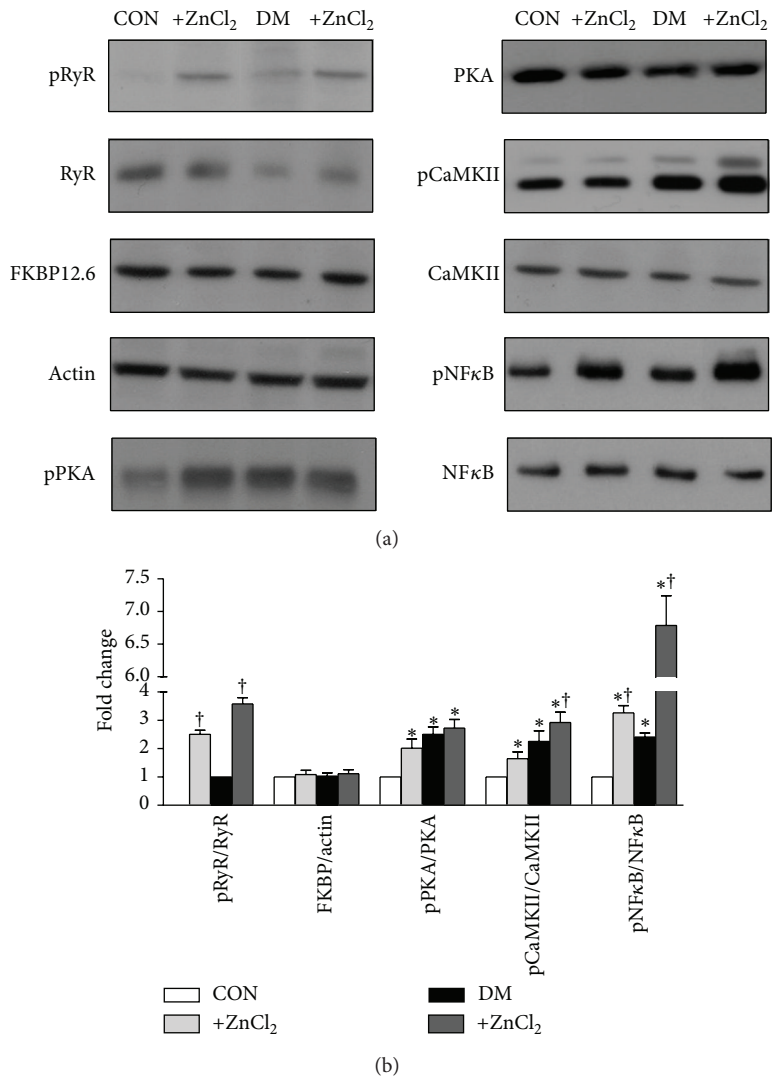

Figure 7: Direct effects of external Zn^{2+} on RyR2 macromolecular complex of ventricular heart tissue. (a) *Top*: representative Western blot images for phospho-RyR2-Ser^{2808} (pRyR2), FK-binding protein, calstabin2 (FKBP), protein kinase A (PKA), phosphorylated PKA (phospho-PKA-Thr198), Ca^{2+}-calmodulin-dependent kinase (CaMKII), phosphorylated CaMKII (phospho-CaMKII-Thr286), nuclear factor kappaB (NF-κB), phosphorylated NF-κB (phosoho-NF-κB), β-actin. (b) Quantification for the ratio of pRyR2 to RyR2, FKBP to β-actin, pPKA to PKA, pCaMKII to CaMKII and pNF-κB to NF-κB. Data presented in (b) obtained from control (CON), 1 μM $ZnCl_2$ incubated control (+$ZnCl_2$, light gray), diabetic (DM) and 1 μM $ZnCl_2$ incubated diabetic (+$ZnCl_2$, dark gray) rat heart homogenates. Bar graphs represent mean ± SEM (n_{rats} = 7–9 for each protocol/group). Significant at $^{*}P < 0.05$ versus CON and $^{\dagger}P < 0.05$ versus DM.

levels of both Zn^{2+} and Ca^{2+} since all these alterations could be prevented with either NAC treatment of diabetic rats or NAC-treatment of diabetic cardiomyocytes. Our electron microscopy data further corroborated these findings fully. Furthermore, we clearly established that these defects in diabetic cardiomyocytes could be attributed to anomalous RyR2 behavior, as revealed by the spatiotemporal properties of both Zn^{2+} and Ca^{2+} sparks that especially exhibited slower kinetics and higher frequencies. The reduced amount of RyR2 and FKBP12.6 levels as well as a marked hyperphosphorylation of RyR2 could be responsible for most of these observations, in part, due to a disbalanced ratio of oxidants/antioxidant-defence. Moreover, the initial findings of this study indicate that supplementation with NAC improves the general status of diabetic rats, with an effect on body weight gain and hyperglycemia, protecting diastolic function, and helping to maintain baseline myocardial mechanics.

4.1. Antioxidant N-Acetyl Cysteine Prevents RyR2 Leak and Plays an Important Role in Diastolic Dysfunction via Increased Levels of Both Zn^{2+} and Ca^{2+} in Diabetic Heart. The present study shows that systemic antioxidant treatment of diabetic rats preserves changes in both Zn^{2+} and Ca^{2+} regulation in diabetic cardiomyocytes without any effect on high blood glucose level and restores normal macromolecular complex composition and function of the RyR2 channels in diabetic

rat hearts. There is associated restoration of myocardial diastolic function and reverse structural remodeling of the left ventricle in diabetic rats with *N*-acetyl cysteine, NAC treatment for 4 weeks. Furthermore, we clearly established that these defects in diabetic cardiomyocytes could be attributed to anomalous RyR2 behavior, as revealed by the spatiotemporal properties of both Zn^{2+} and Ca^{2+} sparks that especially exhibited slower kinetics and higher frequencies. These alterations can coincide perfectly with the behaviour of leaky RyR2 under strong oxidative/nitrosative stress. Indeed, it is known that both acute and chronic hyperglycemia trigger several biochemical and electrophysiological changes resulting in impaired cardiac contractile function [2], at most, due to hypoglycemia-induced big amount of reactive oxygen species, ROS, and followed by tissue/cell damage in several target organs including heart [3–5, 43]. Furthermore, it has been demonstrated that RyR2s are modulated with sulfhydryl oxidation in cardiomyocytes biphasically [25] while high glucose attenuates protein S-nitrosylation via superoxide production [26], and nitric oxide (NO) mediates intracytoplasmic and intranuclear Zn^{2+} release [27]. Moreover, an important contribution of redox modification of RyR2 with direct and/or indirect action of oxidants into SR Ca^{2+} leak in cardiomyocytes has also been shown under various diseased heart models induced in animals [21–24]. Another supporting fact of our current hypothesis arises from the present data on rapidly increased resting free Zn^{2+} level in cardiomyocytes due to Zn^{2+} release from intracellular stores by reactive, ROS/RNS [11]. Moreover, ROS/RNS have been proposed to contribute to direct and/or indirect damage to cardiomyocytes in diabetes [28, 44], providing a close relationship between both increased and deleterious effects of intracellular basal free Zn^{2+} level in the heart. A group of supporting data has been previously shown by our group, in which we demonstrated that inhibiting SR-Ca^{2+} release or increasing Ca^{2+} load in a low Na^{+} solution suppressed or increased Zn^{2+} movements, respectively. Furthermore, we also showed that mitochondrial inhibitors significantly reduced Zn^{2+} transients as well as Zn^{2+} sparks. In addition, either oxidation by H_2O_2 or changing to acidic pH inhibited the Ca^{2+}-dependent Zn^{2+} release. Taken into consideration the previous ones with the present data, we proposed that Zn^{2+} release results, in part, from Zn^{2+} displacement by Ca^{2+} ions from metalloproteins binding sites whose availability depends on pH and redox status of cardiomyocytes, or rather that Ca^{2+} triggers ROS production inducing changes in metal binding properties of metallothioneins and other redox-active proteins as well as more Zn^{2+} release from SR due to defective RyR2 [11, 12, 15, 28, 45]. Additionally supporting this hypothesis, we have also demonstrated that an increase in Zn^{2+} alters several enzymatic activities and leads to RyR2 phosphorylation as seen in pathological conditions. Moreover, another supporting data to this study has been given by Kamalov et al. [46]. Their data showed that the basal intracellular free Zn^{2+} level is increased by 70% in cardiomyocytes from male diabetic rats being parallel to an unbalanced oxidant-status/antioxidant capacity in the same heart preparations, and by over 200% in aldosteronism. Coordinated changes in the basal intracellular free levels of both Ca^{2+} and Zn^{2+} have recently been also reported by our group under experimental conditions (intracellular Zn^{2+} overload or intracellular Ca^{2+} decrease), as well as during a single beat (transients or elementary events) in the cells [12].

Taken together, these data suggest that one of the beneficial effects of NAC treatment, under *in vivo* or *in vitro* conditions, may improve cardiac muscle function by reversing a maladaptive defect in Zn^{2+} signaling besides already known Ca^{2+} signaling, being parallel or individual, in cardiac myocytes of diabetic rats.

4.2. Increased Intracellular Free Zn^{2+} Phosphorylates Intracellular Ca^{2+} Signaling Kinases and Transcription Factor NF-κB. Notably, in here, we have shown that exogenously applied Zn^{2+} caused marked phosphorylation in RyR2 while there was no effect on the protein levels of both RyR2 and an accessory protein of RyR2 macromolecular complex, FKBP12.6, as well as higher phosphorphorylations in both PKA and CaMKII in a concentration-dependent manner, similar to hyperglycemia. These data are further supported, in part, with the fact that a Zn^{2+}-binding protein calsequestrin resides in the SR and can bind up to 200 mol Zn^{2+} per mol, independently of binding up to 50 mol Ca^{2+} per mol calsequestrin. It is known as an association of Zn^{2+} with over 300 enzymes, where it can interact strongly with electronegative sulfur, nitrogen, and oxygen moieties in multiple coordination forms, serving catalytic and structural roles in maintaining active peptide conformations [47]. In addition to metalloenzymes, Zn^{2+} is most known for its ability to bind and stabilize proteins involved in gene regulation in domains called Zn^{2+}-fingers, Zn^{2+}-clusters, and Zn^{2+}-twists [48]. Therefore, it is well accepted that intracellular free Zn^{2+} plays critical roles in the redox signaling pathway and maintains the normal structure and physiology of various cell types while it can be toxic to cardiomyocytes [11, 49, 50]. Although Zn^{2+} is a vital element for mammalian in a certain range, some triggers such as increased ROS/RNS, ischemia, and infarction lead to release of Zn^{2+} from proteins and cause myocardial damage [11, 51–54].

Therefore, it can be hypothesized that Zn^{2+} may compete with or substitute for metal ions crucial for the activity of signaling proteins. In addition to this hypothesis, it has been shown that Zn^{2+} has multiple functional effects on Ca^{2+}/calmodulin-dependent protein kinase II (CaMKII) and modulates RyR1 binding to sarcoplasmic reticulum vesicles in skeletal muscle biphasically [55, 56]. Accordingly, it can be clearly seen that intracellular free Zn^{2+} signaling can easily interfere with that of Ca^{2+} signaling in cardiomyocytes, particularly under pathological conditions, underlying, in part, cardiac dysfunction. Moreover, supporting this last statement, Zn^{2+} is known to induce CaMKII autophosphorylation, inhibit protein tyrosine phosphatases [55–57] and voltage-gated Ca^{2+} channels in mammalian cells [58], and to be highly cytotoxic [59] while divalent metal ions

influence catalysis and active-site accessibility in the cAMP-dependent protein kinase [60]. In here, although a likely role for such intracellular Zn^{2+} signals is the modulation of protein phosphorylation, it is a strong possibility that both activated/phosphorylated CaMKII and PKA due to increased intracellular free Zn^{2+} turn into a hyperphosphorylated RyR2 under high extracellular Zn^{2+} exposure. Therefore, increased intracellular free Zn^{2+}, most probably a contribution of increased intracellular free Ca^{2+}, under increased oxidative stress together with depressed antioxidant-defence in the cells via hyperglycemia induces important defects in excitation-contraction coupling of cardiomyocytes. This statement is further supported with our previous observation related to coordinated changes in the basal intracellular levels of both free Ca^{2+} and Zn^{2+} under experimental conditions, as well as during a single beat in isolated cardiomyocytes [12].

Thus, a major physiological role for Zn^{2+} may be the modulation of cell signaling cascades, especially those involving protein phosphorylation, and considering also that intracellular Zn^{2+} can rise quickly and can influence Ca^{2+} regulation [49, 58], the relative very low abundance of Zn^{2+} in cardiomyocytes suggests its availability as second messengers for gene expression [49, 61]. In an early study, Atar et al. [49] showed that external Zn^{2+} could activate gene expression in GH3 cells due to modification of expression of Zn^{2+} regulating proteins by changes in intracellular free Zn^{2+} cellular systems [62]. In addition, with later findings on a direct regulation of Zn^{2+}-fingers of Zn^{2+}-finger transcription factors by Zn^{2+} availability [61, 63], it can be accepted that intracellular free Zn^{2+} may serve as a second messenger for transcription factor activation, and therefore, gene expression in response to stress. Accordingly, our present data showed that intracellular free Zn^{2+} can directly and markedly phosphorylate a transcription factor NF-κB in cardiomyocytes, of note much more range in hyperglycemia cells. Of particular interest in cardiomyocytes, our data suggest that Zn^{2+} or Zn^{2+} carrying metalloproteins may be released from internal stores during increased oxidative/nitrosative stress and thereby affect transcription/translation pathways [64].

Taken into consideration all present and also previously published data, in here, we report that an enhancement of antioxidant defence in diabetics, directly targeting heart, seems to prevent diastolic dysfunction, being associated with normalization of RyR2 macromolecular-complex, and thereby prevention of both Zn^{2+} and Ca^{2+} leaks leading to normalization of basal levels of intracellular free Ca^{2+} and Zn^{2+} in the heart. This is nicely in line with an early report performed on a rodent heart with hereditary muscular dystrophy, demonstrating accompany of intracellular Ca^{2+} overloading and oxidative stress with increased intracellular free Zn^{2+} [52]. Besides, Kamalov et al. [46] suggested that an optimal range of intracellular free Zn^{2+}/Ca^{2+} ratio in cardiomyocytes and mitochondria must be preserved to combat oxidative stress. Thus, the increased cytosolic and mitochondrial free Zn^{2+} level are coupled to the induction of oxidative stress, while antioxidant effects result from the rise in cytosolic and mitochondrial free Zn^{2+} levels accompanied by a simultaneous activation of metal response element transcription factor-1 and its induction of such antioxidants as metallothionein-1 and glutathione peroxidase. However, with a long-term treatment, by maintaining both a cellular redox-status and intracellular Zn^{2+} level near to control level, antioxidant NAC prevents the subsequent alterations in intracellular Ca^{2+} homeostasis including both Zn^{2+}/Ca^{2+} releases by RyR2, which leads to major defects in cardiac activity.

Conflict of Interests

No potential conflict of interests relevant to this paper was reported. Erkan Tuncay and Esma N. Okatan are equal co-first authors.

Acknowledgments

This work has been supported by grant from TUBITAK SBAG-111S042. The funders had no role in study design, data collection and analysis, decision to publish, or preparation of the paper. No additional external funding was received for this study. The authors would like to thank B. Can for her EM investigation.

References

[1] S. Rubler, J. Dlugash, Y. Z. Yuceoglu, T. Kumral, A. W. Branwood, and A. Grishman, "New type of cardiomyopathy associated with diabetic glomerulosclerosis," *The American Journal of Cardiology*, vol. 30, no. 6, pp. 595–602, 1972.

[2] A. Ceriello, "The post-prandial state and cardiovascular disease: relevance to diabetes mellitus," *Diabetes/Metabolism Research and Reviews*, vol. 16, no. 2, pp. 125–132, 2000.

[3] J. W. Baynes, "Role of oxidative stress in development of complications in diabetes," *Diabetes*, vol. 40, no. 4, pp. 405–412, 1991.

[4] M. Brownlee, "Biochemistry and molecular cell biology of diabetic complications," *Nature*, vol. 414, no. 6865, pp. 813–820, 2001.

[5] L. Cai, W. Li, G. Wang, L. Guo, Y. Jiang, and Y. James Kang, "Hyperglycemia-induced apoptosis in mouse myocardium: mitochondrial cytochrome c-mediated caspase-3 activation pathway," *Diabetes*, vol. 51, no. 6, pp. 1938–1948, 2002.

[6] K. K. Griendling and G. A. FitzGerald, "Oxidative stress and cardiovascular injury part I: basic mechanisms and *in vivo* monitoring of ROS," *Circulation*, vol. 108, no. 16, pp. 1912–1916, 2003.

[7] G. Marra, P. Cotroneo, D. Pitocco et al., "Early increase of oxidative stress and reduced antioxidant defenses in patients with uncomplicated type 1 diabetes: a case for gender difference," *Diabetes Care*, vol. 25, no. 2, pp. 370–375, 2002.

[8] G. Vassort and B. Turan, "Protective role of antioxidants in diabetes-induced cardiac dysfunction," *Cardiovascular Toxicology*, vol. 10, no. 2, pp. 73–86, 2010.

[9] R. L. Charles and P. Eaton, "Redox signalling in cardiovascular disease," *Proteomics*, vol. 2, no. 6, pp. 823–836, 2008.

[10] N. Yaras, A. Bilginoglu, G. Vassort, and B. Turan, "Restoration of diabetes-induced abnormal local Ca^{2+} release in cardiomyocytes by angiotensin II receptor blockade," *American Journal of Physiology*, vol. 292, no. 2, pp. H912–H920, 2007.

[11] B. Turan, H. Fliss, and M. Désilets, "Oxidants increase intracellular free Zn^{2+} concentration in rabbit ventricular myocytes," *American Journal of Physiology*, vol. 272, no. 5, part 2, pp. H2095–H2106, 1997.

[12] E. Tuncay, A. Bilginoglu, N. N. Sozmen et al., "Intracellular free zinc during cardiac excitationcontraction cycle: calcium and redox dependencies," *Cardiovascular Research*, vol. 89, no. 3, pp. 634–642, 2011.

[13] S. L. Sensi, H. Z. Yin, and J. H. Weiss, "Glutamate triggers preferential Zn^{2+} flux through Ca^{2+} permeable AMPA channels and consequent ROS production," *NeuroReport*, vol. 10, no. 8, pp. 1723–1727, 1999.

[14] S. Yamasaki, K. Sakata-Sogawa, A. Hasegawa et al., "Zinc is a novel intracellular second messenger," *Journal of Cell Biology*, vol. 177, no. 4, pp. 637–645, 2007.

[15] B. L. Vallee and K. H. Falchuk, "The biochemical basis of zinc physiology," *Physiological Reviews*, vol. 73, no. 1, pp. 79–118, 1993.

[16] G. Kamalov, P. A. Deshmukh, N. Y. Baburyan et al., "Coupled calcium and zinc dyshomeostasis and oxidative stress in cardiac myocytes and mitochondria of rats with chronic aldosteronism," *Journal of Cardiovascular Pharmacology*, vol. 53, no. 5, pp. 414–423, 2009.

[17] B. Kindermann, F. Döring, D. Fuchs, M. W. Pfaffl, and H. Daniel, "Effects of increased cellular zinc levels on gene and protein expression in HT-29 cells," *BioMetals*, vol. 18, no. 3, pp. 243–253, 2005.

[18] W. Maret, "Oxidative metal release from metallothionein via zinc-thiol/disulfide interchange," *Proceedings of the National Academy of Sciences of the United States of America*, vol. 91, no. 1, pp. 237–241, 1994.

[19] P. I. Oteiza, "Zinc and the modulation of redox homeostasis," *Free Radical Biology and Medicine*, vol. 53, no. 9, pp. 1748–1759, 2012.

[20] N. Yaras, M. Ugur, S. Ozdemir et al., "Effects of diabetes on ryanodine receptor Ca release channel (RyR2) and Ca^{2+} homeostasis in rat heart," *Diabetes*, vol. 54, no. 11, pp. 3082–3088, 2005.

[21] J. Deng, G. Wang, Q. Huang et al., "Oxidative stress-induced leaky sarcoplasmic reticulum underlying acute heart failure in severe burn trauma," *Free Radical Biology and Medicine*, vol. 44, no. 3, pp. 375–385, 2008.

[22] K. Anzai, K. Ogawa, A. Kuniyasu, T. Ozawa, H. Yamamoto, and H. Nakayama, "Effects of hydroxyl radical and sulfhydryl reagents on the open probability of the purified cardiac ryanodine receptor channel incorporated into planar lipid bilayers," *Biochemical and Biophysical Research Communications*, vol. 249, no. 3, pp. 938–942, 1998.

[23] P. Aracena, W. Tang, S. L. Hamilton, and C. Hidalgo, "Effects of S-glutathionylation and S-nitrosylation on calmodulin binding to triads and FKBP12 binding to type 1 calcium release channels," *Antioxidants and Redox Signaling*, vol. 7, no. 7-8, pp. 870–881, 2005.

[24] D. Terentyev, I. Györke, A. E. Belevych et al., "Redox modification of ryanodine receptors contributes to sarcoplasmic reticulum Ca^{2+} leak in chronic heart failure," *Circulation Research*, vol. 103, no. 12, pp. 1466–1472, 2008.

[25] H. Xie and P. H. Zhu, "Biphasic modulation of ryanodine receptors by sulfhydryl oxidation in rat ventricular myocytes," *Biophysical Journal*, vol. 91, no. 8, pp. 2882–2891, 2006.

[26] C. Wadham, A. Parker, L. Wang, and P. Xia, "High glucose attenuates protein S-nitrosylation in endothelial cells: role of oxidative stress," *Diabetes*, vol. 56, no. 11, pp. 2715–2721, 2007.

[27] D. Berendji, V. Kolb-Bachofen, K. L. Meyer et al., "Nitric oxide mediates intracytoplasmic and intranuclear zinc release," *FEBS Letters*, vol. 405, no. 1, pp. 37–41, 1997.

[28] M. Ayaz and B. Turan, "Selenium prevents diabetes-induced alterations in $[Zn^{2+}]_i$ and metallothionein level of rat heart via restoration of cell redox cycle," *American Journal of Physiology*, vol. 290, no. 3, pp. H1071–H1080, 2006.

[29] A. Aydemir-Koksoy, A. Bilginoglu, M. Sariahmetoglu, R. Schulz, and B. Turan, "Antioxidant treatment protects diabetic rats from cardiac dysfunction by preserving contractile protein targets of oxidative stress," *Journal of Nutritional Biochemistry*, vol. 21, no. 9, pp. 827–833, 2010.

[30] E. Tuncay, A. A. Seymen, E. Tanriverdi et al., "Gender related differential effects of Omega-3E treatment on diabetes-induced left ventricular dysfunction," *Molecular and Cellular Biochemistry*, vol. 304, no. 1-2, pp. 255–263, 2007.

[31] B. Turan, M. Désilets, L. N. Açan, Ö. Hotomaroglu, C. Vannier, and G. Vassort, "Oxidative effects of selenite on rat ventricular contractility and Ca movements," *Cardiovascular Research*, vol. 32, no. 2, pp. 351–361, 1996.

[32] E. N. Zeydanli, H. B. Kandilci, and B. Turan, "Doxycycline ameliorates vascular endothelial and contractile dysfunction in the thoracic aorta of diabetic rats," *Cardiovascular Toxicology*, vol. 11, no. 2, pp. 134–147, 2011.

[33] F. Fiordaliso, R. Bianchi, L. Staszewsky et al., "Antioxidant treatment attenuates hyperglycemia-induced cardiomyocyte death in rats," *Journal of Molecular and Cellular Cardiology*, vol. 37, no. 5, pp. 959–968, 2004.

[34] E. Ho, G. Chen, and T. M. Bray, "Supplementation of N-acetylcysteine inhibits NFκB activation and protects against alloxan-induced diabetes in CD-1 mice," *FASEB Journal*, vol. 13, no. 13, pp. 1845–1854, 1999.

[35] P. R. Nagareddy, Z. Xia, K. M. MacLeod, and J. H. McNeill, "N-acetylcysteine prevents nitrosative stress-associated depression of blood pressure and heart rate in streptozotocin diabetic rats," *Journal of Cardiovascular Pharmacology*, vol. 47, no. 4, pp. 513–520, 2006.

[36] M. Ayaz, B. Can, S. Ozdemir, and B. Turan, "Protective effect of selenium treatment on diabetes-induced myocardial structural alterations," *Biological Trace Element Research*, vol. 89, no. 3, pp. 215–226, 2002.

[37] M. Ayaz, S. Ozdemir, M. Ugur, G. Vassort, and B. Turan, "Effects of selenium on altered mechanical and electrical cardiac activities of diabetic rat," *Archives of Biochemistry and Biophysics*, vol. 426, no. 1, pp. 83–90, 2004.

[38] N. Yaras, M. Sariahmetoglu, A. Bilginoglu et al., "Protective action of doxycycline against diabetic cardiomyopathy in rats," *British Journal of Pharmacology*, vol. 155, no. 8, pp. 1174–1184, 2008.

[39] W. Maret, "The function of zinc metallothionein: a link between cellular zinc and redox state," *Journal of Nutrition*, vol. 130, supplement 5, pp. 1455S–1458S, 2000.

[40] W. Maret, "Molecular aspects of human cellular zinc homeostasis: redox control of zinc potentials and zinc signals," *BioMetals*, vol. 22, no. 1, pp. 149–157, 2009.

[41] R. Kumar, Q. C. Yong, and C. M. Thomas, "Do multiple nuclear factor kappa b activation mechanisms explain its varied effects in the heart?" *The Ochsner Journal*, vol. 13, no. 1, pp. 157–165, 2013.

[42] S. Bao, M. Liu, B. Lee et al., "Zinc modulates the innate immune response *in vivo* to polymicrobial sepsis through regulation of

NF-κB," *American Journal of Physiology*, vol. 298, no. 6, pp. L744–L754, 2010.

[43] M. Brownlee, "The pathobiology of diabetic complications: a unifying mechanism," *Diabetes*, vol. 54, no. 6, pp. 1615–1625, 2005.

[44] L. M. Malaiyandi, K. E. Dineley, and I. J. Reynolds, "Divergent consequences arise from metallothionein overexpression in astrocytes: zinc buffering and oxidant-induced zinc release," *GLIA*, vol. 45, no. 4, pp. 346–353, 2004.

[45] S. L. Sensi and J.-M. Jeng, "Rethinking the excitotoxic ionic millieu: the emerging role of Zn^{2+} in ischemic neuronal injury," *Current Molecular Medicine*, vol. 4, no. 2, pp. 87–111, 2004.

[46] G. Kamalov, R. A. Ahokas, W. Zhao et al., "Uncoupling the coupled calcium and zinc dyshomeostasis in cardiac myocytes and mitochondria seen in aldosteronism," *Journal of Cardiovascular Pharmacology*, vol. 55, no. 3, pp. 248–254, 2010.

[47] D. W. Choi and J. Y. Koh, "Zinc and brain injury," *Annual Review of Neuroscience*, vol. 21, pp. 347–375, 1998.

[48] B. L. Vallee, J. E. Coleman, and D. S. Auld, "Zinc fingers, zinc clusters, and zinc twists in DNA-binding protein domains," *Proceedings of the National Academy of Sciences of the United States of America*, vol. 88, no. 3, pp. 999–1003, 1991.

[49] D. Atar, P. H. Backx, M. M. Appel, W. D. Gao, and E. Marban, "Excitation-transcription coupling mediated by zinc influx through voltage- dependent calcium channels," *Journal of Biological Chemistry*, vol. 270, no. 6, pp. 2473–2477, 1995.

[50] Y. Qin, D. Thomas, C. P. Fontaine, and R. A. Colvin, "Mechanisms of Zn^{2+} efflux in cultured cortical neurons," *Journal of Neurochemistry*, vol. 107, no. 5, pp. 1304–1313, 2008.

[51] M. A. Aras and E. Aizenman, "Redox regulation of intracellular zinc: molecular signaling in the life and death of neurons," *Antioxidants and Redox Signaling*, vol. 15, no. 8, pp. 2249–2263, 2011.

[52] A. J. Crawford and S. K. Bhattacharya, "Excessive intracellular zinc accumulation in cardiac and skeletal muscles of dystrophic hamsters," *Experimental Neurology*, vol. 95, no. 2, pp. 265–276, 1987.

[53] H. Fliss and M. Menard, "Oxidant-induced mobilization of zinc from metallothionein," *Archives of Biochemistry and Biophysics*, vol. 293, no. 1, pp. 195–199, 1992.

[54] R. A. Bozym, F. Chimienti, L. J. Giblin et al., "Free zinc ions outside a narrow concentration range are toxic to a variety of cells *in vitro*," *Experimental Biology and Medicine*, vol. 235, no. 6, pp. 741–750, 2010.

[55] I. Lengyel, S. Fieuw-Makaroff, A. L. Hall, A. T. R. Sim, J. A. P. Rostas, and P. R. Dunkley, "Modulation of the phosphorylation and activity of calcium/calmodulin- dependent protein kinase II by zinc," *Journal of Neurochemistry*, vol. 75, no. 2, pp. 594–605, 2000.

[56] R. H. Xia, X. Y. Cheng, H. Wang et al., "Biphasic modulation of ryanodine binding to sarcoplasmic reticulum vesicles of skeletal muscle by Zn^{2+} ions," *Biochemical Journal*, vol. 345, no. 2, pp. 279–286, 2000.

[57] K. A. Skelding and J. A. P. Rostas, "Regulation of CaMKII *in vivo*: the importance of targeting and the intracellular microenvironment," *Neurochemical Research*, vol. 34, no. 10, pp. 1792–1804, 2009.

[58] B. Turan, "Zinc-induced changes in ionic currents of cardiomyocytes," *Biological Trace Element Research*, vol. 94, no. 1, pp. 49–59, 2003.

[59] B. M. Palmer, S. Vogt, Z. Chen, R. R. Lachapelle, and M. M. LeWinter, "Intracellular distributions of essential elements in cardiomyocytes," *Journal of Structural Biology*, vol. 155, no. 1, pp. 12–21, 2006.

[60] J. A. Adams and S. S. Taylor, "Phosphorylation of peptide substrates for the catalytic subunit of cAMP- dependent protein kinase," *Journal of Biological Chemistry*, vol. 268, no. 11, pp. 7747–7752, 1993.

[61] G. K. Andrews, "Cellular zinc sensors: MTF-1 regulation of gene expression," *BioMetals*, vol. 14, no. 3-4, pp. 223–237, 2001.

[62] G. W. Verhaegh, M. O. Parat, M. J. Richard, and P. Hainaut, "Modulation of p53 protein conformation and DNA-binding activity by intracellular chelation of zinc," *Molecular Carcinogenesis*, vol. 21, no. 3, pp. 205–214, 1998.

[63] A. J. Bird, H. Zhao, H. Luo et al., "A dual role for zinc fingers in both DNA binding and zinc sensing by the Zap1 transcriptional activator," *EMBO Journal*, vol. 19, no. 14, pp. 3704–3713, 2000.

[64] S. Pikkarainen, H. Tokola, T. Majalahti-Palviainen et al., "GATA-4 is a nuclear mediator of mechanical stretch-activated hypertrophic program," *Journal of Biological Chemistry*, vol. 278, no. 26, pp. 23807–23816, 2003.

Hindawi Publishing Corporation
Oxidative Medicine and Cellular Longevity
Volume 2014, Article ID 960362, 16 pages
http://dx.doi.org/10.1155/2014/960362

Research Article

Effects of Downregulation of MicroRNA-181a on H_2O_2-Induced H9c2 Cell Apoptosis via the Mitochondrial Apoptotic Pathway

Lei Wang,[1,2] He Huang,[1,2] Yang Fan,[1,2] Bin Kong,[1,2] He Hu,[1,2] Ke Hu,[1,2] Jun Guo,[1,2] Yang Mei,[1,2] and Wan-Li Liu[1,2]

[1] *Department of Cardiology, Renmin Hospital of Wuhan University, Jiefang Road 238, Wuhan 430060, China*
[2] *Cardiovascular Research Institute of Wuhan University, Jiefang Road 238, Wuhan 430060, China*

Correspondence should be addressed to He Huang; huanghe1977@hotmail.com

Received 27 October 2013; Revised 16 December 2013; Accepted 19 December 2013; Published 11 February 2014

Academic Editor: Neelam Khaper

Glutathione peroxidase-1 (GPx1) is a pivotal intracellular antioxidant enzyme that enzymatically reduces hydrogen peroxide to water to limit its harmful effects. This study aims to identify a microRNA (miRNA) that targets GPx1 to maintain redox homeostasis. Dual luciferase assays combined with mutational analysis and immunoblotting were used to validate the bioinformatically predicted miRNAs. We sought to select miRNAs that were responsive to oxidative stress induced by hydrogen peroxide (H_2O_2) in the H9c2 rat cardiomyocyte cell line. Quantitative real-time PCR (qPCR) demonstrated that the expression of miR-181a in H_2O_2-treated H9c2 cells was markedly upregulated. The downregulation of miR-181a significantly inhibited H_2O_2-induced cellular apoptosis, ROS production, the increase in malondialdehyde (MDA) levels, the disruption of mitochondrial structure, and the activation of key signaling proteins in the mitochondrial apoptotic pathway. Our results suggest that miR-181a plays an important role in regulating the mitochondrial apoptotic pathway in cardiomyocytes challenged with oxidative stress. MiR-181a may represent a potential therapeutic target for the treatment of oxidative stress-associated cardiovascular diseases.

1. Introduction

Growing evidence demonstrates that increased levels of reactive oxygen species (ROS) are associated with a variety of cardiovascular diseases [1]. Although ROS can originate from different organelles, mitochondria are considered to be the main producers of ROS. Approximately 80% of anion superoxide ($O_2^{\bullet}$) is produced by mitochondria [2]. In the heart, approximately 30% of the total volume is occupied by mitochondria, and thus the heart is easily subjected to oxidative damage by ROS [3]. To combat the deleterious effects of ROS, mitochondria have evolved an intrinsic antioxidant defense network that mainly consists of the superoxide dismutase (SOD), NADH, and a complete glutathione redox system, formed by glutathione reductase, reduced glutathione (GSH), and glutathione peroxidase (GPx) [4].

GPx converts H_2O_2 and lipid hydroperoxides into water, using GSH as an electron donor. GPx1 is the main isoform, produced in all tissues and expressed in both the cytosol and the mitochondrial matrix. GPx1 prevents the formation of the highly reactive hydroxyl radical [5]. Several genetically modified animal models have been used to show the protective role of GPx1 in cardiac damage caused by ischemia-reperfusion injury [6–8]. Recent findings also indicate that the lack of GPx1 contributes to the risk of atherosclerosis and cardiovascular disease. Mice deficient in GPx1 ($GPx1^{-/-}/ApoE^{-/-}$) developed significantly more atherosclerosis than the control apolipoprotein E-deficient mice [9, 10]. Additionally, transgenic mice overexpressing Gpx1 were protected from aging-related enhanced susceptibility to venous thrombosis compared with wild-type mice [11]. Gpx1 also plays a pivotal role in the protection against angiotensin II-induced vascular dysfunction [12].

The posttranscriptional regulation of GPx1 expression in oxidative stress via nuclear factor κB (NFκB) and activator protein 1 (AP-1) has been shown by many investigators [13, 14]. However, the posttranscriptional mechanism of

Gpx1 in response to H_2O_2-mediated oxidative stress in cardiomyocytes has not been thoroughly studied. MicroRNAs (miRNAs) are one example of a translational mechanism for the regulation of a large number of developmental and physiological processes in the heart [15]. An miRNA is a small, single-stranded RNA that is approximately 22 nucleotides (nt) long. miRNAs are widely distributed and induce both messenger RNA (mRNA) degradation and the suppression of protein translation based on sequence complementarity between the miRNA and its target [16].

The H9c2 rat cardiomyocyte cell line was chosen in the present study as this cell line retains the characteristics of isolated primary cardiomyocytes [17]. We investigated the role of miR-181a in regulating H9c2 cell apoptosis and modulating the mitochondrial apoptotic pathway in the setting of oxidative stress. We found that miR-181a is upregulated in cardiomyocytes with oxidative stress and that the downregulation of miR-181a significantly inhibited the H_2O_2-induced cellular apoptosis, ROS production, mitochondrial structure disruption, and activation of key signaling proteins in the mitochondrial apoptotic pathway. These protective effects were mediated at least partially through the direct targeting of Gpx1.

2. Materials and Methods

2.1. Cell Culture and Determination of Cell Viability. HEK293 cells, myogenic L6 cells, and H9c2 cells (from the Cell Bank of the Chinese Academy of Sciences, Shanghai, China) were cultured in Dulbecco's modified Eagle's medium (DMEM, Invitrogen) supplemented with 5 g/L glucose and 15% (v/v) fetal bovine serum. The cells were maintained in a humidified 37°C incubator with 5% CO_2, supplied with fresh medium every 3 days, and subcultured before reaching confluence. The H9c2 cells were seeded in 96-well microtiter plates and treated with different concentrations of H_2O_2 for 2 h. The MTT assay was used to determine cell viability, following the manufacturer's protocols.

2.2. Bioinformatics Analysis. Rat Gpx1 3′ untranslated region (3′ UTR) sequences were retrieved from the Entrez Nucleotide database (http://www.ncbi.nlm.nih.gov/nuccore). Potential miRNAs targeting Gpx1 were predicted by miRDB (http://mirdb.org/miRDB/), TargetScan (http://www.targetscan.org/), and MicroRNA.ORG (http://www.microrna.org/).

2.3. Transfections, Constructs, and Dual Luciferase Reporter Assay. HEK293 and H9c2 cells were transfected with 50 nM mature miR-181a and miR-CTL (GuangzhouRuiBio Corp., Guangzhou, China) using Lipofectamine 2000 (Invitrogen, USA) as previously described [18]. H9c2 cells were also transfected with a final concentration of 100 nM and for miR-181a knockdown anti-miR-181a (Guangzhou RiBo Corp., Guangzhou, China). The anti-CTL and anti-miR-181a are represented as the scrambled inhibitor and miR-181a inhibitor, respectively. The anti-miR-181a contained 2′-OMe modifications at every base.

The 3′ UTR of the Gpx1 gene was amplified by PCR from total RNA extracted with a Genomic DNA Extraction kit (TaKaRa Bio Inc., Tokyo, Japan) from myogenic L6 cells. The sequences of the primers for the Gpx1 3′ UTR and mutant Gpx1 3′ UTR were as follows: R-Gpx1-3′ UTR-F, CCG**CTCG AG**CCTAAGGCATTCCTGGTATCTGG; R-Gpx1-3′ UTR-R, GAAT**GCGGCCG CTTCTTTGACATTCAGCACTTTATTC**; and R-Gpx1-3′ UTR-Mut-R, GAAT**GCGGC CGC**TTCTTTG**AGAATGA**GCACTTTATTCTTAG. The bold letters in the primers indicate XhoI and SalI restriction sites. The PCR products were excised with XhoI and NotI and cloned into the pmiR-RB-REPORT vector (GuangzhouRuiBio Corp., Guangzhou, China). This plasmid contains hRluc (synthetic renilla luciferase gene), encoding renilla luciferase as the reporter, and hluc (synthetic firefly luciferase gene), encoding firefly luciferase as the internal control. The recombinant plasmid pmiR-RB-Gpx1-3′ UTR was confirmed by restriction enzyme digestion and DNA sequencing.

The luciferase assays were performed according to the manufacturer's protocol. HEK293 cells, seeded into 96-well plates at a density of 1.5×10^4 per well, were transfected with pmiR-RB-Gpx1-WT-3′ UTR (100 ng/well), pmiR-RB-Gpx1-Mut-3′ UTR (100 ng/well), mature miR-181a (50 nM), or miR-control (50 nM) using Lipofectamine 2000. Forty-eight hours after-transfection, the cells were lysed and assayed for luciferase activity using the Dual Glo Luciferase Assay System (Promega). Data recorded by the luminometer were normalized by dividing the firefly luciferase activity with the renilla luciferase activity.

2.4. Measurement of Lactate Dehydrogenase (LDH) and Malondialdehyde (MDA) Levels. H9c2 cells were transfected with miRNAs for 6 h and cultured for 24 h. H_2O_2 (400 μM) was added for the last 2 h. Subsequently, the cells were harvested and lysed. LDH release and MDA content were measured using commercial kits (Jiancheng Bioengineering Institute, China), according to the manufacturer's instructions.

2.5. Intracellular Reactive Oxygen Species (ROS) Assay. H9c2 cells were grown to confluence in a 96-well plate and then transfected with miRNAs for 6 h and cultured for 24 h. H_2O_2 (400 μM) was added for the last 2 h. The cells were then incubated with 2′,7′-dichlorofluorescin-diacetate (DCFH-DA, Sigma) at 37°C for 30 min. The DCFH-DA stain detecting ROS production was observed using a fluorescence microscope (Nikon, Japan). Fluorescence was read at 485 nm for excitation and 530 nm for emission with an Infinite M200 Microplate Reader (Tecan, Switzerland).

2.6. Annexin V and PI Binding Assay. The Annexin V and PI Fluorescein Staining kits (Bender MedSystems, Austria) were utilized to measure H9c2 cell apoptosis, according to the manufacturer's instructions. Briefly, a single-cell suspension was prepared and cultured in a six-well plate at a density of 1×10^5/well. Twenty-four hours after transfection, cells from each group were collected and resuspended in two

hundred microliters of 1x binding buffer. The cells were then incubated with annexin V (1 : 20) for 3 min followed by incubation with propidium iodide (PI, 1 mg/mL) for 15 min. The apoptosis rate was evaluated by flow cytometry (BD).

2.7. Measurement of Mitochondrial Membrane Potential. H9c2 cells were grown on cover slips and incubated with 5 μg/mL JC-1 dye (Enzo Life Sciences, USA) at 37°C for 30 min. The cells were analyzed immediately with a fluorescence microscope. JC-1 accumulates in the mitochondria, selectively generating an orange J-aggregate emission profile (590 nm) in healthy cells. However, upon cell injury, the membrane potential decreases, and JC-1 monomers are generated, resulting in a shift to green emission (529 nm). The orange and green fluorescence intensities were detected using an Infinite M200 Microplate Reader. The $\Delta\psi$m of the H9c2 cells in each treatment group was calculated as the ratio of orange to green fluorescence and expressed as a multiple of the level in the control group.

2.8. Quantitative Real-Time PCR. Total RNA was extracted from H9c2 cells using the Trizol Reagent (Invitrogen). The RT primers and primer sets specific for each miRNA are shown in Tables 1 and 2. The SYBR green stem-loop RT-PCR method was used to assess the expression levels of the miRNAs. The PCR conditions were as follows: 95°C for 10 min, followed by 40 cycles of 95°C for 15 sec and 60°C for 1 min. Samples were run in duplicate with RNA preparations from three independent experiments. The reactions were conducted on the ABI PRISM 7900 system (Applied Biosystems). The fold change in the expression of each gene was calculated using the $2^{-\Delta\Delta CT}$ method, with U6 as an internal control.

2.9. Western Blot Analysis. H9c2 cells growing on six-well plates were transduced with miRNAs and treated with 400 μM H_2O_2, as indicated. The proteins were separated on SDS-polyacrylamide gels and transferred to PVDF membranes. For immunoblotting, PVDF membranes were blocked and probed with antibodies overnight at 4°C. Immunocomplexes were visualized with horseradish peroxidase-coupled secondary antibodies.

2.10. Immunofluorescence Detection of Intracellular Cytochrome c Localization by Fluorescence Microscopy. After the appropriate treatment, the cells were washed with PBS and stained with 200 nM MitoTracker Red CMXRos dye (Molecular Probes, Inc., France), followed by incubation for 30 min at room temperature, to visualize the mitochondria. The cells were fixed with 4% paraformaldehyde for 15 min, permeabilized with 0.1% Triton X-100 for 10 min, and blocked using 3% serum dissolved in PBS for 30 min at room temperature. The cells were then probed with anti-cytochrome c antibody (1 : 40; Santa Cruz Biotechnology) overnight at 4°C. The cells were washed with PBS twice and incubated with FITC-conjugated secondary antibody (1 : 40; Biovision, China) for 2 h in the dark at 37°C. After washing, images of stained cells were obtained using a fluorescence microscope.

2.11. Statistical Analysis. All data are expressed as the mean ± SEM, unless indicated otherwise. Differences among groups were determined by ANOVA. Differences between groups were determined by Student's t-test, with $P < 0.05$ considered statistically significant.

3. Results

3.1. Effects of H_2O_2 on Cell Viability and Protein Expression. The viability of H9c2 cells was determined using the MTT assay by exposing the cells to different concentrations of H_2O_2 for 2 h. Although low concentrations of H_2O_2 had no effect on apoptosis and death, high concentrations (100–800 μM) increased H9c2 cell death in a dose-dependent manner after a 2 h treatment under our experimental conditions (Figure 1(a)).

Because GPx1 is a major antioxidant enzyme that catalyzes the breakdown of H_2O_2, we hypothesized that exogenous H_2O_2 must induce endogenous Gpx1 expression changes in H9c2 cells. As shown in Figure 1(b), compared with untreated cells, a significant increase in GPx1 protein expression was observed in cells treated with H_2O_2 (100 and 200 μM), suggesting that the exposure to moderate concentrations of H_2O_2 induces a compensation response, whereas 400 μM H_2O_2 damages the antioxidant enzyme system, resulting in decreased Gpx1 expression. Therefore, for the remainder of our experiments, a 400 μM concentration of H_2O_2 was used to assess H_2O_2-mediated effects on H9c2 cells.

3.2. Predicted miR-181a as a Negative Regulator of Gpx1. To focus on the role of miRNAs as regulators of Gpx1, three commonly utilized miRNA target prediction algorithms (TargetScan, miRDB, and MiRanda) were interrogated for possible miRNAs interacting with Gpx1. The results of these three algorithms had four potential miRNA candidates in common: miR-7a, 125a, 181a, and 423 (Figure 2(a)). Next, to assess the expression of these candidate miRNAs induced by the apoptotic H_2O_2 concentration, H9c2 cells were exposed to 400 μM $H_2O_2$for 2 h, and the expression levels of the miRNAs were determined by real-time PCR. If an miRNA candidate is a negative regulator of Gpx1, then H_2O_2 should increase its expression in H9c2 cells because the Gpx1 expression was downregulated after stimulation with 400 μM H_2O_2 (Figure 1(b)). At the apoptotic concentration of H_2O_2, only miR-181a expression was increased compared with the control group, whereas the expression of the other candidate miRNAs was decreased (Figure 2(b)). To further confirm the expression change, a 2 h exposure of H9c2 cells to varying concentrations of H_2O_2 resulted in concentration-dependent increases in miR-181a expression, with a peak at approximately 400 μM (Figure 2(b)). Taken together, these results suggest that miR-181a plays a key role in oxidative stress-induced cardiomyocyte apoptosis and that miR-181a may be linked with the expression of Gpx1.

Table 1: Sequences of the RT primers.

Primer name	RT primer sequence
U6	5′CGCTTCACGAATTTGCGTGTCAT3′
rno-miR-7a	5′GTCGTATCCAGTGCGTGTCGTGGAGTCGGCAATTGCACTGGATACGACACAACAA3′
rno-miR-181a	5′GTCGTATCCAGTGCGTGTCGTGGAGTCGGCAATTGCACTGGATACGACCATGGA3′
rno-miR-125a	5′GTCGTATCCAGTGCGTGTCGTGGAGTCGGCAATTGCACTGGATACGACTCACAGG3′
rno-miR-423	5′GTCGTATCCAGTGCGTGTCGTGGAGTCGGCAATTGCACTGGATACGACACTGAGG3′

Table 2: Sequences of the primers used in the SYBR-green-based quantitative RT-PCR validation.

Primer name	Primer sequence	Tm (°C)	Length (bp)
U6	F: 5′GCTTCGGCAGCACATATACTAAAAT3′ R: 5′CGCTTCACGAATTTGCGTGTCAT3′	60	89
rno-miR-423	F: 5′TAAGCTCGGTCTGAGGC3′ R: 5′CAGTGCGTGTCGTGGA3′	60	65
rno-miR-7a	F: 5′GGGGTGGAAGACTAGTGATT3′ R: 5′CAGTGCGTGTCGTGGA3′	60	67
rno-miR-181a	F: 5′GGGCAGCCTTAAGAGGA3′ R: 5′CAGTGCGTGTCGTGGA3′	60	64
rno-miR-125a	F: 5′GCTCCCTGTAGACCCTTTA3′ R: 5′CAGTGCGTGTCGTGGAGT3′	60	67

3.3. Validation of the In Silico Target Analysis of miR-181a. To experimentally validate the computational data, a pmiR-RB-REPORT luciferase construct with the Gpx1-3′-UTR was generated. The purified gel product of Gpx13′-UTR was inserted into the cloning site downstream of the luciferase gene, as described in Section 2. A mutant version, pmiR-RB-Gpx1-3′-UTR-mut, with a three-base-pair mutation within the seed region (Figure 3(a)), was also generated. A significant decrease ($^{*}P < 0.01$) in the relative luciferase activity was observed when the pmiR-RB-Gpx1-3′-UTR was cotransfected with a mature miR-181a into HEK293 cells compared with the miR-control. The miR-181a-mediated suppression was abolished by mutation of the 3′-UTR miR-181a binding site, which disrupts the interaction between miR-181a and the Gpx1-3′-UTR (Figure 3(b)).

Western blotting analyses further confirmed the luciferase assay results. The transfection with the mature miR-181a resulted in decreased Gpx1 protein expression ($^{*}P < 0.01$) compared with the control, whereas the anti-miR-181a protected against the mature miR-181a-mediated inhibition of Gpx1 expression ($^{*}P < 0.05$) (Figure 3(c)).

3.4. Transduction of the Anti-miR-181a Restored the H_2O_2-Altered H9c2 Cell Morphology and Decreased the Levels of LDH and MDA. H9c2 cells were transfected as described in Section 2. As shown in Figure 4(a), the mature miR-181a increased miR-181a expression in H9c2 cells, whereas anti-miR-181a decreased miR-181a expression. The control oligonucleotides had no effect on miR-181a expression.

H_2O_2 treatment changed the spindle-shaped, well-organized cell morphology into a shrunken, round, and distorted morphology. Transduction of the anti-miR-181a, however, almost restored the spindle-shaped morphology observed in untreated cells (Figure 4(b)). MDA levels are indicative of cardiomyocyte oxidativedamage. The H_2O_2 treatment strikingly increased the MDA level, whereas the miR-181a inhibitor significantly decreased the MDA level (Figure 4(c)). LDH release is an indicator of cellular injury. Compared with untreated cells, the LDH levels were markedly increased by H_2O_2-induced injuries. Transduction of the anti-miR-181a decreased LDH release, whereas transduction of the mature miR-181a elevated LDH levels compared with the miR-control (Figure 4(d)).

3.5. Anti-miR-181a Reduced ROS Production. Because Gpx1 catalyzes the reduction of H_2O_2 to water [5] and miR-181a mediates the suppression of Gpx1 expression, we attempted to investigate the effect of miR-181a upon ROS generation. ROS production was detected using an ROS-sensitive dye, 2′,7′-dichlorofluorescein-diacetate (DCFH-DA). As shown in Figure 5(a), H_2O_2 treatment led to strong DCFH-DA staining. Transduction of the mature miR-181a increased the staining intensity, whereas the anti-miR-181a produced relatively dim DCFH-DA staining. These data suggest that the anti-miR-181a attenuates the production of ROS. ROS production was quantified by measuring the cellular fluorescence intensities (Figure 5(b)).

3.6. Anti-miR-181a Attenuated H_2O_2-Induced H9c2 Cell Apoptosis. Compared with the control group, significantly more H_2O_2-treated cells underwent apoptosis, as shown by the bright DAPI staining in the H_2O_2 group.The H_2O_2 treatment caused nuclear condensation, an indicator of apoptosis. Transduction of the anti-miR-181a, however, nearly restored H9c2 nuclei to the normal morphology (Figure 6(a)). Quantitative analysis using flow cytometry confirmed that the

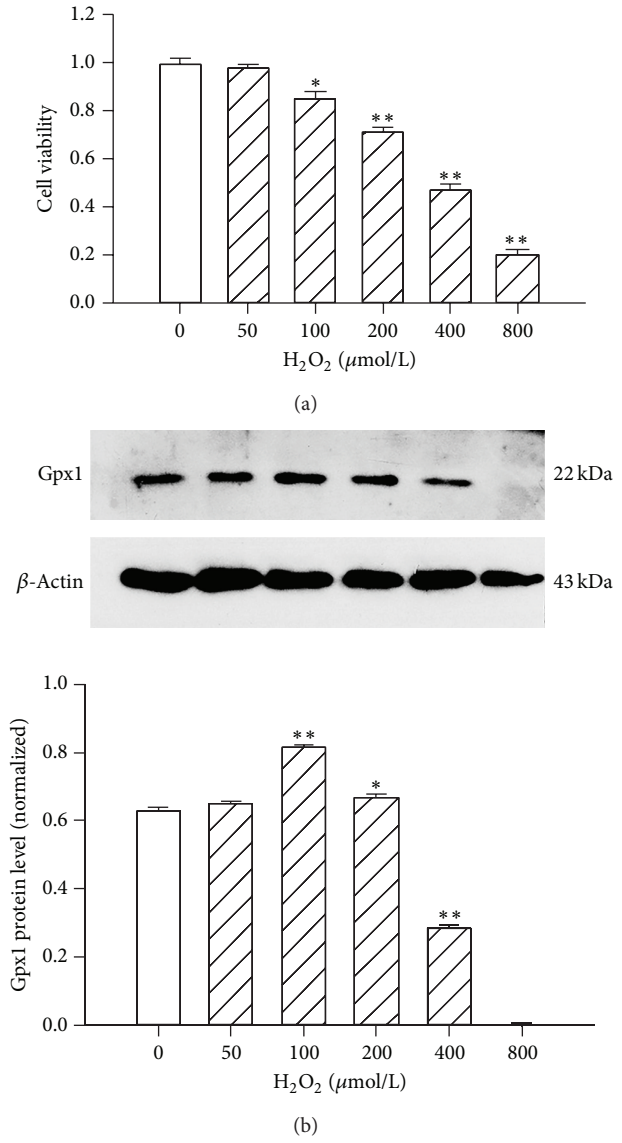

Figure 1: Cell viability and protein expression changes in H_2O_2-treated H9c2 cells. (a) H9c2 cells were treated with various doses of H_2O_2 for 2 h and assessed for cell viability. $^*P < 0.05$ versus control (CTL); $^{**}P < 0.01$ versus control (CTL); the values represent the mean ± SEM, $n = 5$. (b) Gpx1 and β-actin protein levels were detected by western blotting after the treatment of H9c2 cells with different concentrations of H_2O_2 for 2 h. $^*P < 0.05$ versus control (CTL); $^{**}P < 0.01$ versus control (CTL); the values represent the mean ± SEM, $n = 3$.

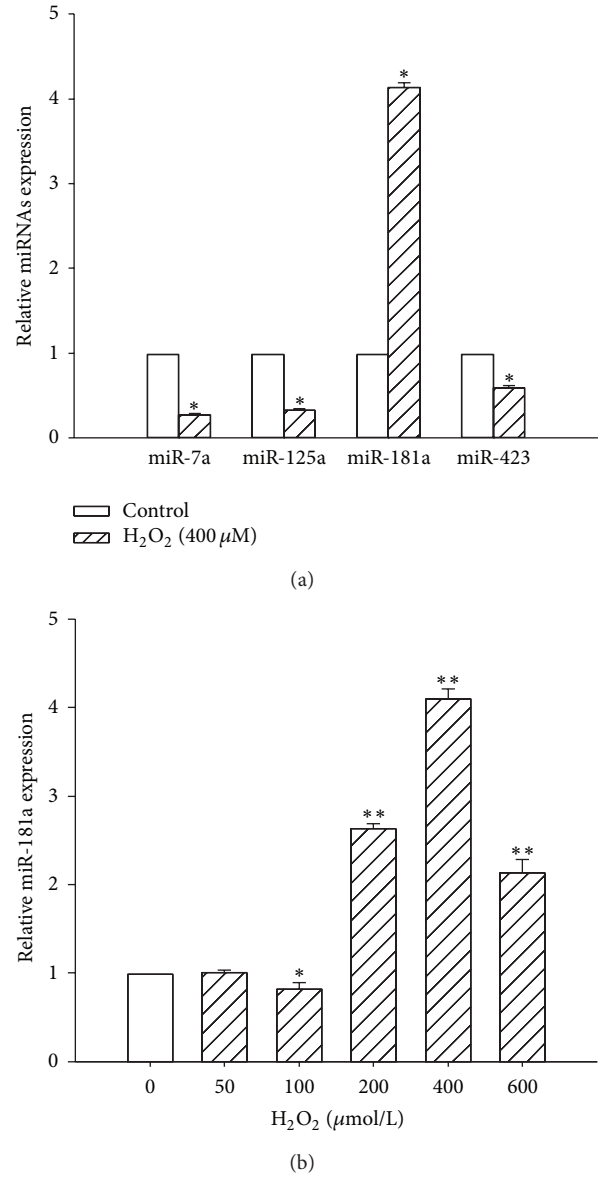

Figure 2: miRNA expression changes in H_2O_2-induced apoptotic cardiomyocytes. (a) Fold change in miR-7a, 125a, 181a, and 423 expression after exposure to H_2O_2 (400 μM) for 2 h. $^*P < 0.01$ versus control (CTL); the values represent the mean ± SEM, $n = 3$. (b) H9c2 cells were treated with different concentrations of H_2O_2, ranging from 50 to 800 μM for 2 h. $^*P < 0.05$ versus control (CTL); $^{**}P < 0.01$ versus control (CTL); the values represent the mean ± SEM, $n = 3$.

anti-miR-181a significantly inhibited H_2O_2-induced apoptosis (Figures 6(b)-6(c)). To investigate the mechanism by which the anti-miR-181a attenuates the H_2O_2-induced H9c2 apoptosis, we examined the protein levels of Bcl-2 and Bax. Western blot analyses showed that Bcl-2 protein levels were markedly increased in the anti-miR-181a-treated cells compared with the miR-CTL group. As expected, Bax expression was markedly decreased by the anti-miR-181a (Figures 6(d) and 6(f)), suggesting that the anti-miR-181a prevents H9c2 cells from undergoing apoptosis by increasing Bcl-2 while inhibiting Bax.

3.7. Anti-miR-181a Restored the H_2O_2-Induced Loss of the Mitochondrial Membrane Potential. Untreated cells contained bright-staining mitochondria that emitted orange fluorescence. The H_2O_2 treatment caused the formation of monomeric JC-1, indicative of a loss of mitochondrial membrane potential. Transduction of the anti-miR-181a, however,

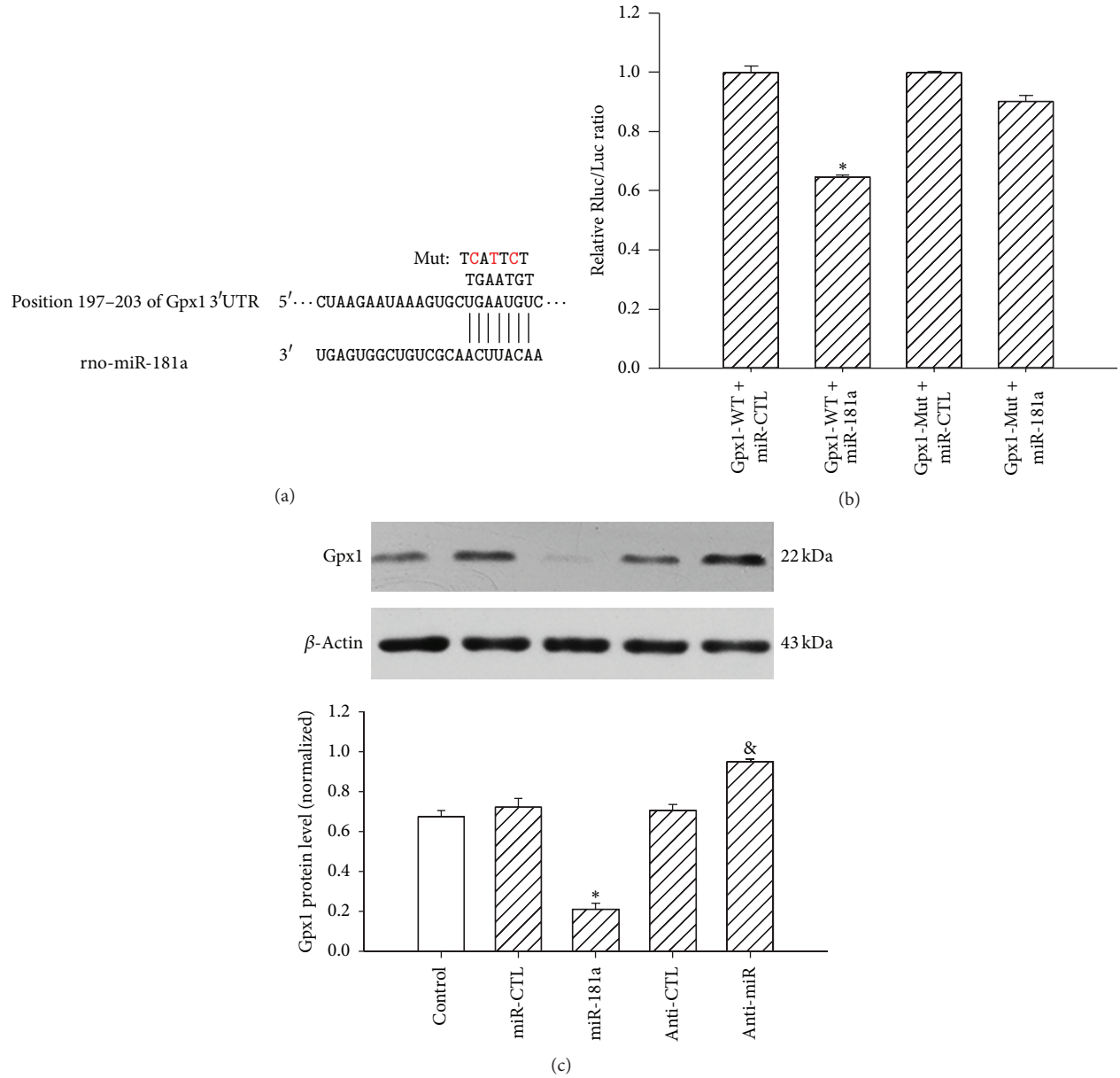

Figure 3: Gpx1 3′-UTR is a direct target of miR-181a. (a) Predicted miR-181a target site in the 3′-UTR of rat Gpx1. The wild-type rat Gpx1 mRNA sequence is shown with the potential binding sites. The mature miR-181a sequence and potential binding between the miR-181a seed region and the rat Gpx1 3′-UTR sequence are shown, with the mutated bases indicated above in red. (b) Rat Gpx1 3′-UTR reporter and the miR-181a binding site mutant reporter were cotransfected with either the mature miR-181a (50 nM) or miR-CTL into HEK 293T cells, followed by cell lysis and luciferase assays 48 h later. $^{*}P < 0.01$ versus Gpx1-WT+miR-CTL group; the values represent the mean ± SEM, $n = 3$. (c) Gpx1 and β-actin protein levels were detected by western blotting 48 h after H9c2 cells were transfected with miR-CTL, miR-181a (50 nM), anti-CTL, or anti-miR-181a (100 nM). $^{*}P < 0.01$ versus miR-CTL; $^{\&}P < 0.01$ versus anti-CTL group; the values represent the mean ± SEM; $n = 3$.

blocked the H_2O_2-induced formation of JC-1 monomers (Figure 7(a)), suggesting that the anti-miR-181a can restore the H_2O_2-induced loss of the mitochondrial membrane potential. The ratio of orange to green fluorescence was used to quantify the $\Delta\psi$m, with a low ratio representing mitochondrial depolarization. We found that the ratio of the H_2O_2 group was lower than that of the control group ($^{*}P < 0.01$), that the anti-miR-181a showed protective effects compared with the anti-CTL-treated groups, and that the upregulation of miR-181a decreased the ratio ($^{\&}P < 0.05$, $^{\#}P < 0.05$; Figure 7(b)).

3.8. Downregulation of miR-181a Blocks the Mitochondrial Apoptotic Pathway. The release of cytochrome c from the mitochondrial intermembrane space into the cytoplasm is

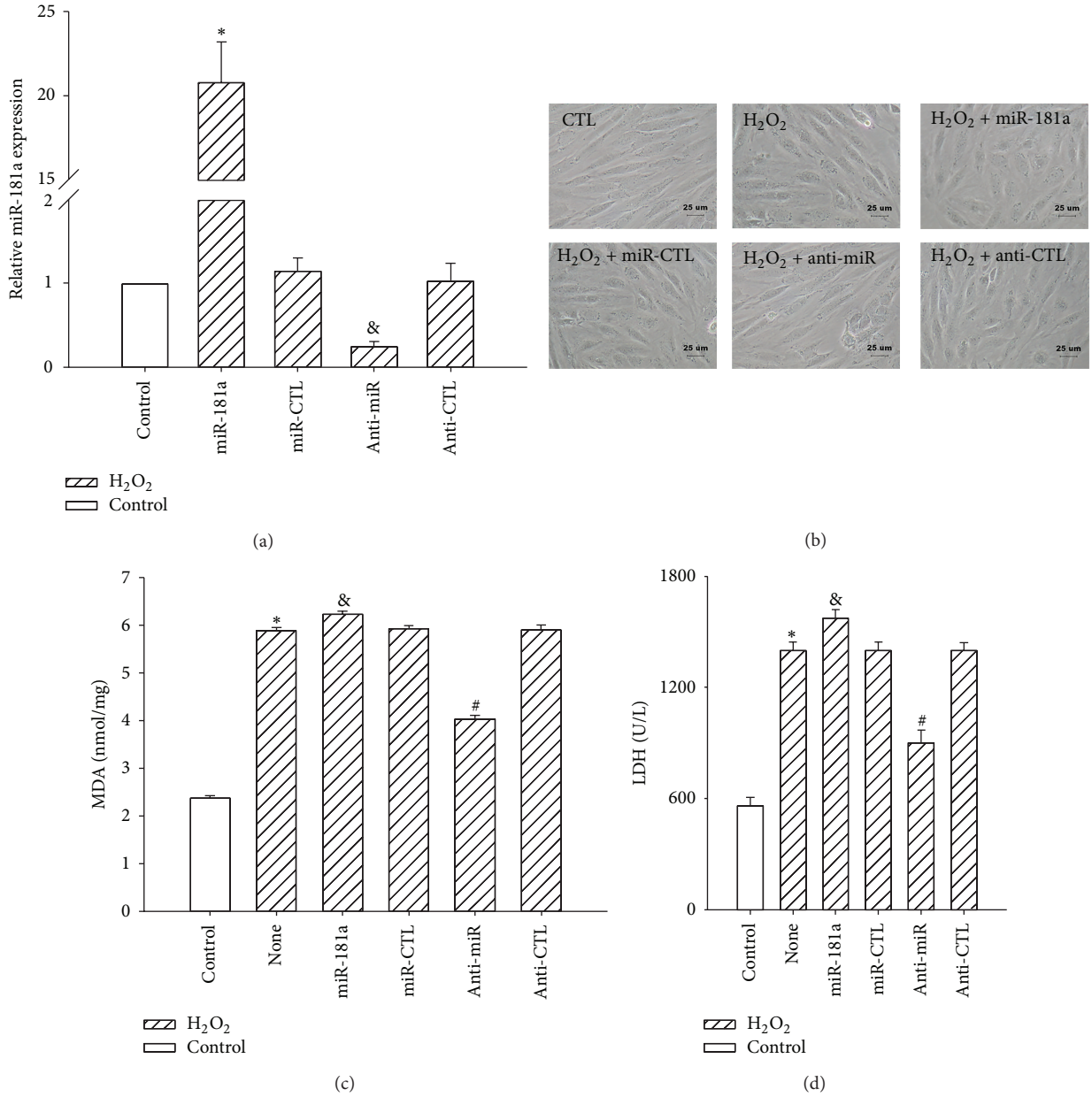

Figure 4: Effects of the down- or upregulation of miR-181a on H_2O_2-induced H9c2 cell morphology and cellular injury. H9c2 cardiomyocytes were treated with miRNAs for 6 h prior to H_2O_2 (400 μM, 2 h) treatment. (a) H9c2 cells were transfected with miR-CTL, miR-181a (50 nM), anti-CTL, or anti-miR-181a (100 nM) for 6 h, followed by real-time PCR analysis of the miR-181a expression levels 24 h later. $^{*}P < 0.01$ versus miR-CTL; $^{\&}P < 0.01$ versus anti-CTL group; the values represent the mean ± SEM; $n = 3$. (b) The downregulation of miR-181a restored the oxidative stress-induced alteration of H9c2 cell morphology, whereas the upregulation of miR-181a exacerbated the morphological changes. Scale bar: 25 μm. (c) The cellular MDA levels were measured using the TBA method, and the concentration of MDA was expressed as nmol/mg protein. $^{*}P < 0.01$ versus control (CTL); $^{\&}P < 0.01$ versus miR-CTL; $^{\#}P < 0.01$ versus anti-CTL group; the values represent the mean ± SEM; $n = 5$. (d) The LDH activity in the culture medium was measured, and the results are expressed as U/L. $^{*}P < 0.01$ versus control (CTL); $^{\&}P < 0.01$ versus miR-CTL; $^{\#}P < 0.01$ versus anti-CTL group; the values represent the mean ± SEM; $n = 5$.

a critical step in the progression of the intrinsic apoptotic pathway [19]. H_2O_2 treatment for 2 h increased the release of cytochrome c from the mitochondria, as shown by the loss of the colocalization of cytochrome c with the mitochondria (Figure 8). The effect of H_2O_2 was attenuated by transduction with the anti-miR-181a, whereas the upregulation of miR-181a exacerbated this effect (Figure 8).

Caspase-3 mediates apoptosis by regulating many important events that lead to the completion of apoptosis [20]. To further investigate the effects of mature miR-181a and

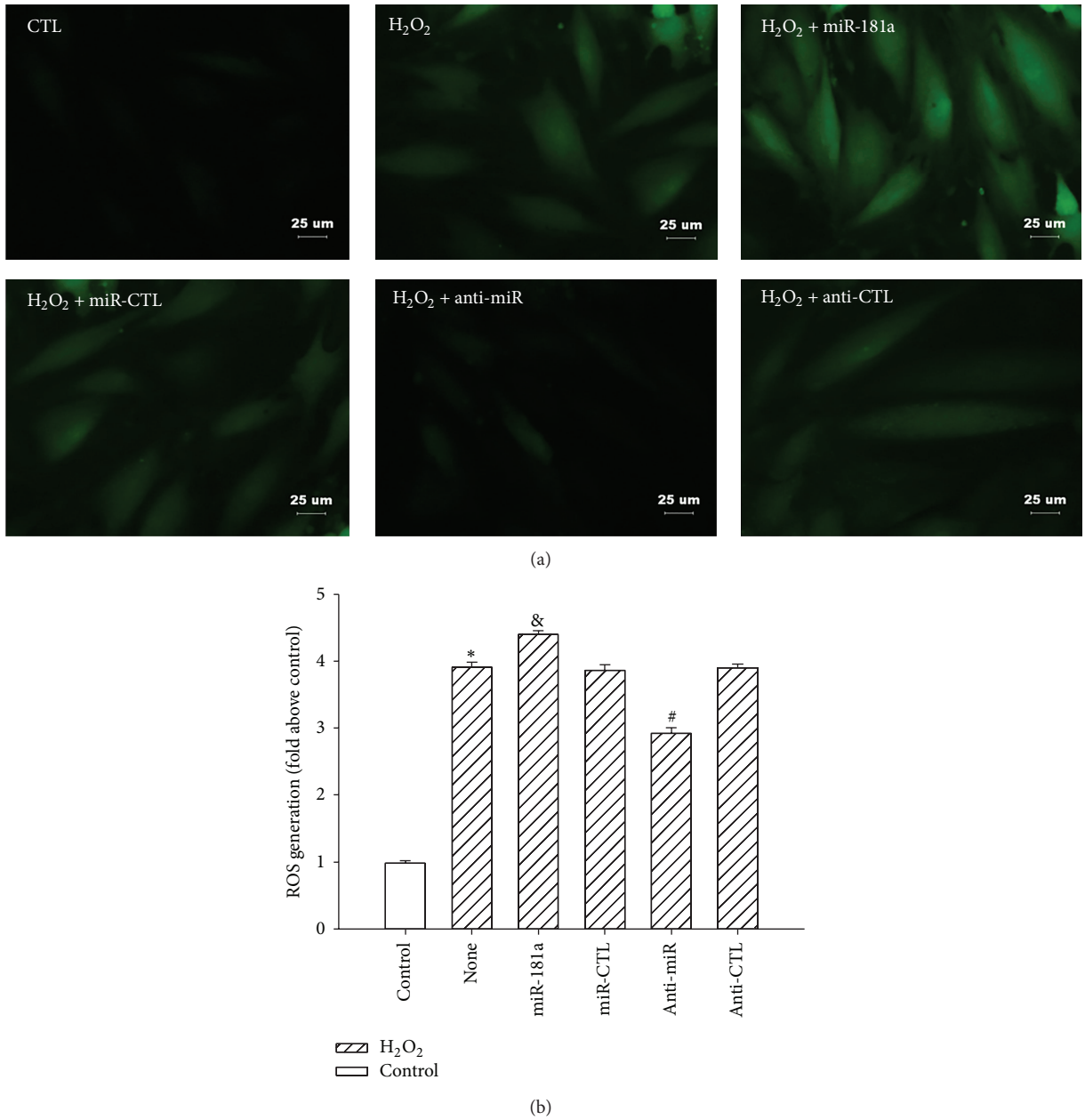

Figure 5: Effects of the miR-181a and anti-miR-181a on H_2O_2-induced H9c2 cell ROS generation. (a) The intracellular ROS levels were estimated using the probe DCFH-DA. ROS production was observed using a fluorescence microscope. (b) The ROS production was quantified by a fluorescence microplate reader, with the fluorescence read at 485 nm for excitation and 530 nm for emission. The cellular fluorescence intensities were expressed as the multiple of the level in the control group. $^{*}P < 0.01$ versus control (CTL); $^{\&}P < 0.01$ versus miR-CTL; $^{\#}P < 0.01$ versus anti-CTL group; the values represent the mean ± SEM; $n = 5$.

anti-miR-181aon cleaved caspase-3 activation, we measured cleaved caspase-3 protein expression (Figures 6(d)-6(e)) by western blots in five different groups. The H_2O_2treatment increased the generation of cleaved caspase-3. This effect was attenuated by transduction with the anti-miR-181a, whereas the upregulation of miR-181a increased cleaved caspase-3 expression (Figure 6(e)). These data suggest that the anti-miR-181a reduces H_2O_2-induced apoptosis by blocking caspase-3-dependent cardiomyocyte apoptosis.

4. Discussion

Increased ROS levels are a hallmark of oxidative stress-induced cardiomyocyte apoptosis. Compared with other ROS, H_2O_2 is a relatively long-lived molecule commonly used in models of oxidative stress in H9c2 cardiomyocytes [21, 22]. High concentrations of H_2O_2 (100–200 μM) have been shown to increase apoptosis, whereas higher concentrations of H_2O_2 (300–1000 μM) cause both apoptosis and

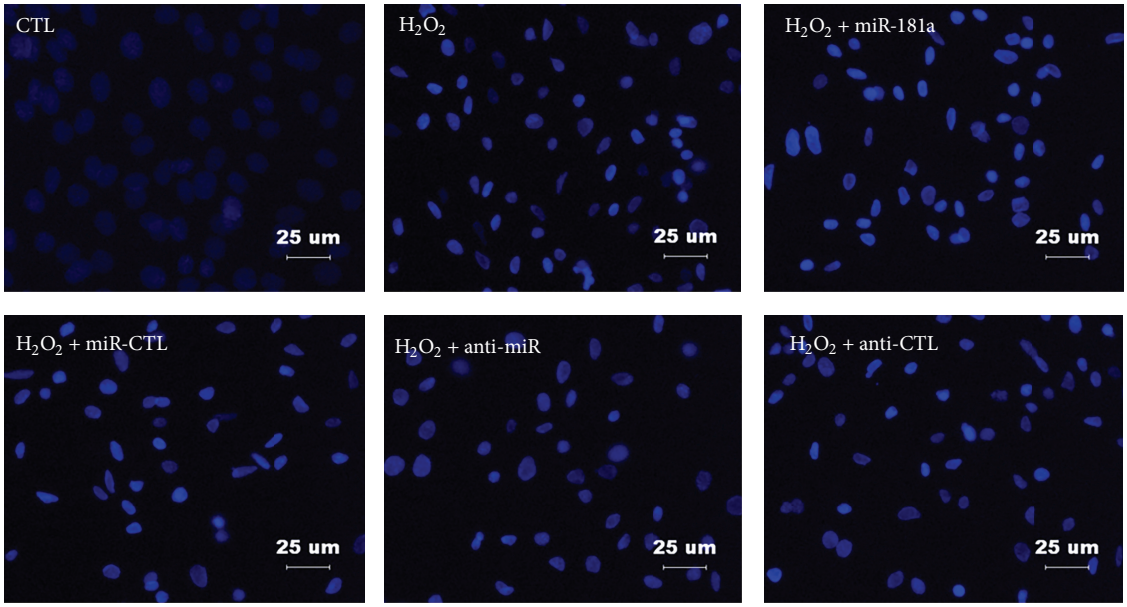

(a)

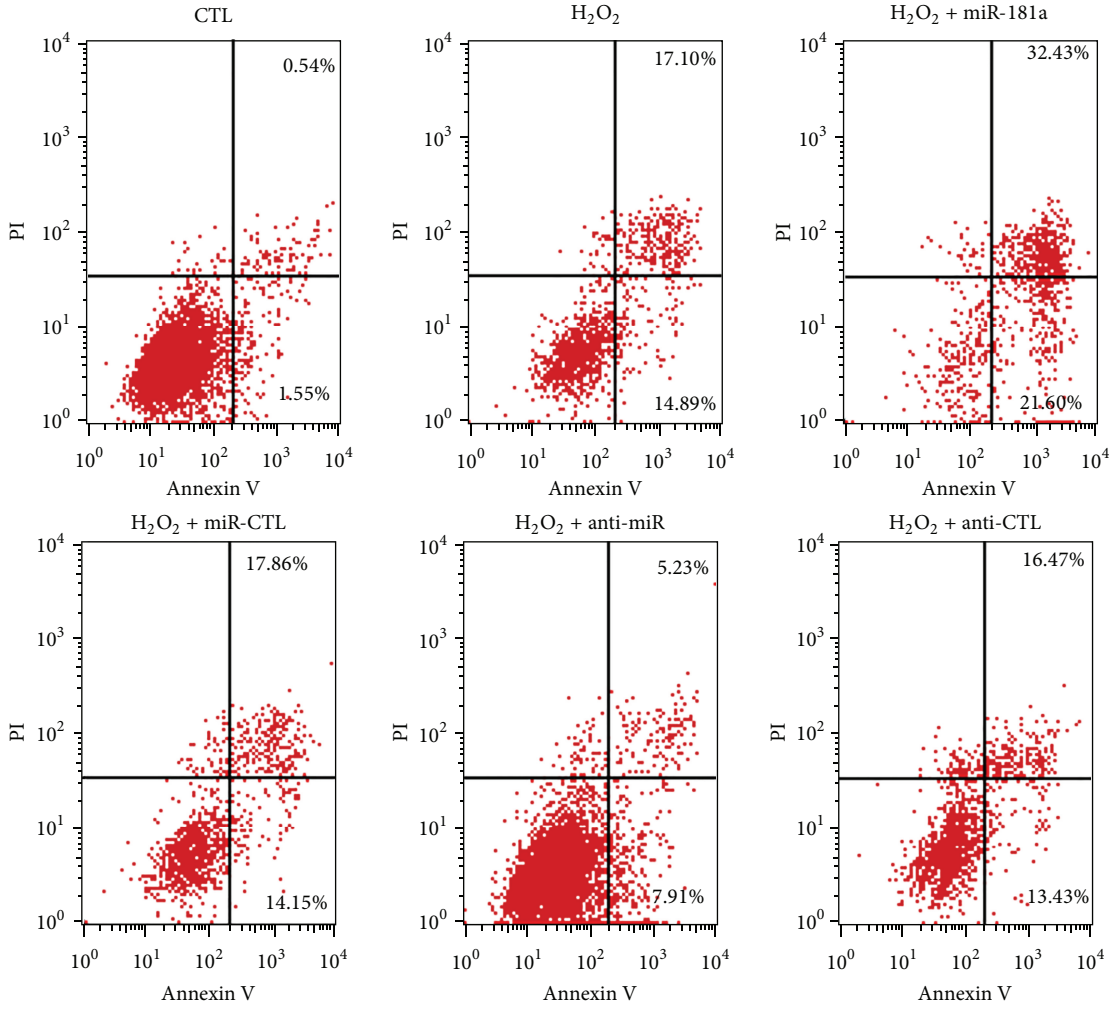

(b)

Figure 6: Continued.

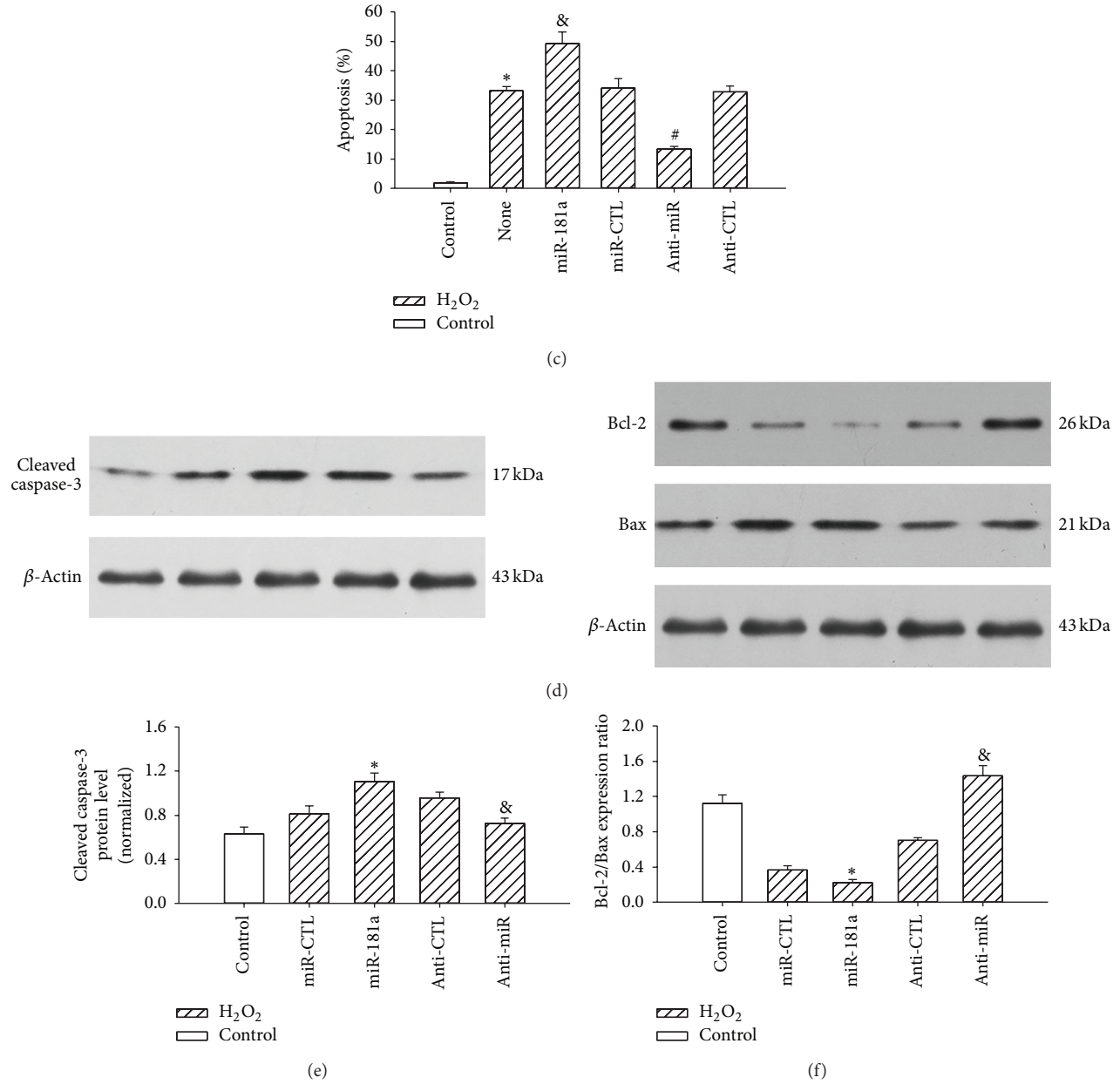

FIGURE 6: Effects of the miR-181a and anti-miR-181a on H_2O_2-induced H9c2 cell apoptosis and the expression levels of key mediators of apoptosis. The cells were transfected with miRNAs for 6 h and cultured for 24 h, with H_2O_2 (400 μM) added for the last 2 h. (a) Oxidative stress-induced DNA damage in the nuclei was shown by DAPI staining. ((b)-(c)) H9c2 cell apoptosis due to oxidative stress was analyzed by flow cytometry. $^{*}P < 0.01$ versus control (CTL); $^{\&}P < 0.01$ versus miR-CTL; $^{\#}P < 0.01$ versus anti-CTL group; the values represent the mean ± SEM; $n = 5$. (d) The cleaved caspase-3, Bcl-2, and Bax protein levels were detected by western blot. (e) The normalization of cleaved caspase-3 expression to that of β-actin. $^{*}P < 0.01$ versus miR-CTL; $^{\&}P < 0.01$ versus anti-CTL group; the values represent the mean ± SEM; $n = 3$. (f) Bcl2/Bax ratio. $^{*}P < 0.01$ versus miR-CTL; $^{\&}P < 0.01$ versus anti-CTL group; the values represent the mean ± SEM; $n = 3$.

necrosis in adult rat ventricular myocytes [23]. In our experiments, the treatment of H9c2 cells with H_2O_2 (50–800 μM) for 2 h caused a dose-dependent decrease in cell viability. A 400 μM dose of H_2O_2 induced both apoptosis and necrosis, as shown by flow cytometry. The dynamic oxidant/antioxidant balance is perturbed following the addition of exogenous H_2O_2 to the medium of cultured cells. In cultured neurons isolated from GPx1 knockout ($GPx1^{-/-}$) mice, the susceptibility to H_2O_2-induced apoptosis correlates with the increasing accumulation of intracellular ROS [24]. We found that the levels of Gpx1 protein were significantly increased in cells exposed to 100 or 200 μM H_2O_2, suggesting that the exposure to moderate concentrations of H_2O_2 induces a compensation response, whereas 400 μM H_2O_2 damages the antioxidant enzymes system and leads to decreased Gpx1 expression.

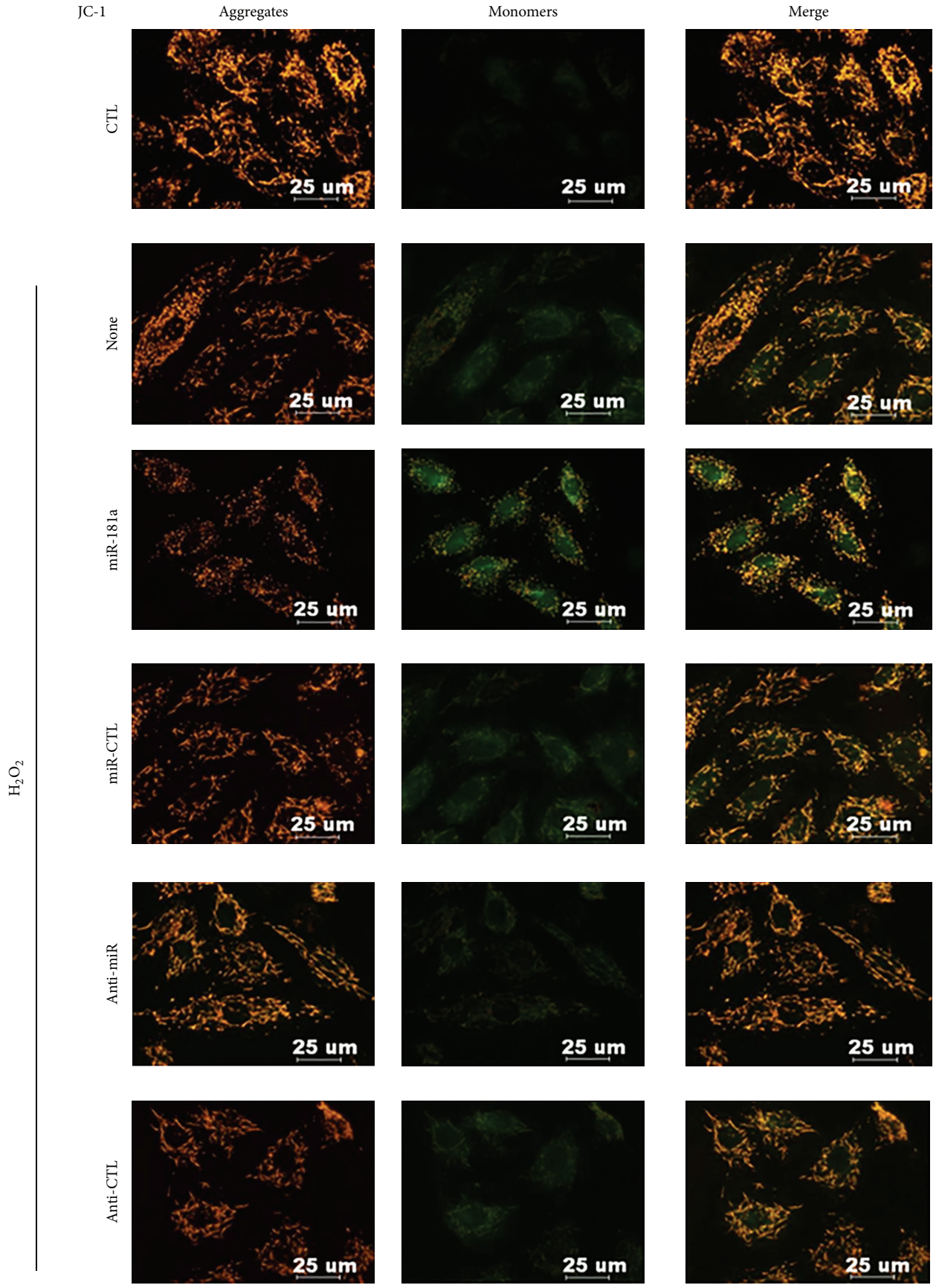

(a)

Figure 7: Continued.

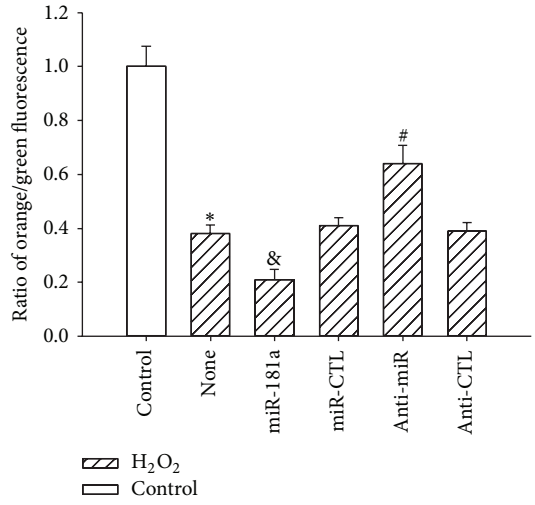

(b)

Figure 7: Effects of the miR-181a and anti-miR-181a on the H_2O_2-induced reduction of the mitochondrial membrane potential. (a) The mitochondrial membrane potential was assessed by the lipophilic cationic probe JC-1. An orange signal indicates the aggregation of JC-1 in the mitochondria. A green signal represents cytosolic JC-1 monomers, indicative of the loss of the mitochondrial membrane potential. Merged images show the colocalization of the JC-1 aggregates and monomers. Scale bar: 25 μm. (b) Quantitative analysis of the membrane potential in (a). The $\Delta\psi$m of the H9c2 cardiomyocytes in each group was calculated as the ratio of orange to green fluorescence, expressed as the multiple of the level in the control group. $^{*}P < 0.05$ versus control (CTL); $^{\&}P < 0.05$ versus miR-CTL; $^{\#}P < 0.05$ versus anti-CTL group; the values represent the mean ± SEM, $n = 3$.

miRNAs are endogenous regulators of gene expression. Previous reports have shown that the binding sites of target mRNAs with as few as seven complimentary base pairs (the seed sequence) to the miRNA 5′ end are sufficient for miRNA regulation in animals [25]. More recently, several studies indicated that miRNA expression levels were sensitive to H_2O_2 in cardiac myocytes. miRNAs can be used as powerful tools to modulate a functional phenotype that involves the participation of multiple proteins, as in the case of ROS-mediated events [26–29]. This finding raises the question of whether the oxidative stress-responsive miRNAs play a role in altering the expression of antioxidant genes that quench ROS to maintain redox homeostasis. With the help of current bioinformatics tools, we predicted several miRNAs that may target Gpx1. Although potential miRNAs can be predicted by computational analysis, these miRNAs must be experimentally verified in cells because the targets and functions of miRNAs are cell-specific and each single protein-coding gene can be regulated by multiple miRNAs [30, 31]. To test which miRNAs target Gpx1 mRNA in H9c2 cells, we first confirmed that the 400 μM H_2O_2 treatment decreased Gpx1 expression. Considering the negative relationship between miRs and Gpx1, the selected miRs were expected to be upregulated in H_2O_2-treated H9c2 cells. By qPCR analyses, we validated that the miR-181a expression was upregulated approximately 4-fold in H_2O_2-treated cells compared with the controls. In addition, Gpx1 expression in H9c2 cells was regulated by miR-181a in unstimulated cells, as determined both by gain-of-function and loss-of-function approaches. To further confirm this effect, we utilized a luciferase vector with the cloned target 3′-UTR region of Gpx1 mRNA. We demonstrated that the negative effect of miR-181a on the Gpx1 levels in H9c2 cells was the result of the direct targeting of Gpx1 mRNA by miR-181a. Hutchison et al. used microarray analysis to assess the effects of miR-181 on the transcriptome in primary astrocytes. Pathway and signaling pathway analyses demonstrated that miR-181 targets genes encoding antioxidant enzymes, including glutathione peroxidases 1 and 4 (Gpx1 and Gpx4, resp.) [32].

To ascertain the role of miR-181a in ROS-mediated H9c2 cells apoptosis, miR-181a expression was modulated via a miR-181a inhibitor and miR-181a mimic. ROS cause damage to intracellular macromolecules, including DNA breakage and lipid membrane peroxidation, both of which can be detected morphologically (cell shrinkage and nuclear condensation) and biochemically (DNA fragmentation and extracellular exposure of phosphatidylserine). We found that the downregulation of miR-181a expression protected against the H_2O_2-induced injury of H9c2 cells by restoring the alterations of H9c2 morphology and nuclear condensation, inhibiting the production of ROS and blocking LDH release and MDA production, two indicators of oxidative stress-induced injury [33].

The pivotal role of mitochondria in cell death and cell survival has been well established: mitochondrial dysfunction constitutes a critical event in the apoptotic process [34, 35]. Excessive levels of ROS damage mitochondria, induce the translocation of Bax and Bad, open the permeability transition pore (PTP), and, thus, lead to mitochondrial depolarization and outer membrane rupture, accompanied by the mitochondrial release of cytochrome c and late activation of caspase-3, finally causing cell apoptosis or death [19].

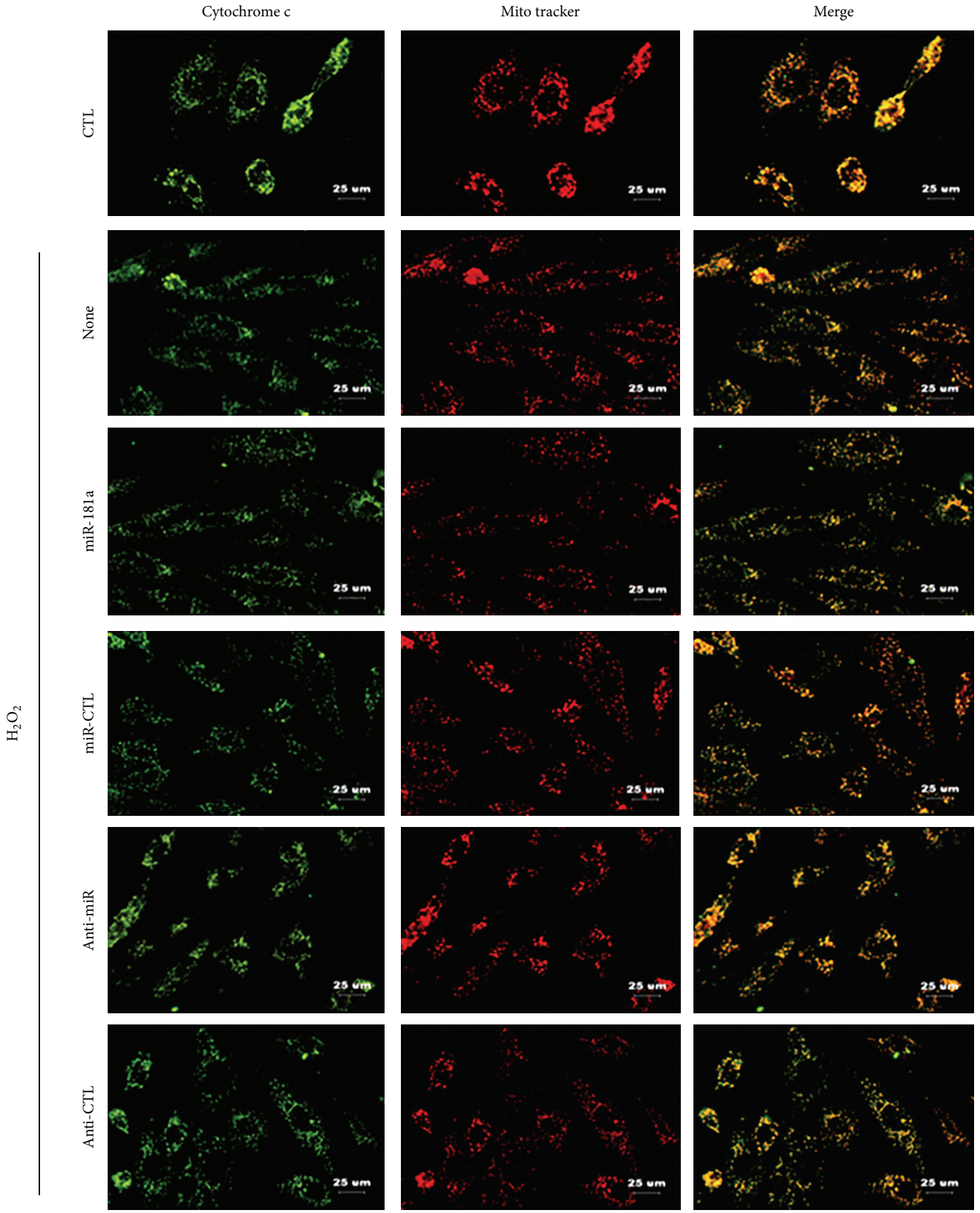

FIGURE 8: Effects of the miR-181a and anti-miR-181a on H_2O_2-induced cytochrome c release from the mitochondria in H9c2 cells. Fluorescence microscopy analysis of H9c2 cells transfected with miRNAs for 6 h prior to exposure to H_2O_2 (400 μM) for 2 h shows immunostaining of cytochrome c (green), Mito tracker staining of the mitochondria (red) and merged images of the two, showing colocalization in yellow. Upon the release of cytochrome c from the mitochondria, green fluorescence can be seen independently. Scale bar: 25 μm. The images presented are representative of three independent experiments.

Our data demonstrate that the anti-miR-181a blocked H_2O_2-induced H9c2 apoptosis by regulating mitochondria-related apoptotic pathways. H_2O_2 induced a decrease in the mitochondrial membrane potential, suggesting an impairment of mitochondrial function. Transduction of the anti-miR-181a, however, restored the mitochondrial membrane potential. These data demonstrate that the anti-miR-181a protected H9c2 cells from H_2O_2-induced apoptosis by maintaining mitochondrial membrane integrity and cardiomyocyte function. Moreover, previous studies indicated that the Bcl-2 family is upregulated during the opening of the PTP [36]. Critical interactions between Bcl-2 family proteins cause permeabilization of the outer mitochondrial membrane, a common decision point early in the intrinsic apoptotic pathway that irreversibly commits the cell to death [37, 38]. Our results demonstrate that miR-181a regulates the expression of the Bcl-2 family. The anti-miR-181a significantly increased Bcl-2 levels while decreasing Bax protein levels, attenuating the alterations caused by H_2O_2-induced injury. One recent study demonstrated that cardiac mitochondria from GPx1$^{-/-}$ mice lost their resistance to hypoxia/reoxygenation damage [39]. Previous studies have indicated that Bcl-2 knockout mice have reduced glutathione levels and glutathione peroxidase activity in brain tissue [40]. Other works have shown that GPx1 may modify the ratio of Bax to Bcl-2 to create a more antiapoptotic environment [41]. Therefore, it is reasonable to conclude that miR-181a regulates the expression of Gpx1 and that Gpx1 directly influences the expression of Bcl-2. However, the direct regulation of Bcl-2 by miR-181a has been confirmed by many investigations, mainly in tumor cells [42–44]. In the future, luciferase reporter assays and western blot analyses should be used to validate Bcl-2 as a direct target of miR-181a in H9c2 cells.

In addition to *cis*-regulation (direct targeting of mRNAs to induce degradation or inhibit protein translation), miRNAs may alter the expression of transcription factors or other regulatory genes that can affect the regulation of the target gene via *trans*-regulatory mechanisms [45]. Prior studies have identified several targets for miR-181a, including GRP78, a major endoplasmic reticulum chaperone and signaling regulator [46, 47], and sirtuin-1, an NAD-dependent protein deacetylase [48]. We assume that these targets may participate in the *trans*-regulation of Gpx1. Furthermore, other studies have demonstrated that miR-181a represses important antiapoptotic targets such as X-linked inhibitor of apoptosis (XIAP), a function that could help explain the proapoptotic effects of this miRNA [32].

In other studies, miRNAs have been shown to be directly linked to the regulation of antioxidant enzymes, including catalase [49], SOD_2 [50], and NADPH oxidase [51]. Our study illustrates the role of miR-181a as a proapoptotic modulator in the regulation of Gpx1. Future studies, especially in ischemia/reperfusion animal models, are necessary to validate the possible therapeutic use of miR-181a regulation.

In summary, we have demonstrated that miR-181a expression is upregulated in H_2O_2-treated H9c2 cells and that inhibition of miR-181a confers cardiac protection against oxidative stress-induced H9c2 cell apoptosis through the direct inhibition of Gpx1 expression and ROS generation, which are important for the maintenance of mitochondrial membrane integrity and the inhibition of mitochondrial apoptotic pathway under oxidative stress conditions. These novel findings may have extensive diagnostic and therapeutic implications for a variety of cardiovascular diseases related to ROS, including atherosclerosis, hypertension, restenosis after angioplasty or bypass, diabetic vascular complications, and transplantation arteriopathy.

Conflict of Interests

The authors declare that they have no competing interests.

Authors' Contribution

He Huang and Lei Wang conceived and designed the experiments. He Huang, Lei Wang, Yang Fan, Ke Hu, Bin Kong, and Jun Guo performed the experiments. Yang Mei and Wan-Li Liu analyzed the data. Lei Wang, Yang Fan, He Hu, Jun Guo, and Bin Kong contributed reagents/materials/analysis tools. He Huang and Lei Wang wrote the paper.

Acknowledgments

This study was supported by Grants from the National Natural Science Foundation of China (81270249).

References

[1] K. Chenand and J. F. Keaney Jr., "Evolving concepts of oxidative stress and reactive oxygen species in cardiovascular disease," *Current Atherosclerosis Reports*, vol. 14, no. 5, pp. 476–483, 2012.

[2] A. Carrière, T. G. Ebrahimian, S. Dehez et al., "Preconditioning by mitochondrial reactive oxygen species improves the proangiogenic potential of adipose-derived cells-based therapy," *Arteriosclerosis, Thrombosis, and Vascular Biology*, vol. 29, no. 7, pp. 1093–1099, 2009.

[3] M. Velayutham, C. Hemann, and J. L. Zweier, "Removal of H_2O_2 and generation of superoxide radical: role of cytochrome c and NADH," *Free Radical Biology and Medicine*, vol. 51, no. 1, pp. 160–170, 2011.

[4] A. J. Kowaltowski, N. C. de Souza-Pinto, R. F. Castilho, and A. E. Vercesi, "Mitochondria and reactive oxygen species," *Free Radical Biology and Medicine*, vol. 47, no. 4, pp. 333–343, 2009.

[5] E. Lubos, J. Loscalzo, and D. E. Handy, "Glutathione peroxidase-1 in health and disease: from molecular mechanisms to therapeutic opportunities," *Antioxidants and Redox Signaling*, vol. 15, no. 7, pp. 1957–1997, 2011.

[6] T. Shiomi, H. Tsutsui, H. Matsusaka et al., "Overexpression of glutathione peroxidase prevents left ventricular remodeling and failure after myocardial infarction in mice," *Circulation*, vol. 109, no. 4, pp. 544–549, 2004.

[7] T. Yoshida, N. Maulik, R. M. Engelman et al., "Glutathione peroxidase knockout mice are susceptible to myocardial ischemia reperfusion injury," *Circulation*, vol. 96, no. 9, pp. II216–II220, 1997.

[8] T. Yoshida, M. Watanabe, D. T. Eagelman et al., "Transgenic mice overexpressing glutathione peroxidase are resistant to

myocardial ischemia reperfusion injury," *Journal of Molecular and Cellular Cardiology*, vol. 28, no. 8, pp. 1759–1767, 1996.

[9] M. Torzewski, V. Ochsenhirt, A. L. Kleschyov et al., "Deficiency of glutathione peroxidase-1 accelerates the progression of atherosclerosis in apolipoprotein E-deficient mice," *Arteriosclerosis, Thrombosis, and Vascular Biology*, vol. 27, no. 4, pp. 850–857, 2007.

[10] P. Lewis, N. Stefanovic, J. Pete et al., "Lack of the antioxidant enzyme glutathione peroxidase-1 accelerates atherosclerosis in diabetic apolipoprotein E-deficient mice," *Circulation*, vol. 115, no. 16, pp. 2178–2187, 2007.

[11] S. Dayal, K. M. Wilson, D. G. Motto, F. J. Miller Jr., A. K. Chauhanand, and S. R. Lentz, "Hydrogen peroxide promotes aging-related platelet hyperactivation and thrombosis," *Circulation*, vol. 127, no. 12, pp. 1308–1316, 2013.

[12] S. Chrissobolis, S. P. Didion, D. A. Kinzenbaw et al., "Glutathione peroxidase-1 plays a major role in protecting against angiotensin II-induced vascular dysfunction," *Hypertension*, vol. 51, no. 4, pp. 872–877, 2008.

[13] L. Z.-H. Zhou, A. P. Johnson, and T. A. Rando, "NFκB and AP-1 mediate transcriptional responses to oxidative stress in skeletal muscle cells," *Free Radical Biology and Medicine*, vol. 31, no. 11, pp. 1405–1416, 2001.

[14] E. Hernandez-Montes, S. E. Pollard, D. Vauzour et al., "Activation of glutathione peroxidase via Nrf1 mediates genistein's protection against oxidative endothelial cell injury," *Biochemical and Biophysical Research Communications*, vol. 346, no. 3, pp. 851–859, 2006.

[15] M. V. G. Latronico and G. Condorelli, "MicroRNAs and cardiac pathology," *Nature reviews*, vol. 6, no. 6, pp. 419–429, 2009.

[16] V. Ambros, "MicroRNA pathways in flies and worms: growth, death, fat, stress, and timing," *Cell*, vol. 113, no. 6, pp. 673–676, 2003.

[17] S. J. Watkins, G. M. Borthwick, and H. M. Arthur, "The H9C2 cell line and primary neonatal cardiomyocyte cells show similar hypertrophic responses in vitro," *In Vitro Cellular and Developmental Biology*, vol. 47, no. 2, pp. 125–131, 2011.

[18] Z. Hua, Q. Lv, W. Ye et al., "Mirna-directed regulation of VEGF and other angiogenic under hypoxia," *PLoS ONE*, vol. 1, no. 1, article e116, 2006.

[19] M. L. Circu and T. Y. Aw, "Reactive oxygen species, cellular redox systems, and apoptosis," *Free Radical Biology and Medicine*, vol. 48, no. 6, pp. 749–762, 2010.

[20] A. Clerk, S. M. Cole, T. E. Cullingford, J. G. Harrison, M. Jormakka, and D. M. Valks, "Regulation of cardiac myocyte cell death," *Pharmacology and Therapeutics*, vol. 97, no. 3, pp. 223–261, 2003.

[21] G. P. Bienert, J. K. Schjoerring, and T. P. Jahn, "Membrane transport of hydrogen peroxide," *Biochimica et Biophysica Acta*, vol. 1758, no. 8, pp. 994–1003, 2006.

[22] H. Han, H. Long, H. Wang, J. Wang, Y. Zhang, and Z. Wang, "Progressive apoptotic cell death triggered by transient oxidative insult in H9c2 rat ventricular cells: a novel pattern of apoptosis and the mechanisms," *American Journal of Physiology*, vol. 286, no. 6, pp. H2169–H2182, 2004.

[23] S. H. Kwon, D. R. Pimentel, A. Remondino, D. B. Sawyer, and W. S. Colucci, "H_2O_2 regulates cardiac myocyte phenotype via concentration-dependent activation of distinct kinase pathways," *Journal of Molecular and Cellular Cardiology*, vol. 35, no. 6, pp. 615–621, 2003.

[24] J. B. de Haan, C. Bladier, P. Griffiths et al., "Mice with a homozygous null mutation for the most abundant glutathione peroxidase, Gpx1, show increased susceptibility to the oxidative stress-inducing agents paraquat and hydrogen peroxide," *Journal of Biological Chemistry*, vol. 273, no. 35, pp. 22528–22536, 1998.

[25] P. Brodersen and O. Voinnet, "Revisiting the principles of microRNA target recognition and mode of action," *Nature Reviews Molecular Cell Biology*, vol. 10, no. 2, pp. 141–148, 2009.

[26] Y. Cheng, X. Liu, S. Zhang, Y. Lin, J. Yang, and C. Zhang, "MicroRNA-21 protects against the H_2O_2-induced injury on cardiac myocytes via its target gene PDCD4," *Journal of Molecular and Cellular Cardiology*, vol. 47, no. 1, pp. 5–14, 2009.

[27] X. Huang, F. Huang, D. Yang et al., "Expression of microRNA-122 contributes to apoptosis in H9C2 myocytes," *Journal of Cellular and Molecular Medicine*, vol. 16, no. 11, pp. 2637–2646, 2012.

[28] J. Fang, X.-W. Song, J. Tian et al., "Overexpression of microRNA-378 attenuates ischemia-induced apoptosis by inhibiting caspase-3 expression in cardiac myocytes," *Apoptosis*, vol. 17, no. 4, pp. 410–423, 2012.

[29] J. H. Suh, E. Choi, M. J. Cha et al., "Up-regulation of miR-26a promotes apoptosis of hypoxic rat neonatal cardiomyocytes by repressing GSK-3beta protein expression," *Biochemical and Biophysical Research Communications*, vol. 423, no. 2, pp. 404–410, 2012.

[30] C. Zhang, "MicroRNomics: a newly emerging approach for disease biology," *Physiological Genomics*, vol. 33, no. 2, pp. 139–147, 2008.

[31] D. P. Bartel, "MicroRNAs: target recognition and regulatory functions," *Cell*, vol. 136, no. 2, pp. 215–233, 2009.

[32] E. R. Hutchison, E. M. Kawamoto, D. D. Taub et al., "Evidence for miR-181 involvement in neuroinflammatory responses of astrocytes," *Glia*, vol. 61, no. 7, pp. 1018–1028, 2013.

[33] L. Zhang, S. Wei, J. M. Tang et al., "PEP-1-CAT protects hypoxia/reoxygenation-induced cardiomyocyte apoptosis through multiple sigaling pathways," *Journal of Translational Medicine*, vol. 11, article 113, 2013.

[34] M. T. Crow, K. Mani, Y.-J. Nam, and R. N. Kitsis, "The mitochondrial death pathway and cardiac myocyte apoptosis," *Circulation Research*, vol. 95, no. 10, pp. 957–970, 2004.

[35] S.-B. Ong and Å. B. Gustafsson, "New roles for mitochondria in cell death in the reperfused myocardium," *Cardiovascular Research*, vol. 94, no. 2, pp. 190–196, 2012.

[36] B. K. Singh, M. Tripathi, B. P. Chaudhari, P. K. Pandey, and P. Kakkar, "Natural terpenes prevent mitochondrial dysfunction, oxidative stress and release of apoptotic proteins during nimesulide-hepatotoxicity in rats," *PLoS ONE*, vol. 7, no. 4, Article ID e34200, 2012.

[37] J.-C. Martinou and R. J. Youle, "Mitochondria in apoptosis: Bcl-2 family members and mitochondrial dynamics," *Developmental Cell*, vol. 21, no. 1, pp. 92–101, 2011.

[38] J. Lindsay, M. D. Esposti, and A. P. Gilmore, "Bcl-2 proteins and mitochondria-Specificity in membrane targeting for death," *Biochimica et Biophysica Acta*, vol. 1813, no. 4, pp. 532–539, 2011.

[39] V. T. Thu, H. K. Kim, S. H. Ha et al., "Glutathione peroxidase 1 protects mitochondria against hypoxia/ reoxygenation damage in mouse hearts," *Pflugers Archiv European Journal of Physiology*, vol. 460, no. 1, pp. 55–68, 2010.

[40] A. Hochman, H. Sternin, S. Gorodin et al., "Enhanced oxidative stress and altered antioxidants in brains of Bcl-2-deficient mice," *Journal of Neurochemistry*, vol. 71, no. 2, pp. 741–748, 1998.

[41] K. Faucher, H. Rabinovitch-Chable, J. Cook-Moreau, G. Barrière, F. Sturtz, and M. Rigaud, "Overexpression of human GPX1 modifies Bax to Bcl-2 apoptotic ratio in human endothelial cells," *Molecular and Cellular Biochemistry*, vol. 277, no. 1-2, pp. 81–87, 2005.

[42] H. Bai, Z. Cao, C. Deng, L. Zhou, and C. Wang, "miR-181a sensitizes resistant leukaemia HL-60/Ara-C cells to Ara-C by inducing apoptosis," *Journal of Cancer Research and Clinical Oncology*, vol. 138, no. 4, pp. 595–602, 2012.

[43] H. Li, L. Hui, and W. Xu, "MiR-181a sensitizes a multidrug-resistant leukemia cell line K562/A02 to daunorubicin by targeting BCL-2," *Acta Biochimica et Biophysica Sinica*, vol. 44, no. 3, pp. 269–277, 2012.

[44] G. Chen, W. Zhu, D. Shi et al., "MicroRNA-181a sensitizes human malignant glioma U87MG cells to radiation by targeting Bcl-2," *Oncology Reports*, vol. 23, no. 4, pp. 997–1003, 2010.

[45] X. Liu, J. Yu, L. Jiang et al., "MicroRNA-222 regulates cell invasion by targeting matrix metalloproteinase 1 (MMP1) and manganese superoxide dismutase 2 (SOD2) in tongue squamous cell carcinoma cell lines," *Cancer Genomics and Proteomics*, vol. 6, no. 3, pp. 134–139, 2009.

[46] Y.-B. Ouyang, Y. Lu, S. Yue et al., "MiR-181 regulates GRP78 and influences outcome from cerebral ischemia in vitro and in vivo," *Neurobiology of Disease*, vol. 45, no. 1, pp. 555–563, 2012.

[47] S. F. Su, Y. W. Chang, C. Andreu-Vieyra et al., "miR-30d, miR-181a and miR-199a-5p cooperatively suppress the endoplasmic reticulum chaperone and signaling regulator GRP78 in cancer," *Oncogene*, vol. 32, no. 39, pp. 4694–4701, 2012.

[48] B. Zhou, C. Li, W. Qi et al., "Downregulation of miR-181a upregulates sirtuin-1 (SIRT1) and improves hepatic insulin sensitivity," *Diabetologia*, vol. 55, no. 7, pp. 2032–2043, 2012.

[49] R. Haque, E. Chun, J. C. Howell, T. Sengupta, D. Chenand, and H. Kim, "MicroRNA-30b-mediated regulation of catalase expression in human ARPE-19 cells," *PLoS ONE*, vol. 7, no. 8, Article ID e42542, 2012.

[50] X.-Y. Bai, Y. Ma, R. Ding, B. Fu, S. Shi, and X.-M. Chen, "miR-335 and miR-34a promote renal senescence by suppressing mitochondrial antioxidative enzymes," *Journal of the American Society of Nephrology*, vol. 22, no. 7, pp. 1252–1261, 2011.

[51] X. Wang, H. Zhu, X. Zhang et al., "Loss of the miR-144/451 cluster impairs ischaemic preconditioning-mediated cardioprotection by targeting Rac-1," *Cardiovascular Research*, vol. 94, no. 2, pp. 379–390, 2012.

Hindawi Publishing Corporation
Oxidative Medicine and Cellular Longevity
Volume 2014, Article ID 481482, 8 pages
http://dx.doi.org/10.1155/2014/481482

Review Article

The Emerging Role of TRα1 in Cardiac Repair: Potential Therapeutic Implications

Constantinos Pantos and Iordanis Mourouzis

Department of Pharmacology, University of Athens, 75 Mikras Asias Avenue, Goudi, 11527 Athens, Greece

Correspondence should be addressed to Constantinos Pantos; cpantos@med.uoa.gr

Received 8 November 2013; Accepted 31 December 2013; Published 9 February 2014

Academic Editor: Neelam Khaper

Thyroid hormone (TH) is critical for adapting living organisms to environmental stress. Plasma circulating tri-iodothyronine (T3) levels drop in most disease states and are associated with increased oxidative stress. In this context, T3 levels in plasma appear to be an independent determinant for the recovery of cardiac function after myocardial infarction in patients. Thyroid hormone receptor α1 (TRα1) seems to be crucial in this response; TRα1 accumulates to cell nucleus upon activation of stress induced growth kinase signaling. Furthermore, overexpression of nuclear TRα1 in cardiomyocytes can result in pathological or physiological growth (dual action) in absence or presence of its ligand, respectively. Accordingly, inactivation of TRα1 receptor prevents reactive hypertrophy after myocardial infarction and results in heart failure with increased phospholamban (PLB) expression and marked activation of p38MAPK. In line with this evidence, TH is shown to limit ischemia/reperfusion injury and convert pathologic to physiologic growth after myocardial infarction via TRα1 receptor. TRα1 receptor may prove to be a novel pharmacological target for cardiac repair/ regeneration therapies.

1. Introduction

Adaptation to the environmental oxygen variations was an evolutionary challenge and allowed life to evolve in earth. Transition from low to high oxygen environments can increase oxidative stress and result in tissue damage. However, living organisms evolved from aquatic to terrestrial environments by developing mechanisms that enabled adaptation to changes in environmental oxygen. These mechanisms have been evolutionary conserved in mammals allowing mammalian birth to oxygen rich environment or implicated in freeze tolerance and arousal from hibernation [1]. Understanding the molecular basis of the adaptive responses of living organisms to stress may be of physiological relevance in the therapy of diseases. In this context, recent experimental and clinical evidence shows that thyroid hormone (TH) may be critical in stress response and low TH in diseased states is associated with increased oxidative stress [2, 3]. With this evidence in mind, this review highlights the role of thyroid hormone signaling and particularly of thyroid hormone receptor alpha1 (TRα1) in cardiac recovery following myocardial injury.

2. Adaptation to Environmental Stress: The Role of Thyroid Hormone (TH)

Amphibian metamorphosis is the most striking paradigm of adaptation to oxygen rich environment. This biological process is entirely dependent on TH. TH is low during embryonic and early larva development and increases as larva approaches metamorphosis. A similar developmental TH secretion pattern is observed in most species and in humans [4]. Furthermore, distinct changes in deiodinases and thyroid hormone receptors (TRs) expression occur and thus, a single hormone can coordinate responses among different cell types and regulate the temporal sequence of remodeling events during amphibian metamorphosis. More importantly, TH can critically determine the amphibian phenotype (low oxygen, aquatic versus high oxygen, and terrestrial habitats). Thus, in salamanders, low TH results in permanent aquatic habitats, delayed metamorphic timing, and large body size, whereas high TH has opposite effects [4]; see Figure 1.

Environmental stress appears to cause changes in the pattern of TH secretion similar to that observed in the early

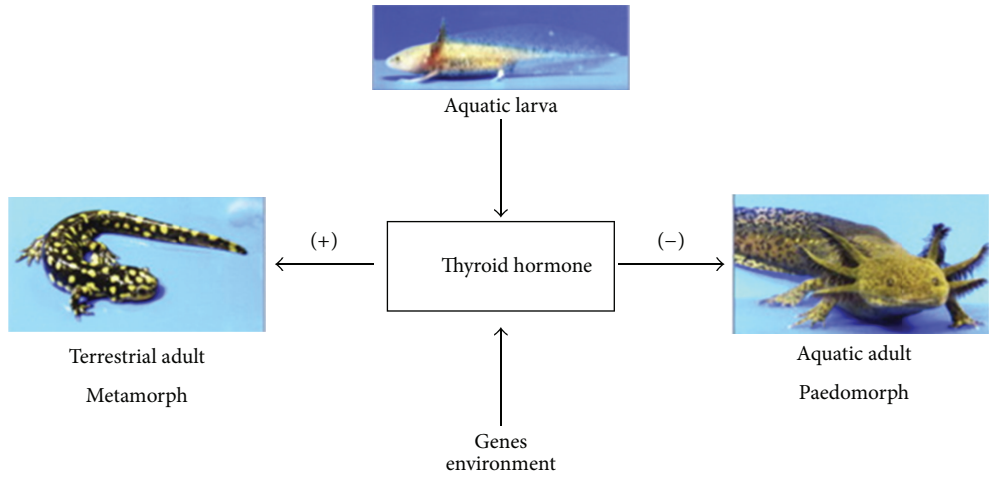

Figure 1: Critical levels of thyroid hormone (TH) induce metamorphosis in salamanders. Low TH can adapt salamander to low oxygen aquatic environment by inducing growth with embryonic characteristics. Addition of TH allows adaptation to terrestrial life and completes metamorphosis. Analogies seem to exist in mammals with TH to determine the phenotypic characteristics of the myocardium (pathological versus physiological growth) after ischemic events. Evolutionary conserved mechanisms of adaptation may be the basis for cardiac repair. (Permission by Johnson and Voss [4].)

embryonic stages. This response is likely to be part of an adaptive response of the living organism to environmental stress. Thus, exposure of air breathing perch to water-born kerosene resulted in low TH and unfavorable metabolic changes, while the administration of TH reversed this response [5]. Along this line, cold stunning in sea turtles resulted in undetectable thyroid hormone levels and recovery induced by rewarming was associated with restoration of TH levels [6]. Similarly, in humans, TH levels decline after various stresses including ischemia, infection, and organ failure, but the physiological relevance of this response in regard to post-stress adaptation remains largely unknown [7, 8].

3. TH Is Critical for the Recovery after Myocardial Injury

A decline in T3 levels occurs within 48 hours(h) after myocardial infarction (AMI) or 6–24 h after cardiac surgery [9, 10]. Low T3 syndrome is present in nearly 20% of patients with AMI, despite primary percutaneous coronary intervention (PCI). Low fT3 levels are associated with lower survival rate particularly in patients with age less than 75 years [11], indicating that TH may have a role in adapting the heart to myocardial injury. In fact, a link of TH to cardiac recovery after myocardial infarction has been recently established in humans and in experimental studies.

In a series of patients with AMI and primary PCI, left ventricular ejection fraction (LVEF%) 48 hours after the index event was strongly correlated with T3 and not T4 levels in plasma. Furthermore, at 6 months, recovery of cardiac function was correlated with T3 plasma levels and T3 was shown to be an independent determinant of LVEF% recovery [12].

In accordance with this clinical evidence, acute T3 (and not T4) administration after ischemia/reperfusion in isolated rat hearts resulted in significant improvement of postischemic recovery of function [13, 14]. Furthermore, in an experimental model of coronary ligation in mice, cardiac function was significantly decreased and this was associated with a marked decline in T3 levels in plasma. T3 replacement therapy significantly improved the recovery of cardiac function [15, 16].

On the basis of these data, it appears that the active T3 and not T4 is critical for the response to stress. In fact, T4 therapy in patients with euthyroid syndrome due to severe illness was not shown to be beneficial [17, 18].

4. TRα1 Receptor and Its Physiologic Actions

T3, the active form of TH, exerts many of its actions through its receptors (TRs): TRα1, TRα2, TRβ1, and TRβ2. TRs, with the exception of TRβ2, are expressed in all tissues and the pattern of expression varies in different types of tissues [19]. TRα1 is predominantly expressed in the myocardium and regulates important genes related to cell differentiation and growth, contractile function, pacemaker activity, and conduction [20–22].

The importance of TH in organ maturation during development and its implication in cell differentiation has long been recognized. This unique action seems to be of physiological relevance in stem cell biology and cancer [23, 24]. T3 can promote differentiation of human pluripotent stem cell derived cardiomyocytes (hips-CM) [23] and glioma tumor cell lines [24]. The implication of TRα1 in cell differentiation is shown in embryonic myoblast cultures (H9c2), which is considered a suitable model to study cell differentiation. Maturation of H9c2 is TH dependent process [25, 26]. TRα1 expression is increased in parallel with the intracellular T3 at the stage of cell differentiation and pharmacological inactivation of TRα1 significantly delays cardiac myoblast

maturation [27]. Along this line, TRα1 is shown to play a critical role in pancreatic β-cell replication and in the expansion of the β-cell mass during postnatal development [28].

T3 can induce physiologic growth and this action involves the activation of PI3 K/Akt/mTOR pathway. T3 regulates this pathway by the interaction of the cytosol-localized TRα1 with the p85α subunit of PI3 K [29, 30].

TRα1 appears to be required to repress basal expression of β-isoform of myosin heavy chain (β-MHC) and T3 induced β-MHC repression [31]. Deletion of TRα1 results in lower levels of α-MHC and SERCA mRNA [32], whereas phospholamban (PLB) expression is greater in the myocardium of animals with mutated TRα1 [33]. TRα1 directly binds at the PLB promoter region. T3 can trigger alterations in covalent histone modifications at the PLB promoter which are associated with gene silencing with lower histone H3 acetylation and histone H3 lysine 4 methylation [34]. In line with this evidence, contractile dysfunction is a consistent observation in all studies using animals with mutated or deleted TRα1 receptor [32, 33].

TH regulates the transcription of pacemaker channel genes such as HCN2 and HCN4 and this action involves TRα1 receptor [32]. Deletion of TRα1 results in bradycardia [32, 35]. TRα1 is also shown to bind to an element of rat connexin 43 promoter region which may be of physiological relevance regarding electrical conduction [36].

TH can control glucose metabolism in the heart via TRα1 receptor. Thus, glucose utilization in the myocardium is impaired in mice with mutated TRα1 [37]. Furthermore, pharmacological inhibition of TRα1 in rats resulted in increased glycogen content in the myocardium [38].

TRα1 is the predominant TR isoform in mouse coronary smooth muscle cells (SMCs) and seems to have a regulatory role in the coronary artery contractile function. Coronary SMCs from TRα1 knock-out mice exhibit a significant decrease in K^+ channel activity. Furthermore, in those arteries, vascular contraction is significantly enhanced [39].

Collectively, it appears that TRα1 has a regulatory role in cardiac homeostasis and thus, it is likely to be implicated in the pathophysiology of cardiac disease. This hypothesis has not, until recently, been explored.

5. TRα1 and Response of the Myocardium to Stress

The potential link of TH signaling to cardiac pathology and particularly of TRα1 receptor has been investigated in several studies with much controversy surrounding this issue. Initial observations showed that TRα1 mRNA is suppressed in left ventricles of patients with dilated cardiomyopathy in comparison with donor hearts [40]. Accordingly, TRα1 mRNA was found to be downregulated in the myocardium of animals with ascending aortic constriction (TAC) [41, 42]. Furthermore, TRα1 mRNA was found to be suppressed after phenylephrine (PE, an alpha1-adrenergic agonist, which is a stimulus for pathologic growth) administration in neonatal cardiomyocytes [42]. Overexpression of TRα1 was shown to reverse PE and TAC induced hypertrophic phenotype [41, 42]. However, this was not a consistent result in all studies. Overexpression of TRα1 resulted in physiologic growth in one study [42] and pathologic growth in another study [43]. Here it should be noted that, in all those studies, TRα1 was measured at mRNA level and not at protein level. TRα1 protein expression was measured in subsequent studies in cardiac specimens from patients with heart failure. TRα1 was found to be upregulated in one study [44] and downregulated in another study [45]. To add to the controversy, TRα1 was shown to be overexpressed [46] or downregulated [47] in animal models of cardiac remodeling after myocardial infarction. On the basis of this conflicting evidence, it is conceivable that clear conclusions cannot be drawn regarding potential role of TRα1 receptor in stressed myocardium.

6. TRα1: A Component of Stress Induced Growth Signaling Pathways

Recent experimental studies have shed more light regarding the role of TRα1 in the response of the myocardium to stress and seem to resolve the controversy. Thus, a distinct pattern of TRα1 expression is shown to occur in the myocardium after acute myocardial infarction, indicating a potential link of TRα1 to reactive cardiac hypertrophy. TRα1 (nuclear part) was shown to be upregulated during the development of compensatory pathological hypertrophy in parallel with a greater activation of ERK and mTOR growth signaling. Consequently, TRα1 declines along with a marked reduction in ERK and mTOR signaling activation on the transition of pathological hypertrophy to congestive heart failure [48]. Studies in cultured cardiomyocytes further showed that TRα1 receptor can be overexpressed in cell nucleus in response to growth stimuli such as phenylephrine (PE) [27]. This response was shown to be due to redistribution of TRα1 from cytosol to nucleus. This process is regulated via ERK and mTOR signaling. In those experiments, overexpression of TRα1 receptor was shown to be associated with pathological growth (with dominant β-MHC expression) only in the absence of TH in culture medium Figure 2. Furthermore, inhibition of ERK and mTOR signaling abolished TRα1 accumulation in cell nucleus and prevented the development of PE induced pathological growth; see Figure 2. This response could be elicited by α1 adrenergic and not β2-adrenergic stimulation (unpublished data) while treatment of neonatal cells with inflammatory mediators, such as TNF-alpha, had no effect on nuclear TRα1 expression [49]. Collectively, these data provide substantial evidence that stress induced accumulation of TRα1 in cell nucleus may be an important component of the mechanisms involved in compensatory growth response after myocardial infarction. This hypothesis has recently been tested in studies in which debutyl-dronedarone (DBD), a TRα1 inhibitor, was administered after AMI in mice [50]. DBD treatment was shown to reduce recovery of cardiac function, prevent compensatory hypertrophy, increase PLB expression (TRα1 responsive gene), and result in marked activation of p38 MAPK [51]. The latter may be of important physiological relevance. Stress induced activation of p38

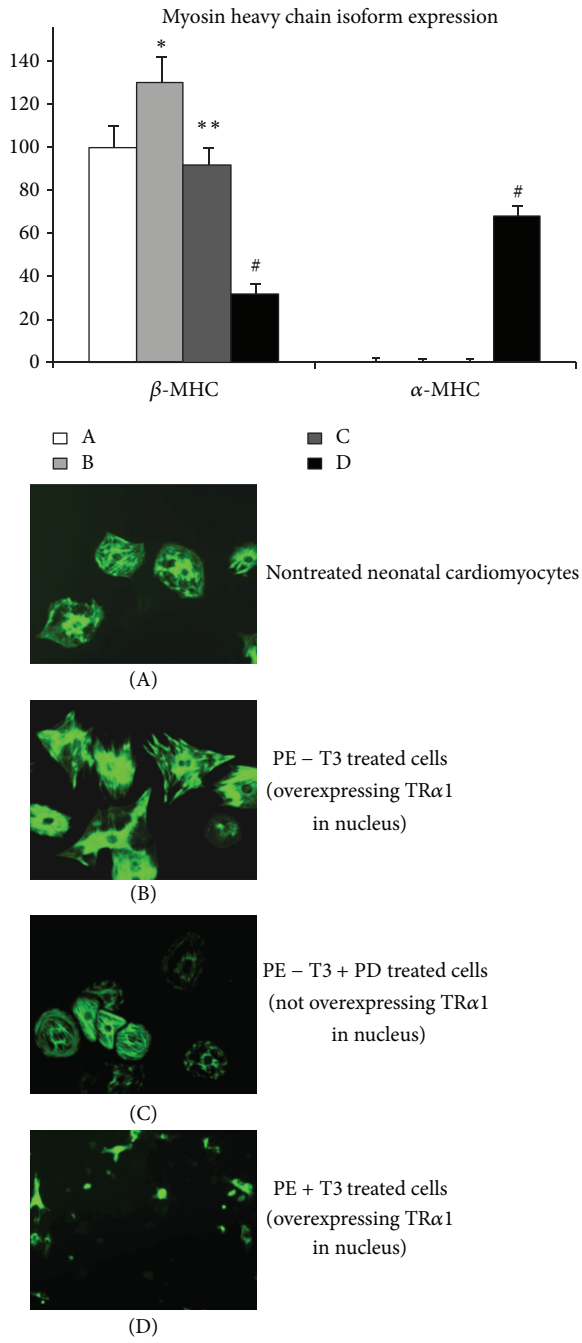

Figure 2: Thyroid hormone (TH) determines the growth response to stress. Stress induced (by PE, a growth stimulus) overexpression of TRα1 in neonatal cardiomyocytes resulted in pathologic growth with dominant beta-MHC expression only in the absence of TH in the cultured medium (PE-T3) (B). This response was abolished after PD98059 administration (an ERK inhibitor) which prevents PE induced TRα1 accumulation in nucleus (PE-T3 + PD) (C). In the presence of TH in cultured medium, PE induced TRα1 accumulation in nucleus resulted in physiologic growth with suppressed beta-MHC and increased alpha-MHC (PE + T3) (D) $^{*}P < 0.05$ versus A, $^{**}P < 0.05$ versus B, $^{\#}P < 0.05$ versus A, B, and C, PE = phenylephrine, MHC = myosin heavy chain.

MAPK can cause apoptosis, low proliferative activity, and impaired tissue repair/regeneration [52–54].

7. TRα1: A Molecular Switch to Convert Pathologic to Physiologic Growth

The potential link of TRα1 to growth response has been revealed in neonatal cardiomyocytes cultures in which phenylephrine (PE) was administered in the presence or absence of TH in culture medium. In this series of experiments, PE administration resulted in increased nuclear TRα1 content and in pathologic growth (dominant β-MHC expression) in the absence of T3 and physiologic growth in the presence of T3 in culture medium [27]; see Figure 2. Thus, TRα1 receptor appears to act as a molecular switch to convert pathologic to physiologic growth. Consistent with this evidence, TH replacement therapy following myocardial infarction in mice resulted in compensatory hypertrophy with adult pattern of myosin isoform expression [16]. Furthermore, increased expression of liganded TRα1 in the myocardium after physical training in patients with heart failure and mechanical support devices was associated with upregulation of physiologic growth kinase signaling [55]. Similarly, TH restored myelination and clinical recovery after intraventricular hemorrhage by converting the unliganded, aporeceptor TRα1 to holoreceptor [56].

8. TRα1 and Ischemia/Reperfusion Injury

TH has long been considered to be detrimental for the response of the myocardium to ischemic stress. However, this long standing belief has been challenged over the past years. In fact, in a series of studies using isolated rat heart models of ischemia/reperfusion, TH pretreatment was shown to be beneficial and mimic the effect of ischemic preconditioning [57]. Furthermore, T3 (and not T4) administration at reperfusion suppressed apoptosis, limited necrosis, and improved postischemic recovery of function [13, 14]. Similarly, TH treatment after myocardial infarction limited infarct size [58] and reduced apoptosis in the border zone of the infarcted area [59]. The reparative effect of TH seems to be mediated via activation of prosurvival signaling pathways. Thus, TH activates Akt [16, 59–61] and regulates PKC isoforms expression [62, 63], HSP70 expression [64], and HSP27 expression and phosphorylation and translocation [65]. Furthermore, TH suppresses ischemia/reperfusion induced p38 MAPK and JNK activation [14, 66]. TH reparative action is shown to be mediated via TRα1 receptor [13]. Here, it is worth mentioning that T3 can also limit streptozotocin (STZ) induced beta pancreatic cell apoptosis via TRα1 receptor. Thus, TH administration in STZ treated animals with myocardial infarction resulted in increased insulin levels in plasma and significant improvement of the postischemic cardiac dysfunction [61].

9. Clinical and Therapeutic Implications

Reperfusion injury and postischemic cardiac remodeling remain still a therapeutic challenge in the management of patients with heart disease [67, 68]. The discovery of novel pharmacological targets such as TRα1 receptor may be of important clinical and therapeutic relevance. TH

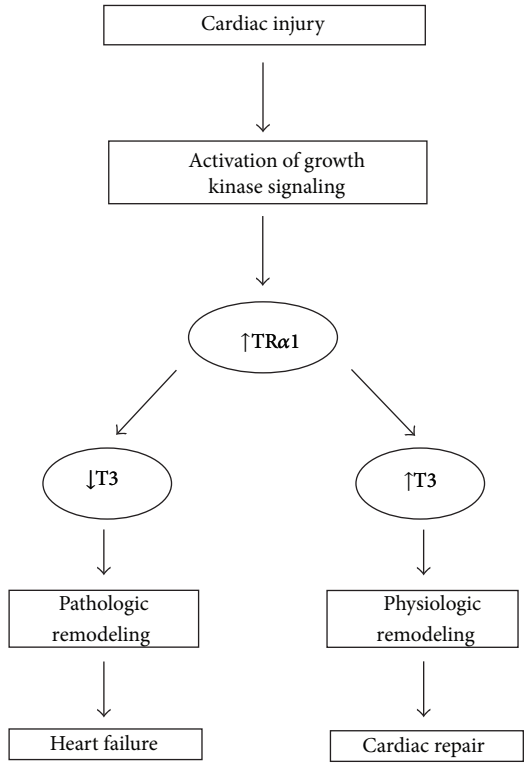

Figure 3: Schematic showing TRα1 involvement in the response of the myocardial tissue to injury.

has already been tried in clinical settings of controlled ischemia/reperfusion, such as CABG or heart donors preservation. Thus, T3 treatment postoperatively limited reperfusion injury and improved haemodynamics in patients undergoing CABG [69]. Furthermore, T3 treatment initiated one week before GABG resulted in improved cardiac index and reduced requirements of inotropes [70]. Similarly, TH has been used in heart donors to increase the probability of success in donor organ transplantation. However, a clear benefit of this treatment has not been demonstrated [71]. This may be due to the fact that most of the patients were receiving T4 instead of the active T3 and TH treatment was used in nonischemic stable donor hearts. In fact, when T3 was administered in a series of 22 unstable (ischemic) heart donors (considered unsuitable for transplantation), 17 of those patients progressed to successful transplantation [72]. Here it should be noted that TH was shown to facilitate recovery in patients with end-stage heart failure and mechanical support devices [73].

On the basis of these preliminary clinical data, large-scale clinical trials may be needed to demonstrate the beneficial effect of TH in clinical settings of ischemia/reperfusion. Furthermore, the recognition that TH can mediate important physiological and pharmacological actions via TRα1 receptor may allow selective pharmacological manipulation of TH signaling via TRα1 agonists. Currently, only TRβ analogs have been synthesized to control cholesterol metabolism. However, a chemical compound (CO23) which is assumed to be a TRα1 selective agonist has recently been synthesized. This compound, although it was shown to be selective for TRα1 receptor in amphibian models, it lost its selectivity in rat [74, 75]. This may be due to differences in TR expression in developing and mature tissues. This issue is of important therapeutic relevance and merits further investigation.

10. Concluding Remarks

TH is long known to be critical in organ maturation and regulation of metabolism. However, recent accumulating evidence shows that TH is crucial for the response of living organisms to environmental stress. In particular, TRα1 receptor seems to be an important determinant for the reactive growth response which occurs after myocardial injury. TRα1 can act as a molecular switch to convert pathological to physiologic growth; see Figure 3. Due to this dual action, TH, via TRα1 receptor, can limit myocardial injury and rebuild the injured myocardium. It is likely that TRα1 receptor may prove a novel pharmacological target for cardiac repair/regeneration.

Conflict of Interests

The authors declare that there is no conflict of interests regarding the publication of this paper.

References

[1] K. B. Storey, "Adventures in oxygen metabolism," *Comparative Biochemistry and Physiology B*, vol. 139, no. 3, pp. 359–369, 2004.

[2] A. Mancini, G. M. Corbo, A. Gaballo et al., "Relationship between plasma antioxidants and thyroid hormones in chronic obstructive pulmonary disease," *Experimental and Clinical Endocrinology & Diabetes*, vol. 120, no. 10, pp. 623–628, 2013.

[3] A. Mancini, S. Raimondo, C. di Segni et al., "Thyroid hormones and antioxidant systems: focus on oxidative stress in cardiovascular and pulmonary diseases," *International Journal of Molecular Sciences*, vol. 14, no. 12, pp. 23893–23909, 2013.

[4] C. K. Johnson and S. R. Voss, "Salamander paedomorphosis: linking thyroid hormone to life history and life cycle evolution," *Current Topics in Developmental Biology*, vol. 103, pp. 229–258, 2013.

[5] V. S. Peter, E. K. Joshua, S. E. W. Bonga, and M. C. S. Peter, "Metabolic and thyroidal response in air-breathing perch (*Anabas testudineus*) to water-borne kerosene," *General and Comparative Endocrinology*, vol. 152, no. 2-3, pp. 198–205, 2007.

[6] K. E. Hunt, C. Innis, and R. M. Rolland, "Corticosterone and thyroxine in cold-stunned Kemp's ridley sea turtles (*Lepidochelys kempii*)," *Journal of Zoo and Wildlife Medicine*, vol. 43, no. 3, pp. 479–493, 2012.

[7] L. J. de Groot, "Non-thyroidal illness syndrome is a manifestation of hypothalamic-pituitary dysfunction, and in view of current evidence, should be treated with appropriate replacement therapies," *Critical Care Clinics*, vol. 22, no. 1, pp. 57–86, 2006.

[8] J. E. Mitchell, A. S. Hellkamp, D. B. Mark et al., "Thyroid function in heart failure and impact on mortality," *Heart Failure*, vol. 1, no. 1, pp. 48–55, 2013.

[9] B. Eber, M. Schumacher, W. Langsteger et al., "Changes in thyroid hormone parameters after acute myocardial infarction," *Cardiology*, vol. 86, no. 2, pp. 152–156, 1995.

[10] F. W. Holland II, P. S. Brown Jr., B. D. Weintraub, and R. E. Clark, "Cardiopulmonary bypass and thyroid function: a 'euthyroid sick syndrome'," *The Annals of Thoracic Surgery*, vol. 52, no. 1, pp. 46–50, 1991.

[11] C. Lazzeri, A. Sori, C. Picariello, M. Chiostri, G. F. Gensini, and S. Valente, "Nonthyroidal illness syndrome in ST-elevation myocardial infarction treated with mechanical revascularization," *International Journal of Cardiology*, vol. 158, no. 1, pp. 103–104, 2012.

[12] I. Lymvaios, I. Mourouzis, D. V. Cokkinos, M. A. Dimopoulos, S. T. Toumanidis, and C. Pantos, "Thyroid hormone and recovery of cardiac function in patients with acute myocardial infarction: a strong association?" *European Journal of Endocrinology*, vol. 165, no. 1, pp. 107–114, 2011.

[13] C. Pantos, I. Mourouzis, T. Saranteas et al., "Acute T3 treatment protects the heart against ischemia-reperfusion injury via TRα1 receptor," *Molecular and Cellular Biochemistry*, vol. 353, no. 1-2, pp. 235–241, 2011.

[14] C. Pantos, I. Mourouzis, T. Saranteas et al., "Thyroid hormone improves postischaemic recovery of function while limiting apoptosis: a new therapeutic approach to support hemodynamics in the setting of ischaemia-reperfusion?" *Basic Research in Cardiology*, vol. 104, no. 1, pp. 69–77, 2009.

[15] K. K. Henderson, S. Danzi, J. T. Paul, G. Leya, I. Klein, and A. M. Samarel, "Physiological replacement of T3 improves left ventricular function in an animal model of myocardial infarction-induced congestive heart failure," *Circulation*, vol. 2, no. 3, pp. 243–252, 2009.

[16] I. Mourouzis, P. Mantzouratou, G. Galanopoulos et al., "Dose-dependent effects of thyroid hormone on post-ischemic cardiac performance: potential involvement of Akt and ERK signalings," *Molecular and Cellular Biochemistry*, vol. 363, no. 1-2, pp. 235–243, 2012.

[17] V. Bacci, G. C. Schussler, and T. B. Kaplan, "The relationship between serum triiodothyronine and thyrotropin during systemic illness," *Journal of Clinical Endocrinology & Metabolism*, vol. 54, no. 6, pp. 1229–1235, 1982.

[18] G. A. Brent and J. M. Hershman, "Thyroxine therapy in patients with severe nonthyroidal illnesses and low serum thyroxine concentration," *Journal of Clinical Endocrinology & Metabolism*, vol. 63, no. 1, pp. 1–8, 1986.

[19] S.-Y. Cheng, J. L. Leonard, and P. J. Davis, "Molecular aspects of thyroid hormone actions," *Endocrine Reviews*, vol. 31, no. 2, pp. 139–170, 2010.

[20] C. Pantos, I. Mourouzis, and D. V. Cokkinos, "Rebuilding the post-infarcted myocardium by activating "physiologic" hypertrophic signaling pathways: the thyroid hormone paradigm," *Heart Failure Reviews*, vol. 15, no. 2, pp. 143–154, 2010.

[21] C. Pantos, I. Mourouzis, and D. V. Cokkinos, "Thyroid hormone and cardiac repair/regeneration: from Prometheus myth to reality?" *Canadian Journal of Physiology and Pharmacology*, vol. 90, no. 8, pp. 977–987, 2012.

[22] C. Pantos, I. Mourouzis, C. Xinaris, Z. Papadopoulou-Daifoti, and D. Cokkinos, "Thyroid hormone and "cardiac metamorphosis": potential therapeutic implications," *Pharmacology & Therapeutics*, vol. 118, no. 2, pp. 277–294, 2008.

[23] C. Y. Ivashchenko, G. C. Pipes, I. M. Lozinskaya et al., "Human-induced pluripotent stem cell-derived cardiomyocytes exhibit temporal changes in phenotype," *American Journal of Physiology*, vol. 305, no. 6, pp. H913–H922, 2013.

[24] A. Liappas, I. Mourouzis, A. Zisakis et al., "Cell type dependent thyroid hormone effects on glioma tumor cell lines," *Journal of Thyroid Research*, vol. 2011, Article ID 856050, 8 pages, 2011.

[25] S. M. van der Heide, B. J. Joosten, B. S. Dragt, M. E. Everts, and P. H. M. Klaren, "A physiological role for glucuronidated thyroid hormones: preferential uptake by H9c2(2-1) myotubes," *Molecular and Cellular Endocrinology*, vol. 264, no. 1-2, pp. 109–117, 2007.

[26] H. H. van der Putten, B. J. Joosten, P. H. Klaren, and M. E. Everts, "Uptake of tri-iodothyronine and thyroxine in myoblasts and myotubes of the embryonic heart cell line H9c2(2-1)," *Journal of Endocrinology*, vol. 175, no. 3, pp. 587–596, 2002.

[27] C. Pantos, C. Xinaris, I. Mourouzis et al., "Thyroid hormone receptor α1: a switch to cardiac cell "metamorphosis"?" *Journal of Physiology and Pharmacology*, vol. 59, no. 2, pp. 253–269, 2008.

[28] F. Furuya, H. Shimura, S. Yamashita, T. Endo, and T. Kobayashi, "Liganded thyroid hormone receptor-α enhances proliferation of pancreatic β-cells," *The Journal of Biological Chemistry*, vol. 285, no. 32, pp. 24477–24486, 2010.

[29] Y. Hiroi, H.-H. Kim, H. Ying et al., "Rapid nongenomic actions of thyroid hormone," *Proceedings of the National Academy of Sciences of the United States of America*, vol. 103, no. 38, pp. 14104–14109, 2006.

[30] A. Kenessey and K. Ojamaa, "Thyroid hormone stimulates protein synthesis in the cardiomyocyte by activating the Akt-mTOR and p70S6K pathways," *The Journal of Biological Chemistry*, vol. 281, no. 30, pp. 20666–20672, 2006.

[31] A. Mansén, F. Yu, D. Forrest, L. Larsson, and B. Vennström, "TRs have common and isoform-specific functions in regulation of the cardiac myosin heavy chain genes," *Molecular Endocrinology*, vol. 15, no. 12, pp. 2106–2114, 2001.

[32] B. Gloss, S. U. Trost, W. F. Bluhm et al., "Cardiac ion channel expression and contractile function in mice with deletion of thyroid hormone receptor α or β," *Endocrinology*, vol. 142, no. 2, pp. 544–550, 2001.

[33] P. Tavi, M. Sjögren, P. K. Lunde et al., "Impaired Ca^{2+} handling and contraction in cardiomyocytes from mice with a dominant negative thyroid hormone receptor α1," *Journal of Molecular and Cellular Cardiology*, vol. 38, no. 4, pp. 655–663, 2005.

[34] M. Belakavadi, J. Saunders, N. Weisleder, P. S. Raghava, and J. D. Fondell, "Repression of cardiac *Phospholamban* gene expression is mediated by thyroid hormone receptor-α1 and involves targeted covalent histone modifications," *Endocrinology*, vol. 151, no. 6, pp. 2946–2956, 2010.

[35] L. Wikström, C. Johansson, C. Saltó et al., "Abnormal heart rate and body temperature in mice lacking thyroid hormone receptor α1," *The EMBO Journal*, vol. 17, no. 2, pp. 455–461, 1998.

[36] A. Stock and H. Sies, "Thyroid hormone receptors bind to an element in the connexin43 promoter," *Biological Chemistry*, vol. 381, no. 9-10, pp. 973–979, 2000.

[37] T. Esaki, H. Suzuki, M. Cook et al., "Cardiac glucose utilization in mice with mutated α- and β-thyroid hormone receptors," *American Journal of Physiology*, vol. 287, no. 6, pp. E1149–E1153, 2004.

[38] C. Pantos, I. Mourouzis, M. Delbruyère et al., "Effects of dronedarone and amiodarone on plasma thyroid hormones and on the basal and postischemic performance of the isolated rat heart," *European Journal of Pharmacology*, vol. 444, no. 3, pp. 191–196, 2002.

[39] A. Makino, H. Wang, B. T. Scott, J. X.-J. Yuan, and W. H. Dillmann, "Thyroid hormone receptor-α and vascular function,"

American Journal of Physiology, vol. 302, no. 9, pp. C1346–C1352, 2012.

[40] C. Sylvén, E. Jansson, P. Sotonyi, F. Waagstein, T. Barkhem, and M. Brönnegård, "Cardiac nuclear hormone receptor mrNA in heart failure in man," *Life Sciences*, vol. 59, no. 22, pp. 1917–1922, 1996.

[41] D. D. Belke, B. Gloss, E. A. Swanson, and W. H. Dillmann, "Adeno-associated virus-mediated expression of thyroid hormone receptor isoforms-α1 and -β1 improves contractile function in pressure overload-induced cardiac hypertrophy," *Endocrinology*, vol. 148, no. 6, pp. 2870–2877, 2007.

[42] K. Kinugawa, K. Yonekura, R. C. Ribeiro et al., "Regulation of thyroid hormone receptor isoforms in physiological and pathological cardiac hypertrophy," *Circulation Research*, vol. 89, no. 7, pp. 591–598, 2001.

[43] K. Kinugawa, M. Y. Jeong, M. R. Bristow, and C. S. Long, "Thyroid hormone induces cardiac myocyte hypertrophy in a thyroid hormone receptor α1-specific manner that requires TAK1 and p38 mitogen-activated protein kinase," *Molecular Endocrinology*, vol. 19, no. 6, pp. 1618–1628, 2005.

[44] G. d'Amati, C. R. di Gioia, D. Mentuccia et al., "Increased expression of thyroid hormone receptor isoforms in end-stage human congestive heart failure," *Journal of Clinical Endocrinology & Metabolism*, vol. 86, no. 5, pp. 2080–2084, 2001.

[45] P. A. Modesti, M. Marchetta, T. Gamberi et al., "Reduced expression of thyroid hormone receptors and beta-adrenergic receptors in human failing cardiomyocytes," *Biochemical Pharmacology*, vol. 75, no. 4, pp. 900–906, 2008.

[46] C. Pantos, I. Mourouzis, C. Xinaris et al., "Time-dependent changes in the expression of thyroid hormone receptor α1 in the myocardium after acute myocardial infarction: possible implications in cardiac remodelling," *European Journal of Endocrinology*, vol. 156, no. 4, pp. 415–424, 2007.

[47] C. Pantos, I. Mourouzis, T. Saranteas et al., "Thyroid hormone receptors α1 and β1 are downregulated in the post-infarcted rat heart: consequences on the response to ischaemia-reperfusion," *Basic Research in Cardiology*, vol. 100, no. 5, pp. 422–432, 2005.

[48] C. Pantos, I. Mourouzis, G. Galanopoulos et al., "Thyroid hormone receptor α1 downregulation in postischemic heart failure progression: the potential role of tissue hypothyroidism," *Hormone and Metabolic Research*, vol. 42, no. 10, pp. 718–724, 2010.

[49] C. Pantos, C. Xinaris, I. Mourouzis, A. D. Kokkinos, and D. V. Cokkinos, "TNF-α administration in neonatal cardiomyocytes is associated with differential expression of thyroid hormone receptors: a response prevented by T3," *Hormone and Metabolic Research*, vol. 40, no. 10, pp. 731–734, 2008.

[50] H. C. van Beeren, W. M. Jong, E. Kaptein, T. J. Visser, O. Bakker, and W. M. Wiersinga, "Dronerarone acts as a selective inhibitor of 3,5,3′-triiodothyronine binding to thyroid hormone receptor-α1: *in vitro* and *in vivo* evidence," *Endocrinology*, vol. 144, no. 2, pp. 552–558, 2003.

[51] I. Mourouzis, E. Kostakou, G. Galanopoulos, P. Mantzouratou, and C. Pantos, "Inhibition of thyroid hormone receptor α1 impairs post-ischemic cardiac performance after myocardial infarction in mice," *Molecular and Cellular Biochemistry*, vol. 379, no. 1-2, pp. 97–105, 2013.

[52] R. Bassi, R. Heads, M. S. Marber, and J. E. Clark, "Targeting p38-MAPK in the ischaemic heart: kill or cure?" *Current Opinion in Pharmacology*, vol. 8, no. 2, pp. 141–146, 2008.

[53] F. B. Engel, M. Schebesta, M. T. Duong et al., "p38 MAP kinase inhibition enables proliferation of adult mammalian cardiomyocytes," *Genes & Development*, vol. 19, no. 10, pp. 1175–1187, 2005.

[54] C. Jopling, G. Suñè, C. Morera, and J. C. I. Belmonte, "p38α MAPK regulates myocardial regeneration in zebrafish," *Cell Cycle*, vol. 11, no. 6, pp. 1195–1201, 2012.

[55] S. Adamopoulos, A. Gouziouta, P. Mantzouratou et al., "Thyroid hormone signalling is altered in response to physical training in patients with end-stage heart failure and mechanical assist devices: potential physiological consequences?" *Interactive Cardiovascular and Thoracic Surgery*, vol. 17, no. 4, pp. 664–668, 2013.

[56] L. R. Vose, G. Vinukonda, S. Jo et al., "Treatment with thyroxine restores myelination and clinical recovery after intraventricular hemorrhage," *The Journal of Neuroscience*, vol. 33, no. 44, pp. 17232–17246, 2013.

[57] C. I. Pantos, V. A. Malliopoulou, I. S. Mourouzis et al., "Long-term thyroxine administration protects the heart in a pattern similar to ischemic preconditioning," *Thyroid*, vol. 12, no. 4, pp. 325–329, 2002.

[58] F. Forini, V. Lionetti, H. Ardehali et al., "Early long-term L-T3 replacement rescues mitochondria and prevents ischemic cardiac remodeling in rats," *Journal of Cellular and Molecular Medicine*, vol. 15, no. 3, pp. 514–524, 2011.

[59] Y.-F. Chen, S. Kobayashi, J. Chen et al., "Short term triiodo-l-thyronine treatment inhibits cardiac myocyte apoptosis in border area after myocardial infarction in rats," *Journal of Molecular and Cellular Cardiology*, vol. 44, no. 1, pp. 180–187, 2008.

[60] J. A. Kuzman, A. M. Gerdes, S. Kobayashi, and Q. Liang, "Thyroid hormone activates Akt and prevents serum starvation-induced cell death in neonatal rat cardiomyocytes," *Journal of Molecular and Cellular Cardiology*, vol. 39, no. 5, pp. 841–844, 2005.

[61] I. Mourouzis, I. Giagourta, G. Galanopoulos et al., "Thyroid hormone improves the mechanical performance of the post-infarcted diabetic myocardium: a response associated with up-regulation of Akt/mTOR and AMPK activation," *Metabolism*, vol. 62, no. 10, pp. 1387–1393, 2013.

[62] C. Kalofoutis, I. Mourouzis, G. Galanopoulos et al., "Thyroid hormone can favorably remodel the diabetic myocardium after acute myocardial infarction," *Molecular and Cellular Biochemistry*, vol. 345, no. 1-2, pp. 161–169, 2010.

[63] V. Rybin and S. F. Steinberg, "Thyroid hormone represses protein kinase C isoform expression and activity in rat cardiac myocytes," *Circulation Research*, vol. 79, no. 3, pp. 388–398, 1996.

[64] C. Pantos, V. Malliopoulou, D. D. Varonos, and D. V. Cokkinos, "Thyroid hormone and phenotypes of cardioprotection," *Basic Research in Cardiology*, vol. 99, no. 2, pp. 101–120, 2004.

[65] C. Pantos, V. Malliopoulou, I. Mourouzis et al., "Thyroxine pretreatment increases basal myocardial heat-shock protein 27 expression and accelerates translocation and phosphorylation of this protein upon ischaemia," *European Journal of Pharmacology*, vol. 478, no. 1, pp. 53–60, 2003.

[66] C. Pantos, V. Malliopoulou, I. Paizis et al., "Thyroid hormone and cardioprotection: study of p38 MAPK and JNKs during ischaemia and at reperfusion in isolated rat heart," *Molecular and Cellular Biochemistry*, vol. 242, no. 1-2, pp. 173–180, 2003.

[67] G. G. Babu, J. M. Walker, D. M. Yellon, and D. J. Hausenloy, "Peri-procedural myocardial injury during percutaneous coronary intervention: an important target for cardioprotection," *European Heart Journal*, vol. 32, no. 1, pp. 23–31, 2011.

[68] T. Springeling, S. W. Kirschbaum, A. Rossi et al., "Late cardiac remodeling after primary percutaneous coronary intervention-five-year cardiac magnetic resonance imaging follow-up," *Circulation Journal*, vol. 77, no. 1, pp. 81–88, 2012.

[69] A. M. Ranasinghe, D. W. Quinn, D. Pagano et al., "Glucose-insulin-potassium and tri-iodothyronine individually improve hemodynamic performance and are associated with reduced troponin I release after on-pump coronary artery bypass grafting," *Circulation*, vol. 114, no. 1, pp. I245–I250, 2006.

[70] M. Sirlak, L. Yazicioglu, M. B. Inan et al., "Oral thyroid hormone pretreatment in left ventricular dysfunction," *European Journal of Cardio-Thoracic Surgery*, vol. 26, no. 4, pp. 720–725, 2004.

[71] A. M. Ranasinghe and R. S. Bonser, "Endocrine changes in brain death and transplantation," *Best Practice and Research*, vol. 25, no. 5, pp. 799–812, 2011.

[72] V. Jeevanandam, "Triiodothyronine: spectrum of use in heart transplantation," *Thyroid*, vol. 7, no. 1, pp. 139–145, 1997.

[73] G. V. Letsou, S. Reverdin, and O. H. Frazier, "Thyrotoxicosis-facilitated bridge to recovery with a continuous-flow left ventricular assist device," *European Journal of Cardio-Thoracic Surgery*, vol. 44, no. 3, pp. 573–574, 2013.

[74] C. Grijota-Martínez, E. Samarut, T. S. Scanlan, B. Morte, and J. Bernal, "*In vivo* activity of the thyroid hormone receptor β- and α-selective agonists GC-24 and CO23 on rat liver, heart, and brain," *Endocrinology*, vol. 152, no. 3, pp. 1136–1142, 2011.

[75] C. A. Ocasio and T. S. Scanlan, "Design and characterization of a thyroid hormone receptor α (TRα)-specific agonist," *ACS Chemical Biology*, vol. 1, no. 9, pp. 585–593, 2006.

Hindawi Publishing Corporation
Oxidative Medicine and Cellular Longevity
Volume 2014, Article ID 159852, 6 pages
http://dx.doi.org/10.1155/2014/159852

Research Article

Catalase Influence in the Regulation of Coronary Resistance by Estrogen: Joint Action of Nitric Oxide and Hydrogen Peroxide

Paulo C. Schenkel, Rafael O. Fernandes, Vinícius U. Viegas, Cristina Campos, Tânia R. G. Fernandes, Alex Sander da Rosa Araujo, and Adriane Belló-Klein

Laboratório de Fisiologia Cardiovascular, Departamento de Fisiologia, Instituto de Ciências Básicas da Saúde, Universidade Federal do Rio Grande do Sul, Sarmento Leite 500, Bairro Farroupilha, 90050-170 Porto Alegre, RS, Brazil

Correspondence should be addressed to Adriane Belló-Klein; belklein@ufrgs.br

Received 22 November 2013; Accepted 25 December 2013; Published 6 February 2014

Academic Editor: Neelam Khaper

We tested the influence of estrogen on coronary resistance regulation by modulating nitric oxide (NO) and hydrogen peroxide (H_2O_2) levels in female rats. For this, estrogen levels were manipulated and the hearts were immediately excised and perfused at a constant flow using a Langendorff's apparatus. Higher estrogen levels were associated with a lower coronary resistance, increased nitric oxide bioavailability, and higher levels of H_2O_2. When oxide nitric synthase blockade by L-NAME was performed, no significant changes were found in coronary resistance of ovariectomized rats. Additionally, we found an inverse association between NO levels and catalase activity. Taken together, our data suggest that, in the absence of estrogen influence and, therefore, reduced NO bioavailability, coronary resistance regulation seems to be more dependent on the H_2O_2 that is maintained at low levels by increased catalase activity.

1. Introduction

Decreased levels of estrogen play a critical role in heart disease development after menopause. The loss of ovarian hormones has a widespread adverse impact, increasing the risk of cardiovascular events, such as myocardial infarction (MI) [1–3].

The ischemic insult caused by MI can be increased during the early moments of reperfusion, referred to as ischemia/reperfusion (I/R) injury [4]. Moreover, myocardial cells tissue damage is aggravated by producing reactive oxygen species (ROS) under ischemic conditions by mitochondrial electron transport chain or by enzymes such as NADPH oxidase, xanthine oxidase, and nitric oxide synthase (NOS) [5].

Under I/R situations, such as in acute MI, endothelial injury decreases the production of nitric oxide (NO) [6], and NOS can become a source of superoxide anion [7, 8]. This process is termed NOS uncoupling. Moreover, NO produced from NOS can react with superoxide anion decreasing NO bioavailability and generating the potent oxidant, peroxynitrite (ONOO−) [9]. On the other hand, Yada et al. demonstrated that endogenous hydrogen peroxide (H_2O_2) contributes to coronary vasodilatation during I/R *in vivo* as a compensatory mechanism for the NO loss [10]. And, according to Cosentino et al. [11], H_2O_2 can be involved in vasorelaxation during uncoupling of NO synthesis. Moreover, it has been shown that H_2O_2 has a critical role as a signaling molecule for cardiac remodeling, probably due to its greater stability and permeability as compared to other ROS. In this context, the H_2O_2 levels modulation by antioxidant enzyme catalase (CAT) seems to play an important role in cardiovascular function [11].

Estrogen therapy (ET) has been considered as a means to reduce cardiovascular risk in postmenopausal women [1] and in animals submitted to I/R injury [12–14]. Furthermore, it has been reported that ET improves NO-mediated vasodilatation in ovariectomized rats [15]. However, the ET effects on H_2O_2 concentrations and its repercussion in coronary tone are not known.

Therefore, the aim in this study was to verify if the influence of estrogen over coronary resistance is modulated by hydrogen peroxide concentrations through catalase

activity control. Another aim of this study was to determine, through the NOS blockade, whether NO participates of this mechanism.

2. Methods

2.1. Animals. Twenty-nine female Wistar rats (60 days, 200 ± 20 g) were obtained from the Central Animal House at Universidade Federal do Rio Grande do Sul, Brazil. The animals were housed in plastic cages (four animals each) and received water and food *ad libitum*. They were maintained under standard laboratory conditions (controlled temperature of 21°C, 12 hours light/dark cycle). They were divided into three groups: SHAM, that was submitted to a sham surgery of bilateral ovariectomy; OVX, which was ovariectomized; and OVX + E_2, that was ovariectomized and received 17β-estradiol replacement. Each group was divided into two groups for the isolated heart perfusion, according to the perfusion solution utilized (Tyrode or Tyrode + L-NAME). Thus, the six experimental groups were TYRODE-SHAM (n = 5); L-NAME-SHAM (n = 4); TYRODE-OVX (n = 6); L-NAME-OVX (n = 4); TYRODE-OVX + E_2 (n = 4); L-NAME-OVX + E_2 (n = 4).

2.2. Ethical Approval. The experimental design was approved by the Committee on Animal Care and Use of the Universidade Federal do Rio Grande do Sul, following the Principles of Laboratory Animal Care published by the Council for International Organizations of Medical Science.

2.3. Ovariectomy (OVX). The rats were anesthetized (ketamine 90 mg kg^{-1}; xylazine 10 mg kg^{-1} i.p.) and bilateral ovariectomy or sham operation was performed. After a week, the animals were submitted to a 17β-estradiol replacement or replacement simulation.

2.4. 17β-Estradiol Therapy. Briefly, 15 mm medical grade tubing (1.02 mm i.d. × 2.16 mm o.d.) was filled with 10 μL of 5% (w : v) 17β-estradiol (Sigma Chemical Co., St. Louis, MO, USA) in sunflower oil and sealed with silicone. Capsules were soaked in sterile saline overnight and implanted subcutaneously between the scapulae under anesthesia. Sham animals were implanted with capsules containing just sunflower oil [16].

2.5. 17β-Estradiol Concentration. Blood samples were collected 28 days after ovariectomy surgery by the retrorbital venous plexus and immediately centrifuged at 1000 g for 10 min. The plasma 17β-estradiol concentration was estimated by chemiluminescence using the Immunolite 2000 apparatus (Biomedical Technologies Inc. Stroughton, MA, USA) at Weinmann Clinical Analysis Laboratory. The results were expressed as pg mL plasma^{-1}.

2.6. Estrous Cycle Determination. In female rats not submitted to ovariectomy, cycle determination was started at the 28th day of the experimental protocol. The cycle of each female rat was determined by observation of vaginal smears, which were taken using plastic tip. Saline was placed on the vaginal opening, aspirated, and then placed on a microscopic slide. Animals in the diestrus phase were used [17].

2.7. Experimental Protocol. After 28 days of the ovariectomy, the rats were killed by decapitation and the hearts were immediately excised and perfused at a constant flow using a Langendorff's apparatus [18]. After the connection of aorta and insertion of the balloon into left ventricle, the hearts were stabilized for 20 min with an end-diastolic pressure set to about 10 mmHg. Animals that did not show stable conditions at the end of this period were discarded. Global ischemia was induced by suspending the coronary flow for 30 min, and after that hearts were reperfused for 20 min.

2.8. Isolated Heart Perfusion. The hearts were rapidly excised through a median sternotomy and aorta was retrogradely perfused (Langendorff model) using a Langendorff apparatus (Hugo Sachs Electronics, March-Hugstetten, Germany). The isolated hearts were perfused with two modified Tyrode solutions. One solution containing 120 mmol L^{-1} NaCl, 5.4 mmol L^{-1} KCl, 1.8 mmol L^{-1} $MgCl_2$, 1.25 mmol L^{-1} $CaCl_2 \cdot 2H_2O$, 2 mmol L^{-1} NaH_2PO_4, 27 mmol L^{-1} $NaHCO_3$, 1.8 mmol L^{-1} Na_2SO_4, and 11 mmol L^{-1} glucose, and, other containing similar composition plus 100 μmol L^{-1} N^{ω}-nitro-L-arginine methyl ester (L-NAME) in a doses capable to inhibit all NOS isoforms [19]. Both solutions were equilibrated with a 95% oxygen and 5% carbon dioxide mixture to give a pH of 7.4 and perfused at a rate of 10 mL min^{-1} with a peristaltic pump (MS-Reglo 4 channels, Hugo Sachs Electronics) and kept at 37°C. A latex balloon was introduced into the left ventricle via the left atrium and was pressurized with a spindle syringe until it reached a preload of 10 mmHg to standardize cardiac work load. Heart rate (HR) and left ventricular end diastolic pressure (LVEDP) as well as the left ventricular developed pressure (LVDP, systolic minus end diastolic pressure) and coronary perfusion pressure (CPP) were monitored with a TPS Statham transducer and used to assess cardiac function.

2.9. Tissue Preparation. After perfusion protocol, the hearts were weighed and homogenized (1.15% w/v KCl and phenyl methyl sulphonyl fluoride PMSF 20 mmol L^{-1}) in Ultra-Turrax. The suspension was centrifuged at 600 g for 10 min at 0–4°C to remove the nuclei and cell debris [20] and supernatants were used for the assay of nitric oxide metabolism and enzymatic activity. Cardiac tissue samples were rapidly removed after perfusion protocol and frozen at −80°C for the evaluation of hydrogen peroxide steady state concentration.

2.10. Determination of Nitrates (NO_3^-) and Nitrites (NO_2^-). Nitrites were determined using the Griess reagent, in which a chromophore with a strong absorbance at 540 nm is formed by reaction of nitrite with a mixture of naphthyl-etilenediamine (0.1%) and sulphanilamide (1%). The absorbance was measured in a spectrophotometer to give

the nitrite concentration. Nitrates were determined as total nitrites (initial nitrite plus nitrite reduced from nitrate) after its reduction using nitrate reductase, from *Aspergillus* species in the presence of NADPH. A standard curve was established with a set of serial dilutions (10^{-8}–10^{-3} mol L^{-1}) of sodium nitrite. Results were expressed as mmol L^{-1} [21].

2.11. Determination of Hydrogen Peroxide. The assay was based in horseradish peroxidase (HRPO)-mediated oxidation of phenol red by hydrogen peroxide, leading to the formation of a compound that absorbs at 610 nm. Tissues were incubated for 30 min at 37°C in phosphate buffer 10 mmol L^{-1}, NaCl 140 mmol L^{-1}, and dextrose 5 mmol L^{-1}. The supernatants were transferred for tubes with phenol 0.28 mmol L^{-1} and 8.5 U mL^{-1} HRPO buffer, where, after 5 min incubation, NaOH 1 N was added and the mixture was read at 610 nm. The results were expressed as nmoles g tissue^{-1} [22].

2.12. Determination of Antioxidant Enzyme Activities. Superoxide dismutase (SOD) activity, expressed as U mg protein^{-1} of protein, was based on the inhibition of superoxide radical reaction with pyrogallol [23]. Catalase (CAT) activity was determined by following the decrease in 240 nm absorption of hydrogen peroxide (H_2O_2). It was expressed as nmoles mg protein^{-1} [24].

2.13. Determination of Protein Concentration. Protein was measured by the method of Lowry et al. [25], using bovine serum albumin as standard.

2.14. Statistical Analysis. Data were expressed as mean ± S.D. and compared using two way ANOVA followed by Student-Newman-Keuls multiple comparison test. Values of $P < 0.05$ were considered significant.

3. Results

3.1. 17β-Estradiol Concentration and Body Weight. 17β-estradiol level was reduced significantly in OVX group (14.3 ± 2.1 pg mL^{-1}) as compared with SHAM, in diestrus phase (30.7 ± 5.6 pg mL^{-1}), and higher in OVX + E_2 group (63.3 ± 2.8 pg mL^{-1}). Body weight showed an opposite profile to 17β-estradiol concentration. OVX rats had significantly higher body weight than SHAM and OVX + E_2 (252 ± 10; 232 ± 9; and 210 ± 7 g, resp.).

3.2. Isolated Heart Perfusion. Tyrode-OVX rats have shown a significant increase in CPP (32% and 28%, resp.) before ischemia and after reperfusion when compared to SHAM. CPP did not differ significantly in OVX + E_2 group before ischemia as compared to SHAM and OVX groups perfused with Tyrode (Figure 1). When NOS blockade by L-NAME was performed, CPP was increased in SHAM (54% and 55%) and in OVX + E_2 (22% and 18%) groups, respectively, before ischemia and after reperfusion as compared to their respective Tyrode control groups (Figure 1). The OVX groups showed no significant differences in CPP when comparing Tyrode and L-NAME perfusion. No significant differences were found in contractile function parameters (Table 1).

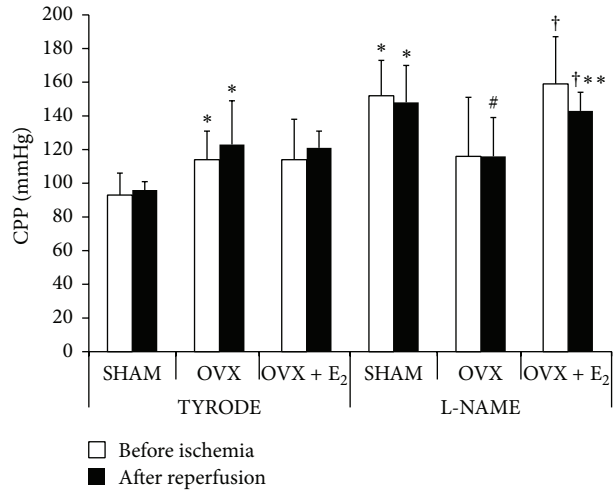

Figure 1: Coronary perfusion pressure (CPP) (in mmHg) of the different experimental groups before ischemia and after reperfusion. Values are expressed as mean ± S.D. of 4–6 animals/group. *Significantly different from TYRODE-SHAM ($P < 0.05$); #significantly different from L-NAME-SHAM ($P < 0.05$); †significantly different from TYRODE-OVX + E_2 ($P < 0.05$); **significantly different from L-NAME-OVX ($P < 0.05$).

3.3. Determination of Nitrates (NO_3^-) and Nitrites (NO_2^-) and Hydrogen Peroxide (H_2O_2). Nitrates/nitrites and hydrogen peroxide levels have shown the same profile of oscillation (Figures 2(a) and 2(b)). In animals perfused with Tyrode, both parameters were lower 35% in the OVX when compared to SHAM. In OVX + E_2 these parameters increased 17% and 34%, respectively, in comparison to OVX (Figures 2(a) and 2(b)). The L-NAME SHAM and OVX + E_2 groups showed a decrease in the nitrates/nitrites levels by 22% and 18%, respectively, and H_2O_2 levels by 36% and 30%, respectively, as compared to their respective Tyrode control groups. No significant differences were found in these parameters evaluated in OVX groups.

3.4. Determination of Antioxidant Enzyme Activities. In the Tyrode perfused groups, CAT activity was elevated in the OVX group as compared to SHAM and was restored in OVX + E_2 group (Table 2). In the L-NAME perfused groups, SHAM and OVX + E_2 showed an increased CAT activity (19% and 31%, resp.), when compared to their respective Tyrode control groups, reaching similar values than those observed in OVX groups, that did not exhibit alterations according to the solution utilized. No significant differences were found in SOD activity in the different experimental groups.

4. Discussion

The main finding of this study was to demonstrate that the protective role of estrogen in attenuating increased coronary

Table 1: Contractile function of the different experimental groups before ischemia and after reperfusion.

	Before Ischemia			After Reperfusion		
	HR (bpm)	LVEDP (mmHg)	LVDP (mmHg)	HR (bpm)	LVEDP (mmHg)	LVDP (mmHg)
TYRODE						
SHAM	214 ± 27	10 ± 1	94 ± 21	188 ± 27	58 ± 12	21 ± 9
OVX	201 ± 38	10 ± 1	87 ± 20	176 ± 46	63 ± 23	31 ± 27
OVX + E_2	184 ± 31	10 ± 1	95 ± 15	169 ± 28	62 ± 24	33 ± 21
L-NAME						
SHAM	202 ± 39	10 ± 1	100 ± 15	190 ± 50	55 ± 21	38 ± 30
OVX	206 ± 36	9 ± 1	84 ± 30	195 ± 31	57 ± 23	32 ± 19
OVX + E_2	186 ± 42	10 ± 1	99 ± 15	165 ± 58	66 ± 31	36 ± 29

Values are expressed as mean ± S.D. of 4–6 animals/group. Heart rate (HR), left ventricle end diastolic pressure (LVEDP), left ventricular developed pressure (LVDP).

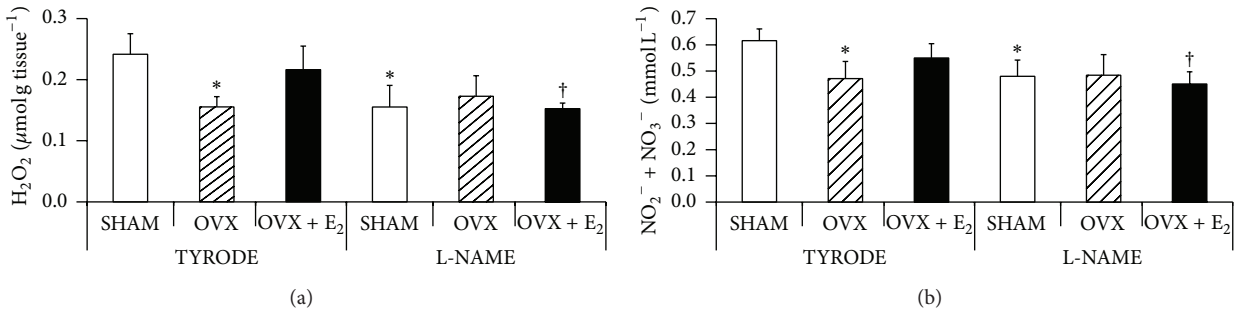

Figure 2: Hydrogen peroxide (H_2O_2) concentration (in μmol g tissue^{-1}) in cardiac tissue slices (a) and nitrites (NO_2^-) and nitrates (NO_3^-) concentration (in mmol L^{-1}) in cardiac muscle homogenates (b) of the different experimental groups at the end of reperfusion. Values are expressed as mean ± S.D. of 4–6 animals/group. *Significantly different from TYRODE-SHAM ($P < 0.05$); †significantly different from TYRODE-OVX + E_2 ($P < 0.05$).

Table 2: Antioxidant activity in cardiac muscle homogenates of the different experimental groups at the end of reperfusion.

	SOD (U mg prot.$^{-1}$)	CAT (pmol mg prot.$^{-1}$)
TYRODE		
SHAM	13.3 ± 2.0	22.4 ± 1.7
OVX	11.7 ± 0.9	26.9 ± 0.7*
OVX + E_2	11.9 ± 1.2	20.8 ± 2.2**
L-NAME		
SHAM	14.4 ± 1.7	26.6 ± 2.0*
OVX	12.0 ± 0.7	27.9 ± 2.6
OVX + E_2	12.2 ± 2.8	27.4 ± 3.1†

Values are expressed as mean ± S.D. of 4–6 animals/group.
*significantly different from TYRODE-SHAM ($P < 0.05$); **significantly different from TYRODE-OVX ($P < 0.05$); †significantly different from TYRODE-OVX + E_2 ($P < 0.05$).

resistance seems to be due to NO influence on the modulation of CAT activity and, by this way, regulating H_2O_2 concentration.

As expected, low estrogen levels were associated with higher coronary resistance in OVX group. The decrease in estrogen levels seems to impair the vascular tone regulation and, thus, has been associated with higher risk of cardiovascular disease [26]. In fact, an increased incidence of acute MI in postmenopausal women has been observed [27]. This fact, combined with the prior knowledge of H2O2 influence on coronary vascular bed by modulating the activity and expression of eNOS via the PI3-kinase and MAPK in-vitro [28], were the main reason to support our choice to develop this study utilizing the classical ex-vivo I/R model. To analyze the importance of estrogen in the coronary tone regulation in adverse heart situations, we simulated menopause by promoting bilateral ovariectomy and used ET to recover its levels. These procedures were effective in reducing and increasing, respectively, 17β-estradiol plasma concentration.

In accordance with the literature, the increase in vascular resistance in ovariectomized rats has been attributed, in part, to a lower NO bioavailability [29]. It has been shown that estrogen may act as an indirect coronary vasodilator mediated by endothelium-derived vasodilatory substances, such as NO [29]. Corroborating these findings, in this study we observed an opposite profile between nitrates/nitrites levels and CPP in the OVX group perfused with Tyrode. It is possible that, with the withdrawal of estrogen influence, endothelial dysfunction takes place, increasing coronary resistance [27]. When NO levels were increased by ET, the coronary resistance was attenuated in Tyrode-OVX + E_2 group. This important role of estrogen in modulation of vascular tone appears to be mediated by PI3-kinase/Akt pathway in endothelial cells resulting in increased expression of NOS and leading to the greater production of NO [28].

Associated with the decrease in NO bioavailability, the OVX group also showed lower H_2O_2 levels as compared to SHAM perfused with Tyrode. The regulation of coronary tone is physiologically modulated in great part by NO. Additionally, numerous other molecules are involved in the regulation of vascular tone. Among these, the more prominent influence of H_2O_2 in pathological situations has been highlighted, when NO influence is reduced [11, 30]. Therefore, the control of these substances appears to be an important mechanism involved in coronary tone regulation. Hydrogen peroxide, a downstream ROS also generate by NADPH-oxidase, has been suggested to be a key molecule in the regulation of the coronary tone by stimulating endothelium-dependent and/or endothelium independent vasorelaxation [30]. These effects, mediated by the regulation of smooth muscle's potassium channel and activation of eNOS, respectively, may represent a cellular adaptation in adverse situations, as in I/R [31, 32]. In this context, the estrogen influence in the vascular tone regulation also appears to be determined by less H_2O_2 production, since this hormone suppresses the activity and expression of NADPH oxidase [33]. In the present study, Tyrode-OVX group presented reduced H_2O_2 levels and higher CAT activity in relation to SHAM group after I/R. Although an inverse association between estrogen and ROS by suppression of the expression and activity of NADPH oxidase has been shown in the literature [33], the lower H_2O_2 levels, showed in this study, were associated with increased activity of CAT in ovariectomized group. Our findings corroborate previous findings of Behr et al. that showed an increase in peroxidases CAT and glutathione in ovariectomized rats [34]. A consequent adaptation of antioxidant enzymes appears to modulate the H_2O_2 levels and thus contribute to vascular tone regulation in rats with low estrogen levels.

Additionally, our findings suggest that this higher CAT activity seems to be resultant from the lower NO bioavailability in animals with reduced estrogen levels, since this group exhibited lower nitrates/nitrites levels. In fact, the antioxidant activity of CAT seems to be modulated by the NO levels. It has been shown in the literature that NO and CAT can quickly react and form a complex that culminate in reduction of NO bioavailability and reduced activity of catalase [35]. In order to determine the role of NO in the estrogen influence on coronary tone, L-NAME was added to the perfusion liquid. As expected, NOS blockade reduced significantly nitrates/nitrites levels in SHAM and OVX + E_2 to values similar to those of OVX group. Furthermore, nitrates/nitrites were not modified in OVX groups perfused with Tyrode or L-NAME, reinforcing our suggestion of a reduced influence of NO in the regulation of coronary tone in ovariectomized rats. Associated with this, CAT was more effective to reduce H_2O_2 levels in SHAM and OVX + E_2 groups perfused with L-NAME since its activity became less inhibited by NOS blockade. These results suggest that estrogen exerts its effects by its capacity to influence NOS activity.

Taken together, our data highlight the influence of estrogen on NOS and the CAT contribution in the regulation of NO and H_2O_2 levels to an important joint action in the control of coronary resistance. Regulating these parameters by negative feedback mechanism, CAT emerges as a key molecule in the regulatory control of the coronary tone. Moreover, the increase in its activity with reduced NO levels suggests a significant influence of H_2O_2 as vasomodulator in adverse situations. This knowledge may be relevant in the proposal of therapeutical strategies capable to diminish the adverse effects observed in the I/R syndrome.

Conflict of Interests

The authors declare that there is no conflict of interest that could be perceived as prejudicing the impartiality of the research reported.

Acknowledgments

This work was supported by CNPq and FAPERGS, Brazilian Research Agencies. The authors would like to acknowledge Weinmann Clinical Analysis Laboratory for 17β-estradiol hormone measurements.

References

[1] M. E. Mendelsohn and R. H. Karas, "The protective effects of estrogen on the cardiovascular system," *New England Journal of Medicine*, vol. 340, no. 23, pp. 1801–1811, 1999.

[2] M. C. Solimene, "Coronary heart disease in women: a challenge for the 21st century," *Clinics*, vol. 65, no. 1, pp. 99–106, 2010.

[3] T. Simoncini and A. R. Genazzani, "Non-genomic actions of sex steroid hormones," *European Journal of Endocrinology*, vol. 148, no. 3, pp. 281–292, 2003.

[4] M. G. Perrelli, P. Pagliaro, and C. Penna, "Ischemia/reperfusion injury and cardioprotective mechanisms: role of mitochondria and reactive oxygen species," *World Journal of Cardiology*, vol. 3, pp. 186–200, 2011.

[5] M. K. Misra, M. Sarwat, P. Bhakuni, R. Tuteja, and N. Tuteja, "Oxidative stress and ischemic myocardial syndromes," *Medical Science Monitor*, vol. 15, no. 10, pp. RA209–RA219, 2009.

[6] J. L. Mehta, W. W. Nichols, W. H. Donnelly, D. L. Lawson, and T. G. P. Saldeen, "Impaired canine coronary vasodilator response to acetylcholine and bradykinin after occlusion-reperfusion," *Circulation Research*, vol. 64, no. 1, pp. 43–54, 1989.

[7] S. Pou, W. S. Pou, D. S. Bredt, S. H. Snyder, and G. M. Rosen, "Generation of superoxide by purified brain nitric oxide synthase," *Journal of Biological Chemistry*, vol. 267, no. 34, pp. 24173–24176, 1992.

[8] I. Huk, J. Nanobashvili, C. Neumayer et al., "L-arginine treatment alters the kinetics of nitric oxide and superoxide release and reduces ischemia/reperfusion injury in skeletal muscle," *Circulation*, vol. 96, no. 2, pp. 667–675, 1997.

[9] J. L. Zweier, J. Fertmann, and G. Wei, "Nitric oxide and peroxynitrite in postischemic myocardium," *Antioxidants and Redox Signaling*, vol. 3, no. 1, pp. 11–22, 2001.

[10] T. Yada, H. Shimokawa, O. Hiramatsu et al., "Cardioprotective role of endogenous hydrogen peroxide during ischemia-reperfusion injury in canine coronary microcirculation in vivo," *The American Journal of Physiology—Heart and Circulatory Physiology*, vol. 291, no. 3, pp. H1138–H1146, 2006.

[11] F. Cosentino, J. E. Barker, M. P. Brand et al., "Reactive oxygen species mediate endothelium-dependent relaxations in

Tetrahydrobiopterin-deficient mice," *Arteriosclerosis, Thrombosis, and Vascular Biology*, vol. 21, no. 4, pp. 496–502, 2001.

[12] E. A. Booth and B. R. Lucchesi, "Estrogen-mediated protection in myocardial ischemia-reperfusion injury," *Cardiovascular Toxicology*, vol. 8, no. 3, pp. 101–113, 2008.

[13] P. Zhai, T. E. Eurell, R. Cotthaus, E. H. Jeffery, J. M. Bahr, and D. R. Gross, "Effect of estrogen on global myocardial ischemia-reperfusion injury in female rats," *The American Journal of Physiology—Heart and Circulatory Physiology*, vol. 279, no. 6, pp. H2766–H2775, 2000.

[14] R. Tissier, X. Waintraub, N. Couvreur et al., "Pharmacological postconditioning with the phytoestrogen genistein," *Journal of Molecular and Cellular Cardiology*, vol. 42, no. 1, pp. 79–87, 2007.

[15] M. Florian, A. Freiman, and S. Magder, "Treatment with 17-β-estradiol reduces superoxide production in aorta of ovariectomized rats," *Steroids*, vol. 69, no. 13-14, pp. 779–787, 2004.

[16] M. Elisa Prediger, G. Duzzo Gamaro, L. MacHado Crema, F. Urruth Fontella, and C. Dalmaz, "Estradiol protects against oxidative stress induced by chronic variate stress," *Neurochemical Research*, vol. 29, no. 10, pp. 1923–1930, 2004.

[17] F. K. Marcondes, F. J. Bianchi, and A. P. Tanno, "Determination of the estrous cycle phases of rats: some helpful considerations," *Brazilian Journal of Biology*, vol. 62, no. 4, pp. 609–614, 2002.

[18] A. S. D. R. Araujo, M. F. S. De Miranda, U. De Oliveira et al., "Increased resistance to hydrogen peroxide-induced cardiac contracture is associated with decreased myocardial oxidative stress in hypothyroid rats," *Cell Biochemistry and Function*, vol. 28, no. 1, pp. 38–44, 2010.

[19] H. Han, R. Kaiser, K. Hu, M. Laser, G. Ertl, and J. Bauersachs, "Selective modulation of endogenous nitric oxide formation in ischemia/reperfusion injury in isolated rat hearts: effects on regional myocardial flow and enzyme release," *Basic Research in Cardiology*, vol. 98, no. 3, pp. 165–174, 2003.

[20] S. F. Llesuy, J. Milei, and H. Molina, "Comparison of lipid peroxidation and myocardial damage induced by adriamycin and 4′-epiadriamycin in mice," *Tumori*, vol. 71, no. 3, pp. 241–249, 1985.

[21] D. L. Granger, N. M. Anstey, W. C. Miller, and J. B. Weinberg, "Measuring nitric oxide production in human clinical studies," *Methods in Enzymology*, vol. 301, pp. 49–61, 1998.

[22] E. Pick and Y. Keisari, "A simple colorimetric method for the measurement of hydrogen peroxide produced by cells in culture," *Journal of Immunological Methods*, vol. 38, no. 1-2, pp. 161–170, 1980.

[23] S. L. Marklund, "Superoxide dismutase isoenzymes in tissues and plasma from New Zealand black mice, nude mice and normal BALB/c mice," *Mutation Research*, vol. 148, no. 1-2, pp. 129–134, 1985.

[24] H. Aebi, "Catalase in vitro," *Methods in Enzymology*, vol. 105, pp. 121–126, 1984.

[25] O. H. Lowry, N. J. Rosebrough, A. L. Farr, and R. J. Randall, "Protein measurement with the Folin phenol reagent," *The Journal of Biological Chemistry*, vol. 193, no. 1, pp. 265–275, 1951.

[26] H. R. Lee, T. H. Kim, and K. C. Choi, "Functions and physiological roles of two types of estrogen receptors, ERalpha and ERbeta, identified by estrogen receptor knockout mouse," *Laboratory Animal Research*, vol. 28, pp. 71–76, 2012.

[27] A. A. Knowlton and A. R. Lee, "Estrogen and the cardiovascular system," *Pharmacology & Therapeutics*, vol. 135, pp. 54–70, 2012.

[28] G. Han, H. Ma, R. Chintala et al., "Nongenomic, endothelium-independent effects of estrogen on human coronary smooth muscle are mediated by type I (neuronal) NOS and PI3-kinase-Akt signaling," *The American Journal of Physiology—Heart and Circulatory Physiology*, vol. 293, no. 1, pp. H314–H321, 2007.

[29] I. Hernández, J. L. Delgado, L. F. Carbonell, M. C. Pérez, and T. Quesada, "Hemodynamic effect of 17β-estradiol in absence of NO in ovariectomized rats: role of angiotensin II," *The American Journal of Physiology—Regulatory Integrative and Comparative Physiology*, vol. 274, no. 4, pp. R970–R978, 1998.

[30] H. Cai, Z. Li, M. E. Davis, W. Kanner, D. G. Harrison, and S. C. Dudley Jr., "Akt-dependent phosphorylation of serine 1179 and mitogen-activated protein kinase kinase/extracellular signal-regulated kinase 1/2 cooperatively mediate activation of the endothelial nitric-oxide synthase by hydrogen peroxide," *Molecular Pharmacology*, vol. 63, no. 2, pp. 325–331, 2003.

[31] H. Cai, J. S. McNally, M. Weber, and D. G. Harrison, "Oscillatory shear stress upregulation of endothelial nitric oxide synthase requires intracellular hydrogen peroxide and CaMKII," *Journal of Molecular and Cellular Cardiology*, vol. 37, no. 1, pp. 121–125, 2004.

[32] J. Cheng, X. Ma, J. Zhang, and D. Su, "Diverse modulating effects of estradiol and progesterone on the monophasic action potential duration in Langendorff-perfused female rabbit hearts," *Fundamental and Clinical Pharmacology*, vol. 26, no. 2, pp. 219–226, 2012.

[33] A. A. Miller, G. R. Drummond, A. E. Mast, H. H. H. W. Schmidt, and C. G. Sobey, "Effect of gender on NADPH-oxidase activity, expression, and function in the cerebral circulation: role of estrogen," *Stroke*, vol. 38, no. 7, pp. 2142–2149, 2007.

[34] G. A. Behr, C. E. Schnorr, and J. C. F. Moreira, "Increased blood oxidative stress in experimental menopause rat model: the effects of vitamin A low-dose supplementation upon antioxidant status in bilateral ovariectomized rats," *Fundamental and Clinical Pharmacology*, vol. 26, no. 2, pp. 235–249, 2012.

[35] G. C. Brown, "Reversible binding and inhibition of catalase by nitric oxide," *European Journal of Biochemistry*, vol. 232, no. 1, pp. 188–191, 1995.

Hindawi Publishing Corporation
Oxidative Medicine and Cellular Longevity
Volume 2014, Article ID 657512, 9 pages
http://dx.doi.org/10.1155/2014/657512

Research Article

Antiapoptotic Actions of Methyl Gallate on Neonatal Rat Cardiac Myocytes Exposed to H_2O_2

Sandhya Khurana,[1] Amanda Hollingsworth,[1,2] Matthew Piche,[1] Krishnan Venkataraman,[3] Aseem Kumar,[4,5] Gregory M. Ross,[1] and T. C. Tai[1,2,4,5]

[1] *Medical Sciences Division, Northern Ontario School of Medicine, Laurentian University, Sudbury, ON, Canada P3E 2C6*
[2] *Department of Biology, Laurentian University, Sudbury, ON, Canada P3E 2C6*
[3] *Department of Gerontology, Huntington University, Sudbury, ON, Canada*
[4] *Department of Chemistry and Biochemistry, Laurentian University, Sudbury, ON, Canada P3E 2C6*
[5] *Biomolecular Sciences Program, Laurentian University, Sudbury, ON, Canada P3E 2C6*

Correspondence should be addressed to T. C. Tai; tc.tai@nosm.ca

Received 12 August 2013; Revised 15 October 2013; Accepted 11 November 2013; Published 12 January 2014

Academic Editor: Adriane Belló-Klein

Reactive oxygen species trigger cardiomyocyte cell death via increased oxidative stress and have been implicated in the pathogenesis of cardiovascular diseases. The prevention of cardiomyocyte apoptosis is a putative therapeutic target in cardioprotection. Polyphenol intake has been associated with reduced incidences of cardiovascular disease and better overall health. Polyphenols like epigallocatechin gallate (EGCG) can reduce apoptosis of cardiomyocytes, resulting in better health outcomes in animal models of cardiac disorders. Here, we analyzed whether the antioxidant N-acetyl cysteine (NAC) or polyphenols EGCG, gallic acid (GA) or methyl gallate (MG) can protect cardiomyocytes from cobalt or H_2O_2-induced stress. We demonstrate that MG can uphold viability of neonatal rat cardiomyocytes exposed to H_2O_2 by diminishing intracellular ROS, maintaining mitochondrial membrane potential, augmenting endogenous glutathione, and reducing apoptosis as evidenced by impaired Annexin V/PI staining, prevention of DNA fragmentation, and cleaved caspase-9 accumulation. These findings suggest a therapeutic value for MG in cardioprotection.

1. Introduction

Reactive oxygen species (ROS), a product of normal cellular metabolism, are usually handled effectively by the cellular defense systems, thereby having little bearing on cellular health. Cellular redox balance is maintained by antioxidant enzymes, such as superoxide dismutase and catalase, and by signaling mechanisms to conserve a state of oxidative homeostasis. However, under situations of exaggerated stress or hypoxia, the cellular defenses may be insufficient to overcome ROS overload. Oxidative stress has been clinically shown to be relevant in the progression of cardiac diseases and heart failure [1, 2]. Excess ROS can cause a variety of cellular damage including mitochondrial dysfunction, DNA damage, and ultimately lead to apoptosis with apoptosis of cardiomyocytes being critical in tissue damage and eventually heart failure. Hence, protection of cardiomyocytes and their increased survival is a putative target for cardioprotection [3].

Increasing evidence suggests that fetal hypoxia and resultant increased ROS are factors that can program for adult diseases, a phenomenon known as developmental programming; the activation of oxidative stress pathways *in utero* can program for cardiac dysfunction in adulthood such as responses to ischemia/reperfusion, cardiac function, coronary flow, and hypertension [4–7]. Hypoxia due to intrauterine stress during fetal development affects cardiogenesis and can have adverse effects on the developing heart, affecting fetal heart morphology and function [5]. In this scenario, fetal cardiomyocytes undergo hypertrophy, likely due to increased cardiomyocyte loss resulting from increased apoptosis [8]. Antioxidants such as vitamin C administered during pregnancy to rats have proven effective in preventing

oxidative stress-mediated cardiovascular dysfunction in the offspring of this animal model [9, 10]. Cardiomyocytes also undergo cell death under a variety of other physiological stimuli such as oxidative stress due to hypoxia induced during cardiac ischemia and glucose limitation amongst others [11]. Further, sustained volume and pressure overload, seen in hypertension and other cardiac disorders, ultimately lead to cardiac hypertrophy and result in cell death.

Naturally occurring polyphenols are antioxidants that are well acclaimed for their protective effects particularly in situations of oxidative stress and have been associated with inhibiting cell apoptosis, increasing viability, and being cytoprotective in nature [12]. Epidemiological studies have provided strong evidence in support of improved cardiovascular health in populations with consumption of diets rich in polyphenols [13, 14]. Studies using polyphenols have shown their beneficial effects in alleviating the effects of oxidative stress or modulating signaling pathways or both thereby reducing cardiovascular disease sequelae [15–17].

The goal of the current study was to examine the effect of polyphenols on survival of cultured neonatal rat cardiomyocytes (RCMs) under oxidative stress to evaluate mechanisms of polyphenols in cardioprotection, with an emphasis on effects on oxidative stress-related parameters. Hypoxia and oxidative stress induce apoptosis in neonatal cardiac myocytes [18–21]; further, these cells have been extensively employed as a model to study the mechanisms underlying electrophysiological heart functions and responses of myocytes to various stimuli including responses to oxidative stress and ROS, making them a suitable model for this study [22]. Previously, we have shown that the polyphenol methyl gallate (MG) is capable of protecting adrenal medulla-derived neuronal rat PC12 cells against H_2O_2-mediated apoptosis [23]. Cell type specificity in the mode of action of polyphenols has been reported. For example, gallic acid (GA) behaves as an antioxidant and protects HeLa cells from H_2O_2-induced cytotoxicity; however, in A549 cells it behaves as a prooxidant and induces apoptosis [24, 25]. Similarly, in the case of epigallocatechin gallate (EGCG), its pro-oxidant properties have been demonstrated in certain cancer cell lines; however, its antioxidant and cytoprotective capability has also been well recognized [26–28]. Hence, to assess the action of polyphenols and ascertain cell-specific differences in the mode of protection from apoptosis between PC12 and neonatal RCMs, the polyphenols EGCG, GA, and MG were employed to analyze recovery of neonatal RCMs from oxidative stress induced by H_2O_2 or $CoCl_2$ to compare with our previous work. This study shows that, similar to the PC12 cells, in RCMs too, MG can enhance cell viability, reduce ROS, increase mitochondrial stability, and restrict progression to apoptosis in neonatal rat cardiomyocytes stressed with H_2O_2.

2. Materials and Methods

2.1. Cell Culture. Neonatal rat cardiac myocytes (RCMs) isolated from 2-day-old rat heart ventricle were purchased from ScienCell Research Laboratories, Carlsbad, CA, USA. The cells were maintained in a humidified incubator at 37°C with 5% CO_2, in cardiac myocyte medium (CMM) supplemented with 5% FBS, 1% cardiac myocyte growth supplement, and 1% penicillin/streptomycin (ScienCell Research Laboratories; Carlsbad, CA).

2.2. Cell Treatment. To determine LD_{50}, various concentrations of H_2O_2 or $CoCl_2$ were used in an MTT assay for 24 hours. Once LD_{50} was determined, oxidative stress was induced using the LD_{50} concentration for 24 hours, specifically H_2O_2 (800 μM) or $CoCl_2$ (900 μM). The polyphenols were chosen based on a prior screening study performed in our lab identifying polyphenols that were able to reduce ROS in PC12 cells under oxidative stress [29]. Polyphenol concentrations were consistent with previous studies from our lab using PC12 cells; pretreatment with N-acetylcysteine (NAC) was a positive control [23, 29]. Epigallocatechin-3-gallate (EGCG, 100 μM), gallic acid (GA, 50 μM), methyl gallate (MG, 50 μM), or NAC (5 mM) (Sigma-Aldrich; Oakville, ON) were added to RCMs, incubated for 30 minutes, and then stressed with H_2O_2 or $CoCl_2$ for 24 hours. The downstream processing was assay/experiment specific. Cells were imaged using an inverted microscope (Nikon ECLIPSE TS100) and processed with Adobe Photoshop CS4.

2.3. Viability Assays. The MTT assay was used to determine LD_{50} concentrations of $CoCl_2$ and H_2O_2 and in the polyphenol protection experiments to determine cell viability. Cells, cultured in a 96-well plates, were treated as above, and MTT dye was added at 1/10th volume (5 mg/mL in PBS) (Sigma-Aldrich; Oakville, ON). Cells were incubated at 37°C with 5% CO_2 in the dark for 4 hours, medium aspirated, 50 μL of DMSO added (Fisher Scientific; Whitby, ON), and incubated in the dark for 15 minutes. The OD_{570} was measured on a plate reader (BioTek, PowerWave XS; Winooski, VT, USA). Optical densities of samples were normalized to controls.

2.4. Intracellular ROS. Intracellular ROS was measured using a fluorogenic dye, CM-H_2DCFDA (5-(and-6)-chloromethyl-2′7′-dichlorodihydrofluorescein diacetate, acetyl ester) (Invitrogen Canada; Burlington, ON) as per the manufacturer's instructions. Fluorescence was measured at 495 nm and emission at 525 nm via flow cytometry (FACS Canto II, BD Biosciences; San Jose, CA). The fluorescence from 10,000 events was averaged and relative fold changes determined by comparing with controls.

2.5. JC-10 Staining. Mitochondrial membrane potential was assessed by flow cytometry using a fluorogenic dye, JC-10 (Abcam; Cambridge, MA). Treated cells were loaded with JC-10 dye according to the manufacturer's instructions with modifications: spent medium was aspirated and complete medium added to scrape cells. JC-10 solution was added at equal volume and incubated in the dark at 37°C for 15 minutes prior to analysis. For the positive control, cells were incubated with FCCP (carbonyl cyanide 4-(trifluoromethoxy) phenylhydrazone), preceding the JC-10 solution. Monomeric (green) and J-aggregate (red) fluorescence were measured

using the FL1 and FL2 channels, respectively, and analyzed following compensation for spectral overlap.

2.6. Annexin V and PI Staining. Apoptosis was measured by flow cytometry using CytoGLO Annexin V-FITC Apoptosis Detection Kit (IMGENEX Corporation; San Diego, CA) as per the manufacturer's instructions. Relative fold changes in the percentage of Annexin V^+/PI^+ and Annexin V^-/PI^- were compared to controls.

2.7. Total Glutathione. Total glutathione was quantified enzymatically as per the manufacturer's instructions (Enzo Life Sciences, Plymouth Meeting, PA) and absorbance normalized to protein concentration quantified by BCA assay (Pierce, Thermo Scientific; Rockford, IL). Relative change was determined by comparing with controls.

2.8. DNA Fragmentation. DNA from treated and control cells was isolated as previously described [30], resolved on a 2% agarose gel, and imaged with Biorad Chemidoc XRS and Quantity One software.

2.9. Fluorescence Microscopy. RCMs were planted on acid washed coverslips and treated as above. The cells were washed with PBS, fixed with 3.7% p-formaldehyde, permeabilized with 0.2% Triton X100, and stained with anticleaved caspase-9 (rat specific Clone, Asp353, Cell signaling) for 1 hour. Alexa 488 conjugated secondary and DAPI were then applied for 30 minutes in the dark (Invitrogen, Burlington, ON, Canada). The coverslips were visualized on a confocal microscope (Zeiss TE2000). A minimum of 10 fields and 50 cells were counted, $n = 3$, and images processed using Adobe Photoshop CS4.

2.10. Statistical Analysis. Data are represented as mean ± SEM. with a minimum $n = 3$. Comparisons of treatment groups were made to controls by one-way ANOVA and Dunnett's *post hoc* test (GraphPad Prizm, La Jolla, CA). Values of $P \leq 0.05$ were considered statistically significant.

3. Results

3.1. MTT Assay. The MTT assay was employed to assess LD_{50} for each stressor as a function of cellular metabolic activity. Varying concentrations of H_2O_2 or $CoCl_2$ were added to the cells and viability analyzed at 24 hours of treatment. The LD_{50} was determined to be 800 μM for H_2O_2 and 900 μM for $CoCl_2$ (Figures 1(a) and 1(b), resp.). Applying the LD_{50} concentrations, rescue of viability was assessed after oxidative stress, in the presence or absence of NAC or the polyphenols EGCG, MG, or GA. NAC was used as a positive control because of its well-documented antioxidant effects, including the scavenging of ROS, stimulation of glutathione synthesis, and detoxification [31]. Viability of $CoCl_2$-stressed cells did not significantly change with prior exposure to EGCG, GA, MG, or NAC (Figure 1(c)). However, pretreatment with NAC, EGCG, or MG significantly increased viability of RCMs stressed with H_2O_2 from 49.5% to 209.9%, 76.9%, and 123.2%, respectively (Figure 1(c)), indicating their protective effect only against H_2O_2 but not cobalt. The assessment of viability by the MTT assay was verified with trypan blue exclusion, since the former detects mitochondrial functionality, while the latter depends on the integrity of the limiting membrane; the data from both assays were consistent (data not shown). A morphological assessment of treated RCMs was done to visualize cellular damage. The images show that cells treated with NAC or EGCG, MG, or GA were virtually indistinguishable from controls (Figure 1(d)). In contrast, cells treated with H_2O_2 or $CoCl_2$ appeared stressed and did not have the same attachment properties as controls. The H_2O_2-stressed cells appeared to lose membrane integrity with signs of membrane damage. Cells treated with $CoCl_2$ appeared rounded and lost their attachment properties. In both stressors, pretreatments with NAC, EGCG, and MG treatment considerably reversed these morphological effects, while GA had little to no effect (Figure 1(d)).

Although EGCG improved viability and maintained cell integrity, the cardioprotective effects of MG was further examined due to its more potent ability to increase cell viability and considering our prior investigations on MG's ability to prevent apoptosis in PC12 cells. Also, subsequent experiments were restricted only to H_2O_2 since no rescue was seen with cobalt.

3.2. Intracellular Reactive Oxygen Species. Since excess H_2O_2 causes accumulation of intracellular ROS (iROS), which is detrimental to cellular health, the ability of MG to reduce iROS and thereby increase cell viability was examined. Flow cytometry was used to quantify iROS in treated cells compared to healthy controls. Exposure to H_2O_2 resulted in a 3.4-fold increase in production of iROS; both NAC and MG significantly decreased H_2O_2-driven generation of iROS as pretreatment with these compounds decreased iROS levels to 2.3-fold and 1.4-fold, respectively (Figure 2(a)).

3.3. Mitochondrial Potential. This study further evaluated whether the increased iROS in H_2O_2-stressed cells was accompanied by of a loss of mitochondrial potential and if MG pretreatment could affect this phenomenon. The cells were analyzed with the JC-10 dye that forms red J-aggregates in healthy cells but stays a green monomer in cells that have lost mitochondrial integrity; treatment with FCCP was used as a positive control for functionality of the JC-10 dye. The scatter plots show that majority of the cells treated with H_2O_2 shifted towards green fluorescence when compared to controls (Figure 2(b)). Remarkably, in cells pretreated with the antioxidants NAC or MG, a population shift to the red channel was observed indicating preservation of mitochondrial potential. Consequently, H_2O_2-stressed cells maintained mitochondrial potential when pretreated with either NAC or MG (Figure 2(c)).

3.4. Total Glutathione. The synthesis of glutathione, a key antioxidant produced endogenously by cells to overcome oxidative stress, can be modulated by polyphenols [32]. Thus, to assess the antioxidant capacity of the cells, total

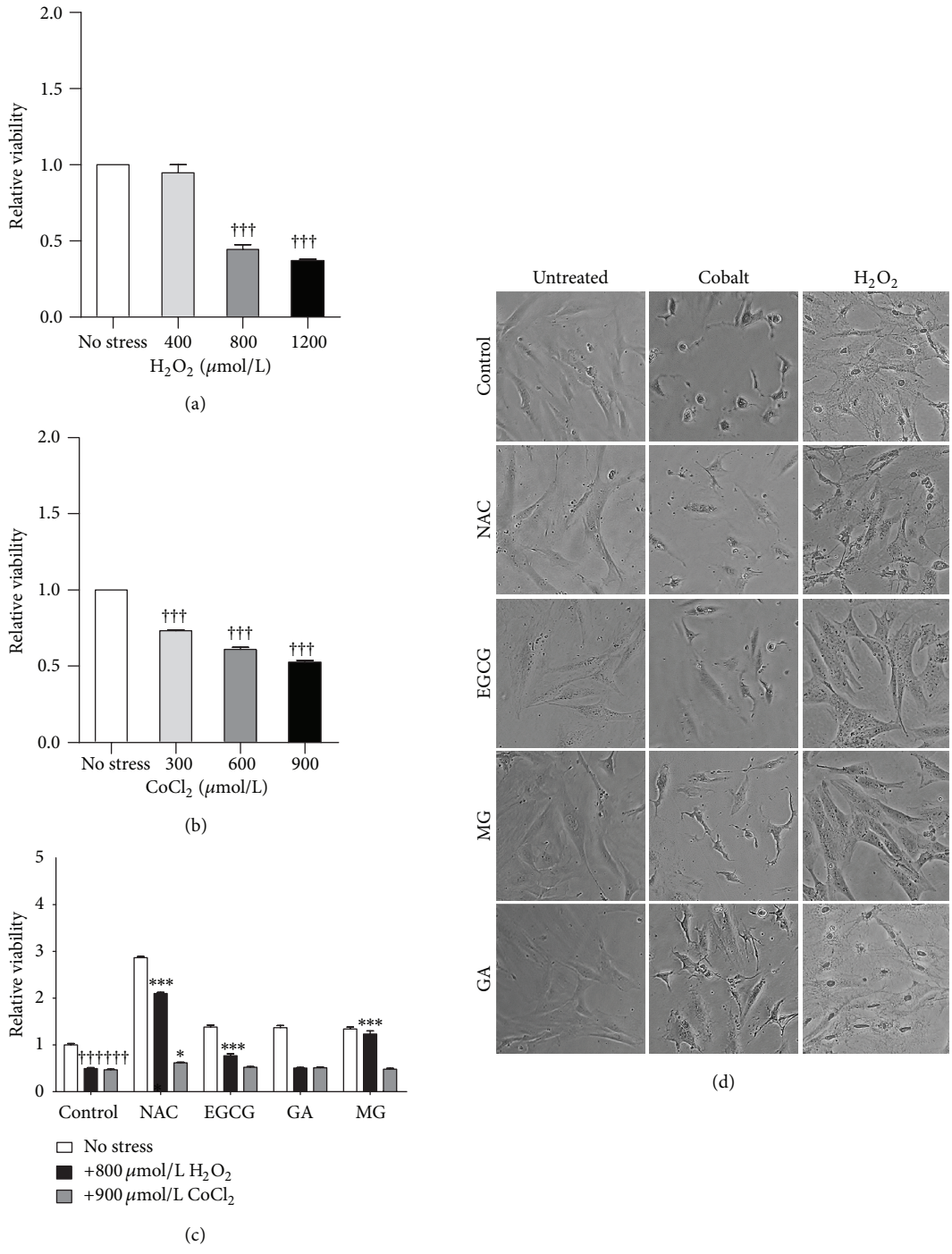

Figure 1: Oxidative stress affects viability and morphology of neonatal rat cardiac myocytes. LD_{50} concentrations were determined for RCMs using varying concentrations of H_2O_2 (a) or $CoCl_2$ (b). RCMs, pretreated with 5 mM NAC, 100 μM EGCG, 50 μM GA, or 50 μM MG, were exposed to 800 μM H_2O_2 or 900 μM $CoCl_2$ for 24 hours before proceeding to MTT assay (c) or imaging (d) as described in the methods. Stressed cells versus unstressed controls ($^{\dagger\dagger\dagger}P < 0.001$) and versus stressed cells pretreated with NAC or polyphenols ($^{***}P < 0.001$, $^{*}P < 0.05$). Data is expressed as mean ± S.E.M., $n = 3$.

glutathione was measured in H_2O_2-stressed cells and in those that were treated with MG prior to the stressor. The level of endogenous glutathione was significantly diminished upon H_2O_2 exposure. However, pretreatment of stressed RCMs with NAC or MG significantly increased total glutathione to normalcy (Figure 2(d)).

3.5. Apoptosis Assays. Numerous studies have established H_2O_2 as an inducer of cell apoptosis via loss of mitochondrial integrity and DNA damage. Evidence suggests that polyphenols mediate cell protective effects by interfering with apoptosis. Since MG seemed to increase viability, reduce ROS, and protect mitochondria, we wanted to further analyze

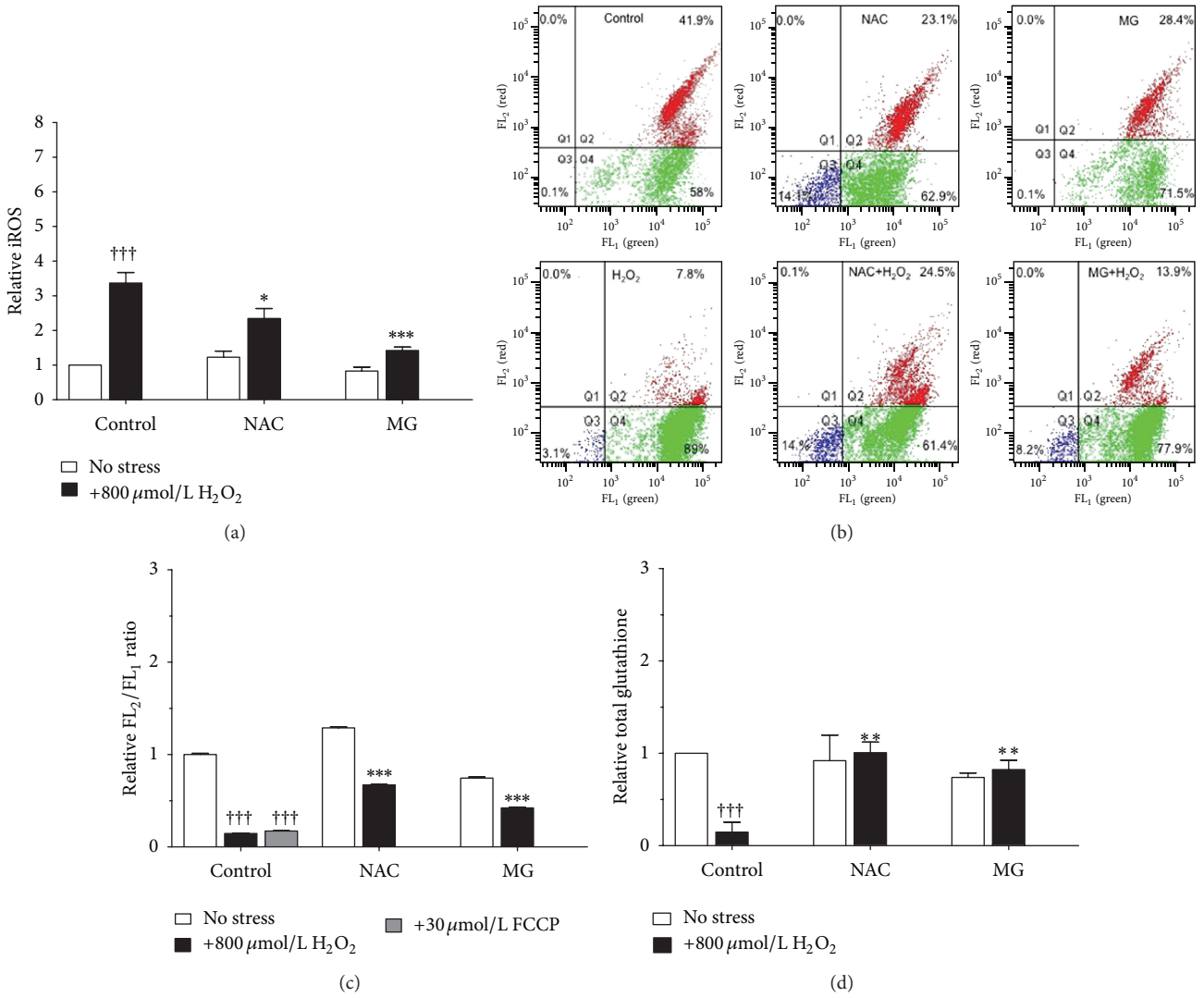

FIGURE 2: Methyl gallate represses oxidative stress. Neonatal RCMs pretreated with 5 mM NAC or 50 μM MG were exposed to 800 μM H_2O_2 for 24 hours before proceeding to measurements of either intracellular ROS (a), or mitochondrial membrane potential presented as a representative scatterplot (b) or graphically (c) and total glutathione levels as described in methods (d). Stressed cells versus unstressed controls ($^{\dagger\dagger\dagger}P < 0.001$) and versus stressed cells pretreated with NAC or MG ($^{***}P < 0.001$, $^{**}P < 0.01$, $^{*}P < 0.05$). Data is expressed as mean ± S.D, $n = 3$.

whether MG could potentially affect progression to apoptosis in H_2O_2-stressed cells. To determine this, we used flow cytometry to quantify Annexin V^+ and Propidium Iodide (PI^+) populations; late apoptotic cells are the dual positive fluoresced population in Q2 while unstained cells segregate in Q3 in the scatter plots (Figure 3(a)). Majority of the control cells and MG or NAC treated cells were Annexin V^-/PI^- indicating their healthy status (Figures 3(a) and 3(b)). However, H_2O_2-stressed RCMs showed a shift to dual stained with a 2.3-fold increase in this population when compared to the controls (Figures 3(a) and 3(c)). Eminently, MG reduced binding of Annexin V and PI in H_2O_2-stressed RCMs, with a significant shift from Q2 to Q3 suggesting that MG protects RCM cells from late apoptotic events (Figures 3(a) and 3(b)). NAC also demonstrated similar trends (Figures 3(a), 3(b), and 3(c)).

Further DNA fragmentation assays were performed to determine whether MG is capable of protecting DNA from damage in cells undergoing H_2O_2-mediated apoptosis. Indeed, pretreatment of RCMs with MG protected DNA; the typical DNA laddering pattern seen in apoptotic cells was significantly rescued in cells pretreated with MG (Figure 4(a)). This corroborates the interpretation from the Annexin V/PI data that MG protects cells under oxidative stress by preventing apoptotic events. To understand a potential cellular mechanism, levels of cleaved caspase-9 were analyzed, with caspase-9 being an initiator caspase upregulated in apoptotic cells. A microscopy-based approach was used to determine the intensity of cleaved caspase-9 and nuclear architecture revealed by DAPI staining. Control cells demonstrated a weak signal in the green channel reflective of the absence of cleaved caspase-9, with healthy rounded nuclei (Figure 4(b), Control

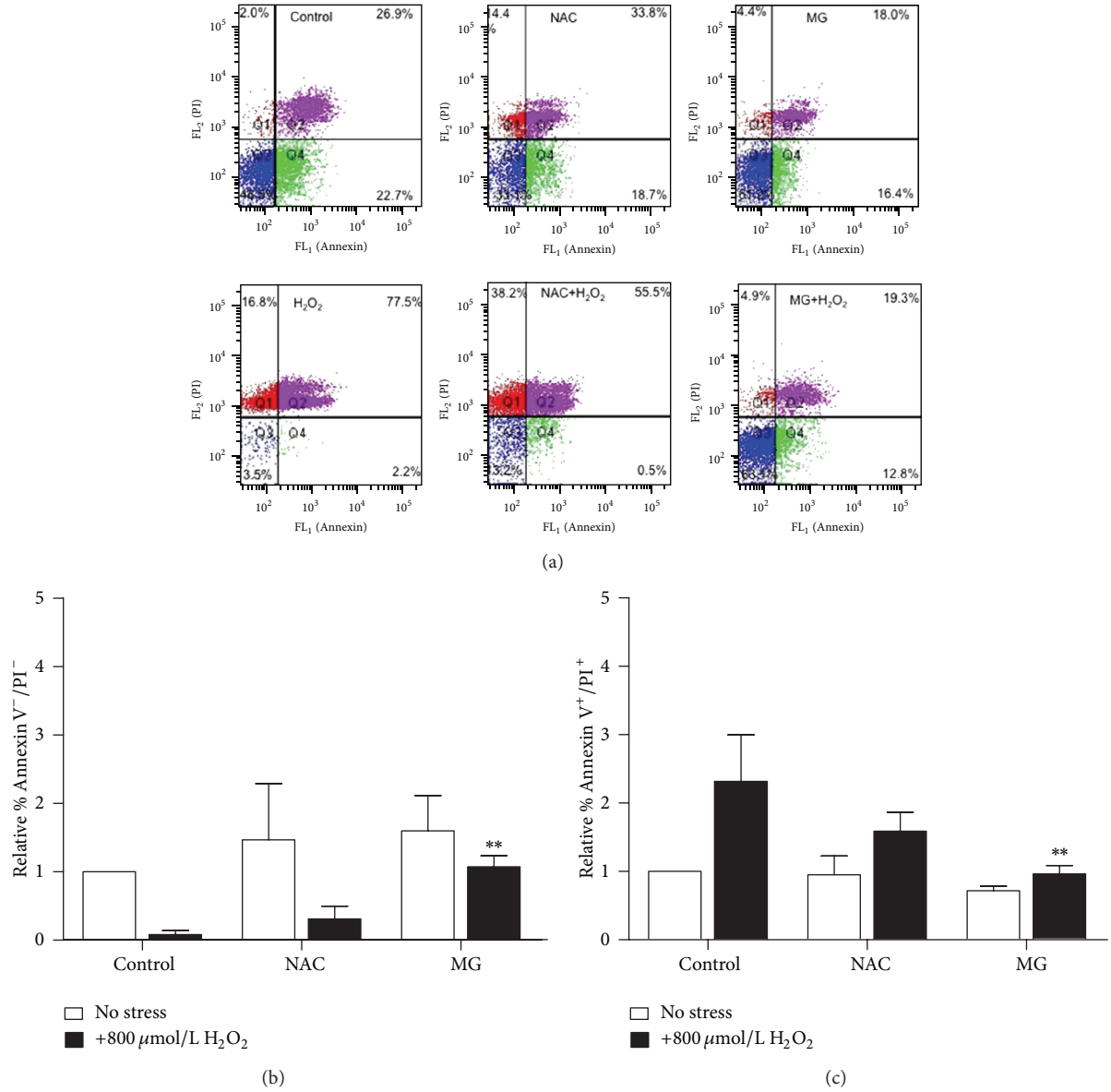

Figure 3: Methyl gallate protects cell viability by preventing apoptosis. Neonatal RCMs, pretreated with 5 mM NAC or 50 μM MG prior to stress induction with H_2O_2 for 24 hours, were stained with Annexin V and PI and analyzed by flow cytometry to assess apoptotic events by scatter distribution (a). The data is graphically represented asunstained Annexin$^-$/PI$^-$ (healthy) RCMs (b) and late apoptotic Annexin$^+$/PI$^+$ cells (c). Stressed cells versus unstressed controls ($^{\dagger\dagger}P < 0.01$) and versus stressed cells pretreated with NAC or MG ($^{**}P < 0.01$, $^{*}P < 0.05$). Data is expressed as means ± S.D, $n = 3$.

panel). The MG or NAC alone treated cells showed a similar pattern as control (Figure 4(b), MG panel and data not shown). Upon treatment with H_2O_2, an increase in intensity is apparent in the green channel indicative of cleaved caspase-9 accumulation, with the nucleus exhibiting a condensation of chromatin into crescent-shaped structures and increased blue intensity (Figure 4(b), H_2O_2 panel). Remarkably, treatment with MG rescued the cells from nuclear damage and blocked the accumulation of cleaved caspase-9 (Figure 4(b), H_2O_2 + MG panel); similar results were seen with NAC (data not shown). It must be noted that a 100% effect was not observed, with both healthy and unhealthy appearing cells present in the H_2O_2 + MG group. Therefore, cells were counted; a significant 30% reduction was calculated in the number of unhealthy cells that were observed in the MG pretreated group as compared to the H_2O_2 alone. Consequently, MG protects the nuclear architecture and prevents cleaved caspase-9 accumulation in H_2O_2-stressed cells.

Altogether, this study demonstrates the ability of MG to protect neonatal RCMs exposed to H_2O_2 from apoptosis by preserving mitochondrial membrane integrity, reducing ROS, increasing glutathione, protecting DNA from damage, and reducing activation of caspase-9 due to oxidative stress.

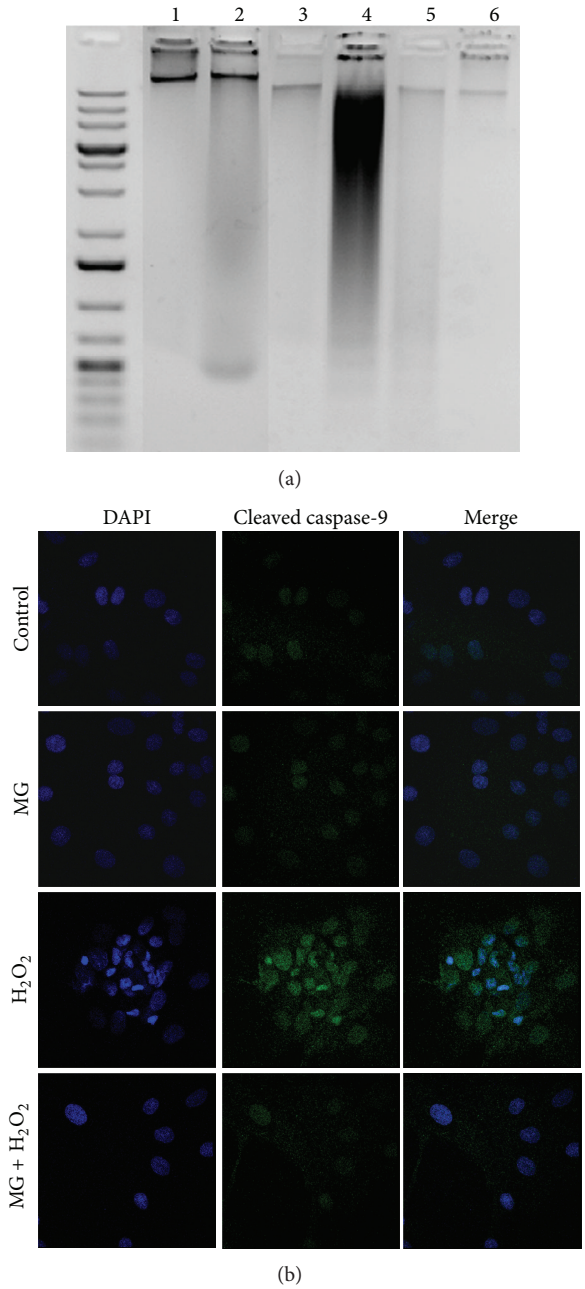

Figure 4: Methyl Gallate prevents DNA damage and inhibits caspase-9 activation. Total DNA was isolated from treated neonatal RCMs as described in methods. The lanes were regrouped from different parts of a representative gel (a) showing: 1Kb + ladder, Lane 1: Control, Lane 2: NAC, Lane 3: MG, Lane 4: H_2O_2, Lane 5: NAC + H_2O_2, and Lane 6: MG + H_2O_2. Fluorescent microscopy images of RCMs stained for cleaved caspase-9 and DAPI (b) showing: Panel 1: Control, Panel 2: MG, Panel 3: H_2O_2, and Panel 4: MG + H_2O_2.

4. Discussion

Oxidative stress, a major contributor to cell death, has been widely implicated in cellular damage and progression to cardiovascular disease [1]. Apoptosis is a significant cause of ROS-mediated cardiomyocyte cell loss during hypoxia, prenatal stress, ischemia-reperfusion, and other cardiac disorders. Polyphenols have been widely studied for their beneficial effects in reversing the effects of ROS thereby protecting cells from death. Our data demonstrates that, of the polyphenols analyzed, none were able to restore viability of neonatal RCMs from $CoCl_2$ stress. Further, only EGCG and MG restored cell viability of H_2O_2-stressed cells to the same as untreated controls. GA was unable to increase viability of either $CoCl_2$- or H_2O_2-stressed cells indicating a different mechanism of action from EGCG or MG. Additionally, EGCG and MG were able to rescue only from H_2O_2 stress implying source-dependent specificity in protection from oxidative stress; while cobalt reacts with H_2O_2 via a Fenton-based reaction to increase ROS, H_2O_2 generates highly reactive superoxide and hydroxyl radicals via the Haber-Weiss reaction [33, 34]. Moreover, certain polyphenols like EGCG and GA can behave as prooxidants and increase intracellular ROS ([35] and data not shown). The ability of MG to reduce iROS indicates direct antioxidant potential by acting as a scavenger for ROS or an indirect mediation of ROS reduction by modulating cellular signaling pathways; both mechanisms have been reported for polyphenols [36, 37].

Glutathione (GSH) is a crucial cellular antioxidant as it interacts directly with ROS, thereby oxidizing it to GSSG, which can be eliminated or converted by glutathione reductase (GSR) back to GSH. GSH also acts as a substrate for glutathione S-transferase (GST) which complexes it with electrophilic molecules destined for removal, like end products of oxidation and other toxics. GSH is also required in the reaction for glutathione peroxidase- (GPx-) mediated detoxification of H_2O_2 [38]. Because of its ROS scavenging properties, as evident by overall decreased iROS in cells pretreated with MG prior to the stressor, it is plausible that increased available GSH is a direct consequence of a reduced demand to counteract ROS. The ability of MG to increase cellular GSH has also been demonstrated in MDCK cells and, by our group, in PC12 cells exposed to H_2O_2 stress [29, 39]. The ability of MG to increase cellular GSH content is in keeping with other polyphenols shown to increase phase II enzymes in the oxidative stress response like GSR and GPx by gene activation via antioxidant response elements (ARE); in this regard, polyphenols have been noted to have mechanisms of protection that are distinct from their antioxidant capabilities alone [32]. However, based on the current data, we cannot pinpoint the exact mechanism by which MG increases cellular GSH or mediates iROS reduction.

The MTT assay data correlates with the JC-10 assay, both indicators of mitochondrial functionality, implying that MG rescued viability by preserving mitochondrial integrity. Mitochondrial health and maintenance of mitochondrial membrane potential are critical to cell survival. The exposure of cells to H_2O_2 has been shown to collapse the mitochondrial membrane potential in a variety of cell types. Damage to the mitochondrial membrane is a proven central player in the initiation of intrinsic apoptotic events, with cytochrome c release from the inner mitochondrial membrane being a factor that can be modulated by ROS [40]. In the ensuing steps, caspase-9 is cleaved subsequently acting as an initiator caspase and activates effector caspases like caspase-3 [41].

Active caspase-3 ultimately leads to mobilization of caspase activated DNase (CAD) into the nucleus, DNA fragmentation, and end-stage apoptosis. Early apoptosis is marked by the exposure of phosphatidylserine groups on damaged limiting membranes, which can bind to Annexin V with high affinity. In addition, damaged membranes are permeable, thus allowing the otherwise impermeable PI to enter cells and intercalate with DNA. Healthy intact cells are Annexin V^-/PI^-; cells in early apoptosis are characterized by Annexin V^+/PI^-, while the dual stained population Annexin V^+/PI^+ characterizes late apoptotic/necrotic cells [42]. Our lab has previously demonstrated MG's protective abilities against apoptosis in PC12 cells, specifically in preventing activation of caspase-9 [23, 29]. In the current study, MG showed similar cytoprotection in RCMs by diminished Annexin/PI staining, reversal of DNA laddering, and reduction of caspase-9 activation.

However, not all H_2O_2-stressed cells showed cleaved caspase-9^+ staining, but the endpoint of apoptosis was observed in the form of degraded DNA implying that the extrinsic pathway of apoptosis was also likely activated by H_2O_2. In the extrinsic pathway, the engagement of Fas ligand (Fas L) to cell surface Fas leads to Fas trimerization, followed by caspase-8 activation and recruitment of the death complex; FLIP (FLICE inhibitory protein) can inhibit cell death by the Fas/FasL pathway [43]. Previous studies showed that ROS can regulate FLICE and that H_2O_2 exposure can sensitize cardiomyocytes to Fas-mediated cell death [44]. However, in the current study, the role of extrinsic apoptotic factors was not examined, with the primary focus on mitochondrion-mediated intrinsic pathway. Nevertheless, polyphenols such as EGCG can modify Fas receptor expression and modulate STAT-1 phosphorylation thereby reducing apoptosis of cardiomyocytes [45]. Therefore, it is plausible that MG may have played some role in inhibiting the extrinsic pathway, demonstrated in the complete protection from DNA degradation upon MG pretreatment.

In summary, our data emphasizes the role of MG in repressing apoptosis progression in neonatal cardiomyocytes subjected to H_2O_2 stress by scavenging of ROS, increased endogenous glutathione, safeguarding mitochondria and cellular DNA, and inhibiting the intrinsic apoptotic pathway. In conclusion MG has the potential to combat oxidative stress in neonatal cardiomyocytes and could have therapeutic value in cardioprotection.

Conflict of Interests

The authors declare that there is no conflict of interests regarding the publication of this paper.

Authors' Contribution

Amanda Hollingsworth contributed equally to this paper.

Acknowledgments

This study was supported by grants from the Natural Sciences and Engineering Research Council of Canada to T. C. Tai.

References

[1] N. S. Dhalla, R. M. Temsah, and T. Netticadan, "Role of oxidative stress in cardiovascular diseases," *Journal of Hypertension*, vol. 18, no. 6, pp. 655–673, 2000.

[2] S. K. Maulik and S. Kumar, "Oxidative stress and cardiac hypertrophy: a review," *Toxicology Mechanisms and Methods*, vol. 22, no. 5, pp. 359–366, 2012.

[3] J. L. V. Reeve, A. M. Duffy, T. O'Brien, and A. Samali, "Don't lose heart—therapeutic value of apoptosis prevention in the treatment of cardiovascular disease," *Journal of Cellular and Molecular Medicine*, vol. 9, no. 3, pp. 609–622, 2005.

[4] K. H. Al-Gubory, P. A. Fowler, and C. Garrel, "The roles of cellular reactive oxygen species, oxidative stress and antioxidants in pregnancy outcomes," *International Journal of Biochemistry and Cell Biology*, vol. 42, no. 10, pp. 1634–1650, 2010.

[5] A. J. Patterson and L. Zhang, "Hypoxia and fetal heart development," *Current Molecular Medicine*, vol. 10, no. 7, pp. 653–666, 2010.

[6] D. Hauton, "Hypoxia in early pregnancy induces cardiac dysfunction in adult offspring of *Rattus norvegicus*, a non-hypoxia-adapted species," *Comparative Biochemistry and Physiology Part A*, vol. 163, no. 3-4, pp. 278–285, 2012.

[7] J. Nanduri, V. Makarenko, V. D. Reddy et al., "Epigenetic regulation of hypoxic sensing disrupts cardiorespiratory homeostasis," *Proceedings of the National Academy of Sciences of the United States of America*, vol. 109, no. 7, pp. 2515–2520, 2012.

[8] S. Bae, Y. Xiao, G. Li, C. A. Casiano, and L. Zhang, "Effect of maternal chronic hypoxic exposure during gestation on apoptosis in fetal rat heart," *American Journal of Physiology—Heart and Circulatory Physiology*, vol. 285, no. 3, pp. H983–H990, 2003.

[9] D. A. Giussani, E. J. Camm, Y. Niu et al., "Developmental programming of cardiovascular dysfunction by prenatal hypoxia and oxidative stress," *PLoS One*, vol. 7, no. 2, Article ID e31017, 2012.

[10] A. D. Kane, E. A. Herrera, E. J. Camm, and D. A. Giussani, "Vitamin C prevents intrauterine programming of *in vivo* cardiovascular dysfunction in the rat," *Circulation Journal*, vol. 77, no. 10, pp. 2604–2611, 2013.

[11] M. T. Crow, K. Mani, Y.-J. Nam, and R. N. Kitsis, "The mitochondrial death pathway and cardiac myocyte apoptosis," *Circulation Research*, vol. 95, no. 10, pp. 957–970, 2004.

[12] C. Giovannini and R. Masella, "Role of polyphenols in cell death control," *Nutritional Neuroscience*, vol. 15, no. 3, pp. 134–149, 2012.

[13] S. Khurana, M. Piche, A. Hollingsworth, K. Venkataraman, and T. C. Tai, "Oxidative stress and cardiovascular health: therapeutic potential of polyphenols," *Canadian Journal of Physiology and Pharmacology*, vol. 91, no. 3, pp. 198–212, 2013.

[14] I. C. W. Arts and P. C. H. Hollman, "Polyphenols and disease risk in epidemiologic studies," *The American Journal of Clinical Nutrition*, vol. 81, no. 1, pp. 317S–325S, 2005.

[15] V. Stangl, H. Dreger, K. Stangl, and M. Lorenz, "Molecular targets of tea polyphenols in the cardiovascular system," *Cardiovascular Research*, vol. 73, no. 2, pp. 348–358, 2007.

[16] C. A. Hamilton, W. H. Miller, S. Al-Benna et al., "Strategies to reduce oxidative stress in cardiovascular disease," *Clinical Science*, vol. 106, no. 3, pp. 219–234, 2004.

[17] A. Basu, M. Rhone, and T. J. Lyons, "Berries: emerging impact on cardiovascular health," *Nutrition Reviews*, vol. 68, no. 3, pp. 168–177, 2010.

[18] M. Tanaka, H. Ito, S. Adachi et al., "Hypoxia induces apoptosis with enhanced expression of Fas antigen messenger RNA in cultured neonatal rat cardiomyocytes," *Circulation Research*, vol. 75, no. 3, pp. 426–433, 1994.

[19] S. J. Chen, M. E. Bradley, and T. C. Lee, "Chemical hypoxia triggers apoptosis of cultured neonatal rat cardiac myocytes: modulation by calcium-regulated proteases and protein kinases," *Molecular and Cellular Biochemistry*, vol. 178, no. 1-2, pp. 141–149, 1998.

[20] X. Long, M. O. Boluyt, M. L. Hipolito et al., "p53 and the hypoxia-induced apoptosis of cultured neonatal rat cardiac myocytes," *Journal of Clinical Investigation*, vol. 99, no. 11, pp. 2635–2643, 1997.

[21] H. Zhu, S. McElwee-Witmer, M. Perrone, K. L. Clark, and A. Zilberstein, "Phenylephrine protects neonatal rat cardiomyocytes from hypoxia and serum deprivation-induced apoptosis," *Cell Death and Differentiation*, vol. 7, no. 9, pp. 773–784, 2000.

[22] S. Chlopcíková, J. Psotová, and P. Miketová, "Neonatal rat cardiomyocytes—a model for the study of morphological, biochemical and electrophysiological characteristics of the heart," *Biomedical papers*, vol. 145, no. 2, pp. 49–55, 2001.

[23] J. A. G. Crispo, M. Piché, D. R. Ansell et al., "Protective effects of methyl gallate on H_2O_2-induced apoptosis in PC12 cells," *Biochemical and Biophysical Research Communications*, vol. 393, no. 4, pp. 773–778, 2010.

[24] B. R. You and W. H. Park, "Gallic acid-induced lung cancer cell death is related to glutathione depletion as well as reactive oxygen species increase," *Toxicology in Vitro*, vol. 24, no. 5, pp. 1356–1362, 2010.

[25] Ö. Erol-Dayi, N. Arda, and G. Erdem, "Protective effects of olive oil phenolics and gallic acid on hydrogen peroxide-induced apoptosis," *European Journal of Nutrition*, vol. 51, no. 8, pp. 955–960, 2012.

[26] S. Azam, N. Hadi, N. U. Khan, and S. M. Hadi, "Prooxidant property of green tea polyphenols epicatechin and epigallocatechin-3-gallate: implications for anticancer properties," *Toxicology in Vitro*, vol. 18, no. 5, pp. 555–561, 2004.

[27] S. C. Forester and J. D. Lambert, "The role of antioxidant versus pro-oxidant effects of green tea polyphenols in cancer prevention," *Molecular Nutrition and Food Research*, vol. 55, no. 6, pp. 844–854, 2011.

[28] R. Sheng, Z.-L. Gu, M.-L. Xie, W.-X. Zhou, and C.-Y. Guo, "EGCG inhibits cardiomyocyte apoptosis in pressure overload-induced cardiac hypertrophy and protects cardiomyocytes from oxidative stress in rats," *Acta Pharmacologica Sinica*, vol. 28, no. 2, pp. 191–201, 2007.

[29] J. A. G. Crispo, D. R. Ansell, M. Piche et al., "Protective effects of polyphenolic compounds on oxidative stress-induced cytotoxicity in PC12 cells," *Canadian Journal of Physiology and Pharmacology*, vol. 88, no. 4, pp. 429–438, 2010.

[30] A. Kumar, A. Kumar, P. Michael et al., "Human serum from patients with septic shock activates transcription factors STAT1, IRF1, and NF-κB and induces apoptosis in human cardiac myocytes," *Journal of Biological Chemistry*, vol. 280, no. 52, pp. 42619–42626, 2005.

[31] G. S. Kelly, "Clinical applications of N-acetylcysteine," *Alternative Medicine Review*, vol. 3, no. 2, pp. 114–127, 1998.

[32] R. Masella, R. Di Benedetto, R. Varì, C. Filesi, and C. Giovannini, "Novel mechanisms of natural antioxidant compounds in biological systems: involvement of glutathione and glutathione-related enzymes," *Journal of Nutritional Biochemistry*, vol. 16, no. 10, pp. 577–586, 2005.

[33] K. Jomova and M. Valko, "Advances in metal-induced oxidative stress and human disease," *Toxicology*, vol. 283, no. 2-3, pp. 65–87, 2011.

[34] F. J. Giordano, "Oxygen, oxidative stress, hypoxia, and heart failure," *Journal of Clinical Investigation*, vol. 115, no. 3, pp. 500–508, 2005.

[35] H. Babich, A. G. Schuck, J. H. Weisburg, and H. L. Zuckerbraun, "Research strategies in the study of the pro-oxidant nature of polyphenol nutraceuticals," *Journal of Toxicology*, vol. 2011, Article ID 467305, 12 pages, 2011.

[36] M. Lorenz, S. Wessler, E. Follmann et al., "A constituent of green tea, epigallocatechin-3-gallate, activates endothelial nitric oxide synthase by a phosphatidylinositol-3-OH-kinase-, cAMP-dependent protein kinase-, and Akt-dependent pathway and leads to endothelial-dependent vasorelaxation," *Journal of Biological Chemistry*, vol. 279, no. 7, pp. 6190–6195, 2004.

[37] D. Vauzour, A. Rodriguez-Mateos, G. Corona, M. J. Oruna-Concha, and J. P. E. Spencer, "Polyphenols and human health: prevention of disease and mechanisms of action," *Nutrients*, vol. 2, no. 11, pp. 1106–1131, 2010.

[38] V. I. Lushchak, "Glutathione homeostasis and functions: potential targets for medical interventions," *Journal of Amino Acids*, vol. 2012, Article ID 736837, 26 pages, 2012.

[39] T.-J. Hsieh, T.-Z. Liu, Y.-C. Chia et al., "Protective effect of methyl gallate from *Toona sinensis* (Meliaceae) against hydrogen peroxide-induced oxidative stress and DNA damage in MDCK cells," *Food and Chemical Toxicology*, vol. 42, no. 5, pp. 843–850, 2004.

[40] M. Ott, V. Gogvadze, S. Orrenius, and B. Zhivotovsky, "Mitochondria, oxidative stress and cell death," *Apoptosis*, vol. 12, no. 5, pp. 913–922, 2007.

[41] S. A. Cook and P. A. Poole-Wilson, "Cardiac myocyte apoptosis," *European Heart Journal*, vol. 20, no. 22, pp. 1619–1629, 1999.

[42] I. Vermes, C. Haanen, H. Steffens-Nakken, and C. Reutelingsperger, "A novel assay for apoptosis. Flow cytometric detection of phosphatidylserine expression on early apoptotic cells using fluorescein labelled Annexin V," *Journal of Immunological Methods*, vol. 184, no. 1, pp. 39–51, 1995.

[43] P. Waring and A. Müllbacher, "Cell death induced by the Fas/Fas ligand pathway and its role in pathology," *Immunology and Cell Biology*, vol. 77, no. 4, pp. 312–317, 1999.

[44] J. Nitobe, S. Yamaguchi, M. Okuyama et al., "Reactive oxygen species regulate FLICE inhibitory protein (FLIP) and susceptibility to Fas-mediated apoptosis in cardiac myocytes," *Cardiovascular Research*, vol. 57, no. 1, pp. 119–128, 2003.

[45] P. A. Townsend, T. M. Scarabelli, E. Pasini et al., "Epigallocatechin-3-gallate inhibits STAT-1 activation and protects cardiac myocytes from ischemia/reperfusion-induced apoptosis," *The FASEB Journal*, vol. 18, no. 13, pp. 1621–1623, 2004.